

Development of Novel Operational Stability Control Systems for embedded High Voltage DC Links

A thesis submitted for the degree of Doctor of Philosophy

By

Shadi Khaleghi Kerahroudi

Supervisor: Prof Gareth Taylor

Brunel Institute of Power Systems (BIPS)

Department of Electronic and Computer Engineering
College of Engineering, Design and Physical Sciences
Brunel University London

August 2015

Abstract

In order to achieve the ambitious decarbonisation targets of the UK government, up to 30GW of wind generation could be connected to the GB transmission system by 2020. The challenges imposed when incorporating this volume of renewable energy are significant, introducing new technical challenges for National Grid as the system operator for the Great Britain transmission system. The majority of this new renewable generation will be connecting in Scotland and offshore in the UK as a whole. This results in greater uncertainty in the system from significant changes to the direction and volume of power flows across the network. In addition this implies a higher power transfer capacity requirement on the AC transmission lines, which are currently stability-limited, connecting SPT (Scottish Power Transmission) and National Grid networks. The required power transfer capability increases every year because of the large-scale increase in wind generation. Therefore, there is insufficient transmission capacity in the existing network to accommodate the increasing power transfer without constraining output of some generation plants. A range of new state of art technologies such as embedded HVDC link and Thyristor Controlled Series Compensation (TCSC) are planned to be added to the GB system in order to provide additional capacity and consequently facilitate the integration of large-scale renewable generation. It is, therefore essential that National Grid explores new ways of operating the transmission network and new devices to gain additional benefit from the HVDC link and the TCSC capabilities with regard to the system stability enhancement. This thesis investigates the effectiveness of the HVDC link and the TCSC with a view to system stability enhancement. A hierarchical stability control system to enhance the stability limit and achieve the best transient and dynamic performance using the HVDC link and the TCSCs as actuators in the feedback control system is proposed. In addition, a stability control system, using a robust and stabilising Sample Regulator multivariable control design method , to guarantee the system robustness and stability is proposed and designed. The performance and capability of the designed controller in co-ordinated control of the forthcoming power flow control devices are demonstrated on benchmark networks as well as full dynamic models of the GB transmission system using various study cases. Finally, the effectiveness of the West Coast HVDC link in improving the inter-area oscillation damping is presented using the developed model of the future GB transmission system.

Acknowledgements

I would like to express my gratitude to my supervisor Prof. Gareth Taylor for his guidance, advice and encouragement throughout this research.

A special acknowledgement must also go to the Engineering and Physical Sciences Research Council (EPSRC) and National Grid Electrical Transmission plc (NGET) who have sponsored this project. I would particularly like to thank Dr. Fan Li and Dr. Martin Bradley who have provided valuable insight and helped me to strengthen my knowledge of the industrial context into which this research is placed.

My deep appreciation also goes to Victor Mtembo and Dr. Phil Ashton for their help and advice throughout writing the thesis.

Also, I am extremely appreciative of the support provided to me by the Brunel Institute of Power Systems (BIPS) at Brunel University London.

Most importantly, I would like to thank My Family for their patience throughout this research – and particularly during the writing of this thesis. Without their support and encouragement this period would have been far more stressful, and far less enjoyable.

To my Family

Author's Declaration

The work described in this thesis has not been previously submitted for a degree in this or any other university and unless otherwise referenced it is the author's own work.

Table of Content

Chapter 1	1
Introduction	1
1.1. Environmental targets and Future Energy Scenarios	1
1.2. Generation capacity based on Future Energy Scenarios	2
1.3. Existing National Electricity Transmission System (NETS)	3
1.4. Future system requirements	5
1.5. Research objectives	9
1.6. Principal contributions to knowledge	10
1.7. Background to the Engineering Doctorate	12
1.8. List of publications arising from the PhD	12
1.8.1 Journal publications	12
1.8.2 Book Chapter publications	12
1.8.3 International Conference publications	12
1.8.4 Joint International Conference publications	13
1.9. Organisation of the thesis	14
Chapter 2	16
Literature review	16
2.1 Introduction	16
2.2 Historical power system stability issues	16
2.2.1 Power system reliability and security	17
2.3 Power system stability	18
2.4 Classification of power system stability	19
2.4.1 Rotor angle stability	20
2.4.2 Voltage stability	21
2.4.3 Frequency stability	22
2.5 Potential solution to power system stability enhancement	22
2.5.1 Review on application of TCSC in power system enhancement	23
2.5.1.1 History of TCSC implementation	23

2.5.1.2	Impact of optimal TCSC placement on the system performance enhancement	23
2.5.1.3	Capability of TCSC in the enhancement of the transfer capacity of tie lines limited by transient stability constraint	25
2.5.1.4	Capability of the TCSC to enhance the damping of power system oscillations	25
2.5.1.5	The capability of the TCSC in damping Sub-Synchronous Resonance (SSR)	27
2.5.2	Review of HVDC technology and its application in power system enhancement	29
2.5.2.1	The major advantages and applications of HVDC systems	30
2.5.2.2	HVDC link's technologies	32
2.5.3	Interaction between the AC and DC systems	34
2.5.4	Past research on the application of the HVDC link in power system stability enhancement	35
2.5.4.1	Capability of the HVDC link to enhance the damping of power system oscillation	38
2.5.4.2	Capability of the HVDC link to enhance transient stability	40
2.5.5	Future development of embedded and interconnector DC links	41
2.5.5.1	Future embedded HVDC links	42
2.5.5.2	Future off-shore DC grid	42
2.6	Concluding remarks	43
Chapter 3		45
Power system modelling in PowerFactory		45
3.1	Introduction	45
3.2	Introduction to DIgSILENT PowerFactory	45
3.3	Modelling and control of CSC-HVDC link	46
3.3.1	CSC- HVDC link configuration and components	46
3.3.2	CSC-HVDC link modelling	47
3.3.3	Control strategies for CSC-HVDC link	49
3.3.3.1	Rectifier control mode	49
3.3.3.2	Inverter control mode	50
3.3.4	Hierarchy control system for the CSC-HVDC link	51
3.4	TCSC modelling	53
3.5	Static Var Compensators (SVC) model	54
3.5.1	Target voltage mode	54

3.5.2	Constant MVar mode.....	55
3.6	Characteristics of the test systems used throughout the thesis.....	55
3.6.1	Test system 1	55
3.6.2	Test system 2 (Multiple TCSC line)	56
3.6.3	Test system 3 (Single HVDC link)	56
3.6.4	Test system 4 (Multiple HVDC links)	57
3.6.5	Test system 5 (Including the HVDC link and SVC).....	58
3.6.6	Test system 6 (Two-area four-machine system)	59
3.7	Concluding remarks	60
Chapter 4		61
Framework and requirements of hierarchical stability control system.....		61
4.1	Introduction to current and future control schemes in the GB transmission system	61
4.2	Requirement for hierarchical stability system.....	62
4.3	Control problems in the GB transmission system.....	64
4.4	Introduction to National Grid operational tools	65
4.4.1	Security constrained dispatch program (EBS).....	65
4.4.2	On Line Stability Assessor (OSA).....	66
4.4.3	Operational Tripping Schemes (OTS)	67
4.5	Framework of hierarchical stability control system for the GB transmission system	67
4.5.1	Proposed solution.....	68
4.6	The supervisory stability control system design	69
4.7	Introduction to Matlab/PowerFactory interface	70
4.7.1	Requirement for interfacing	70
4.7.2	Structure of the Matlab to DIgSILENT PowerFactory interface	71
4.8	Validation of the correct creation of interface between PowerFactory to Matlab/Simulink	72
4.8.1	Test system	73
4.8.2	The external PI controller in Matlab/Simulink (Setting up the required structure on the PowerFactory side to create an Interface).....	74
4.8.3	Initial conditions definition and calculation.....	77
4.8.4	Setting up the required structure (on Matlab/Simulink side) to create the Interface	78
4.8.5	Performance comparison of Built-in and external controllers	78
4.9	Concluding remarks	80

Chapter 5	81
Principle of the Sample Regulator control.....	81
5.1 Introduction.....	81
5.2 Feedback control system design.....	82
5.2.1 Primary and secondary control system	82
5.2.2 Requirements for the feedback control system	83
5.2.3 Multivariable feedback control system overview	84
5.3 Multi-variable control system design methods	85
5.4 Theory of the multi-variable Sampled Regulator control design method.....	87
5.4.1 Introduction.....	87
5.4.2 Assumption, notations and definitions.....	88
5.4.3 Stability of the Sampled Integral Regulators	90
5.4.4 Passivity method.....	90
5.4.5 Algorithm and theorem of passivity design method	93
5.4.6 Discussion on main features of the SR control.	94
5.5 Comparison of the linear characteristics of the actuators under control.....	95
5.5.1 Characteristics of the TCSC as an actuator.....	95
5.5.2 Characteristics of the HVDC link as an actuator	97
5.5.3 Characteristics of the SVC as an actuator.....	97
5.6 Implications to the stability control system design	98
5.7 Considerations affecting the stability control system	98
5.8 Application of SISO SR control in the stability enhancement.....	99
5.8.1 Development of a SISO SR control for the TCSC power flow control (Study case 1) .	99
5.8.1.1 Open-loop step response for design of SR controller	100
5.8.1.2 Test system.....	101
5.8.1.3 Simulation results and analysis on study case 1	101
5.8.2 Development of SISO SR controller for the HVDC link power flow control (Study case 2)	104
5.8.2.1 Test system.....	104
5.8.2.2 Overall structure of the secondary SISO SR controller for the HVDC link .	105
5.8.2.3 Simulation results and analysis on study case 2	105
5.9 Application of MIMO SR control for coordinated control of power flow and voltage control devices.....	108

5.9.1	Development of MIMO SR control for coordinated control of two TCSC lines (Study case 3)	108
5.9.1.1	Test System	108
5.9.1.2	Simulation results and analysis on study case 3	109
5.9.1.3	Limitation of the SR controller for the TCSC line.....	111
5.9.2	Development of the MIMO SR control for coordinated control of two HVDC links (Study case 4).....	112
5.9.2.1	Test System	112
5.9.2.2	Overall structure of the secondary MIMO SR control for multiple HVDC links	113
5.9.2.3	Simulation results and analysis on study case 4	114
5.9.3	Coordinated control of the HVDC link and SVC (Study case 5)	117
5.9.3.1	Test system.....	118
5.9.3.2	Simulation results and analysis on study case 5	119
5.10	Concluding remarks	123
Chapter 6		125
Stability control and management system in future GB transmission system		125
6.1	Introduction	125
6.2	Study set-up.....	125
6.2.1	Main steps of setting up a study case which represents 2016 demand and generation profile.....	126
6.2.2	Description of the Full GB Transmission system model	128
6.3	Stability analysis performed for the GB transmission system	129
6.4	Planning criteria	130
6.5	Definition of Study cases and scenarios.....	131
6.6	Capability of the West Coast HVDC link in stability enhancement.....	132
6.7	Simulation results and analysis for the study case 1.1 vs. study case 1.2.....	132
6.8	Simulation results and analysis for the study case 2.....	139
6.9	Concluding remarks	141
Chapter 7		142
Wide-area power oscillation damping control for embedded HVDC link		142
7.1	Introduction	142

7.2	History of transient and dynamic instability in GB transmission system	142
7.3	Principle of modal analysis	143
7.4	Application of the TCSC and the HVDC link in damping the inter-area oscillation	144
7.5	Supplementary power oscillation damping control design approaches and specification	145
7.5.1	PSS-based damping controller design	145
7.5.2	Principle of the MLQG control design method	146
7.6	Test systems under study	148
7.6.1	Two Area , four- machine concept proving test network.....	148
7.6.2	Full GB Transmission system model	150
7.7	Design of the supplementary power oscillation damping controller for the TCSC line	150
7.7.1	Characteristics of modified the test system under the study for design of the TCSC's damping controller	151
7.7.2	Simulation results on performance of the PSS-based damping controller for TCSC .	152
7.8	Impact of the sharing of active power on the AC and DC lines on the system small-signal stability	154
7.9	Design of supplementary power oscillation damping control for the CSC-HVDC link (study case on small test system)	155
7.9.1	Requirements for the MLQG-based damping controller for the HVDC link	155
7.9.1.1	Selection of signals for system identification	156
7.9.1.2	System model validation and reduction	156
7.9.2	Linearised model of the test system using system identification	157
7.9.3	Main features of the MLQG damping controller design.....	159
7.9.4	Capability of the MLQG and PSS-based damping controller for the HVDC link...	160
7.9.4.1	Definition of the study cases to investigate the effectiveness of both designed damping controllers for the HVDC link	161
7.9.4.2	Simulation results on the performance of the PSS-based and MLQG-based damping controller (study case1).....	162
7.9.4.3	Simulation results on the performance of the PSS-based and MLQG-based damping controllers (study case 2)	164
7.10	Capability of the West Coast HVDC link's damping controller in the system stability improvement (Study case on the full GB transmission system model)	166
7.10.1	Inter-area oscillation studies using the full GB transmission system model.....	166
7.10.2	Structure of the PSS-based damping controller for the bipole West Coast CSC-HVDC link	168

7.10.3	Definition of the study cases to investigate the effectiveness of the HVDC link's damping control (using full GB transmission system mode 1).....	170
7.10.4	Simulation results and analysis on study case 1	172
7.10.5	Simulation results and analysis on study case 2	175
7.10.6	Discussion on effectiveness of the West Coast HVDC link damping controller at various operating points.....	178
7.11	Comparative study on effectiveness of a range of supportive control actions for stability enhancement.....	179
7.11.1	Introduction to smart demand control and generator inter-trip.....	179
7.11.1.1	Generator inter-trip.....	179
7.11.1.2	Smart demand control	180
7.11.2	Simulation results and analysis on the effectiveness of introduced supportive control actions (comparative study)	181
7.12	Concluding remarks	184
Chapter 8	186
Conclusions and Further work	186
8.1	Summary and conclusions	186
8.2	Further research opportunities	193
Appendix A	195
A.1:	Dynamic parameters of the SMIB test system 1	195
A.2:	Dynamic parameters of the SMIB test system 2.....	197
A.3:	Dynamic parameters of the SMIB test system 3.....	197
A.4:	Dynamic parameters of the SMIB test system 4.....	198
A.5:	Dynamic parameters of the SMIB test system 5.....	198
A.6:	Dynamic parameters of the test system 6.....	200
Appendix B	203
B1:	The converters' control model associated with HVDC link	203
Appendix C	206
C 1:	Model and parameters of the PSS-based power oscillation damping control for the TCSC.....	206
C 2:	Model and parameters of the PSS-based power oscillation damping control for the HVDC link	207

C 3: Model and parameters of the MLQG-based power oscillation damping control for the HVDC link 208

C 4: Parameters of the PI control for TCSC 208

Appendix D 209

D.1: Procedure and steps of the system identification routine to identify the linear model of non-linear systems are presented in Figure D.1 209

Appendix E 210

E.1: The overall structure of the West coast HVDC link supplementary damping controller in Power Factory 210

E 2: Model and parameters of the PSS-based power oscillation damping control for the West coast HVDC link 210

Table E 2. 1: PSS-based damping control design parameters for the West coast HVDC link 210

Appendix F 212

F.1 Overview of Inter-area oscillation/small signal stability 212

F.2 Power System linearisation for stability analysis 212

References 214

List of Figures

Figure 1.1: Demand and generation background, Gone Green scenario [6].....	3
Figure 1.2: Required transfer capability for B6 boundary [4][5].....	6
Figure 1.3: B6 required transfer capability using various system enforcements [4].	8
Figure 1.4: Geographical location of future enforcements as shown in Figure1.3.....	8
Figure 2.1:Classification of the power system stability [22]	20
Figure 2.2: The main steps and process of control system design	37
Figure 3.1: The CSC-HVDC single line diagram modelled in DIgSILENT PowerFactory	46
Figure 3.2: The equivalent circuit diagram of the CSC-HVDC Systems [22].....	48
Figure 3.3: Schematic of the hierarchy control for the CSC-HVDC link at Rectifier and Inverter side.....	52
Figure 3.4: structure of the TCSC model	53
Figure 3.5: Schematic of concept proving test system1 in PowerFactory	56
Figure 3.6: Schematic of test system 2 (or multiple TCSC line) in PowerFactory.....	56
Figure 3.7: Schematic of test system 3 in PowerFactory including the HVDC link & AC lines	57
Figure 3.8: Schematic of test system4 in PowerFactory with multiple HVDC links	58
Figure 3.9: Schematic of concept proving test system5 in PowerFactory	59
Figure 3.10: Schematic of Two-area four-machine test system6 in PowerFactory	59
Figure 4.1: Future reinforcements for England and Wales [132]	63
Figure 4.2: Hierarchical stability control system	68
Figure 4.3: Overall structure of the Interface.....	72
Figure 4.4: Test system1 in PowerFactory.....	73
Figure 4.5: Structure of the Interface for design of the PI controller in Simulink.....	77
Figure 4.6: Matlab script to execute Simulink file.....	78
Figure 4.7: Comparison of built-in and external PI controller performance.....	79
Figure 5.1: Structure of MIMO controller	85
Figure 5.2: Algorithm of Sample Regular design method	94
Figure 5.3: TCSC step response.....	96
Figure 5.4: HVDC link step response	97
Figure 5.5: SVC step response	98

Figure 5.6: Structure of the Interface for SR Control design in PowerFactory	100
Figure 5.7: Unit step Response of TCSC line for SR Controller Design.....	101
Figure 5.8: Comparison of SR and PI controller Performance	103
Figure 5.9: Comparison of SR and PI Controller Performance	103
Figure 5.10: Concept proving PowerFactory SMIB test model 3 for study case 2	104
Figure 5.11: Structure of the Interface for the SISO SR control design for the HVDC link in PF.....	105
Figure 5.12: Dynamic time responses of the system following a step change to the HVDC link under control of a SISO SR design with different sampling rate.	106
Figure 5.13: Dynamic time responses of the system at post-fault with HVDC link under controls of internal PI controller or the cascade SISO SR control with sampling rate of 80ms	108
Figure 5.14: Concept proving PowerFactory SMIB test model for study case 3	109
Figure 5.15: Individual SISO PI controller for each TCSC line.....	110
Figure 5.16: Performance comparison of the SISO PI control vs. MIMO SR control for the TCSC power flow control	110
Figure 5.17: Concept proving PowerFactory SMIB test model 4 used for study case 4	113
Figure 5.18: Structure of the Interface for the MIMO SR control design for two HVDC links in PowerFactory	114
Figure 5.19: Per-fault coordinated control of the two-HVDC links following a step change on one of the HVDC links	115
Figure 5.20: Post-fault control of the multiple HVDC links with the immediate increase of both HVDC links' flows to enhance the system stability.....	116
Figure 5.21: Concept proving PowerFactory SMIB test model for study case5	119
Figure 5.22: Per-fault coordinated control of the HVDC link and SVC using a MIMO SR control	121
Figure 5.23: Post-fault control of the HVDC link and SVC using MIMO SR control for the immediate increase of the HVDC link's flows to enhance the system stability	122
Figure 6.1: Demand curve for typical minimum and maximum winter and summer including Cardinal points such as Peak (P), trough (T) and fixed point (F) [152]	126

Figure 6.2: GB transmission system with the future West and East Coast embedded HVDC links[6]	129
Figure 6.3.: Schematic diagram of B6 boundary in parallel with west coast HVDC link for study case 1.....	132
Figure 6.4: Study case 1: operation point B: Dynamic response of the system with/without implementing the HVDC link's fast ramp-up capability through the MIMO SR control following the occurrence of the AC fault when the B6 transfer is at point B ..	136
Figure 6.5: Study case 1-operation point C: Dynamic response of the system with/without implementing the HVDC link's fast ramp-up capability through the MIMO SR control following the occurrence of the AC fault when the B6 transfer is at point C. .	137
Figure 6.6: Study case 1-operation point D: Dynamic response of the system with/without implementing the HVDC link's fast ramp-up capability through the MIMO SR control following the occurrence of the AC fault when the B6 transfer is at point D ..	139
Figure 6.7: Comparison of the SISO PI and MIMO SR control performance for coordinated control of SVC and HVDC link using the full GB transmission system model.....	140
Figure 7.1: Unstable 0.5Hz oscillations between the Scotland and England [157]	143
Figure 7.2: Structure of PSS-base damping controller.....	146
Figure 7.3: Structure of the MLQG damping controller	148
Figure 7.4: Four-machine test system in DIgSILENT	149
Figure 7.5: Four-machine test system in DIgSILENT including the TCSC line	151
e) and f) Generators 3 and 4 rotor angle oscillation with /without damping control	
Figure 7.6: The effect of the TCSC damping controller on the system stability	153
Figure 7.7: Impact of the HVDC link power flow variation on the damping ratio of the oscillation mode	154
Figure 7.8: Impact of the HVDC link power flow variation on the damping ratio of the oscillation mode	154
Figure 7.9: a) The injected signal for system identification, b) System response (rotor oscillations) following the injection of the PRBS signal	158
Figure 7.10: a) Model order selection using the singular value, b) Validation of the estimated linear model and actual non-linear system	158
Figure 7.11.: LTR with different value of q	159

Figure 7.12: Modes of the four-machine test system in complex plane	160
Figure 7.13: Damping of system poles with and without damping controller.....	162
Figure 7.14: Comparative study on performance of PSS and MLQG damping controller, system response with/ without damping controller following a small disturbance	163
Figure 7.15: Comparative study on performance of PSS and MLQG damping controller, system response with/ without damping controller following a large disturbance	164
Figure 7.16: Damping constant for various system variables following a large disturbance	165
Figure 7.17: GB transmission system including embedded West Coast HVDC link presenting the location of generators monitored for the inter-area oscillation assessment and location of required damping controller's input signal on the GB transmission system.....	167
Figure 7.18: Supplementary damping controller for the Bipole CSC-HVDC link.....	169
Figure 7.19: Location of line monitored for inter-area assessment and location of faults simulated on the GB transmission system in study case1 and study case 2	171
Figure 7.20: Study case 1.1: Response of the full GB transmission system with/without damping controller following occurrence of F1 when B6 transfer is at point1	174
Figure 7.21: Study case 1.2: Response of the full GB transmission system with/without damping controller following occurrence of F2 when B6 transfer is at point1	175
Figure 7.22: Study case 2.1: Response of the full GB transmission system with/without damping controller following occurrence of F1 when B6 transfer is at point2	176
Figure 7.23: Study case 2.2: Response of the full GB transmission system with/without damping controller following occurrence of F2 when B6 transfer is at point2	177
Figure 7.24: Comparison of damping controller effectiveness at operating point 1& 2 when F1 occurs	178
Figure 7.25: Comparison of damping controller effectiveness at operating point 1& 2 when F2 occurs	178
Figure 7.26: Response of the full GB transmission system following a fault occurrence using various supportive actions	183
Figure A.1. 1: SMIB test system 1	195
Figure A.3. 1: Test system 3 with HVDC link.....	197
Figure A.5. 1: Test system 5 with SVC and HVDC link	198

Figure A.6. 1: Single line diagram of the four-machine test system 6 with TCSC	200
Figure B. 1: Overall framework of CSC-HVDC link convertors control	203
Figure B. 2: CSC-HVDC link DC power control	204
Figure B. 3: CSC-VDC link Voltage Dependant Current Order Limiter (VDCOL) model.....	204
Figure B. 4: The HVDC link CC, CV and CEA control framework	205
Figure C. 1: PSS-based damping control model for TCSC	206
Figure C. 2: PSS-based damping control model for HVDC link in PowerFactory	207
Figure C. 3: MLQG-based damping control model for HVDC link in PowerFactory	208
Figure D. 1: System identification procedure	209

List of Tables

Table 1.1: Advantages and main features of control design techniques proposed in the thesis in addressing the transient and dynamic stability issues.....	11
Table 2.1: Main feature of CSC-HVDC link compared to VSC-HVDC link [70][73] ...	35
Table 3.1: Definition of the CSC-HVDC link parameters.....	49
Table 6.1: Power transfer limit across the B6 boundary at various operating points ...	134
Table 7.1: Definition of parameters	144
Table 7.2: Eigenvalues /Modes of the two-area, four-machines test system with HVDC link	149
Table 7.3: Eigenvalues /Modes of the two-area, four-machines test system with No POD for TCSC	152
Table 7.4: Eigenvalues /Modes of the two-area, four-machines test system with POD for TCSC.....	152
Table 7.5: Eigenvalues /Modes of the two-area, four-machines test system.....	160
Table 7.6: Impact of the damping controllers on the modes of the system's frequency , damping ratio and damping constant	161
Table A.1 1: Synchronous machine dynamic parameters.....	195
Table A.1 2: Bus type and load flow data.....	196
Table A.1 3: Generators' exciter data	196
Table A.1 4: Generators' governor parameters.....	196
Table A.1 5: Generators' transformer parameters.....	196
Table A.1 6: Load data.....	196
Table A.1 7: TCSC's Reactor and Capacitor parameters.	197
Table A.1 8: Lines parameters	197
Table A.3 1: Load data.....	197
Table A.3 2: lines parameters.....	198
Table A.3 3: Bus type and load flow data.....	198
Table A.3 4: Generators' transformer parameters.....	198
Table A.5 1: Synchronous machine dynamic parameters.....	199
Table A.5 2: Bus type and load flow data.....	199
Table A.5 3: Generators' transformer parameters.....	199
Table A.5 4: Load data.....	199

Table A.5 5: lines parameters.....	200
Table A.5 6: SVC parameters	200
Table A.5 7: SVC voltage control parameters	200
Table A. 6. 1: Synchronous machine dynamic parameters.....	201
Table A. 6. 2: Bus type and load flow data.....	201
Table A. 6. 3: Generators' AVR data.....	201
Table A. 6. 4: Generators' governor parameters.....	201
Table A. 6. 5: Generators' transformer parameters.....	202
Table A. 6. 6: Load data.....	202
Table A. 6. 7: Shunt capacitors data	202
Table A. 6. 8: Shunt capacitors data	202
Table A. 6. 9: TCSC Reactor and Capacitor parameters.	202
Table B. 1: West coast HVDC link design aspects [156]	203
Table C.1: PSS-based damping control design parameters for TCSC.....	206
Table C. 2: PSS-based damping control design parameters	207
Table C 3: MLQG-based damping control design parameters	208
Table C 1: PI controller parameters.....	209
Table E 2. 1: PSS-based damping control design parameters for the West coast HVDC link	210

Abbreviations

AVR	Automatic Voltage Regulator
BMU	Balancing Mechanism Units
BSP	Bulk Supply Point
CSC	Current Source Converter
CEA	Constant Extinction Angle
CCC	Constant Current Control
CSG	China Southern Power Grid
DEAF	Demand Forecasting
EA	Evolutionary Algorithm
EBS	Energy Balancing System
EMR	EMR Electricity Market Reform
EMS	Energy Management System
ENTSO	ENTSO-E European Network of Transmission System Operators
ENSG	Electricity Networks Strategy Group
EU Union	EU European Union
EMT/RMS	Electro-Mechanical Simulation
EWEA	European Wind Energy Association
FACT	Flexible AC Transmission Network
FSC	Fixed Series Compensation
FES	Future Energy Scenarios
IFA	France- Interconnector
IEMS	Integrated Energy Management System

GA	Genetic Algorithm
GPS	Global Positioning System
GHGE	Green House Gas Emissions
LMI	Linear Matrix Inequality
LQR	Linear Quadratic Regulator
LTR	Loop Transfer Regulator
HVDC	High Voltage Direct Current
MITS	Main Interconnected Transmission System
MIMO	Multi Input Multi output
MTC	Multi-Terminal Configuration
MLQG	Modal Linear Quadratic Gaussian
NETSO	National Electricity Transmission System Operator
NGETN	National Electricity Transmission Network
NSPSO	Non-dominated Sorting Particle Swarm Optimization
NG	National Grid
NGET	National Grid Electricity Transmission
OFGEM	Office For Gas and Electricity Markets
OLTA	Off-Line Transmission Analyses tool
OSA	On Line Stability Assessor
OTS	Operational Tripping Schemes
PSO	Particle Swarm Optimisation
PF	DIgSILENT PowerFactory
PFA	Post Fault Action

PI/PID	Proportional-Integral
PMU	Phasor Measurement Unit
PNA	Power Network Analysis
POD	Power Oscillation Damping
PRBS	Pseudo Random Binary Sequence
PSS	Power System Stabilizer
PTDF	Power Transfer Distribution Factor
PT	Power Transfer
QBs	Quadrature Boosters
RIIO	Revenue = Incentives + Innovation + +Outputs
RPL	Reduce Real Power Losses
SPICE	Schedule Process in Control Environment
SQP	Quadratic Programming
SCADA	SCADA Supervisory Control And Data Acquisition
SPWM	Sinusoidal Pulse Width Modulation
SO	System Operator
SHETL	Scottish Hydro Electric Transmission Limited
SPTL	Scottish Power Transmission Limited
SPS	Special Protection Systems
SVC	Static Variable Compensator
SISO	Single Input Single Output
SR	Sample Regulator
SMIB	Single Machine Infinite Bus

STATCOM	Static Synchronous Compensator
SVSM	Static Voltage Stability Margin
SRDM	Sample Regulator Design Method
SSDC	Sub-Synchronous Resonance Damping Controller
SSR	Sub-Synchronous Resonance
SQSS	Security and Quality of Supply Standard
TCSC	Thyristor Controlled Series Compensation
TLFS	Transmission Line Flow Sensitivity
TO	Transmission Owner
TCR	Thyristor Controlled Reactors
TIRG	Transmission Investment for Renewable Generation
VSC-HVDC	Voltage Source Converter
VDCOL	Voltage Dependant Current Order Limiter
WAMS	Wide Area Monitoring System
WP	Winter Peak

Chapter 1

Introduction

This research has been conducted in order to gain a greater understanding of how embedded High Voltage Direct Current (HVDC) systems can be employed to improve system stability and investigate the best operating strategy for the HVDC link with regards to system security and overall stability enhancement. Therefore, a description is provided, in various sections of this chapter, of relevant background information and the main motivations for the research presented in this thesis. The overall objectives of this research project are presented within the context of power system stability enhancement of the GB transmission system whilst increasing the penetration of renewable generation to the grid.

1.1. Environmental targets and Future Energy Scenarios

Climate change legislation enforced from both the EU and UK Governments has set two environmental targets relating to renewable energy and Green House Gas Emissions (GHGE). Based on the first target, 20% of European energy is required to come from renewable sources by 2020 [1]. Also, the 2020 target, set by the Renewable Energy Directive for the UK states that 15% of energy is to be provided from renewable sources.

The second target commenced by Climate change Act of 2008, set up the GHGE reduction target of 80% below the 1990 baseline by 2050, and a minimum reduction of 34% by 2020 [1][2][3]. In order to achieve the above mentioned ambitious environmental targets, contribution from all sectors in the UK such as transport, heat and power is required. However, the power sector in Great Britain (GB), as a main contributor is required to deploy drastic changes in order to cater for future renewable developments.

The Electricity Networks Strategy Group (ENSG), the Office for Gas and Electricity Markets (Ofgem) and the Transmission Owners (TO) of GB, have developed a vision for future electricity networks in the UK reported in [4][5]. Furthermore, based on this

vision, the Electricity Ten Year Statement in 2013 [6], which is a report published by National Grid (NG) , has provided a detailed analysis of credible future energy scenarios up to 2050 as well as the requirement on future development and changes in generation and demand patterns and predicted technologies in order to secure the future electricity supply [6][7].

1.2. Generation capacity based on Future Energy Scenarios

The range of energy scenarios developed through the Future Energy Scenarios (FES) process by the National Electricity Transmission System Operator (NETSO), NG for the UK is to meet these 2020 environmental targets. Also, the developed energy scenarios are implemented to determine the range of future transmission capacity requirements. The main developed scenarios are outlined in [6] as follows:

- **Slow Progression;** slower development in renewable energy is expected. Based on this scenario, the renewable target by 2020 is not met.
 - Wind capacity reaches to 13GW by 2020 and 29GW by 2035. Other renewables stay static. Coal capacity shows slower decrease compared to the Gone Green scenario.
- **Gone Green;** designed to meet these legally binding environmental targets (including Renewable energy and emissions target) by 2020. Therefore, a balanced approach is taken in assuming a generation mix from various generation sectors. The Gone Green scenario is a stake holder supported scenario. It is updated annually to reflect the changes in the energy market. The key features of the Gone Green scenario are [6]:
 - It is predicted that the total installed capacity of wind generation will increase to approximately 20GW by 2020 (including 11GW of offshore) and 51GW by 2035 (including 37GW of offshore). Also, other renewables including hydro, biomass and marine will increase by 2.6GW by 2020.
 - Coal capacity decreases considerably over the period to 2035, from 20GW to 16GW by 2020 and to 2GW by 2035 whereas Gas/CHP increases to 38 GW over the period between 2025 and 2030

It should be noted that the level of renewable generation assumed for both Gone Green and Slow Progression is both from the network development and operational perspective. Also, for both scenarios, demand is assumed to be unchanged due to improvements in energy efficiency and an increase in the level of embedded and micro generation. However, demand increase is anticipated toward 2030 due to growth in industrial demand and the use of electric cars.

Overall the Gone Green scenario could suffer from larger renewable intermittency. However, it is less vulnerable to gas shocks, due to lower levels of gas demand under these scenarios. These risks can potentially be mitigated using greater interconnection with TSOs in central Europe and the Nordic system. Nevertheless, security of supply could be jeopardised in the Gone Green scenario if periods of no wind during cold winter weather coincided with gas supply shocks [8]. The generation mix and demand based on the Gone Green scenario (out to 2035) is illustrated in Figure 1.1.

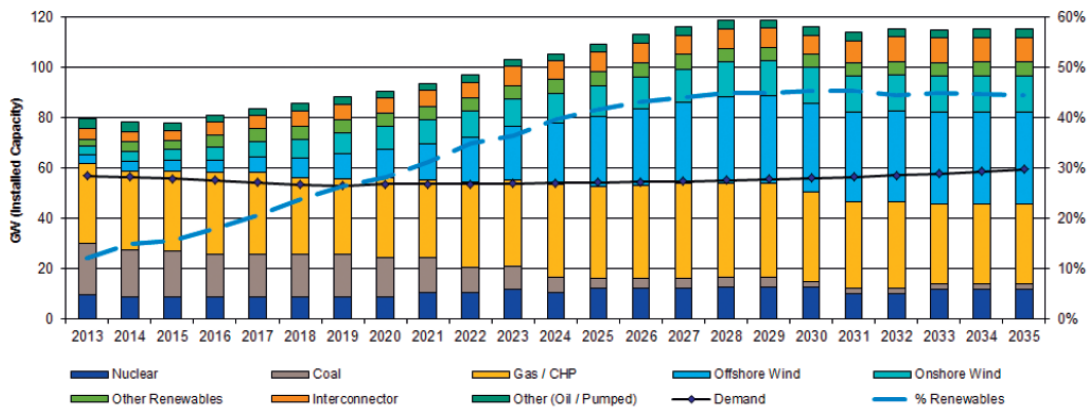


Figure 1.1: Demand and generation background, Gone Green scenario [6].

1.3. Existing National Electricity Transmission System (NETS)

The onshore transmission system consists of the England and Wales transmission network, owned by National Grid Electricity Transmission plc (NGET) and the Scottish transmission network, owned by two separate transmission companies, Scottish Power Transmission Limited (SPTL) in south and central Scotland and Scottish Hydro Electric Transmission Limited (SHETL) in the north of Scotland. The offshore transmission systems are also separately owned. Also, the generators and interconnectors are separately owned and operated. In England and Wales, networks at 275kV or above are classed as transmission network, whereas assets at 132kV or above are classed as transmission network in Scotland.

National Grid (NG) has been the Great Britain System Operator (GBSO) since 1st April 2005. National Grid, as SO for England and Wales, carries out energy balancing and coordinates and directs power flow across the transmission system. In addition, National Grid extended its GBSO operations to include the offshore transmission systems following the “Go Active” of offshore transmission.

The Summer Outlook report for 2014 announced a summer peak demand of 46.4GW and the summer minimum demand was forecasted at 19GW. The expected generation capacity at the start of the summer was 76.4GW including interconnectors and the minimum generating availability over the summer was 43.1GW [9]. Also, based on the winter outlook report, NG was required to accommodate a winter peak of around 56GW with a forecast mid-winter generation capacity for 2013/2014 of 79.1GW [10].

Currently there are four interconnectors between GB and other markets (the French interconnector, IFA with 2GW, Moyle with 450MW, BritNed with 1GW and East West interconnector, EWIC, with 500MW) to facilitate competition and support the efficient integration of renewable generation. There are more interconnectors contracted to be commissioned by 2020 [6].

Originally, Electricity networks were designed to transport power from large groups of generation centrally located around the fuel sources and transport corridors in the North to demand centres located mainly in the South East. Such a network configuration resulted in a typical North to South power flow direction from predominantly thermal generation plants with controllable generation output. However, with the expected growth in wind as the primary source of energy, generation is moving further away from the demand centres, which results in a requirement of transferring power over longer distances. Since wind generation is mainly being developed to the north and east of the system, particularly in Scotland, there will be a significant rise in the volume of power transfers from North to South. Therefore, the network needs to be reconfigured to manage electricity flows from a much larger number of smaller renewable plants, which will connect to the networks. Also, [11] identified tighter capacity margins, due to large combustion plant power station closures in 2014/2015.

These radical changes to Britain’s energy industry require larger investment to deliver smarter and more innovative networks. Ofgem’s Project Discovery identified £200

billion investment required in the next ten years to secure sustainable energy supplies and maintain system security at lower costs for consumers [12]. Electricity Market Reforms would contribute to providing the required investment partly by attracting enough investment to build new forms of generation. However, it is estimated that the cost of delivering such an investment would increase customers' energy bills by between 14-25%. In order to attract efficient investment in Britain's energy networks at lower prices, Ofgem has implemented the new RIIO (Revenue = Incentives + Innovation + Outputs) framework and performance-based model to which rewards companies that are more innovative in running their networks to better meet the needs of consumers [12]. NETS have been split into a number of regions specified by boundaries crossing critical circuits. There are three main boundaries (B6, B7 and B7a) that provide the capacity for generation in Scotland and the North of England to supply the major demand centres in the South. The existing transmission network across these boundaries mainly consists of two double circuit 400kV routes, one on the western side of the country and the other on the east which has 4.4 GW thermal power transfer capability. However, currently power transfer across this boundary is limited to 2.5 GW by stability constraints across the boundary.

1.4. Future system requirements

As mentioned above, following the Crown Estate Round 3 offshore wind farms program, a large volume of renewable generation is scheduled to be connected to Scotland over the coming years [13][14]. In addition to offshore wind generation, small embedded generation within Scotland (up to 2GW by 2030) can make a significant change to the boundary requirements. Also, according to all Future Energy Scenarios, there is a significant increase in the export from Scotland to England due to the connection of additional wind generation in Scotland. This results in exceeding the maximum capability of the existing network and consequently results in the transmission system being non-compliant with the requirements of the NETS System Security and Quality of Supply Standards (SQSS) [15]. Therefore the boundary capability needs to be increased through network reinforcement in order to restore the SQSS compliance. Figure 1.2 shows the required transfer capability by 2030 based on the Future Energy Scenarios discussed in this section.

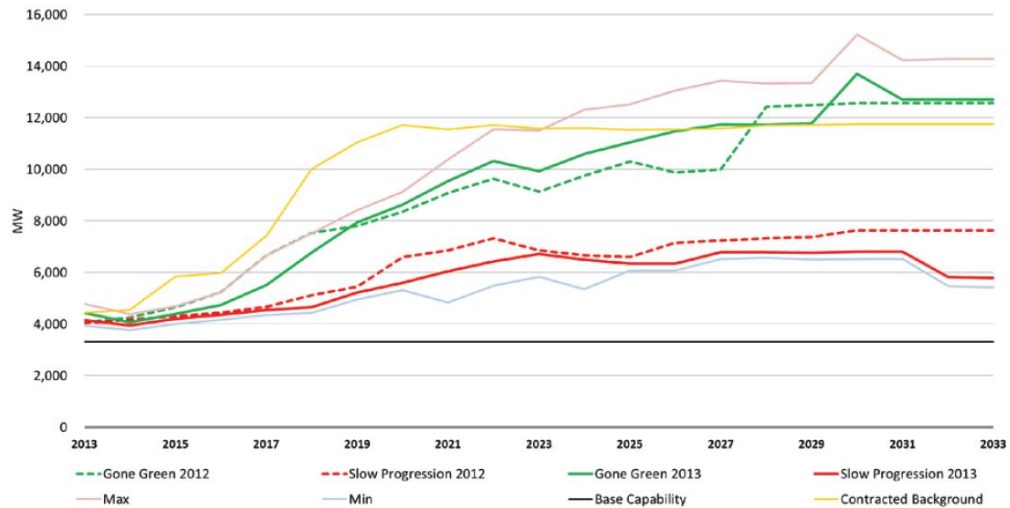


Figure 1.2: Required transfer capability for B6 boundary [4][5].

A series of potential network reinforcements, as shown in Figure 1.3, are defined against two main criteria including; NETS SQSS Compliance and Cost Benefit Analysis. The approved potential reinforcements are expected to come into operation by 2020 to increase the B6 boundary capability to accommodate the ever increasing power transfer from Scotland to England as outlined below [4][5].

- Western HVDC Link with 2.2GW of capacity between Deeside to Hunterston by 2017.
- Series Compensation on Harker-Hutton route, Eccles-Stella West route, Strathaven-Harker route and compensation on Harker-Stella West circuit by 2015.
- Shunt Compensation (MSCs) at: at Harker. (2*225MVar), Hutton (1*225MVar) and MSCs at Stella West (2*225MVar) by 2015
- NGET-SHETL East Coast HVDC Link with 2.1GW capacity from Peterhead to Hawthorn Pit by 2018.

Also, a number of alternative onshore solutions to increase the boundary capability such as the construction of two new double 400kV transmission circuits were considered. However, it was abandoned as a result of higher costs. The Western HVDC link connects Hunterston substation in Scotland and Connah’s Quay substation in North Wales via an undersea cable sited along the West coast of GB. This DC link will extend across all three boundaries and will provide an increase in capacity of around 2.2GW.

The main delivered outputs of the HVDC project comprise maintaining the security of supply, reducing expected constraint costs, increasing the boundary capability and eventually from the environmental point of view; it facilitates the decarbonisation target by adding the connection of a large volume of wind generation.

An alternative option to building the HVDC link as system reinforcement is to pay constraint costs to generators to ensure that total transfers do not exceed the boundary capability. The conducted cost benefit analysis revealed that by 2015 the annual constraint costs will rise to approximately £185m. Considering the constraint cost over the life time of the HVDC link, it was concluded that the capital cost for the Western HVDC link (which is estimated to be around £1bn) would represent a significant saving over the life time of the DC link.

Since the boundaries B7 and B7a would also become non-compliant based on SQSS requirements by 2014 under the Gone Green scenario, additional offshore HVDC links are planned to connect Round 3 offshore wind farms from Dogger Bank to the main AC transmission system. Following DC links increase in the B7 and B7a boundary power transfer capability.

- NGET-SHETL East Coast HVDC link 1, with 2.1GW capacity from Peterhead to Hawthorn Pit by 2018.
- NGET-SPT East Coast HVDC link 2, with 2.1GW HVDC link between Lackenby and Torness by 2018.
- NGET-SHETL East Coast HVDC Link 2 with 2.1 GW capacities from Peterhead to England by 2020.

In addition to the above development, the number of interconnectors to Europe is expected to double by 2030 following the sustained development of the European energy markets. Hence, the total capacity of the future planned interconnectors such as Norway, Belgium, and France is anticipated to increase to 8.6GW [7][16][17]. The complexity of the transmission networks is now increasing due to the closure of conventional thermal generation; higher volumes of variable renewable generation, lower system inertia and growing number of interconnections. As a result, the transmission networks are now being driven a lot closer towards their designed limits

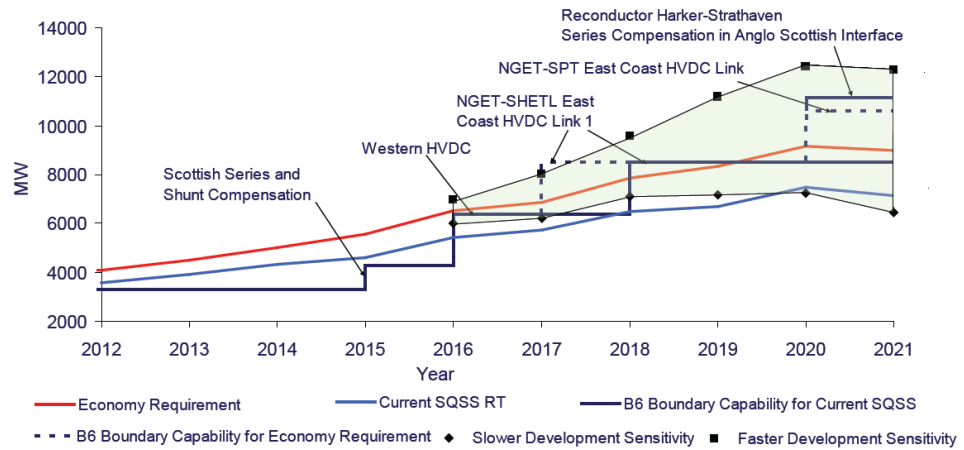


Figure 1.3: B6 required transfer capability using various system enforcements [4].

and are required to be more flexible and smarter. In line with that, NG is incentivised under the RIIO price control structure [12] to enhance the system performance and optimise the existing network capacity in an innovative manner. It is therefore necessary to develop tools and technologies with the right strategy to facilitate the network capability optimisation.

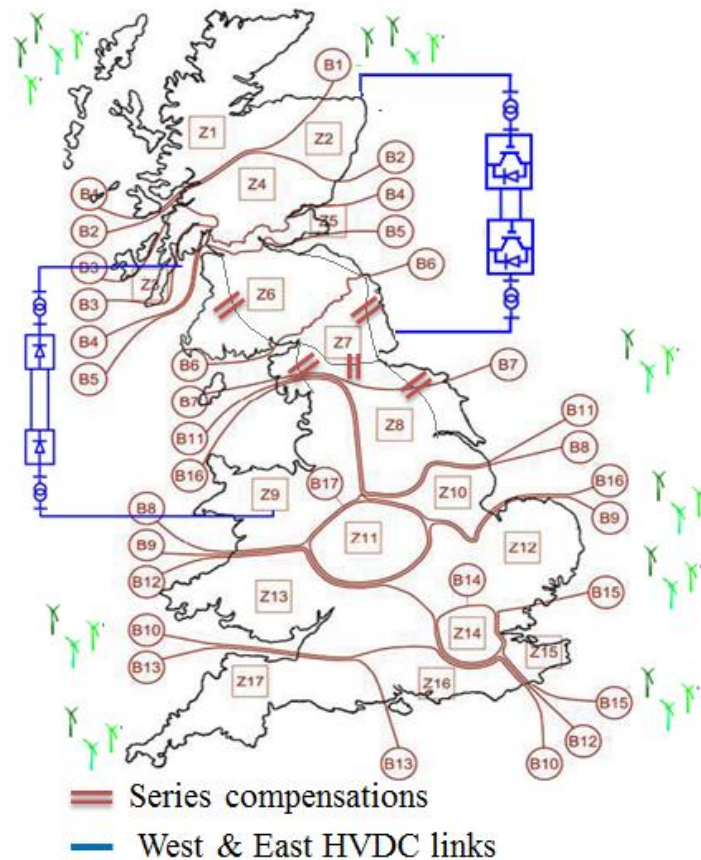


Figure 1.4: Geographical location of future enforcements as shown in Figure1.3

1.5. Research objectives

To meet the environmental target and decarbonise the UK electricity supply an increasing volume of variable renewable generation is coming into operation in UK. Consequently an unprecedented amount of change is required to the GB transmission system to accommodate the upcoming renewable generations. To that extent, more state-of-the-art technologies such as FACTS devices and Power Flow Control (PFC) devices including embedded West Coast HVDC link are being commissioned to provide the additional capacity to the network. However, the network in this area is now congested with many types of new and automatic control devices and without proper analysis, there is a risk of interaction between various control devices. Therefore, a stability control system is required to guarantee the optimal dynamic performance and co-ordination of power flow control devices at pre-fault and enhance the stability limit at post-fault. A research project, jointly supported by National Grid and Brunel University with following defined objectives was started in 2011:

- Identify the requirement of the NG stability control system
- Establish the framework of the control strategy that meets NG requirements and can fit into the NG operational business process that takes consideration of other existing operational tools.
- Carry out off-line studies to investigate the performance of the proposed stability controllers for their:
 - Multi-objective regulating and tracking abilities
 - Multiple device coordination
 - Robustness at post-fault
 - Pre- and post-fault actions
- Investigating the optimal operational strategies of the embedded West coast HVDC link with regards to the B6 boundary transient stability enhancement.
- Investigating the capability of the West coast HVDC link in improving inter-area power oscillation damping using a supplementary damping controller by conducting off-line studies on the full future GB network model.

1.6. Principal contributions to knowledge

The principal contributions to knowledge, as presented in this thesis, can be summarised as follows:

- A comprehensive review is conducted on past research surrounding the issue of power system stability and the latest proposed solutions for stability enhancement using the HVDC link and the TCSC through the deployment of various controller design methods and the implementation of various control schemes and strategies.
- Requirements for a hierarchical stability control system which guarantees the coordinated control and optimal dynamic performance of the power flow controller devices in a large integrated power system such as the GB transmission system is investigated. Also, a framework of strategies for the hierarchical stability control system at the transmission level, which takes into account NG's requirements, is proposed.
- A novel multivariable feedback control is designed for such a stability control system using a non-parametric control design method. This design method, Sample Regulator (SR) control, is developed for unknown systems and is based on their open loop step responses. Therefore, this method is mostly attractive for applications in large integrated power systems since the controller design only requires knowledge of the nonparametric model of the power system i.e. the open-loop step response, which is easily obtainable compared to development of a parametric model of the power system.
- As the initial part of developing the required stability control system, the interfacing between PowerFactory and Matlab tool is developed and deployed. This is done in order to extend the computational facilities and capability of PowerFactory for the implementation of the advanced control design methods. The interfacing is necessary due to the fact that PowerFactory cannot directly provide all control system components required for the specific computation or design of a complex control law.

- The performance of the non-parametric time domain, MIMO SR control design method is further investigated for the control of various types of control devices. The investigated devices include the HVDC link and SVC using the full GB transmission system model representing the 2016 demand and generation profiles. Moreover, the optimal operational strategy for the embedded West Coast HVDC link in the GB transmission system with regard to the enhancement of the stability limit across the B6 boundary is investigated using the MIMO SR controller.
- The capability of the HVDC link in improving inter-area power oscillation damping is investigated using a PSS-based (this name is commonly used by NG as this type of damping controller has similar structure to generators' PSS) and Modal Linear Quadratic Gaussian (MLQG) oscillation damping control method for the design of a supplementary damping controller. A comparative study on the performance of both damping controllers is presented using a simple test system. Afterwards, the capability of the West Coast HVDC link in improving the system dynamic stability is investigated using the full future GB system model in PowerFactory.

TABLE 1.1: Advantage and main features of control design techniques proposed in the thesis in addressing transient and dynamic stability issues

Proposed control design	Advantages in responding to control challenges	Main features of controller	Stability issue covered by controller	Actuators under control
Sample Regulator (SR)	Complexity doesn't increase by size of network, easy to tune	Non-parametric MIMO	Transient Stability	HVDC link, SVC, TCSC
PSS-based Damping control	Easy to tune, similar structure to generators' PSS	Non-parametric SISO	Dynamic Stability	HVDC link, SVC, TCSC
MLQG Damping control	Complex to tune, tuned to target poorly damped oscillatory modes of interest	Linear Model - based MIMO	Dynamic Stability	HVDC link, SVC, TCSC

1.7. Background to the Engineering Doctorate

The Engineering Doctorate (PhD) provided by Brunel University, is a three year advanced degree focused around industry relevant research. The scheme, funded by the Engineering and Physical Sciences Research Council (EPSRC) and a sponsoring organisation, presents the opportunity to design and research practical techniques for solving an industry led research problem with a focus on environmental significance. The vast majority of the research is therefore carried out with the sponsoring organisation providing the researcher with valuable industrial experience. The research outcomes need to satisfy, at least, the same requirements as a traditional PhD [18] . This PhD project was supported by National Grid and the majority of the work was conducted at the ENCC (Electricity National Control Centre) near Wokingham.

1.8. List of publications arising from the PhD

The work detailed in this thesis has resulted in number of refereed publications as follows:

1.8.1 Journal publications

- Kerahroudi Shadi.K, F.Li, Taylor G.A, M.Abbod and M.E.Bradley “Evaluating the Novel Application of a Class of Sampled Regulators for Power System Control “*IEEE Transactions on Control Systems Technology - Paper ID TCST-2015-0052, Accepted.*
- Kerahroudi Shadi.K, F.Li, M.M.Alamuti, Rabbani R, M.E.Bradley and Taylor G.A “Novel Operational Stability Control Schemes for Embedded HVDC Links in the Future GB Transmission System “*IEEE Transactions on Power Delivery, Submitted Sept. 2015.*
- M.Mohammadi Alamuti, Kerahroudi Shadi.K, Rabbani.R, Taylor G.A “Probabilistic Evaluation of Power System Stability Enhancement Using Supplementary MLQG and MPC Schemes for Embedded HVDC ink ” *IEEE Transactions on Power Delivery , Submitted Sept. 2015.*

1.8.2 Book Chapter publications

- Kerahroudi. Shadi.K, M.M.Alamuti1, F.Li, Taylor G.A, M.E.Bradley “Application and Requirement of DIgSILENT PowerFactory to Matlab/Simulink Interface” Springer publication, ISBN 978-3-319-12957-0

1.8.3 International Conference publications

- Kerahroudi, Shadi.K, Zobaa. A.F, Taylor G.A, M.E.Bradley, Yang,L "Investigating the impact of stability constraints on the future GB transmission

system," *Universities Power Engineering Conference (UPEC), 2012 47th International*, vol., no., pp.1, 6, 4-7 Sept. 2012

- Kerahroudi, Shadi.K; Taylor G.A, M.E.Bradley, Zobia A.F "A framework for coordinated stability control in the future GB transmission system using HVDC and power flow controller devices," *AC and DC Power Transmission (ACDC 2012), 10th IET International Conference* , vol., pp.1,6, 4-5 Dec. 2012
- Kerahroudi, Shadi. K, Taylor G.A, F.Li, M.E.Bradley "Initial development of a novel stability control system for the future GB transmission system operation," *Power Engineering Conference (UPEC), 2013 48th International Universities'* , vol., no., pp.1,6, 2-5 Sept. 2013
- Kerahroudi, Shadi. K, F.Li, Taylor G.A, M.E.Bradley “ Application of a Novel Stability Control System for Coordination of Power Flow Control Devices in the Future GB Transmission System” *IEEE PES General Meeting, USA, Washington DC* , July 2014
- Kerahroudi, Shadi.K, Rabbani.R, F.Li, Taylor G.A, Alamuti. M. Mohammadi, M.E.Bradley "Power system stability enhancement of the future GB transmission system using HVDC link," *Power Engineering Conference (UPEC), 2014 49th International Universities* , vol., no., pp.1,6, 2-5 Sept. 2014
- Kerahroudi, Shadi.K, Taylor G.A, Ma, Zhibo, Redfern, Miles, M.E.Bradley "Transmission system stability enhancement using demand management technology," *Power Engineering Conference (UPEC), 2014 49th International Universities* , vol., no., pp.1,5, 2-5 Sept. 2014
- Kerahroudi, Shadi.K, F.Li, Z. Ma, M.M.Alamuti, Rabbani.R, Taylor G.A, M.E. Bradley “Critical Evaluation of the Power System Stability Enhancement in the Future GB Transmission Using the HVDC link ,” *AC and DC Power Transmission (ACDC 2015), 11th IET International Conference on* , vol., no., pp.1,6, 4-5 Feb. 2015

1.8.4 Joint International Conference publications

- Rabbani.R, Mohammadi M, Kerahroudi Shadi.K, Zobia, Ahmed F, Taylor G.A. "Modelling of reduced GB transmission system in PSCAD/EMTDC," *Power Engineering Conference (UPEC), 2014 49th International Universities* , vol., no., pp.1,6, 2-5 Sept. 2014
- Alamuti,M.Mohammadi; Rabbani.R, Kerahroudi Shadi.K, Taylor G.A, "System stability improvement through HVDC supplementary Model Predictive Control," *Power Engineering Conference (UPEC), 2014 49th International Universities* , vol., no., pp.1,5, 2-5 Sept. 2014
- Alamuti, M.Mohammadi; Rabbani, R.; Kerahroudi Shadi.K, Taylor G.A, Youbo Liu, Junyong Liu "A critical evaluation of the application of HVDC supplementary control for system stability improvement," *Power System Technology (POWERCON), 2014 International Conference on* , vol., no., pp.1172,1177, 20-22 Oct. 2014

1.9. Organisation of the thesis

Chapter 1 - Introduction

The sections in this chapter will outline the motivations of the research presented in this thesis. This research has been conducted in order to gain a greater understanding of how embedded HVDC systems can be employed to improve system stability and investigate the best operating strategy for the HVDC link with regard to system security and stability enhancement. Therefore, a description of the relevant background information is provided. The overall objectives of this research project are presented within the context of power system stability enhancement of the GB transmission system whilst increasing the penetration of renewable generation to the grid.

Chapter 2 – Review of technologies and Literature

This Chapter details the history of stability issues in power systems and reviews the latest proposed solutions by researchers for system stability enhancement using HVDC links and TCSCs. The Chapter also reviews various control design methods for the control of power flow control devices in transmission systems and the capability and requirement of various proposed control design approaches are examined and commentary on the relevant available literature is provided.

Chapter 3 –Power system modelling in PowerFactory

This Chapter outlines an overview on the HVDC link technology and their control scheme particularly the modelling of the Current Source Converter (CSC) based HVDC transmission networks and its primary and hierarchy control strategy. Also, the benchmark test networks that have been modelled and used for studies are described in this Chapter. The models are validated through a number of case studies using time domain (EMT/RMS) simulation in DIgSILENT PowerFactory.

Chapter 4–Framework and requirements of hierarchical stability control system

This Chapter describes current and future control issues with specific reference to the GB transmission system, as well as explaining the requirement for a hierarchical stability control system. In addition, the need for interfacing simulation programs such as DIgSILENT PowerFactory (PF) with MATLAB control tool box is discussed. Their capability in performing comprehensive mathematical calculations and offering a wide

range of control system functions is also discussed, as an initial step to develop such a hierarchical stability control system.

Chapter 5–Principle of the Sample Regulator control

This Chapter discusses the requirements for the feedback control system for coordinated control of the various power control devices and focuses on the technical development of multivariable feedback control systems. Also, introduced in this Chapter is the fundamental theory and techniques of a stabilising Sample Regulator (SR) control system design method following an overview on other choices of control design method. Finally, several study cases are presented to demonstrate the application of SR controller in stability enhancement. The presented study cases investigate the capability and performance of the designed SR controller as a Single Input Single Output (SISO) and Multi Input Multi Output (MIMO) for the control of various power control devices such as HVDC link, TCSC and SVC.

Chapter 6–Stability control /management system in future GB transmission system

In this Chapter the performance of the non-parametric time domain, MIMO SR control design approach is further tested for the control of various types of control devices including the HVDC link and SVC with its associated auxiliary POD functions using the full scale GB transmission system using a full model representing the 2016 generation profile.

Chapter 7–Wide-area Power Oscillation Damping Control for the HVDC link

This Chapter presents a brief description of two damping controller design methods such PSS-based and MLQG damping control which are implemented for the design of the supplementary oscillation damping controller for HVDC link and TCSC. Following that a comparative study on the performance of both damping controllers is presented. Finally, the capability of the West Coast HVDC link in improving system stability is demonstrated using the full model of the GB transmission system.

Chapter 8–Conclusions and Further Work

In the final Chapter a summary is provided on the work presented in this thesis and the main contributions of this research are discussed. In addition, outlines of proposed future work are presented.

Chapter 2

Literature review

2.1 Introduction

This Chapter details the history of stability issues in power systems and reviews the latest proposed solutions by researchers for system stability enhancement using HVDC link and TCSC. Also, this Chapter reviews various control design methods for the control of Power Flow Control (PFC) devices in transmission systems. The capabilities and requirements of the various proposed control design approaches are examined through a comprehensive literature review.

2.2 Historical power system stability issues

The importance of power system stability issues was first recognised in the 1920s (Steinmetz, 1920). Later on, the black out of Northeast US and Ontario in November of 1965, drew the attention of regulatory agencies and power system industries to the problem of stability and the importance of power system reliability. At first, transient (rotor angle) stability had been the focus of most industries' concerns and considerable improvements in the transient stability performance of power systems has been achieved through the utilisation of fast fault clearing, high-response exciters, series capacitors and special protection schemes. However, the decreasing strength of transmission systems has resulted in an increased focus on small signal stability. In addition, an investigation into the underlying causes of frequency instability was initiated following the frequency stability problems experienced in 1970s and 1980s [19].

The early dynamic stability issues were related to the fact that power generation and local demand centres were becoming more dispersed and remote power plants were feeding consumers over long transmission lines [19][20]. However, in recent years, as the electric power systems have evolved and the complexity of power systems increased due to higher implementation of interconnections and integration of large scale wind generation, the complexity of the stability problems also increased and different forms

of instability have emerged. In addition, power systems are being operated under ever more stressed conditions due to the deregulation of the power industries, increases in bulk power exchange between distant regions of a transmission network to meet the growing demand, open transmission access, as well as construction and environmental constraints. Consequently, transmission system operators are facing greater challenges to maintain system security, due to transmission networks being pushed closer to their physical limits to make the most of existing facilities' capabilities. The power systems operating close to their stability limits are particularly vulnerable to any sudden disturbance and cascade tripping could happen if the necessary pre-fault or post-fault actions are not taken. Thus, the planning and operation of modern dynamic power systems requires a caution and consideration of all forms of system instability.

2.2.1 Power system reliability and security

Reliability of a power system, which is defined as the probability of satisfactory operation of the system consistently in the long term, is the main objective in power system design and operation [21]. To be reliable, the power system must be secure all of the time. To be secure, the system must be stable. However, a system may be stable following a contingency, yet insecure due to components' overloads or voltage violations at post-fault. Author in [21] defines reliability as *"the level that the performance of power system results in power being delivered to consumers within accepted standards and desired amounts"*. In this definition reliability contains two key features; adequacy and security. Adequacy is an ability of the power system to provide customers' required energy consistently, and security is known as the ability of a power system to withstand sudden disturbances. Thus, security relates to the robustness of the system to disturbances and depends on the system operating conditions and the probability of a disturbances occurrence. In other words, security implies that power systems should withstand any single contingency such as an outage or failure of any component, without the system and customers services interruption, loss of system stability and exceeding the system variable limit and constraint [22]. Therefore security analysis includes two key components:

- Static security analysis—this entails steady-state analysis of the post-disturbance system conditions to ensure no ratings and constraints are violated.

- Dynamic security analysis—this entails investigating different kinds of power system stability issue.

Under challenging network conditions, where power systems are moving closer to their physical limits, maintaining the security of the system is becoming the main concern of system operators. Whereas in normal operating conditions the main focus is on the optimisation and economical operation of the system. Since modern power systems are being operated under ever more stressed conditions, maintaining the dynamic security and stability of the system can, at times, take a higher priority compared to other objectives such as optimal power flow and economical system operation [20].

2.3 Power system stability

There are various definitions of power system stability to be found in the literature. A formal definition, which is applied to an interconnected power system as a whole, is provided in [22] as follows:

“The stability of an interconnected power system is defined as ability of the power system, at a given initial operating condition, to return to a stable operation condition following being subjected to any sudden physical disturbance, with most system variables bounded so that practically the entire system remains intact”.

The power system is a highly nonlinear system and its dynamic response is influenced by a wide range of devices with different characteristics and response rates. Also, such a system operates in a constantly changing environment and could be subjected to a small or large disturbance. Small disturbances are in the form of load changes, which occur constantly and large disturbances are in the form of a short circuit on a transmission line or loss of a large generator. Therefore, system stability depends on many factors such as network topology, the initial operating condition as well as the nature and severity of the disturbance. In fact, stability is a condition of equilibrium between opposing forces which are dependent on the aforementioned factors. Various forms of instability may happen if the opposing forces experience a continued imbalance. In other words, system instability implies a condition where a loss of synchronism or generator pole slip or a progressive decrease in bus voltages has occurred. Conversely, the power system is considered stable, if following the occurrence of a disturbance, it will reach a new

equilibrium state with the system remaining intact. It should be noted that a power system may remain stable following a given disturbance and be unstable for another. However, it is impractical to design the power systems to be stable for every possible contingency. Hence, the power system is usually designed to be stable only for credible contingencies, which have a realistically high probability of occurrence [22]. Protective relays are set to isolate the faulty part of network and restore the system to normal state. However, system stability cannot always be guaranteed after a fault clearance, as it is influenced by many elements with different dynamic responses. It is therefore essential to understand the cause of the power system instability issues and this will assist power system industries in the planning and secure operation of the system. The deregulation, privatisation, transmission congestion, weak connection, unexpected event and hidden error or failures in protection systems are some of the well-known and recognised power system issues.

2.4 Classification of power system stability

Basically, power system stability is a single problem. However, power systems may experience various forms of instabilities that cannot be effectively addressed by treating it as one. The classification of system stability into appropriate categories facilitates the analysis of system stability, identifying key causes of instability and devising methods of improving system stability. The classification of power system stability is conducted based on the size of the disturbances, physical nature of the resulting mode of instability, the devices, processes, and the time span that must be taken into consideration for stability assessment [22]. Figure 2.1 describes the various form of stability as follows:

- Rotor angle stability
- Voltage stability
- Frequency stability

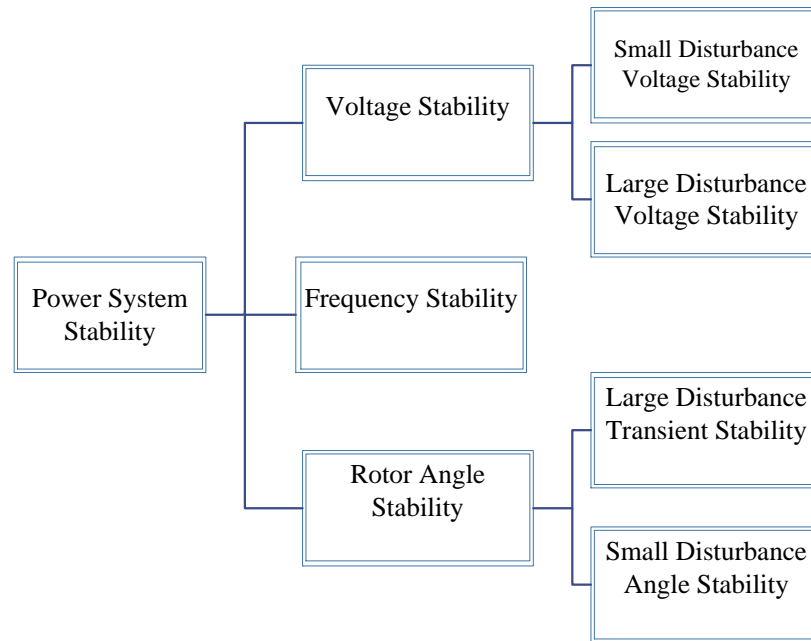


Figure 2.1:Classification of the power system stability [22]

2.4.1 Rotor angle stability

Rotor angle stability is the ability of synchronous machines of an interconnected power system to stay in synchronism after being subjected to a disturbance. In fact it is the ability of maintaining equilibrium between the input mechanical torque and the output electrical torque of each generator. If this equilibrium is disturbed, acceleration or deceleration of the generators rotors happens according to the laws of motion of a rotating mass, which results in advancing the angular position of the accelerating generator and consequently angular separation. Beyond a certain limit an increase in angular separation is followed by further angular separation and instability at the end. The electromagnetic torque of a synchronous machine following a perturbation can be resolved into two components: synchronising torque (in phase with rotor angle deviation) and damping torque (in phase with the speed deviation). Insufficient synchronising torque results in a *periodic* instability, whereas lack of damping torque results in *oscillatory* instability. To gain better insight into the nature of rotor angle stability problems, rotor angle stability is divided into the following two subcategories:

- Small-disturbance stability
- Large-disturbance rotor angle stability or transient stability

Small-disturbance rotor angle stability mostly depends on the initial operating state. Either periodic instability (due to lack of synchronising torque) or oscillatory instability (lack of sufficient damping torque) can occur in this case. However, nowadays due to the use of continuously acting generator voltage regulators, periodic instability is less likely to happen following a small disturbance. Small-disturbance rotor angle stability problems can be either local or global in nature. Local rotor angle oscillation modes depend on the strength of the transmission system, generator excitation control systems and plants' output [22]. Global rotor angle oscillations, which are referred to as inter-area mode oscillations, caused by interactions among large groups of generators and involve oscillations of a group of generators connected through relatively weak tie-lines. They involve oscillation of a group of generators in one area swinging against a group of generators in another area. Their characteristics are very complex and have a major effect on the stability of inter-area modes.

Large-disturbance rotor angle stability or transient stability is the ability of the power system to maintain synchronism when subjected to a severe disturbance, such as a short circuit on a transmission line. Transient stability depends on both the initial operating state of the system and the severity of the disturbance. Transient Instability is usually in the form of a periodic angular separation due to insufficient synchronising torque and known as first swing instability. Transient instability could be the result of superposition of a slow inter-area swing mode and a local-plant swing mode causing a large excursion of rotor angles after the first swing [22].

2.4.2 Voltage stability

Voltage stability refers to the ability of a power system to maintain steady state voltages within the operational statutory limit at all buses in the system following a disturbance for a given initial operating condition. Voltage instability could result in a loss of load or tripping of transmission lines or other elements by their protective systems and finally cascading outages. A progressive drop of voltages is the most common form of voltage instability. However, overvoltage instability also exists. Similarly, voltage stability is also divided into two subcategories of small-disturbance stability and large-disturbance rotor angle stability or transient stability.

2.4.3 Frequency stability

Frequency stability refers to the ability of a power system to maintain steady state frequency within the operational statutory limit at all times following a severe imbalance between generation and load.

2.5 Potential solution to power system stability enhancement

The fast development and integration of large scale wind generation in the power system has led to bottlenecks in the flow of power and an increasing complexity in maintaining system security. Also it has resulted in the requirement for a higher power transfer capacity across the network. The GB transmission network is now being operated closer to its physical limit with a risk of losing N-1 security criteria. Therefore, system enhancement will be essential. However, due to the difficulty in obtaining support to build new transmission lines, more advanced solutions are required to be employed to provide the required system enhancements. The concept of FACTS was first introduced by N.G. Hingorani, in 1988 [23]. These devices are power electronic based systems capable of controlling various electrical parameters to provide more controllability and increase power transfer capability.

The family of FACTS devices including TCSC, FSC, QB, UPFC, STATCOM, SVC and HVDC link have been commonly implemented to improve the performance of long distance AC transmission networks. Also, they have been used for various power system issues such as voltage stability, power flow control and power transfer enhancement. Although, FACTS devices enhance the power network efficiency, their benefits are dependent on their type, size, number and location in the transmission system [24]. A study on the effectiveness of the five different types of FACTS devices (including SVC, TCSC, UPFC and STATCOM) on the steady-state performance of the Hydro-Québec network is presented in [25]. In this study the optimal locations and values of different types of FACTS devices were determined using a Genetic Algorithm (GA) optimisation method [25].

With regards to the optimal location and parameter setting of the multiple FACTS devices in the power system, investigation on performance of the several optimization methods such GA, Particle Swarm Optimisation (PSO) and Evolutionary Algorithm (EA) has been reported in the literatures [26][27][28][29][30][31][32][33].

2.5.1 Review on application of TCSC in power system enhancement

2.5.1.1 History of TCSC implementation

TCSC consists of a series capacitor shunted by a Thyristor-Controlled Reactor (TCR), which allows the impedance of the AC lines to be reduced. It is now a key device in the FACTS family playing several roles in the operation and control of power systems. It has been increasingly implemented with long AC transmission lines by utilities in modern power systems as an effective and economical way to solve a range of power system issues such as: optimal power flow control, voltage support, transient stability enhancement, congestion management by increasing the power transfer capacity, mitigating sub synchronous resonance; damping the power oscillation and reducing losses in transmission lines [34]. There are several reports on the satisfactory operation of TCSC in system performance enhancement on long transmission lines across the world. For example, a report in [35] has shown how the problem of large inter-area oscillations has been mitigated using TCSC on a 1000km, 500kV interconnection between the north and south of Brazil. Similarly, an installation of TCSC or FSC on the long transmission distances in China, has improved the poor power oscillations damping after faults. The observation of systems has shown that without the operation of series compensation these systems would have been unstable in the case of some contingencies leading to severe outages [36].

2.5.1.2 Impact of optimal TCSC placement on the system performance enhancement

Due to the high cost of TCSC, finding the optimal location and size is one of the key considerations in the implementation to obtain the maximum benefit and capability. This problem has been the focus of much research and different single or multi objective optimisation techniques have been proposed, as explained in the next section [34]. The objectives considered by the researchers in either single or multi objective optimisation methods consist of optimal power flow control, voltage stability improvement, transient stability enhancement, congestion management and loss minimisation. Studies in [37][38][39] investigate the optimal location of the TCSC using a single objective optimisation technique which, considers optimal power flow as the main objective, whereas in [40] voltage stability has been the single objective of the optimisation problem. On the other hand [41][42][43] have proposed various methods

such as quadratic stabilising control, MPC and PSO control for determining the optimal location of TCSC from a transient stability viewpoint. A similar study in [44] determines the optimal allocation of the TCSC controllers that satisfies the transient stability requirements. In this study a robust controller is designed to improve the stability of a multi-machine power system using TCSC. The H_{∞} norm method is used as indices of performance and measures the degree of effects of an input disturbance on the outputs of the controlled system. The results show that this approach has led to a satisfactory result in stabilising the system with least number of TCSC implementation [44]. The sensitivity analysis approach has also been employed in conjunction with GA to find the optimal placement and setting of the TCSCs with an objective function of reducing system loading in congested lines [45].

Furthermore, TCSC placements, as a multi-objective optimisation problem are investigated by researchers which are presented in [46] [47] [48] [49] [50] [51] i.e. [46] examines the effects of the TCSC on voltage stability and transient stability (as a multi-objective) by changing the reactive power distribution in the power system. Trajectory Sensitivity Analysis (TSA) was used in [47] to measure the transient stability condition of the system and trace the optimal location of the TCSC for different fault conditions.

In addition, in [48] Eigenvalue-based methods have been used, and transient stability as well as steady state stability of the system has improved using TCSC. In another multi objective optimisation problem studied in [49] the application of the TCSC to mitigate small signal stability problem as well as congestion management of a heavily loaded line in a multi machine system is investigated using PSO and the Transmission Line Flow Sensitivity (TLFS) method for curtailment of non-firm load to limit power flow congestion.

In another study [28] the application of GA and PSO is applied for determining the optimum number, the optimal locations and the best possible parameters of multiple TCSC to achieve both objectives of maximum system load ability with minimum installation cost. Locating multi-type FACTS controllers in order to optimise multi-objective voltage stability problems is also investigated in [50] using Non-dominated Sorting Particle Swarm Optimisation (NSPSO). The presented results in this study

shows that TCSC maximizes the Static Voltage Stability Margin (SVSM), reduces Real Power Losses (RPL) and Load Voltage Deviation (LVD). A novel TCSC placement approach is proposed in [98] to decrease the congestion in the transmission lines while increasing the static security margin and voltage profile of a given power system using Sequential Quadratic Programming (SQP) problem [51][35].

2.5.1.3 Capability of TCSC in the enhancement of the transfer capacity of tie lines limited by transient stability constraint

The installation of TCSC will considerably improve power system stability. However, an appropriate control scheme is required for selection of the TCSC mode conversion time. The moment at which a generator's angular velocity reaches maximum acts as the start time of the TCSC having maximum capacitance value. This is because the kinetic energy is at its maximum when the equivalent generator angular velocity reaches maximum so the TCSC needs to reach its maximum capacitance value in order to ensure system stability. Furthermore, when the derivative of the corrected potential energy is zero just at the moment when the equivalent generator angular velocity is less than zero, the TCSC immediately operates in bypass mode [52].

2.5.1.4 Capability of the TCSC to enhance the damping of power system oscillations

Power systems are continually subjected to small disturbances, which can result in oscillations in the power systems. Low frequency oscillations are a detrimental phenomenon in power systems, which increase the risk of system instability and limit the steady-state power transfer. These electromechanical oscillations can be classified as local mode oscillations, inter area mode oscillations, control mode oscillations and torsional modes. These oscillations may be sustained and lead to growing oscillations which eventually cause system separation and cascading failures if no adequate damping is available. An example of the detrimental effects of un-dampened low frequency oscillation is islanding and loss of 30MW of load in the Western Systems Coordinating Council (WSCC) grid in the USA in 1996, which happened following a chain of events. The post event analysis concluded that system instability could have been avoided by employing damping controllers [53]. Conventionally, the local oscillations are damped cost-effectively and sufficiently by installing Power System Stabilisers (PSS). Performance of the generator's PSS with regard to inter-area modes is

insufficient due to the complexities of coordinated tuning and the sacrifice in local mode damping that must be made [54][55][56]. Therefore, PSSs are normally tuned for local modes and settings remain unaltered unless any issues arise [57]. However, with the fast development of FACTS devices, further oscillation damping can be achieved by adding supplementary Power Oscillation Damping (POD) control to the installed FACTS devices in power systems. It should be noted that the damping duty of a FACTS controller is not the primary functions. Several approaches based on modern control theory have been applied to FACTS devices such as TCSC for the design of the supplementary power oscillation damping control.

One key consideration in the design of a cost-effective POD controller is the fact that the designed controller should be able to provide desired damping as well as generating moderate transients in the POD output signal following severe disturbances. This is because a large POD output signal may cause the TCSC to hit its limits and result in reducing the POD damping control action. Therefore, examination of equipment performance for severe disturbances is an integral part of POD controller design.

In addition, another key point in the design of an effective and robust POD controller is the selection of an input signal that can be employed to modulate the TCSC reactance. Input signals could be local signals (such as lines 'current, active-power flow, bus voltage or local bus frequency) or wide-area remote signals (such as rotor-speed deviation of remote generators or rotor angle, speed or frequency difference across the system). As the local signals are more readily available, the majority of practical installations of TCSCs use local measurements for controlling power flows and damping power oscillations. Research shows that locally available signals can provide good damping depending on the location of installed devices [58]. However, in practice, POD designer does not have control over the location of devices when the device is not primarily installed for the POD purposes [59]. Also, the entire system oscillatory modes are not observed by local signals. Therefore, optimal stability enhancement cannot be achieved using only local input signals. The study presented in [60] also demonstrates that the TCSC's POD controllers using the remote rotor angle deviations measurement signals supplied from the Phasor Measurement Units (PMUs) improve transient stability

much better compared with the case where local control signals are employed for modulating the TCSC reactance.

The main issue with the design of a wide-area damping controller is the time delay of remote/wide-area signals. Author in [61] proposes an approach in the design of a TCSC wide-area damping controller using the free weighting matrices method, which is expressed with a set of Linear Matrix Inequality (LMI) constraints, and the pole placement method. The simulation results on the test system reveals that the designed TCSC damping controller not only reduces inter-area oscillation, but is also robust to various time delays [61]. Selection and tuning of the TCSC damping controller parameter has been investigated by many researchers and several approaches based on modern optimisation techniques such as PSO has been applied to find the optimal parameters [62].

2.5.1.5 The capability of the TCSC in damping Sub-Synchronous Resonance (SSR)

Although series capacitors are capable of improving the power transfer capacity in the transmission system, there is great concern with regard to the SSR issues. This issue is a dynamic phenomenon that is primarily exhibited by series capacitor compensated transmission networks fed by thermal generation, particularly in cases of high degrees of compensation. It occurs due to adverse interaction between the turbine-generator mechanical system and fixed series compensated Electrical networks when the frequency of the compensated line coincided with some poorly damped torsional vibration frequency of the turbo-generator shaft, and could hence induce increased mechanical stresses in the shafts [63]. In comparison, the TCSC does not have the same dynamic characteristics as a fixed series capacitor and would not cause SSR issue. This is because TCSC acts to eliminate this risk for coinciding resonance frequencies by making the series capacitor(s) act inductive in the sub-synchronous frequency. Therefore, The SSR problem can be avoided by reducing the percentage of compensation provided by the fixed series capacitors and replacing that with TCSC as a substitute.

The use of the TCSC in conjunction with fixed series compensation offers more economical options due to the high cost of the TCSC. However, the proportion of

variable compensation, the TCSC, has to be chosen suitably to prevent SSR. Hybrid schemes in the implementation of the TCSC and fixed series compensation is another proven, effective and economical approach to avoid SSR. This scheme utilises a combination of a single-phase TCSC and a fixed series capacitor in one phase of the compensated transmission line and fixed capacitors on the other two phases. The created phase imbalance results in a suppression of interaction between the electrical and mechanical sides of the turbine-generator and eventually reduction of the growing torsional stresses at SSR mode. The proposed scheme is economically attractive compared with a full three phase TCSC, which has been used for power oscillation damping [64][65][66]. Moreover the TCSC can be employed for the design of a Sub-Synchronous Resonance Damping Controller (SSRDC). An application of SSRDC in improving the instability of torsional modes caused by external fixed capacitors used in conjunction with a TCSC is presented in [67]. The designed SSRDC is based on generator slip signals using the damping torque analysis method and gives satisfactory damping for torsional modes. Further analysis indicates that although improved damping for torsional modes can be achieved, a robust design is more difficult, especially when several sub-synchronous torsional modes are present[67].

In addition, there is risk of interaction between the series compensation and other FACTS devices used in a network. For example, in the GB transmission system, increasing levels of wind penetration has resulted in a requirement for higher power transmission capacity across the Scottish boundary. Series compensation has been installed as part of onshore reinforcement. The potential damaging effect of SSR caused by installed series compensation on GB system is studied in [63]. In addition, the impact of existing Quadrature Boosters (QBs) in the GB transmission system on the safe levels of compensation is assessed with particular emphasis on the occurrence of SSR. The assessment and eigenvalue analyses show that change of QB's tap changer may trigger SSR if the series compensation is tuned near the natural modes of the shaft of synchronous generators. Therefore it is critical that the level of series compensation is selected with awareness [63] [68].

2.5.2 Review of HVDC technology and its application in power system enhancement

The first electricity transmission systems were direct current systems. However, HVAC electrical systems replaced the DC transmission system as the power at low voltage could not be transmitted over long distances. With the development of high voltage valves, it was possible to once again transmit power over the long distances using HVDC transmission links. The world's first commercial HVDC link between the Swedish mainland and the island of Gotland was built in 1954 with a rating of 20MW. The initial scheme took 25 years to develop. In 1970, the Gotland scheme was extended to 30MW and 150kV using the first Thyristor valves technology in a HVDC application. Since the first commercial HVDC link installation a vast amount of the HVDC links have been installed across the world [69]. The energy challenges of the 21st century have resulted in the use of more sustainable energy solutions, such as wind and other renewable resources. Therefore, more offshore wind generation is coming into operation. However, transmitting a high volume of power from wind farms to the demand centres over long distances presents a significant challenge due to the need for a cost effective, robust and reliable transmission solution.

Developments in advanced power electronic devices and fully controlled semiconductors have had an immense impact on the development of HVDC technology. As a result, the HVDC transmission network is now considered to be one of the best transmission solutions for the transfer of bulk power over long distances [70] and has been increasingly used in many parts of the world such as China and India where energy resources are dispersed far away from the load centres [71]. Nevertheless, a comprehensive study for each application is required to find out the best transmission solution for connecting offshore wind farms located at very long distances from the onshore grid. The necessary procedures to determine the most cost effective transmission solution are presented in [70]. Based on this guideline, in order to select the optimal transmission solution and configuration, specific project parameters such as average output power of a wind farm, transmission losses, energy unavailability, investment and energy transmission cost are required [70]. Globally, the total installed capacity of the HVDC transmission system had reached up to 50GW in 2001. This capacity was increased to 100 GW by 2010 after only nine years. According to current

planned projects, it is expected that this will have doubled again to 200 GW by 2016 [72] [73].

2.5.2.1 The major advantages and applications of HVDC systems

Overall, the major advantages of HVDC links over HVAC links are [71]:

- The foremost advantage of the DC transmission system is the elimination of reactive power. Therefore, power can be transferred over long distances with no reactive power losses and constant voltage at the receiving end. Whereas, in the case of long AC cables, compensating devices such as SVCs or STATCOMs are required to keep the AC voltage constant.
- Higher power transfer up to 30% for the same size and insulation level by HVDC links compared to the AC lines due to two main reasons: the effective voltage can be higher, and the wires can be bigger (wire diameter is limited for AC lines due to the skin effect whereas a DC line can be arbitrarily thick).
- Lower losses on DC cables, hence DC cable has smaller insulation and copper size.
- Cross section of AC cables are limited, due to the skin effect that prevents an AC current from penetrating to the centre of a large wire, whereas in the case of the DC cables, there is no limitation to the size of DC cables, except for thermal issues.
- As explained in second bullet point, the HVDC overhead lines can transport significantly more power for the same size by the HVAC line. Therefore by having smaller cable sizes in the DC system, the required ground area and support towers are smaller.
- No contribution to the network short circuit levels and fault-blocking for the blackout prevention in the case of cascade events.

Moreover, HVDC link has the capability to rapidly control the transmitted power. Thus, HVDC transmission lines may be used in a coordinated manner to improve transient stability as well as damping oscillations in power system. This in turn will allow the system operator to transfer more power through system corridors.

The main disadvantages of HVDC links over HVAC lines are associated with:

- Transformers for voltage stepping and circuit breakers are dramatically less complex and expensive for the HVAC than for the HVDC power. Meanwhile DC Circuit Breakers (CBs) for the VSC-HVDC links are also a huge problem, due to the complexity in the design of the DC CBs, especially at high power levels above one megawatt (MW). The feasibility of different solutions concerning the DC CBs is presented in a small number of scientific publications in [73].
- Multi-terminal systems are not feasible with the CSC-HVDC links due to power reversal issues with CSC-HVDC links. Also, the point to point CSC-HVDC link does not require HVDC CBs, since the AC CBs can be used instead. Multi-terminal systems though, which use VSC technology, will require HVDC CBs so that, the whole system does not have to shut down.
- Higher cost of construction due to the power electronics and converter transformers. However, beyond a certain distance, the investment costs of HVDC link are much smaller than those AC transmission lines since e.g. a bipolar system only has two lines compared to three lines in an AC system. This results in smaller costs in tower design and construction for delivering the same capacity of power.

Typical applications of the HVDC link comprise:

- *Interconnecting two asynchronous AC systems or two AC systems with unlike frequencies.* HVDC has the ability to interconnect two separate asynchronous AC systems as a tie line .e.g. where one operates at a frequency of 50Hz and the other at 60Hz (such as a back to back 500MW HVDC link between Uruguay and Brazil.) or where the two systems are operated at the same frequency but different phase angles (such as a back to back HVDC link connecting the asynchronous Eastern and Western American system). This is mainly because; DC power is independent of the frequency and phase of the power systems.
- *Submarine power transmission,* for cables longer than 40-70Km HVDC cables are a more economical solution.

- *Long distance bulk power delivery*, for both overhead lines and cables longer than 600-800Km, thus HVDC link is a more economical solution. Also, HVDC link represents good performance in long distance bulk power delivery as in AC systems the reactive power flow limits the transmission distance and consequently makes it more costly [71].
- *Trading*, due to the ability of controllable power exchanges between two AC networks. A typical example is France-Angleterre Interconnector (IFA).

2.5.2.2 HVDC link's technologies

Various types of HVDC links based on the methods of AC to DC conversation are introduced in [74][75]. Currently two main converter technologies, which are explained in the next section, are commercially available for use in the HVDC transmission. In both technologies, there is no reactive power along the DC transmission line. Therefore, there is no technical limit to the transmission distance.

- **Line Commutated Current Source Converter (CSC-HVDC)**: This began with the use of mercury valves and now utilises high power Thyristors. It is also known as classic HVDC link.
- **Voltage Source Converter (VSC-HVDC)** using Insulated Gate Bipolar Transistors (IGBTs).

Line-Commutated Current-Sourced Converter (CSC-HVDC)

The classical HVDC link is mainly designed for bulk power transportation over long distances and is based on Thyristor valves with only turn-on capability that requires a strong network voltage to commute. Due to this characteristic of Thyristors, classical HVDC link can only reverse the power by changing the voltage polarity. Moreover, it requires reactive power support at both ends and costly filters to remove system harmonics. Also, one of the key drawbacks of classical HVDC link is a lack of black start capability. However, this problem can be solved by combining CSC-HVDC with an auxiliary source of reactive power [70][71]. On the contrary, CSC-HVDC link has the inherent ability to withstand short circuits during the faulty operating conditions on DC side. The VSC-HVDC link is more exposed to short circuits on DC side and therefore cables are more suitable for the VSC-HVDC applications [73].

Voltage Source Converter (VSC-HVDC)

The world's first VSC-HVDC link was installed in March 1997 in Sweden (3MW, 10km overhead line). Currently about 17, VSC-HVDC links have been installed worldwide with another 520km in production [71]. VSC-HVDC link, which is based on IGBTs technology, is a well-established technology for capacity ranging around 500MW. IGBT is a fully-controllable power electronic device, with turn on or turn off capability. The utilisation of IGBTs allows a rapid switch of power flow direction by reversing the current direction [71]. The converters are typically controlled through Sinusoidal Pulse Width Modulation (SPWM) and the harmonics are directly associated with the switching frequency of each converter [73]. In addition, the VSC-HVDC is not only beneficial to all kinds of applications provided by classical HVDC link, but also the use of VSC-HVDC as opposed to CSC-HVDC offers many other advantages as explained [76] [74] [77][69]:

- The commutation of VSC-HVDC is independent of the AC grid voltage due to its capability to be turned on and off by the IGBTs. Therefore, it can be connected to a weak AC network.
- VSC-HVDC link is self-commutated, hence unlike the CSC-HVDC link, commutation failures and associated power interruptions would be a pressing issue.
- VSC-HVDC links are very flexible because of its ability to control active and reactive power independently without an extra compensating component.
- VSC-HVDC can be effectively used for Multi-Terminal Configurations (MTC). From a technology point of view, VSC-HVDC technology has the capability to be implemented in other key areas including; power supply to island, infeed to load centres, DC segmented grid and offshore generation.
- Lower construction time and site area are required. The study in [78] presents a comparison study on the overall site footprint and converter buildings aspect of VSC-HVDC projects and CSC-HVDC projects of a similar rating. The results reveal that due to no reactive power compensation requirements on the 2-Level VSC-HVDC technology the overall site area required for 2-Level VSC-HVDC is only 77% of that required for CSC-HVDC. Whereas, the overall converter

building footprint for 2-Level VSC-HVDC is 190% of that for CSC-HVDC [78].

Due to recent developments in HVDC technologies, ratings of VSC-HVDC links are further increasing to play an essential role in system stability enhancement. Since the West Coast HVDC link is designed to be a CSC-HVDC and the East Coast is expected to be a VSC-HVDC link, a comparison between CSC-HVDC and VSC-HVDC is presented in Table 2.1 [76][71][74][75][73] [69].

2.5.3 Interaction between the AC and DC systems

As more and more HVDC interconnection is scheduled to come into operation, the potential interactions between HVDC and HVAC in hybrid systems as well as interactions between multiple HVDC links has become the key source of concern in maintaining the stability of hybrid power systems. As faults cannot be entirely prevented, it is crucial for power system engineers to determine the impact of AC and DC faults on the stability of the whole power system [79]. If an AC fault on a system results in commutation failure and blocking of a DC link (particularly in CSC-HVDC), it could be difficult to avoid system instability. The operational experience of China Southern Power Grid (CSG) in the operation of AC/DC hybrid transmission systems shows that the influence on the HVDC system caused by the AC system faults could be restrained by selection of the right control strategy for the HVDC system [80].

The authors in [79] concluded that, in the case of a DC fault, the transient stability of the system and voltage drop is improved when longer HVDC transmission lines are used in parallel with moderately shorter HVAC transmission lines [79]. Also, an actual comparative case study in Taiwan was conducted to evaluate the impact of offshore wind farm integration on systems using HVDC or HVAC as the transmission solution. It was shown that when the fault happens on the offshore grid, the voltage and frequency responses in the onshore grid are more stable under the HVDC link compared to the HVAC link. This implies that HVDC link can offer the wind farm better voltage and frequency stability. Whereas, in the case of utilising HVDC link, the terminal voltages and frequencies of the wind turbines would be slightly affected by the fault that occurs in the onshore grids, but it is not the case for HVAC link [81].

TABLE 2.1::Main feature of CSC-HVDC link compared to VSC-HVDC link [70][73]

Attributes	CSC-HVDC	VSC-HVDC
Converter Technology	Thyristor valve, grid-com.	IGBT valve, self-com
Max converter rating	6400 MW \pm 800kV (OHL)	1200 MW \pm 320kV , cable
Relative size	4	1
Reactive Power demand	Reactive Power demand =	No reactive power demand
Reactive power compensation &	Discontinuous control	Continuous control
Independent control of P& Q	No	Yes
Scheduled maintenance	Typically < 1%	Typically < 0.5%
Typical Converter system losses in single level HVDC	2.5 – 4.5 %	3-5%
MTC	Complex, limited to two terminals	Simple – no limitation

2.5.4 Past research on the application of the HVDC link in power system stability enhancement

HVDC link has proven to be an effective means to stabilise the transmission system with resulting higher energy transfer capability. A number of research presented in technical papers have shown the capability of HVDC links in enhancing power system stability [79]. Also, power system restoration is proposed by the author in [76] using HVDC link support. In fact, HVDC Links can be implemented for both large-disturbance rotor angle stability enhancement, known as transient stability, and small-disturbance rotor angle stability enhancement by means of power oscillation damping improvement using various control design approaches and schemes. This is explained further in the next section. Numerous control design approaches have been developed over the last decades for power system control devices, gaining an insight into the small-signal electromechanical nature of a power system.

In general, the objective of a control system is to make the plant output signal behaves in a desired way by manipulating the plant input signal. However, there are different kinds of problems including the regulator problem, which manipulates the input to

counteract the effect of the disturbance whereas the servo problem manipulates the input to keep the output close to the set-point. Control system design and mode estimation methods can be classified as either model-based analysis methods or measurement-based methods. Model-based methods involve linearising the differential equations of the power system around a given operating point. This method is widely used for the analysis of low-frequency oscillations such as eigenvalue analysis. The main downside of this approach is the requirement for highly intensive computation and its complexity increases with the size of the network under study. Also, the system model varies with the changes of operating conditions. Thus, this approach is not desirable for large integrated power systems due to the level of complexity involved in presenting the entire system model in detail. However, with a measurement-based method, a linear model of the system can be estimated from system measurements. In comparison, the required effort in building a measurement-based model is far less than that required for a model-based method [59].

In both approaches the main process of control system design is elaborated in Figure 2.2 in order to have a better insight into the requirements of control system design [82]. The control design approach developed for power system stability improvement and reported in various papers is summarised in the next section.

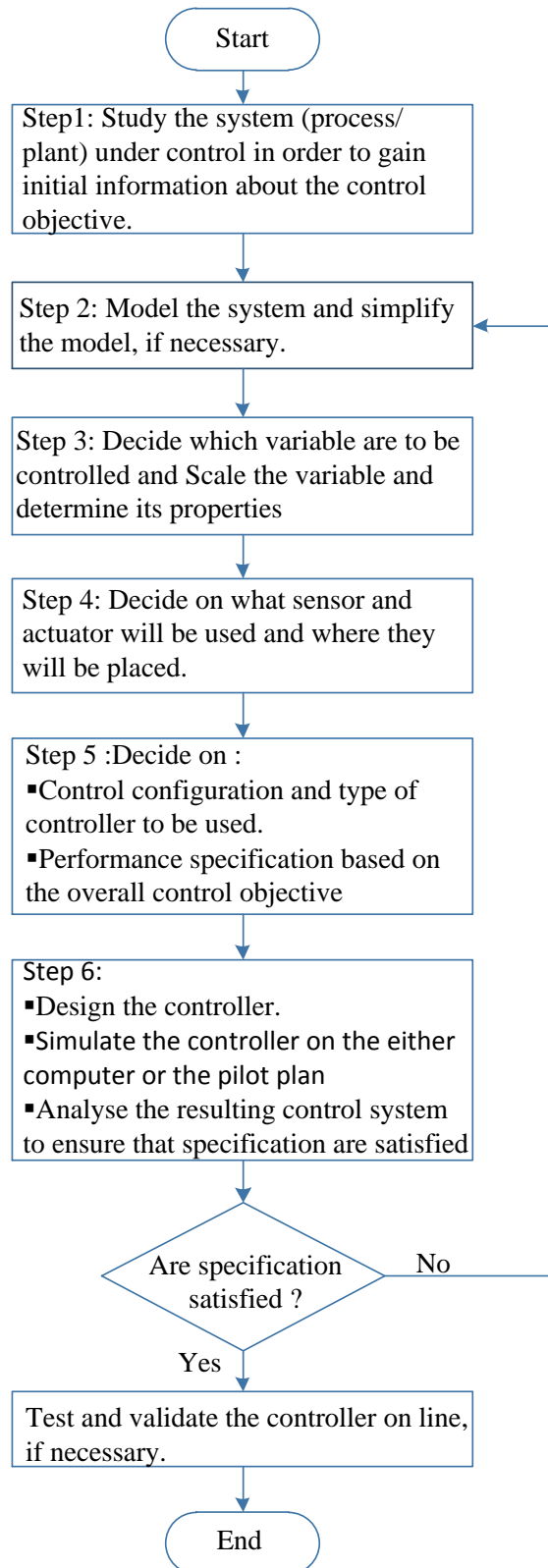


Figure 2.2: The main steps and process of control system design [82]

2.5.4.1 Capability of the HVDC link to enhance the damping of power system oscillation

Power oscillation damping control through modulation of HVDC link's power flow was introduced in 1976 in order to improve the transmission capacity of parallel AC tie lines [83]. Since then, due to a call for improved inter-area mode damping, the focus of the majority of studies have been on improving small-disturbance rotor angle stability by providing better damping of the inter-area oscillation modes using supplementary oscillation damping control for HVDC link. Furthermore, large investments in the installation of CSC-HVDC links in China (with existing operational capacity of 45GW) has encouraged extensive research in the field of power oscillation damping within the Chinese grid. These researches include both single POD controllers design and coordinated schemes for multiple controllers [59][84][85][86]. Several factors are important and must be considered in the design of power oscillation damping controllers including the performance of the controller to ensure sufficient damping, the robustness of the controller to changes of operating conditions, the simplicity and scalability of the control design method for deployment in large power systems. Also, the selection of effective input signals for power modulation is increasingly of concern and it has been the focus of many researchers [69]. Fundamentally, both WAMS-based global signals and local signals can be exploited for modulating HVDC link's power flow. However, WAMS-based global signals have proven to be more effective in improving un-dampened mode of oscillations due to their ability to provide higher system observability [87][88][89][90][91]. The evaluation on the effectiveness of the local and WAM'S signals presented in [69] demonstrates that the local signal can also efficiently damp oscillations depending on their location. Numerous signals can be used for modulating HVDC transmitted power such as frequency (rotor speed) or phase angle difference at the two ends of the HVDC-link. Alternatively, the rate of change of power flow can be used [92][93].

In addition to the aforementioned factors, a dynamic model of the system with an adequate level of system dynamics is required in the design of oscillation damping control to guarantee accurate results and a good level of damping factor. For the purpose of small disturbance rotor angle stability analysis, a generic small disturbance HVDC model based on injection modelling is presented in [94].

The identification of optimal connection points of the HVDC link to improve the stability of parallel AC systems is another factor, which has been intensively studied [59][57]. However, in practice, due to logistical considerations, options for points of connection are very limited. In general, despite these potential limitations, the HVDC–Wide area control could be a better option for damping inter-area oscillations. This is because HVDC transmission is normally used to interconnect regional grids, which means it can effectively influence the operating characteristics of the networks [95]. However, in large interconnected power systems with various inter-area oscillation modes and shapes, single FACTS or HVDC-based POD is not sufficient to provide the required level of damping. Therefore, the wide-area damping controllers are required to provide effective wide-area control for damping the multiple inter-area oscillation modes and consequently enhance the overall system stability [95]. On the other hand, multiple wide-area damping controllers require co-ordinated control.

Another area of concern is the co-ordination of existing generators' PSS and FACTS devices' damping control. The research presented in [96] demonstrated that co-ordinated FACTS and PSS damping control can provide improved oscillation damping with a simple low order control structure. Some other studies implemented nonlinear optimisation for co-ordination purposes [97][98]. On the contrary, the study presented in [99] shows that the supplementary damping controller implemented for HVDC link is not effective when there is no low frequency inter-area oscillation damping issue in the network with the generators' PSS are in service to damp the local oscillatory modes.

Basically, both HVDC technologies can be used for damping control and generally any technique proposed for active power modulation is applicable for both systems. However, VSC-HVDC link can not only provide input for active power modulation but also, provide input for reactive power modulation for the purpose of dynamic stability enhancement. The studies presented in [100][57][101] show that active power modulation is more effective compared to reactive power modulation.

Numerous control design methods have been implemented in the design of HVDC-based POD control, including extensions of traditional linearisation-based residue techniques [99], the novel use of fuzzy control laws [102], sliding mode controls [103], relative gain array [104], H_2/H_∞ [95], pole placement techniques [105], Model

Predictive Control (MPC) [106], energy function formulations [107], non-linear optimisation of PSS-based designs using local [86] and global [108] signals, and adaptive controllers with self-tune using the Prony method [109]. Also, the authors in [59] presented both the LQG-based state feedback techniques and the particle swarm optimisation for POD design [59] [110]. The authors in [110] also assessed the topological change and time delay variations [101]. Although LQG control was reported to be highly suitable for wide-area damping applications, assigning the right weighting only to the states that participate in critical oscillatory modes is a difficult task to perform and sometimes even adverse results can be observed due to complex weight tuning.

Wide-area MPC control schemes are also proposed as a mode-based approach [111]. The study presented in [112] compares the performance of the MPC and the LQG controllers in improving the system inter-area oscillation damping. Results demonstrated that the MPC controller could provide better performance due to its capability to consider the system constraint while optimising the objective function.

In all the proposed approaches a good performance in improving the post-disturbance response of the network has been demonstrated. However, the robustness of the controllers and coordination of multiple wide-area damping controllers have hardly been investigated. Also, the majority of the proposed methods have only been demonstrated on ideal test systems rather than a realistic model of large interconnected power systems.

2.5.4.2 Capability of the HVDC link to enhance transient stability

As discussed in the previous sections, much research has focused on the application of HVDC link for oscillation damping using a supplementary controller. Whereas, the available studies on enhancing transient stability of the hybrid HVDC-HVAC systems are limited and many aspects related to this subject are still open for investigation [92][93]. Between the limited amount of research in this area, the authors in [113] introduces an inertia emulation control strategy for VSC-HVDC converters to improve transient stability of the AC system. Another study conducted by Liu investigates a hybrid multi-infeed HVDC system. An adaptive limiter for the current controller has been employed to improve the HVDC performance to stabilise the AC system after a

fault incident [114]. In addition to the HVDC link converter control, a DC chopper controller can contribute to the stability improvement of an AC network. The DC chopper controller can be categorised as an important member of the family of Discrete Supplementary Controllers (DISCOS). Such controllers are not part of the continuous system operation and will be activated at the time of severe faults in the system. The complete range of DISCOS includes dynamic braking, fast valving, single-pole switching, series capacitor insertion, controlled system separation and load shedding, generator dropping etc. [92][115]. The capability of the DC chopper to perform DISCOS has been tested by the authors in [92].

Another approach to enhance the transient stability of the system is exploiting the fast ramp-up capability of HVDC link as corrective control. The corrective control actions are activated after the disturbance occurrence to minimise the impact of the disturbance on the stability of the system. These actions have proved to be effective in increasing transmission network capacity [116][117].

Both HVDC technologies allow fast changes of the power flow through them. Also, short-term overload capability is available for the majority of HVDC links depending on different conditions like ambient temperature, availability of redundant cooling equipment, etc. [118]. For example short-term overload capability of the West coast HVDC link which is the focus of this research is up to 2.4GW. This fast control and short-term overload capability (within ms time scale) could be exploited for corrective control actions to enhance system stability.

2.5.5 Future development of embedded and interconnector DC links

The HVDC links are commonly used for the application of both interconnection and embedded links in parallel with AC lines. Due to a significant increase in the requirement for higher transmission capacity and offshore development, a large and growing area of demand for HVDC links is predicted in the future. Therefore, more and more HVDC links are expected to be installed, which have the potential to be employed for system stability enhancement.

2.5.5.1 Future embedded HVDC links

With the EU's ambitious plans for changing the energy infrastructure in order to reduce GHGEs, higher level of renewable energy generation (predominantly wind generation) is installed far from the load centres. This will result in a pressing need for additional transmission capacity to accommodate renewable generation. This can be very challenging for densely populated power systems where securing right-of-way permissions for new transmission lines are almost impossible.

An option for the increase of transmission capacity due to the increased power density is the use of embedded HVDC links. Therefore, another potential application of HVDC link refers to the prospect of embedding HVDC lines into the meshed AC system. As embedded HVDC lines become more widespread, there is increasing interest in the unique opportunities that they provide to enhance system stability. A good example of that is Chandrapur-Padghe Bipole HVDC link, in India, which adds another 1500MW to the existing capacity of the 400kV system [119]. An example in the UK is the Western HVDC link where the unavailability of HVAC transmission lines has resulted in the employing of a CSC-HVDC link across the Scottish boundary to add another 2.2GW of capacity in this area by 2016. When DC links are connected in parallel with AC transmission lines, apart from providing higher capacity, additional benefit from HVDC links can be obtained if the appropriate control scheme is implemented including varying the power flow rapidly to improve transient stability or modulation of power on the DC link to provide damping of existing inter-area oscillations.

2.5.5.2 Future off-shore DC grid

In addition to the increase in the implementation of embedded HVDC links, there has been a significant increase in the use of interconnection links to facilitate the sharing of the installed wind generation across the EU. The European Wind Energy Association (EWEA) revealed that in the EU power sector, the current installed wind energy capacity has reached to 117.3GW by the end of 2013 [120][121]. However, the fulfilment and deliverability of the EU's targets for renewable energy is directly linked to the development of an offshore grid in the North Sea, which is considered as one of the building blocks in the European Super-grid [77]. A DC super-grid can provide improved system reliability and market operation by taking advantages of both AC and

DC technologies. The potential of a meshed HVDC grid for power supply security and market integration in the North Sea area is investigated in [122]. The results demonstrated that improvement in grid frequency control can be achieved by employing suitable control schemes for meshed HVDC grids. Also, this significantly assists managing the outage conditions such as loss of wind power generation [122].

Due to the capability of the VSC-HVDC link in fast power reversal and fast switching nature of VSC-HVDC, it is considered as the main HVDC technology for multi-terminal applications and building a large interconnected offshore grid. This is because VSC-HVDC link does not depend on the effective short circuit ratio or on reactive power support at the connection points in order to present a reliable commutation process. One key issue in implementing VSC-HVDC for super grid construction is their limited rating. However, future technological developments of VSC-HVDC towards increased power ratings may allow future applications of the VSC-HVDC system in bulk power systems and DC super grids [123]. Furthermore, the importance of standardisation in future DC grids should not be ignored [122].

2.6 Concluding remarks

This Chapter detailed the history of stability issues in power systems and reviewed the latest proposed solutions by researchers for system stability enhancement using the HVDC link and the TCSC. Generally, the two main approaches that have been proposed in the literature for power system stability enhancement are implementation of new state of the art transmission devices or the implementation of various control schemes for the existing and upcoming devices.

Also, the Chapter reviewed the various control design methods for the control of power flow control devices in transmission systems and the requirements of various proposed control design approaches are discussed along with commentary on the relevant available literature. As previously discussed, in the last few decades several researches have investigated FACTS devices and HVDC links active power set-point modulation for the purpose of achieving power oscillation damping using a variety of control schemes. Although, many proposed schemes have shown to be effective, very few control schemes have been implemented on a real power system. Also, available studies on the transient stability improvement of the hybrid HVDC and AC networks are scarce

and many aspects related to this area is still open for further research. For example, no studies have considered the co-ordination of various power control devices such as the HVDC link and the TCSC with regards to strategy to select the optimised set-point for each device.

Chapter 3

Power system modelling in PowerFactory

3.1 Introduction

The following sections will outline the modelling and primary control of Current Source Converter (CSC) based HVDC transmission networks and the benchmark test networks that have been used in this thesis. The models are validated through a number of case studies using time domain (EMT/RMS) simulation in DIgSILENT PowerFactory.

3.2 Introduction to DIgSILENT PowerFactory

As the complexity of the integrated electric power networks grows, the need for more comprehensive simulation tools rises.

DIgSILENT PowerFactory is the leading high-end simulation tool for applications in generation, transmission, distribution and industrial systems. It integrates all the required functions for power system modelling analysis and simulation. Some of these functions include power flow, fault analysis, RMS stability, small signal analysis and interfaces for SCADA integration and PSS/E compatibility [124].

It also has the capability to integrate new state of art technologies such as power electronic based devices FACTS, HVDC links and wind generation.

The focus of this thesis is on investigating the ability of the HVDC link to improve system stability using various control schemes. Several concept proving test models are implemented throughout the thesis, which will be described in the following sections. The concept of a designed controller will be first applied to a test model then to a more realistic system in the full developed future GB network model.

3.3 Modelling and control of CSC-HVDC link

3.3.1 CSC- HVDC link configuration and components

For the CSC-HVDC link model incorporated in the test models, the CIGRE benchmark model is used. The single-line diagram of a CSC-HVDC link as modelled in DIgSILENT PowerFactory is shown in Figure 3.1. The detailed models of the associated converters' control are provided in Appendix B.

The model that represents the West coast HVDC link is a 600kV, 2.2GW Bipolar HVDC system with a 12-pulse configuration for converters' bridges at both ends. Each 12-pulse converter comprises two 6-pulse valves connected in series of equal rated voltage at the rectifier and inverter terminals to enhance the DC voltage level for transmitting more power. The neutral point is grounded as shown in Figure 3.1.

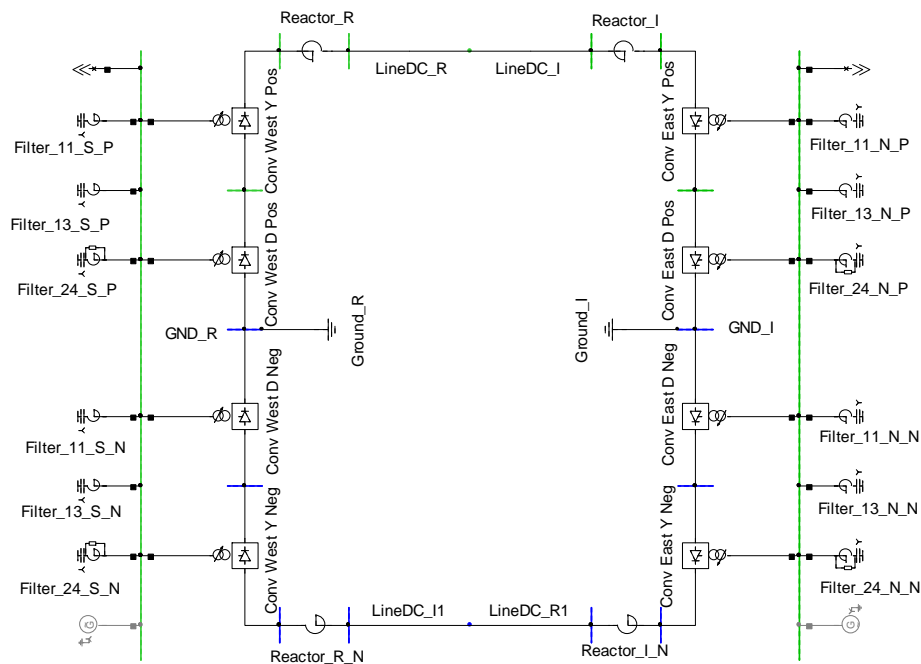


Figure 3.1: The CSC-HVDC single line diagram modelled in DIgSILENT PowerFactory

The main components of the system include [22]:

Converters: DC/AC and AC/DC conversion is performed in the converter units and each unit consists of two 6-pulse Thyristor bridges (also each bridge consists of 6 Thyristor valves) and a built-in transformers with tap changers. The built-in converter

transformers are designed to work with high harmonic current and withstand AC/DC voltage stress.

AC and DC side filters: In a 12-pulse converter all harmonics of the order $12k \pm 1$ ($k=0, 1, 2, \dots$) appear on the AC side. Therefore, a typical 12-pulse Thyristor terminal requires an 11th, 13th, 23rd, 25th ... filter on the AC side. Some HVDC designs with overhead lines also implement a DC filter.

Reactive power compensation: CSC-HVDC link has high reactive power demand which varies with DC power. Typically a large percentage of reactive power compensation is required, which is up to 60% of the DC power rating, to be provided by the filter banks and the rest is supplied by switchable capacitor banks or FACTS-based devices such as a STATCOM or SVC.

Control system: The rectifier and inverter include various hierarchical control systems which will be explained further in the next section.

Smoothing reactors: The DC-side of the converter consists of smoothing reactors, which are mainly required to reduce harmonics at the DC-side, prevent commutation failures and protect valves at post fault. It is usually determined based on DC fault current, communication failure and dynamic stability [125].

3.3.2 CSC-HVDC link modelling

The equivalent circuit of a CSC-HVDC system is illustrated in Figure 3.2 to show the relationship between DC voltage, (V_{dc}) at the rectifier and inverter side. Also, the principal equations for V_{dc} and DC current, (I_{dc}) at a multi-bridge HVDC links' converter are defined in (3.1) to (3.5). Also, all the parameters are defined in Table 3.1.

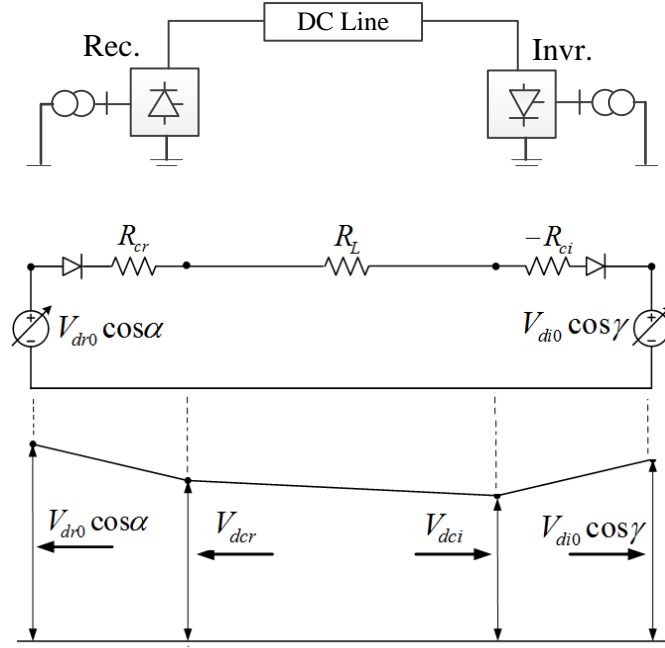


Figure 3.2: The equivalent circuit diagram of the CSC-HVDC Systems [22]

It is evident that V_{dc} can be changed by varying the firing angle. However, as can be seen in (3.4) the Power factor angle is dependent on the firing angle. Therefore, the nominal firing angle is desired to be kept low, around 15° - 20° in order to reduce the reactive power consumption. A sufficient margin is also required to compensate for any AC voltage drop following a disturbance [125]. Also, V_{ac} and the inductance of the converter transformer, (L_{tr}) can affect the V_{dc} . In fact (L_{tr}) prevents instantaneous commutation from one Thyristor switch to another and eventually results in commutation overlap denoted by (μ).

$$V_{dcr} = B \frac{3\sqrt{2}}{\pi} V_{LLr} \cos \alpha - B \frac{3}{\pi} \omega L_{tr} I_{dc} \quad (3.1)$$

$$V_{dci} = B \frac{3\sqrt{2}}{\pi} V_{LLi} \cos \beta - B \frac{3}{\pi} \omega L_{ti} I_{di} \quad (3.2)$$

$$I_{dc} = \frac{V_{dcr} - V_{dci}}{R_{dc}} \quad (3.3)$$

$$\cos(\phi) \approx \frac{\cos \alpha + \cos \delta}{2} \quad (3.4)$$

$$Q_{ac} = P_{ac} \tan(\phi) \quad (3.5)$$

In addition, as shown in (3.3), I_{dc} is proportional to the difference between the converters' voltage. Therefore, I_{dc} can be controlled by using the inverter or rectifier voltage.

TABLE 3.1: Definition of the CSC-HVDC link parameters

α	Firing delay angle (start of commutation)	I_{dc}	DC current
δ	Extinction delay angle (end of commutation)	V_{LLi}	Line to line AC voltage at inverter side
μ	Commutation overlap angle ($\mu = \delta - \alpha = \beta - \gamma$)	V_{LLr}	Line to line AC voltage at rectifier side
β	Ignition advance angle ($\beta = 180 - \alpha$)	ϕ	Powerfactor angle
γ	Extinction advance angle ($\gamma = 180 - \delta$)	L_{tr}	Reactance at Rectifier side
V_{dcr}	DC voltage at Inverter side	L_{ti}	Reactance at Inverter side
V_{dci}	DC voltage at Rectifier side	B	Number of series connected 6-pulse bridge

3.3.3 Control strategies for CSC-HVDC link

Under normal conditions, the rectifier end operates in Constant Current Control (CCC) mode to control the I_{dc} , while the inverter controls the V_{dc} . In fact the I_{dc} and V_{dc} are controlled in order to maintain the desired power transfer on the DC link. It is essential therefore to continuously measure the required system quantities such as the I_{dc} , V_{dc} , firing delay angle, (α) and inverter Extinction angle. The roles of converters could reverse under abnormal operating conditions such as reduced AC voltage or a fault occurrence. This is further explained in the next section.

3.3.3.1 Rectifier control mode

The rectifier of CSC-HVDC link typically operates at CCC mode. However, the rectifier voltage can be increased until the firing angle reaches the minimum firing angle

limit of $\alpha=2^\circ$. Under this condition, the rectifier moves to constant firing angle mode where ($\alpha = \text{constant}$).

3.3.3.2 Inverter control mode

The inverter could operate in three different control modes depending on system conditions.

- In normal operating conditions, the inverter operates at constant V_{dc} mode to stabilise the system while the rectifier is controlling I_{dc} .
- If the AC voltage at the rectifier side reduces, the rectifier assists in improving the voltage reduction by reducing its firing angle until it reaches to the firing angle limit and from that point it would operate at $\alpha = \text{constant}$ mode. Whereas, the inverter keeps the I_{dc} constant and operates at CCC with current reference, (I_{ref}) reduced by a current margin, (I_{margin}). Therefore, there is a 10-15% margin between the I_{order} at the rectifier side and I_{order} at the inverter point.
- If the AC voltage at the inverter side is reduced, the rectifier carries on controlling the I_{dc} and the inverter moves to a Constant Extinction Angle (CEA) mode to prevent commutation failure.

Overall, the CSC-HVDC system is not desirable for maintaining the rated DC current, I_{dc} , when the AC voltage drops more than 25%. This is because; following the AC voltage depression, the rectifier firing angle reaches its minimum limit to compensate the AC voltage drop. In case of further AC voltage drops, the rectifier moves to constant mode and I_{dc} will be controlled by the inverter at the reduced level. Since V_{dc} is not controlled by any of the converters, V_{dc} might drop further. Therefore, the Voltage Dependant Current Order Limiter (VDCOL) control is implemented to reduce the maximum allowable DC current when the voltage drops below a predetermined value. The VDCOL characteristics may be a function of the V_{dc} or AC commutating voltage [125].

All of the operating control modes are designed to ensure the DC system stability and minimum reactive power consumption, as the high firing angle or extinction angle results in high reactive power absorption.

3.3.4 Hierarchy control system for the CSC-HVDC link

An overview of CSC-HVDC link's control hierarchy is illustrated in Figure 3.3. In a bidirectional HVDC link the inverter and rectifier can interchange modes rapidly. The inverter provides three control modes, including Constant DC or AC voltage control mode, CEA and CCC mode. In inversion mode, it is critical to maintain the Extinction angle at minimum to avoid commutation failure. Hence, the CEA (Gamma or Extinction angle control) is a default control at the inverter side. However, this mode of control is less stable during a disturbance or in cases where the DC link is connected to a weak AC network. Therefore, DC or AC voltage control is the main control at the inverter side using a Proportional Integral (PI) feedback control to maintain the voltage at the target level.

The I_{dc} (or active power control) is not active throughout normal operation. This back-up control is very favourable during a fault on the DC side or when the rectifier loses its I_{dc} control during a depressed AC voltage at the rectifier side following any disturbance. The inverter CCC controller compares the I_{order} with a reference current (I_{ref}) reduced by margin current. ($I_{ref} = I_{order} - I_{margin}$, with $I_{margin} = 0.1$ p.u.).

A hierarchy master level control, as presented in Figure 3.3, is provided at the rectifier side, which in fact provides the current reference (I_{ref}) to the main DC current controller. The rectifier also facilitates the power control by continuously calculating the DC power at the DC voltage reference value and outputs the scheduled I_{order} . [125].

As shown in Figure 3.3, frequency control and power oscillation damping can be employed at the rectifier side. Power oscillation damping can be implemented to improve the stability of networks with poorly damped oscillations. This signal is usually added to I_{order} . Also, the active power order override is provided, which can be implemented for post-fault action and other events. All three controllers calculate the firing angle and the lowest outputs from these controllers are selected through minimum gamma logic selection to determine the firing pulse for the inverter valves. The firing angle is limited between 110° and 170° to reduce the possibility of commutation failure and at the same time to avoid unplanned switch over to the rectification mode.

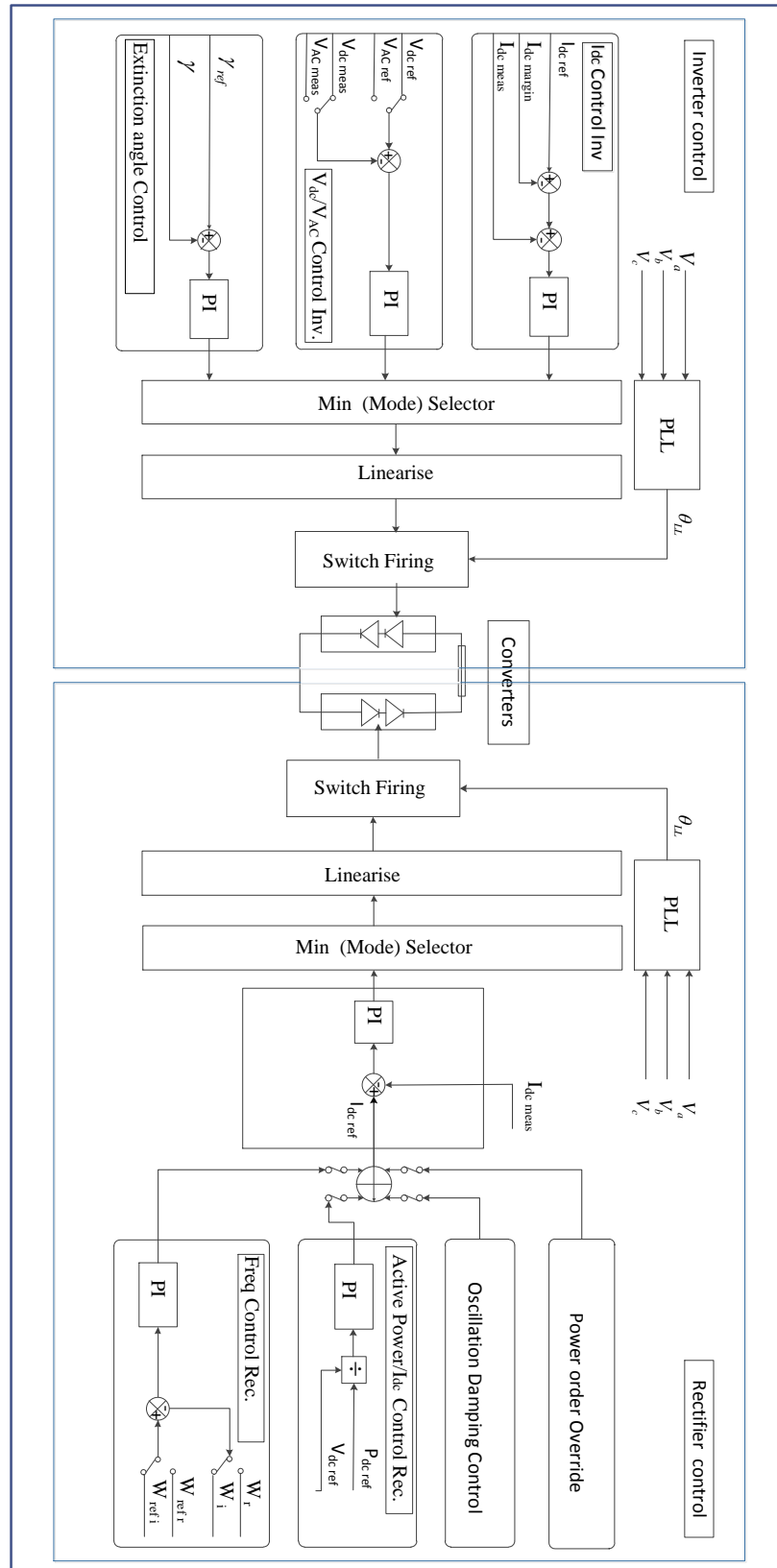


Figure 3.3: Schematic of the hierarchy control for the CSC-HVDC link at Rectifier and Inverter side

3.4 TCSC modelling

As explained in Chapter 2, the TCSC can be implemented in a heavily loaded transmission line to increase the capacity of the transmission line. In addition, it can provide improvements in power oscillation damping, SSR mitigation and transient stability [126][127].

The TCSC circuit consists of a Thyristor-Controlled Inductor branch (TCR) in parallel with a capacitor, which is inserted directly in series with the transmission line. Therefore, the TCSC can be simply modelled by using the concept of variable reactance as shown in Figure 3.4.

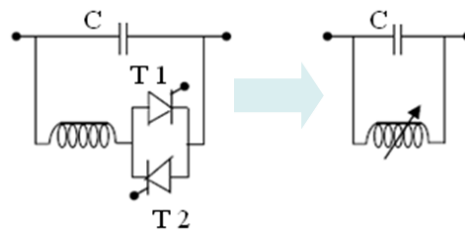


Figure 3.4: structure of the TCSC model

The variable inductive reactor of the TCR branch, (X_L) can be controlled by varying the Thyristor firing angle, (α) as shown in Equation (3.6) and the TCSC effective reactance X_{TCSC} is calculated using (3.7)-(3.9) [128][129].

$$X_L(\alpha) = X_L \frac{\pi}{\pi - 2\alpha - \sin 2\alpha} \quad (3.6)$$

$$X_{TCSC}(\alpha) = X_{LC} + C_1(2(\pi - \alpha) + \sin(2(\pi - \alpha))) - C_2 \cos^2(\pi - \alpha)(\varpi(\pi - \alpha)) - \tan(\pi - \alpha) \quad (3.7)$$

Where:

$$X_{LC} = \frac{X_C X_L}{X_C - X_L}, \quad \varpi = \sqrt{\frac{X_C}{X_L}} \quad (3.8)$$

$$C_1 = \frac{X_C + X_L}{\pi}, \quad C_2 = 4 \frac{(X_{LC})^2}{X_L \pi} \quad (3.9)$$

The TCSC is capable of operating in both the inductive ($90 < \alpha < \alpha_{Llim}$) and the capacitive regions ($\alpha_{Clim} < \alpha < 180$) by varying the Thyristor firing angle [129]. When

the value of $X_L(\alpha) = X_C$ the effective X_{TCSC} becomes infinity and the TCSC starts resonating, which has to be avoided.

3.5 Static Var Compensators (SVC) model

The SVC is a voltage controlling device, consisting of Thyristor Switched capacitors (TSC), Thyristor Controlled Reactors (TCR) and filters. Its main application is to provide fast acting MVAR response to system voltage changes. Similar to the TCSC, the variable inductive reactor of the TCR branch (X_L) can be controlled by varying the Thyristor firing angle (α). The SVC effective reactance (X_{SVC}) and the equivalent susceptance as a function of (α) are defined in (3.10) and (3.11) respectively [130].

$$X_{SVC} = \frac{X_C X_L}{\frac{X_C}{\pi}(2(\pi - \alpha) + \sin(2\alpha)) - X_L} \quad (3.10)$$

$$B_{eq} = \frac{\frac{X_C}{\pi}(2(\pi - \alpha) + \sin(2\alpha)) - X_L}{X_C X_L} \quad (3.11)$$

SVC operation modes include:

- Target voltage mode (fast voltage controller)
- Constant MVAR mode (reactive power)

3.5.1 Target voltage mode

Despite the name, at this mode the SVC will not adjust its output to maintain a constant voltage. In fact the target voltage is the intercept voltage at which the SVC output will in fact be zero and maximum reserve is available. The output of the SVC is determined by a predefined slope characteristic (setting is typically 4 - 5%.) and an intercept or target voltage (that is normally set within the range 0.95 – 1.00 – 1.05p.u.). In case of voltage deviation from the target voltage, the output of the SVC will be adjusted along the pre-set slope. This means that with a slope of 5% the output of the SVC will be changed from zero to maximum capacitive output for a 5% fall in voltage from the target. This implies that if the steady state voltage is allowed to deviate from the intercept (target) then the reactive reserves will be consumed and only a limited response will be available for voltage support in the event of a fault. It is, therefore vital to observe the SVC output in this mode at all times.

3.5.2 Constant MVar mode

In this mode, the MVar output of the SVC will be maintained at a predefined constant value. The reactive controller will achieve this MVar target by adjustment of the target voltage (set-point) of the voltage controller with the δV_Q in order to maintain the SVC reactive power output at a specified value given by the target MVar set-point. This mode ensures the SVC dynamic reactive power reserves are available for fast regulation [130].

3.6 Characteristics of the test systems used throughout the thesis

3.6.1 Test system 1

A Single Machine Infinite Bus (SMIB) system, which is presented in Figure 3.5, is set up and implemented to demonstrate the process of interfacing PowerFactory to Matlab/Simulink. The test system consists of two AC lines (ElmLine) which connects the two areas. The generator (ElmSym) in each area is represented by a full order synchronous machine model, which is equipped with both governors and voltage regulators in PowerFactory. One of the AC lines is equipped with a TCSC, where the initial Fixed Series Compensation (FSC) is 30% of the total line reactance. The TCSC can provide up to 75% compensation to the total reactance of a single line route by changing the reactance of the TCR. As discussed in section 3.4, the TCR is modelled as a variable reactance (ElmSind) “VarReactor” and the steady state value of the inductance, which is 20 Ohms, is defined in the load-flow model. When the Thyristors of the TCSC are blocked, the TCSC operates as a conventional series compensator with a fixed reactance “XC” and when the Thyristors are conducting the device can vary its net reactance. This series reactance could be adjusted within its limits to keep the specific amount of active power flow across the line. It is essential that the initial condition of the TCSC reactance is defined and set in the design of the controller in PowerFactory. The control variable is the reactance of the TCR branch. In fact the active power in Line1 is regulated by varying the reactance of the series reactor to minimise inter-machine / inter-area oscillations under normal operations such as tracking of the set-point changes. The specific details and parameters of test system1 are provided in Appendix A.1.

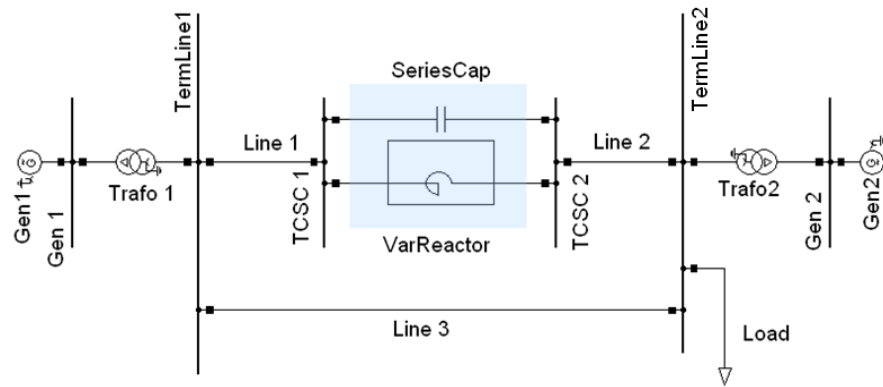


Figure 3.5: Schematic of concept proving test system1 in PowerFactory

3.6.2 Test system 2 (Multiple TCSC line)

The second SMIB model, as depicted in Figure 3.6 , with two parallel TCSC lines, is set up to investigate the performance and capability of a MIMO controller in the coordinated control of multiple TCSC lines in order to enhance system stability. The test system consists of two AC lines in parallel with two TCSC lines. Each TCSC line has an initial FSC of 30%. The TCR branch of the TCSC lines can produce up to 75% compensation to the total reactance of a single line route. The other characteristics of the system are similar to test system1.

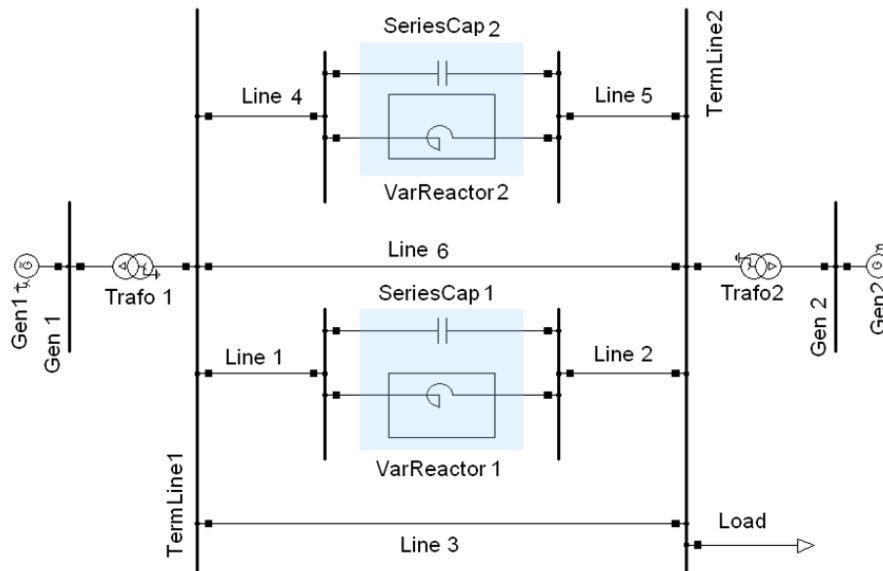


Figure 3.6: Schematic of test system 2 (or multiple TCSC line) in PowerFactory

3.6.3 Test system 3 (Single HVDC link)

The third SMIB test system, shown in Figure 3.7, is set up in DIgSILENT PowerFactory to investigate the capability of an embedded HVDC link in parallel with

an AC line for improving system stability. The dynamic model of the CSC-HVDC link and generators are implemented in the test system. The HVDC link in this model is to represent the future West Coast HVDC link of GB system. The main parameters of test system 3 are provided in Appendix A.3.

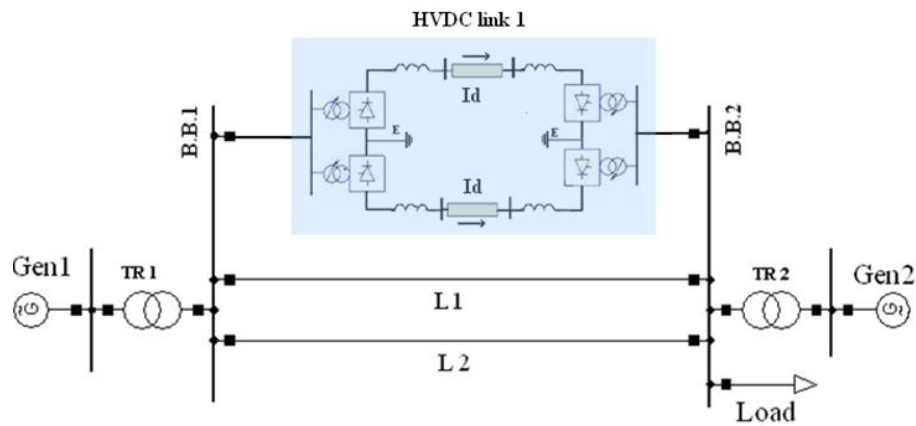


Figure 3.7: Schematic of test system 3 in PowerFactory including the HVDC link & AC lines

3.6.4 Test system 4 (Multiple HVDC links)

The fourth SMIB test system, shown in Figure 3.8, is set up in DIgSILENT PowerFactory to represent the transmission network connections between the North of England and Scotland. In this test system two parallel HVDC links are integrated to the AC system. The power transfer from generator 1 to the load is around 1.3GW including each HVDC link carrying 500MW of power. Also, the dynamic model of the generators and the CSC-HVDC links are implemented. The specific details and parameters of test system 4 are provided in Appendix A.4.

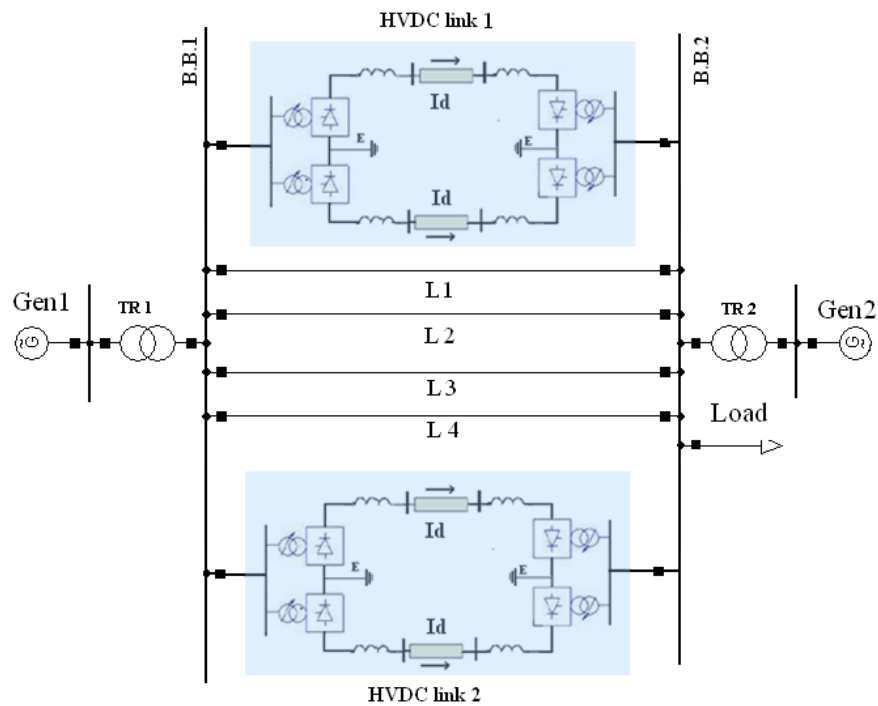


Figure 3.8: Schematic of test system4 in PowerFactory with multiple HVDC links

3.6.5 Test system 5 (Including the HVDC link and SVC)

Another test system, with initial transfer levels of 2GW and 500MW power on HVDC link, shown in Figure 3.9, is set up for demonstrating the coordinated control of the HVDC link and SVC together under a single MIMO SR feedback control. This test system is set up to represent the system across the B6 boundary, with the HVDC link along the West Coast and the SVC at Harker side. In addition to the voltage regulation function, this SVC is also equipped with a POD for damping control. The damping control senses system oscillations from either frequency or active power feedback signals. In the SMIB system, power flows on AC lines L1, L2, L5 and L6 are monitored by the POD, as is the case in the GB transmission system on the West-side of the AC inter-connectors. The specific details and parameters of test system 5 are provided in Appendix A.5.

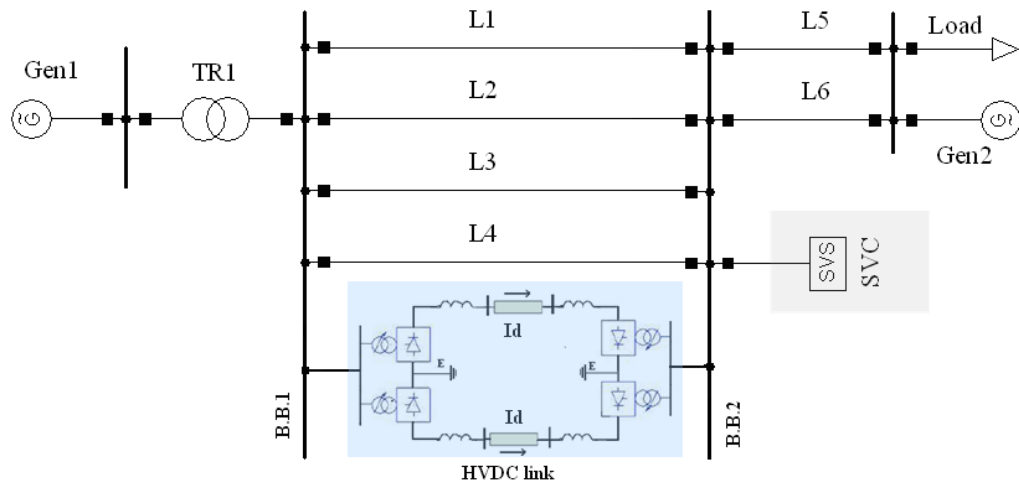


Figure 3.9: Schematic of concept proving test system5 in PowerFactory

3.6.6 Test system 6 (Two-area four-machine system)

The test system 6 shown in Figure 3.10 is used for dynamic stability assessments and illustrating the application of the TCSC and HVDC link in providing supplementary damping control. This model is based on the two-area four-machine system with an extra AC line which is extracted from [22]. In the mid-point of the additional AC line there is a TCSC that provides 40% compensation of the line reactance. In studies where the HVDC link capability for oscillation damping control is under investigation, the TCSC line is replaced by a HVDC link. The parameters of test system 6 are provided in Appendix A.6.

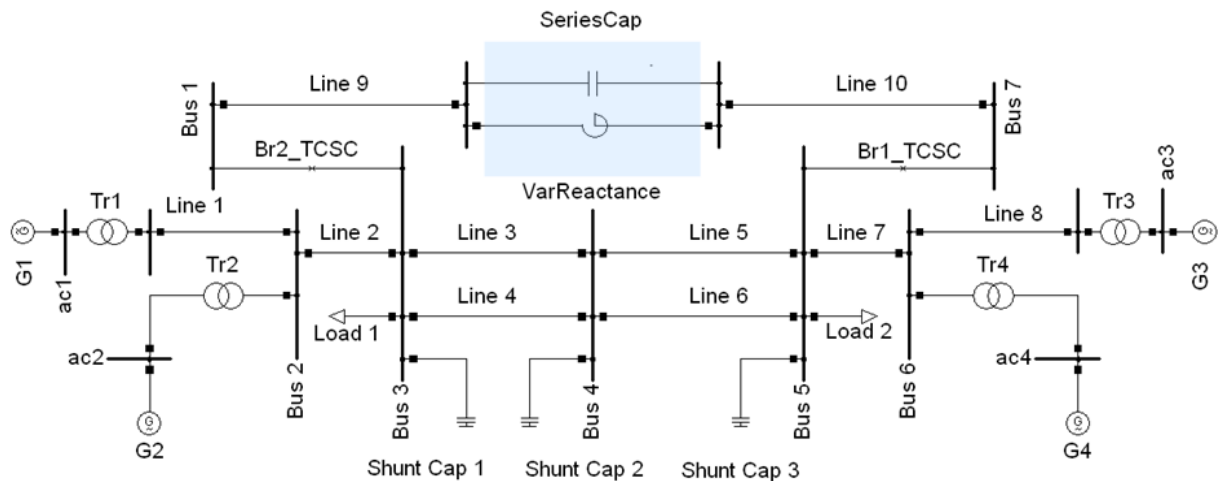


Figure 3.10: Schematic of Two-area four-machine test system6 in PowerFactory

3.7 Concluding remarks

In this Chapter, following a brief overview of the principles and background theory of the TCSC, SVC and CSC-HVDC link, the overall control strategies for the CSC-HVDC link are discussed. In addition, all the test systems, modelled in DIgSILENT PowerFactory are presented in this Chapter. The details of these models, which include the CSC-HVDC and benchmark test systems, are provided in Appendix A and B. In the subsequent Chapters, these models are implemented with an objective to study the capability of the HVDC link in transient and dynamic stability enhancement for the future GB transmission networks.

Chapter 4

Framework and requirements of hierarchical stability control system

This Chapter describes current and future control issues with specific reference to the GB transmission system, as well as explaining the requirement for a hierarchical stability control system. In addition, the need for interfacing simulation programs such as DIgSILENT PowerFactory (PF) with MATLAB control tool boxes, which are capable of performing comprehensive mathematical calculations and offering a wide range of control system functions are discussed, as an initial step to develop such a hierarchical stability.

4.1 Introduction to current and future control schemes in the GB transmission system

In the operation of High Voltage (HV) transmission systems the major control actions are carried out via generation dispatch optimisation, which are for the control of a given steady state operating point and can be for both pre and post fault situations. Ultimately, the balance of generation and demand is controlled at this level. In addition to the generation dispatch control, other controls actions usually involve are substation configuration, compensation equipment switching control and demand side management etc. The purpose of these control actions are for short-circuit fault levels, flow control, voltage and reactive power regulation and system stability. The devices deployed in a HV transmission system for either voltage or power flow control could be both manual and automatic. For example, the voltage control devices include transformer tap changers, Manually Switched Capacitor (MSC) banks and Static Var Compensation (SVC) systems, while the flow control devices consist of Phase Shifting Transformer (PST), known as ‘Quadrature Boosters’ (QB), Fixed or Thyristor Controlled Series Compensation (FSC/TCSC) devices and the HVDC link. Within the National Grid transmission network, tap changers, MSC, SVC, QB and inter-system HVDC interconnectors have been installed as mature technologies for many years. National Grid is currently considering using various system controllers to reinforce the GB transmission system to meet various 2020 energy scenarios including the ‘Gone

Green' scenario[131] [8]. The Series compensation and HVDC link are the top two system controllers amongst others that have already been entered into the ENTSOE's Ten-Year Network Development Plan. The new Series Compensations and the West Coast embedded (inter-area) HVDC link are now expected to be commissioned in 2015 and 2016 respectively. With the nearing addition of these automatic devices to the system, how to control and operate them to achieve the maximum benefit from the view of a System Operator (SO) is a pressing issue that needs urgent answers.

4.2 Requirement for hierarchical stability system

As previously mentioned in Chapter 1, following the CO₂ reduction legislation, all the EU countries are committed to maximise their power output from low carbon resources such as renewable energy sources. A significant portion of these renewable resources is expected to be from wind farms, both onshore and offshore. Also, it is predicted that the installed capacity of wind generation will increase to around 30GW by 2020 compared to the current installed capacity of around 10GW[132] [1].

The majority of the new wind generation will be installed in Scotland, and offshore in the UK as a whole, where the maximum levels of wind resources are available. Such an increase in variable renewable generation will result in significant changes to the direction and volume of power flows across the network. A good example is a significant increase in the required power transfer between SPT (Scottish Power Transmission) and National Grid networks [1][2] [132][133][134]. The SPT and National Grid Electricity Transmission (NGET) networks boundary (known as Anglo Scottish boundary) contains two double 400kV AC lines; on the Western and the Eastern sides of the boundary. The Anglo Scottish boundary (also known as B6) has a current transfer capability of around 2.2GW due to stability issues. The stable operation of the network following a certain disturbance is guaranteed by reducing the power transfer on this boundary. The range of the required power transfer capability over the boundary increases every year, due to the increase in the potential output from the intermittent wind generation [133]. As a result it is essential that the GBSO and TOs maximise the use of existing transmission lines operating them closer to their thermal limits in order to avoid constraining some generation plant and also to develop methods to improve the stability limit. A potential solution to provide the higher transfer capacity

required to integrate this additional generation is to use some of the new transmission technologies, such as TCSC and embedded HVDC links. These will come into operation in the GB system between 2013 and 2021 as shown in Figure 4.1. Such power flow controller devices could dynamically change the overall structural and oscillatory behaviour of the system and consequently affect system stability. National Grid may have to resort to costly pre-fault constraint management to maintain system stability if these system changes cannot be controlled quickly via power flow control. However, without investment in stability control systems much of the potential advantages and effectiveness of all these costly reinforcements on the transmission system could be wasted. Consequently, this could result in constraining the output of renewable energy sources which ultimately increases the operating costs of the UK electricity market. Therefore, a stability control system is required to guarantee the optimal dynamic performance for the co-ordination of power flow control in such a large integrated power system [135][136][137].



Figure 4.1: Existing and future reinforcements for England and Wales [133]

4.3 Control problems in the GB transmission system

The embedded HVDC link and TCSC's are fast acting and automatically controlled devices, which are primarily designed for power flow control purposes whereas SVCs are used for voltage regulation. Both the new HVDC link and SVCs in the GB transmission system are capable of incorporating additional feedback signals to enhance system oscillation damping.

Current thinking on the operation of the TCSC in the GB system is to be implemented only for a small range of load flow regulation during normal operation, while the ability for tuning the controllable series reactance is to be utilised to avoid SSR.

The future West Coast embedded HVDC link in the GB transmission system, also known as "bootstraps" for this type of HVDC applications, are supposed to tie the two parts of the weakly connected AC sub-systems in the GBSO network together under both pre and post-fault conditions.

With regard to power flow control, the HVDC link is primarily intended to control the pre-fault flow and enhance the boundary transfer capacity, while at the immediate post-fault, it's fast ramping and short-term capacities can be utilised to enhance the transient stability. While the HVDC link provides fast ramping in order to take on extra flows from faulted AC circuits, the SVC can be regulated within the statutory operation limits ($\pm 10\%$ on the GB HV system) to provide useful support such as post-fault actions. It is important to note that all of these controls are in transient time scales (i.e. in milliseconds).

As explained previously in section 4.2, the Anglo-Scottish boundary is such a critical boundary both traditionally and in the future due to the penetration of renewable energy sources in the GB system. National Grid has therefore; put a huge investment into this area. Hence, the network in this area is now congested with many types of new and automatic control devices. For example, conductor upgrades have been ongoing in the last few years; new transmission technologies such as the TCSC and the embedded HVDC links down the East and West coast are coming into operation in the GB system by 2016 and 2018 respectively. Without proper analysis, there is a risk of interaction between various control devices [14] [134] [138].

4.4 Introduction to National Grid operational tools

As aforementioned, the constant challenge to National Grid as the GBSO is to improve the stability limit across the B6 boundary. Therefore, it is critical to investigate whether the stability limit can be pushed close to the thermal load flow limits under all operational conditions by implementing a Stability Control System (SCS). However, such a stability control system is required to reconcile with all other control systems on the National Grid system which are built for overall operational control. These control systems include the Energy Balancing System (EBS), Operational Tripping Schemes (OTS) equipped as Special Protection Systems (SPS) and On Line Stability Assessor (OSA). Therefore, a brief introduction to all operational tools used in National Grid that might be linked with the proposed SCS is provided. Then the framework and role of the proposed SCS within the entire National Grid control system is outlined in the next section [135][136][137].

4.4.1 Security constrained dispatch program (EBS)

System security is a crucial issue in operating the transmission system. A secure pre-fault optimal power flow solution assures both the pre-fault and post-fault constraints. The security constrained dispatch program at National Grid will incorporate a network model to secure thermal constraints directly by placing limits on the output of sets of generators. In the future security constrained dispatch program, which is known as EBS, the voltage constraints and thermal constraints will also be secured in terms of group constraints. Stability constraints will be secured by limiting generation in the constraint group based on the constraint limit calculated by off-line studies using Off-Line Transmission Analyser (OLTA) and fed to the security constrained dispatch program.

This implies that all thermal, stability and voltage group constraints are secured for the optimal power flows solution obtained from the future security constrained dispatch program. Therefore, the SCS, which will be explained in the Section 4.5, will also honour all thermal, stability and voltage constraints if the set-point of the SCS is obtained from the security constrained dispatch program. This allows the SCS to follow the optimal power flows from the future security constrained dispatch program [135][136][137].

4.4.2 On Line Stability Assessor (OSA)

“OSA” stands for Online Stability Assessment tool while Power Network Analysis (PNA) is commonly used in the context of the Integrated Energy Management System (IEMS) for power network analysis. Control engineers at the ENCC in National Grid use the PNA tool to assess the GB HV transmission system security using online measurements in real-time. The PNA tool can be used to study thermal and voltage violations. However, there is no facility to study the dynamic behaviour of the system and to assess system stability in near real-time.

With more wind farms and other types of renewable energy coming into our transmission system, National Grid is facing increasing difficulties to manage the uncertainty due to the intermittency nature of renewable energy. The traditional planning process studies system stability once or twice a day at the system peak loading period(s). However, the wind can never be predicted precisely as we expected. Consequently, wind power generation always has the element of uncertainty. In the GB transmission system we have limited transmission capacities at some locations. Sudden changes of power over these ‘weak’ parts of the network may cause thermal overloads, voltage stress and power swings or stability problems. Clearly, only a couple of stability studies per day are becoming less and less adequate to cope with this more variable situation. The solution to manage the uncertainty is to move away from the reliance on off-line studies and assess the stability online continuously. Therefore, OSA is required to complement and enhance the PNA performance for the real-time stability security assessment. OSA uses full system dynamic models for stability analysis. All studies for all credible system contingencies are run every 10-15 minutes based on the current system snapshot which is produced by the IEMS ‘state estimation’ from the real-time measurements which are typical SCADA, RTU measurements.

In OSA, system stability is quantified against our Standards of Quality and Security of Supply (SQSS) [15]. Unlike the power flow contingency analysis, stability could be affected by both location of faults and timing of post-fault actions. These differences give added complexity to computation. Therefore, the processing speed is extremely critical to the OSA application. For that reason, an efficient algorithm on the powerful

parallel computer servers is implemented for stability analysis to capture any potential stability issue in real-time [139].

4.4.3 Operational Tripping Schemes (OTS)

The generation intertrip is a conventional technology that is used by TSOs to alleviate overload and improve system stability. It is a protection controlled automatic action that will disconnect a selected generator and solve system thermal overload, voltage and stability issues and improve system security. As specified in the connection agreement, TSOs can ask generators to select their contracted machines to be armed to intertrip to attain a more secure situation post fault/disturbance. Should the fault happen the selected generator circuit breaker will open in a specified time [140]. This service is also known as generation curtailment or Operational Tripping Scheme (OTS). In National Grid, OTS operates to a set of operating rules that determine the action of the scheme in response to power system events and states. In general, an OTS will monitor the terminating circuit breakers and/or disconnectors of certain circuits and trip generation according to a selection by the ENCC control engineer and power station control staff.

4.5 Framework of hierarchical stability control system for the GB transmission system

The proposed hierarchical SCS shown in Figure 4.2 is a Feedback control system intended to deliver the best stability and dynamic performance. The hierarchical components of the control system defined as follows [135][136][137].

- A security constrained dispatch program which acts as a master control to provide a set-point for the SCS in order to secure all thermal and voltage constraints as described in section 4.4.1.
- A feedback SCS in which fast power flow controller devices such as the TCSC and the embedded HVDC link are defined as an actuator. A stabilising control algorithm is employed to ensure that the mismatch between the set-point and actual active power on the individual lines are minimised. The Phasor Measurement Unit (PMU) will be used to provide the measured data of the actual power on the individual lines.
- The OSA will be implemented for Special Protection Action (SPA).

When the control actions of the SCS feedback control are inadequate as predicted by OSA, a generator intertrip scheme should be deployed as the final special protection action. Therefore, the future OSA will be utilised to manage the intertrip actions as the last solution.

An issue will be raised at the immediate post-fault. As the security constrained dispatch program takes time to be updated and will not be updated immediately after a fault. As a result, the areas either side of the tie-lines or the boundaries will be destabilised if the SCS still follows the pre-fault results of the security constrained dispatch at the post-fault. A solution for this issue is proposed in section 4.5.1 [135][136][137].

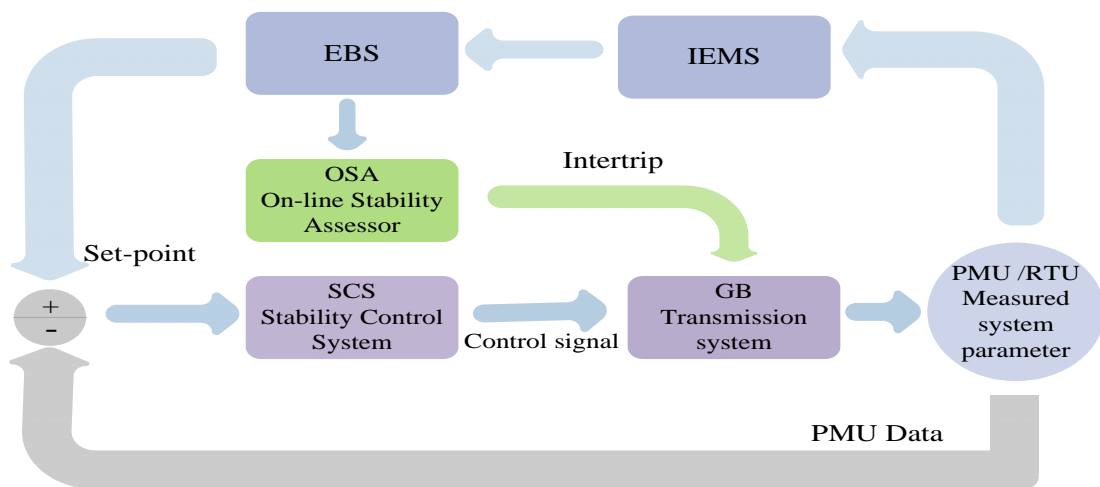


Figure 4.2: Hierarchical stability control system

4.5.1 Proposed solution

The objective of the control system is to maintain system stability by reducing the swing of the areas either side of the boundaries against each other or minimising the frequency deviation. The SCS could minimise the frequency deviation and the power swing of the areas either side of the boundaries if it manages to keep the total boundary power flow as constant as pre-fault. In order to do that the power set-point at the immediate post fault is defined as follows [4-5]:

$$P_{i,Ref}^* = P_{i,Ref} + \frac{\left[\sum_{k=1}^K (1 - Z_k) \right] P_{k,OPF-Ref}}{\sum_{m=1}^i (Z_m)} \quad (4.1)$$

$$\text{Where: } \begin{cases} Z_k = 1 \text{ when CB}_k \text{ is closed} \\ Z_k = 0 \text{ when CB}_k \text{ is open} \end{cases} \quad (4.2)$$

K: Number of lines not under the SCS control;

i: Number of lines with the power flow controller devices.

In (4.1), “ Z_k ” represents the circuit breaker position and “ Z_k ” becomes zero when the line K^{th} is open or tripped. “ Z_m ” represents the circuit breaker position of line with power flow control devices. “ $P_{k,OPF-Ref}$ ” and “ $P_{i,Ref}$ ” denotes the pre-fault optimal power flow on the each line obtained from the security constrained dispatch program. When a fault occurs on the K^{th} line, at immediate post-fault, the loss of that line will be picked-up and shared by the lines under the control of the SCS by modifying the pre-fault set-point of the SCS “ $P_{i,Ref}$ ” to the new set-point “ $P_{i,Ref}^*$ ” as defined in (4.1).

4.6 The supervisory stability control system design

As described in section 4.2, an overall stability control strategy at the transmission system level is needed for the best dynamic performance and co-ordination of power flow in the GB transmission system. However, coordination of different types of devices with their internal control systems in the GB transmission system requires a computerised system controller to command the individual actuators. This system controller must be designed in view of the GB transmission system as an entity. It is proven that discrete control law is more applicable to computer control system design. In order to design such a controller, there is a need to interface simulation programs such as PowerFactory (DIgSILENT) with some control tool boxes that are capable of performing comprehensive mathematical calculations and offering a wide range of control system functions. The Matlab program offers a large control toolbox and a wide range of computerised algorithms. Thus, when one is investigating a new control technique, either continuous or discrete, for power systems, it is more convenient to use Matlab. Access to the Matlab program from the simulation is achieved by using an interface to PowerFactory. This section briefly describes the process of interfacing

PowerFactory and Matlab program as an initial step of developing an stability control system for the GB transmission system [137][141].

4.7 Introduction to Matlab/PowerFactory interface

Simulation tools have been used extensively by manufacturers, designers and system operators for the analysis and assessment of various aspects of the design and operation of power systems with ease and without resorting to costly and potentially harmful tests on the real system. As the complexity in the integrated electric power network grows, the need for more comprehensive simulation tools rises. The simulation tools are expected to cater for all the standard power system analysis needs including high-end applications in new technologies such as wind power and distributed generation. Therefore, modern simulation tools have been developed in line with this ever increasing need by means of the integration of improved user interfaces. Interfacing between the simulation tools and external programs or mathematical tools extends the capability of the simulation tools in the execution of simulation more effectively, particularly in areas where the external programs or algorithms provides more advanced techniques and flexibility, i.e. advanced control system design in the Matlab control tool box [137][141] .

4.7.1 Requirement for interfacing

The standard library of the simulation tools which normally include models of synchronous/asynchronous machines, transmission lines, transformers, semiconductors, power electronic devices and simple processing functions (such as gain blocks and Proportional-Integral (PI/PID) controllers) facilitate the fast modelling and assembling of the electrical network. However, not all control system components are readily available to perform the specific computation or design of a complex control law. A comprehensive analysis /design requires computational facilities and advanced control blocks, digital processors, capability of modelling of nonlinear elements, etc. Therefore, it is sometimes essential to combine the two programs so that each could provide particular features either for more detailed modelling of certain aspects of a complex power network or for higher computational capability [142]. For that reason, the majority of simulation programs can extend their capability by interfacing to external

programs or software. In this approach, each software tool follows certain standards to allow software developed with various vendors to be implemented together through the use of interfaces [143].

The application of interfacing has been reported in the simulation of power electronic convertors, design of complex protection systems, design of advanced digital control systems and simply adding another feature such as optimization to the main simulator [142]. The interfacing allows the full exploitation of both packages' capabilities. Consequently the powerful mathematical and control functions including the various toolboxes available in the Matlab program could be implemented with the fast and powerful modelling and simulation capability of PowerFactory.

4.7.2 Structure of the Matlab to DIgSILENT PowerFactory interface

The overall structure of the interface is illustrated in Figure 4.3. In the process of linking Matlab/Simulink to PowerFactory the following programs interact throughout the simulation time [141][144][145].

- PowerFactory.
- Matlab data and data models in the form of m.files (.m)
- Matlab/Simulink model (.mdl)

The m.files and Matlab/Simulink models represent the model and algorithms of the external controllers, while the PowerFactory model represents the power system. In order to implement a Matlab model/algorithm in a PowerFactory project, it needs to be included in a frame similar to the *Dynamic Simulation Language* (DSL) model definition. The first step is to create a 'slot' inside a composite frame (ElmComp) in the PowerFactory project where the model/algorithm should be inserted. A block definition (BlkDef) is also required to be created in the 'type' library, which allows a definition of the Matlab code to be imported by ticking the Matlab m-file check box in the classification section and providing the address of the m.file (as shown in Figure 4.5.e). It is important to note that users need to insert the address of the location where the provided m.file is stored.

In the block definition (BlkDef) of this composite frame, all of the required inputs from PowerFactory, the outputs obtained from Matlab and the state variables must be defined. In addition, all the defined inputs, outputs and state variables in this block must be declared properly in the m.file. In each step of the simulation, PowerFactory inserts all the signals defined as ‘global variables’ into a ‘common workspace’ that can then be used by the external models or algorithms in Matlab. It is therefore crucial that all signals including the controller parameters, inputs, outputs and state variables are defined as a global variable in the m.file [144]. The function that the Matlab/Simulink program is tasked to perform can either be a built-in Matlab function or a user-defined algorithm [141][144][145] .

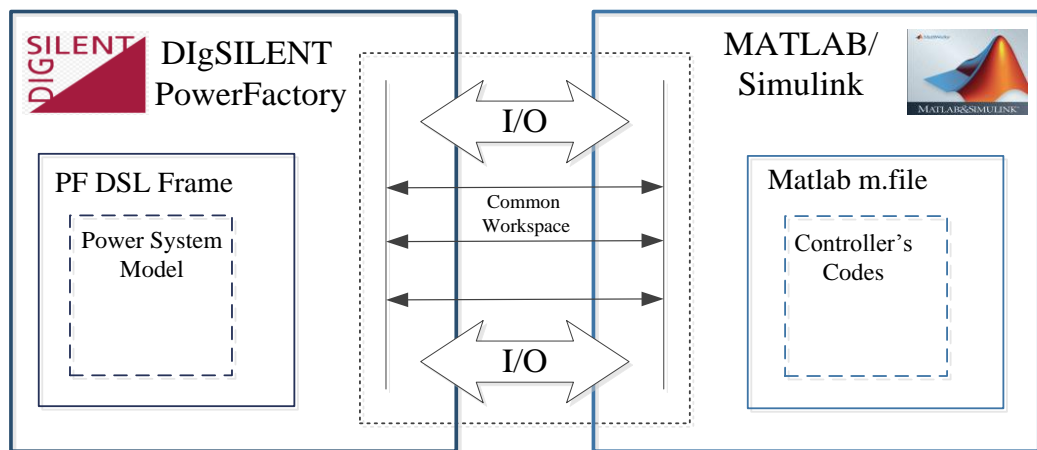


Figure 4.3: Overall structure of the Interface

In order to provide an illustrative instruction on how the interface between PowerFactory DIGSILENT and Matlab/Simulink can be created a study case is provided in this section to demonstrate the design of an external PI controller for the control of a TCSC line. In addition, this study case validates the correct creation of the interface between two programs for the design of an external controller in Matlab.

4.8 Validation of the correct creation of interface between PowerFactory to Matlab/ Simulink

This study case is set up to show the process and aspects related to interfacing the PowerFactory and Matlab/Simulink programs. In this study case, a PI controller is designed externally in Simulink to regulate the power flow in line1 and line2 (which are modeled in PowerFactory) using the Matlab to PowerFactory interface capability.

Regulation of the power in these lines minimises the inter-machine/ inter-area oscillations under normal operations by tracking the TCSC's set-point changes. To examine the correct linking between the two tools, the performance of the externally designed PI controller in Simulink is compared with the case when the built-in PI controller from the PowerFactory library is used to regulate the power in line1 and line2 [141].

4.8.1 Test system

The SMIB test system1, described in Chapter 3, is used to show the validation and process of interfacing PowerFactory to Matlab/Simulink. The initial state of the pre-fault system can be read from the power flow in the diagram shown in Figure 4.4. The characteristic of this model is provided in more detail Section 3.6.1. As explained in section 3.6.1, one of the AC lines is equipped with a TCSC which can provide up to 75% compensation to the total reactance of a single line route by changing the reactance of the TCR. Therefore, the control variable is the reactance of the TCR branch. The control system, in this example, is designed to regulate the power flow on line1 and line2 by varying the reactance of the series reactor in order to minimise inter-machine/inter-area oscillations under normal operations such as the tracking of the set-point changes [146].

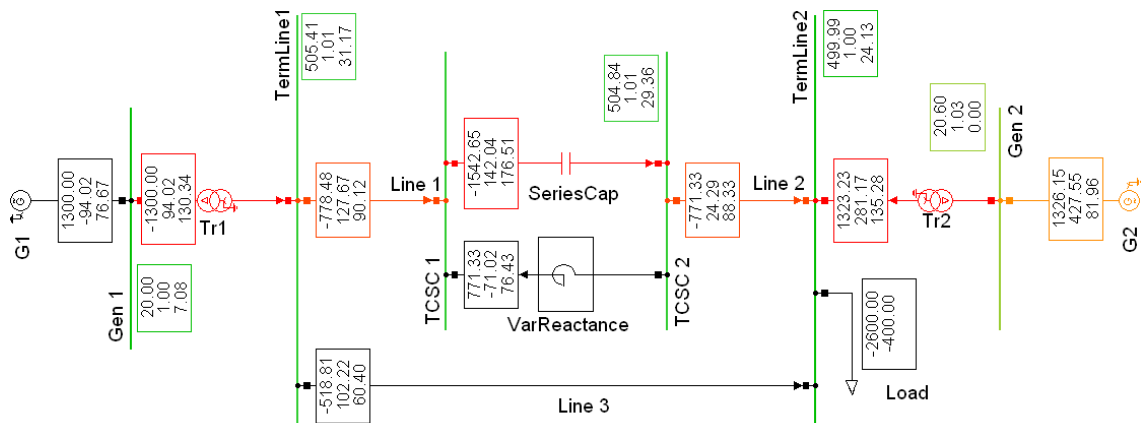


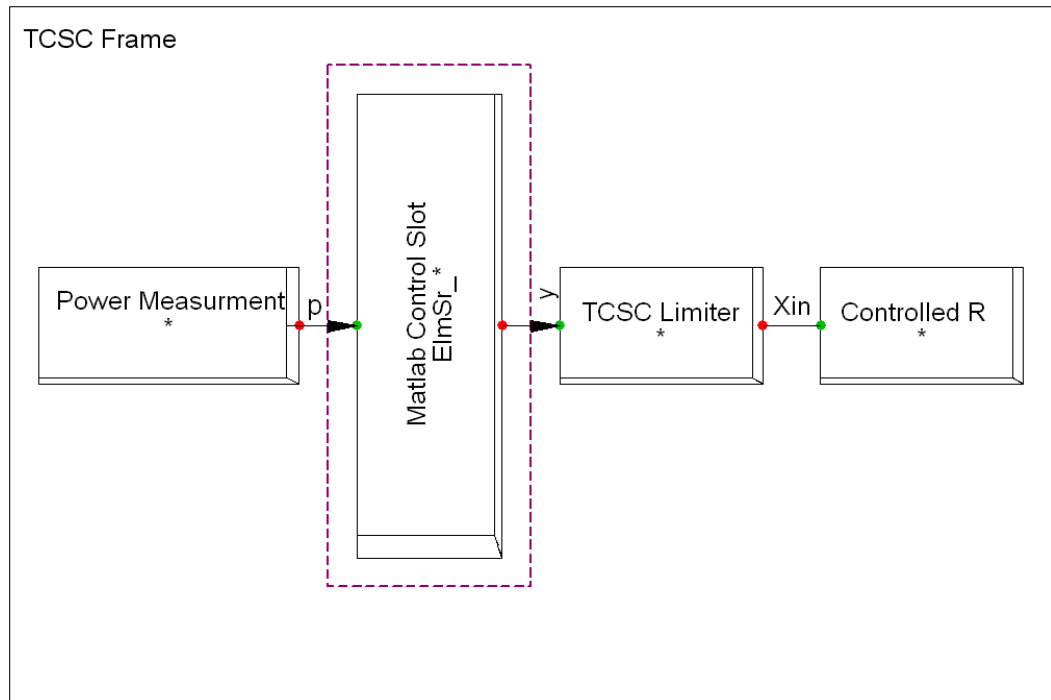
Figure 4.4: Test system1 in PowerFactory

4.8.2 The external PI controller in Matlab/Simulink (Setting up the required structure on the PowerFactory side to create an Interface)

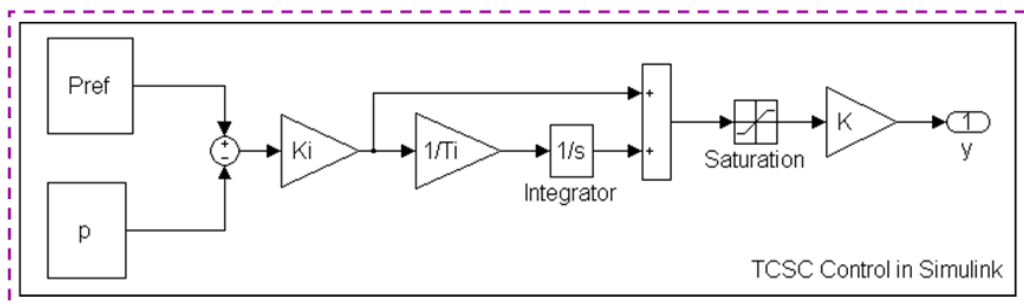
As described in section 4.7.2, the three programs (PowerFactory model, Matlab m.files (m) and Matlab/Simulink model (mdl)) interact throughout the simulation time when the interface capability is implemented. In this example, the Simulink model (mdl), shown in Figure 4.5.b, represents the externally designed PI controller. The parameters of the external PI controller are defined in a common DSL model (ElmDsl) of PowerFactory, as shown in Figure 4.5.d and Figure 4.5.e.

As described in section 4.7.2, the first step of creating the interface to allow the insertion of the Matlab/Simulink model, is to create a slot (ElmDsl) inside the TCSC composite frame in the PowerFactory project, which in this study case is named “Matlab TCSC control” shown in Figure 4.5.a. This slot represents the PI controller model in Simulink (mdl). Each slot in the TCSC frame is linked and sourced to the relevant component using the created composite model (ElmComp) for the TCSC frame presented in Figure 4.5.c. Since all of the required inputs from PowerFactory, the outputs obtained from Matlab/Simulink and the state variables must be defined, a block definition (BlkDef) for the Matlab TCSC control slot is created and all inputs, outputs and state variables are defined as shown in Figure 4.5.e. In addition, all the initial conditions (Figure 4.5.f) are defined in this block definition (BlkDef).

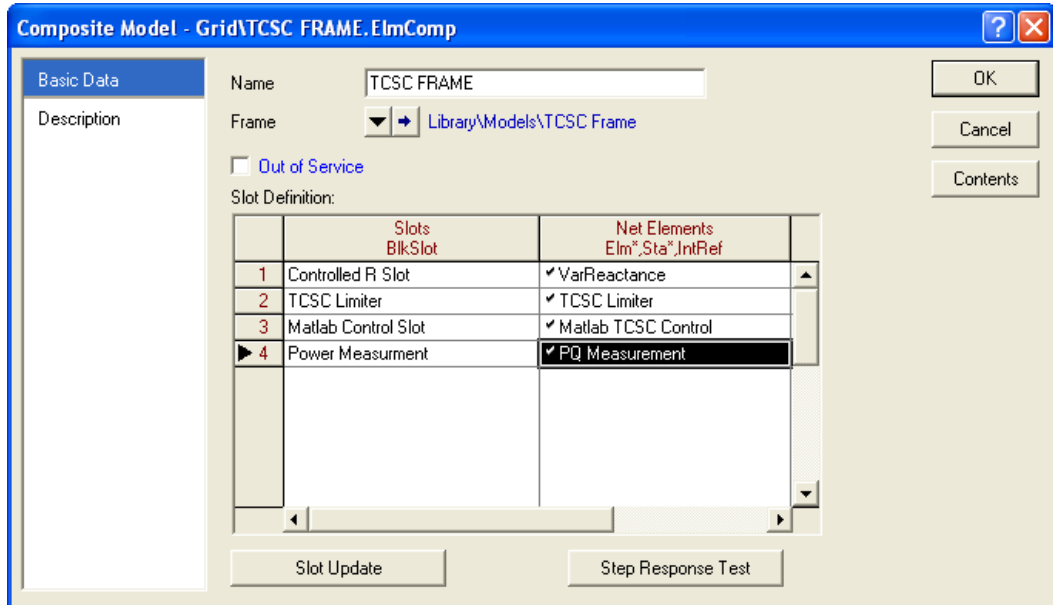
In this example, the input signals are measured power in Line1 (defined as P in Figure 4.5.a, Figure 4.5.b) and set-point of the TCSC line (defined as Pref in Figure 4.5.b) which are sent from PowerFactory to the Simulink model. The output of the Simulink model (y) is the control signal of the PI controller that is sent to PowerFactory at each step of the simulation (defined as X_{in} in Figure 4.5.a, Figure 4.5.b). It is essential that all the inputs, outputs and state variables defined in the created block definition (BlkDef) (shown in Figure 4.e.) are declared as a global variable in the m.file which is presented in section 4.3.2. The parameters of the PI controller in Simulink (mdl) are defined in a common DSL (ElmDsl) model in PowerFactory as shown in Figure 3.d [141].



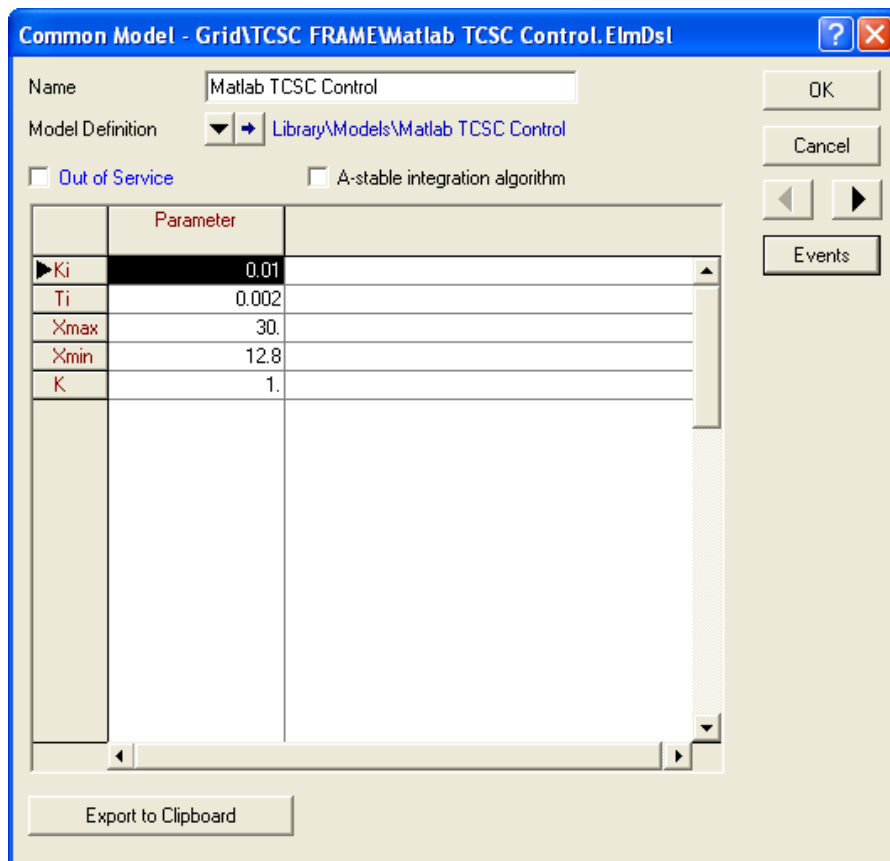
a) Composite TCSC Frame model in PowerFactory



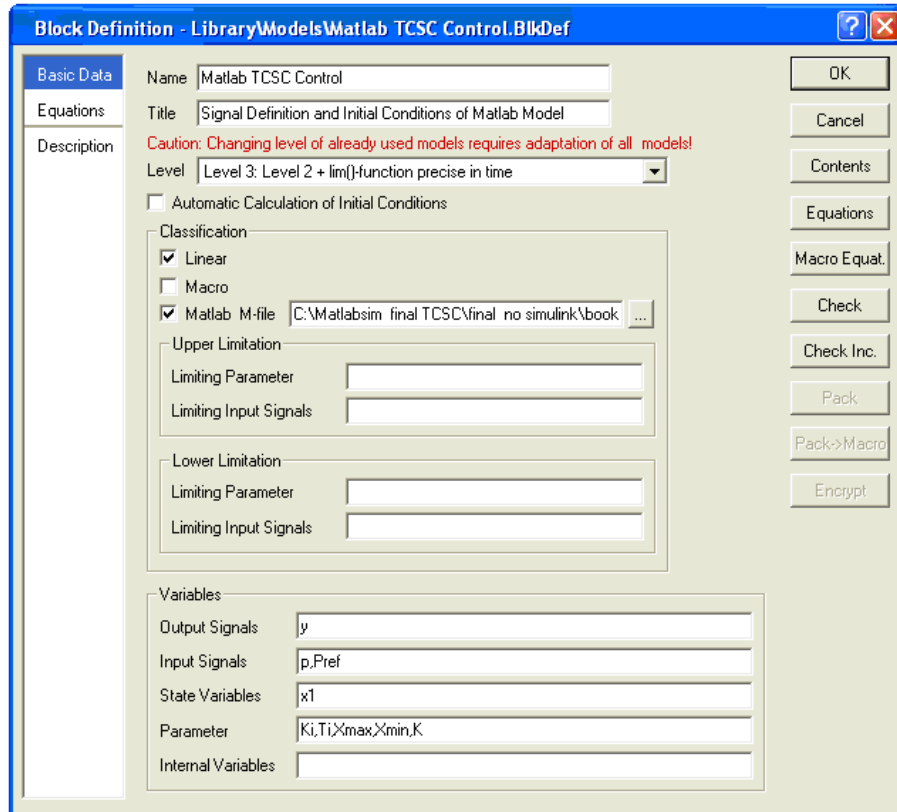
b) External PI controller in Matlab/Simulink



c) Composite model for the TCSC Frame in PowerFactory



d) Common DSL model for Matlab TCSC control



e) Matlab TCSC control, block definition (Basic Data page)

```
!The following equations are required for initial
conditions calculation

inc(Pref)=p

inc(x1)=y/K

y=0.001
```

f) Matlab TCSC control block definition (Equations page)

Figure 4.5: Structure of the Interface for design of the PI controller in Simulink

4.8.3 Initial conditions definition and calculation

Setting incorrect initial conditions for a newly defined controller frames can stop the program or introduce unnecessary oscillations at the beginning of the simulation. The initial conditions have to be defined for any block that contains state variables. This can

be implemented within the block itself (i.e. the PI controller) or within the controller frame which contains the mentioned block.

Since the system is in a steady state condition when initialised, all the error signals (if any feedback controller is employed) have to be zero. The initial conditions have to be defined for all the state variables in the frame. In most cases the initial value of the frame output is known to DIgSILENT through the load flow analysis which is executed prior to the initial condition calculation (if not it can be given the initial value). The initial value of the next block in line that has a state variable is given in a way that the calculated output value matches the known output value [141].

4.8.4 Setting up the required structure (on Matlab/Simulink side) to create the Interface

After creating the correct structure for implementing the interface in PowerFactory, an external PI controller is created in Simulink, as shown in Figure 4.5.b. Since DIgSILENT PowerFactory is only able to call scripts, any Simulink file has to be executed via a script or Matlab function as presented in Figure 4.6.

```
%%%%%%%%%%  
Function [t, x, y] = TCSCcontrol  
global p Pref ki Ti Xmax Xmin k x1  
% Get the simulation parameters  
options = simget('TCSCcontrol_model');  
% Set updated initial conditions  
options = simset('InitialState',[x1]);  
% Run the simulation and update the output and states  
value  
[t, x, y] = sim('TCSCcontrol_model', [], options);  
%%%%%%%%%%
```

Figure 4.6: Matlab script to execute Simulink file

4.8.5 Performance comparison of Built-in and external controllers

The performances of both the built-in and external PI controllers following the change of set-point of the TCSC line (Prep) are presented in Figure 4.7. The control signals

generated by both controllers and the active power in line1 that is under the control of PI controllers are shown in Figure 4.7. The simulation results show that the behavior and performance of the external PI controller in Simulink is identical with it perfectly matching the performance of the built-in PI controller in PowerFactory. This implies that the interface between PowerFactory and Matlab/Simulink is conducted correctly and that the inputs and outputs are exchanged accurately between the two tools at each simulation step[141].

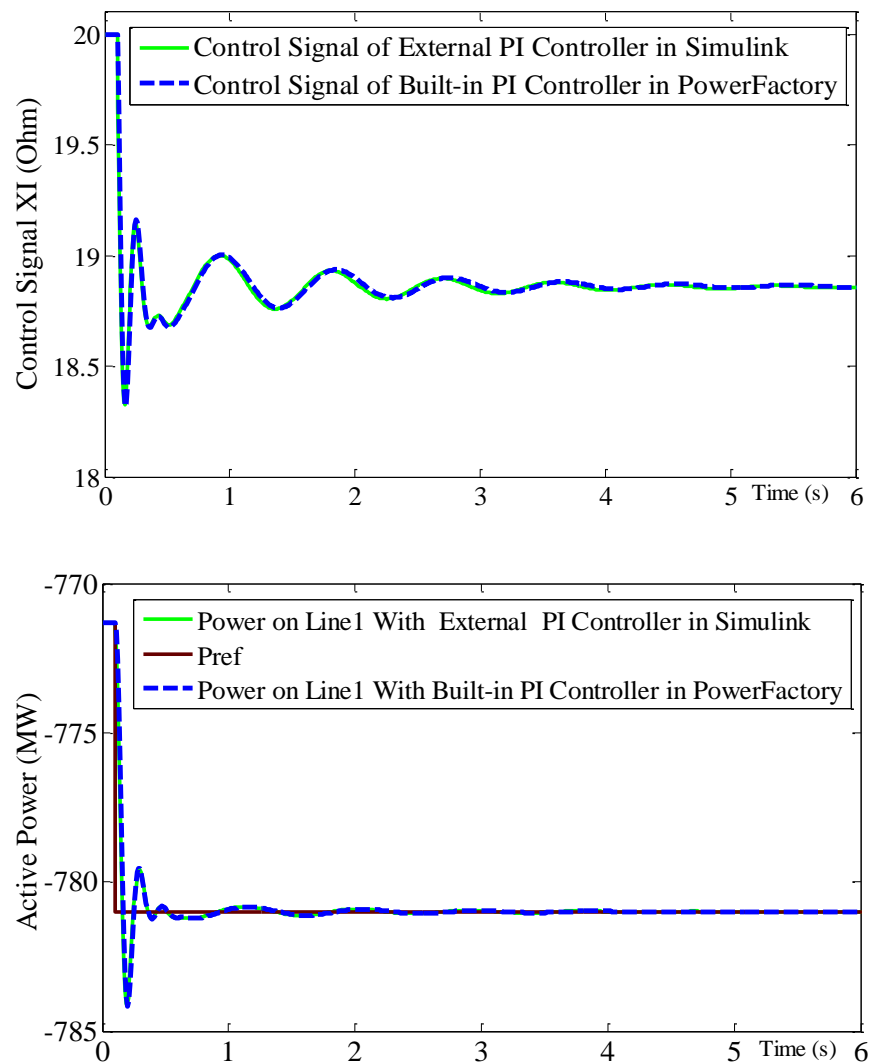


Figure 4.7: Comparison of built-in and external PI controller performance

4.9 Concluding remarks

The necessity for the stability control system to guarantee coordinated and optimal dynamic performance of the power flow controller devices in a large integrated power system such as the GB transmission system has been described in detail in this Chapter. Furthermore, a hierarchical framework for the future stability control system was proposed in order to enhance stability and push the stability limit beyond the thermal limits under all the operational conditions as follows:

Implementation of security constrained dispatch program:

- To ensure that the power flows observe all constraints.

Implementation of the SCS for the best stability and dynamic performance:

- To satisfy all thermal, stability and voltage constraints by following the optimal power flow solution obtained from the security constrained dispatch program.
- To control the inter-area swing and increase the synchronising power utilising TCSC and HVDC link as an actuator in a feedback stability control system.

Implementation of the OSA as a predictive special protection:

- To manage the generator intertrip as the final special protection action.

In addition, the requirement for interfacing Matlab/Simulink to PowerFactory is presented and validated in this Chapter.

Chapter 5

Principle of the Sample Regulator control

5.1 Introduction

As previously discussed in Chapter 4, it is essential that the GBSO maximises the use of existing transmission lines by operating them closer to their thermal limits, improving the stability limits to avoid constraining some generation plants, particularly renewable generation across the B6 boundary. Therefore, National Grid is implementing a huge program of investment i.e. circuit conductor upgrades have been ongoing in the last few years and new transmission technologies such as the TCSC and the embedded HVDC links down the East and West coast are coming into operation in the GB system by 2016 and 2018 respectively. To that extent the network in this area will comprise many types of new and automatic control devices[138][147].

Without thorough analysis, there is a risk of interaction between various control devices i.e. the interaction between POD controllers from SVC and HVDC links, interaction between devices with flow control, such as the West coast HVDC link, affecting the regulation of the future East coast HVDC link. Ultimately, these power flow control devices could potentially affect system stability. Without investment in a supervisory stability control system some of the potential advantages of these costly reinforcements on the transmission system could be lost. Consequently, this will result in constraining the output of renewable energy sources, which ultimately increases the operating costs of the UK electricity system. Therefore, a stability control system is required to guarantee the optimal dynamic performance and coordination of power flow control at pre-fault enhancing the stability limit at post-fault in such a large integrated power system.

A framework for such a feedback control system to enhance system stability was proposed in Chapter 4. Also, the role of the proposed stability control system within the entire National Grid control systems was outlined in the previous Chapter 4 [136].

Following that the Sample Regulator control design method is introduced in this Chapter for the design of the feedback stability control system.

5.2 Feedback control system design

This Chapter focuses on the technical development of fundamental feedback control systems. Before further development the term controller, as used in this Chapter, should be explained first. Although, being regarded as ‘controllers’ in power systems, devices such as phase shifters, SVC, TCSC and HVDC links in a control system are regarded as actuators. Therefore for the purpose of control system design the above mentioned devices are named actuator in this Chapter. The controllers used in this study refer to the devices that produce the control command signals based on various system measurements. Actuators carry out commands from controllers that are either built within the actuators or are external.

5.2.1 Primary and secondary control system

The overall control strategy and a hierarchical stability control system structure are outlined in Section 4.5. Thermal and voltage security are provided by the security constraint optimal dispatch program (known as future EBS) under a normal operating point whereas the feedback SCS enhances the system stability and avoids as much as possible the use of generator OTS. Finally, special protections such as OTS are deployed based on the OSA assessment as the last defence to stability enhancement.

This section focuses on the design of the feedback stability control systems. In general, for the GBSO there are three options for type or structure of the control system design.

1. Utilising internal control systems within actuators, e.g. SVC, TCSC and HVDC link.
2. The POD compensation feedback loops added to the actuators as an auxiliary signal.
3. Cascade control systems incorporate a secondary control system to further enhance the primary control systems within the actuators.

Similar to PSS, POD is only a complementary control system, which could be incorporated into either type (1) or (3) by adding an additional feedback signal.

Therefore, type (2) is not considered as a separate control system configuration here. For that reason, the two following configurations are discussed in this Chapter.

- A single-level control by utilising the internal controllers.
- A cascade control by introducing an additional secondary controller on top of the primary internal controllers.

5.2.2 Requirements for the feedback control system

Internal control systems may be able to provide certain functions to the feedback control system within the SCS if there is a built-in controller within the actuator. Internal controllers are primarily required to perform rapid pre and post-fault voltage and power flow regulations and oscillation damping control.

Cascade control is often used for servo-control systems where the primary control can regulate the controlled variables around command points and the secondary control can manipulate these commands for better trajectory tracking. In such a cascade system the regulation can be separated from the command optimisation with primary and secondary controls set to different regimes and control at different speeds.

Although both options can be developed into either Single Input-Single Output (SISO) or Multi-Input and Multi-Output (MIMO) control systems, internal controllers from manufacturers are usually based on the SISO design and tuned only for a single control variable. SISO design may be sufficient for the cases where the individual controls are near ‘optimal’ on their own, and variables under control in the system are relatively uncoupled.

The built-in SISO controllers will not be able to coordinate several individual actuators and control all outputs coherently to meet the overall SCS objectives as a whole in the feedback control system. With the presence of interactions the overall system stability and control performance can be severely compromised. Similar to linearity, interactions in a real system may depend on the system operating conditions. Within power systems, planned or unplanned outages may change the interactions between control variables and this can be fairly rapid and severe. In these cases, the control systems designed based on the SISO approach will be challenged.

For the SCS research, it is desired to investigate the feasibility of a control system that can take care of the needs of all control systems such as those of SVC, TCSC and the HVDC link with their associated POD control, at the same time and under the same framework to make the control from various actuators in the system to be coherent. Therefore, a MIMO control design approach would be required in order to meet these objectives. The MIMO controller used for SCS is desired to address simultaneously the issues of:

- Stability
- Coordination
- Optimisation

Both single-level and cascade control systems can be designed for either SISO or MIMO systems. For the SCS MIMO feedback control system, if using the single-level control, the built-in controllers would need to be replaced by the corresponding part of the MIMO controller, while for cascade control, secondary control could be developed directly to be part of the MIMO controller.

5.2.3 Multivariable feedback control system overview

The dynamics of actuators can either be considered as part of the Controller or combined together with the rest of the power system in the block diagram shown below in Figure 5.1. In this block diagram:

- y_{i0} , are set-points of respective controlled variables.
- y_i , is the actual controlled variables (e.g. power flow on circuits i , or voltage on bus i).
- u_i , the controlling variables in channel i .

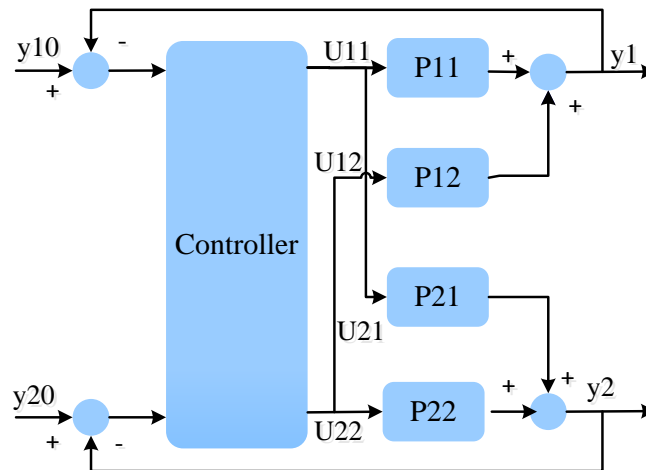


Figure 5.1: Structure of MIMO controller

The multivariable controller is represented by the block *Controller* and the system dynamics are represented as P_{ij} (with or without actuator dynamics). The block diagram shown in Figure 5.1 is a 2x2 MIMO system and input/output variables and control variables are expressed in vectors as (y) and (u) . The corresponding state transition functions are matrices with appropriate dimensions.

5.3 Multi-variable control system design methods

There are two main approaches in the design of a multivariable control system; the non-parametric control system design method and the parametric (model-based) control system design method. In contrast to the parametric approach, one clear advantage of the non-parametric approach is that the complexity and dimensions of the problems do not increase with the size of the network and details of dynamic models represented in the analysis.

Based on the time domain approach, Åström has introduced a class of sampled integral regulators and ensured stability of the closed loop systems with their designs in a series of developments [148][149][150]. These design methods are developed for unknown systems and it is based on the system open loop step responses. This approach therefore is termed as ‘non-parametric’, which is in contrast to any model based or ‘parametric’ methods. Since the models are non-structural time responses, these algorithms can be applied to the design of control systems for large, nonlinear and complex power systems

without any need to simplify the model. However, the trade-off to the dimensionality in the non-parametric approach is the length of the time series that would be needed to capture a dynamic process. For a parametric approach, when stability is obtained using system simplification, it is critical to justify the validity of a reduced model to the original system, while in the non-parametric time response approach an estimate of the truncation errors can be established with relative ease. Between these two approximations, quantifying the impacts of structural simplification can often be a more open problem than formulating the truncation error from a well-constructed sequence.

The ‘black box’ or ‘input-output’ approach adopted in the feedback control system design has been a traditional engineering practice. For example, the Nyquist theorem is the foundation of stability analysis for linear systems based on the frequency domain analysis. Successes were achieved in 1960-80’s in generalising the Nyquist method from SISO to MIMO [151]. However, the time domain approach has been attracting more attention due to its suitability to direct computer implementation.

Also, compared to the frequency domain analysis approach, such as modal analysis/pole placement or the state feedback algorithms, which are often used for PSS tuning, the time domain design approach is more suitable for computer implementation and results can be directly interpreted to meet the GB SQSS [15].

In this research the proposed SCS should be able to be applied to the full GB system with its full dynamic model representation. Therefore, a non-parametric approach is chosen here.

Åström’s work has been extended by many researchers, particularly Lu and Kumar [149] and Mossaheb [150]. Later it has been extended to MIMO controller for non-monotonic and uncertain systems.

Developments of the aforementioned Sampled Regulators have paved a novel approach to the designs of computer controlled systems, achieving both stability and optimality by exploring the time domain input and output properties of an unknown system. In addition, discrete control laws are more applicable to the computer control system design. In order to coordinate several different types of actuator devices with their internal control systems in the GB transmission system, the system control would

require a computerised system controller to command the individual actuators. Also, this system controller must be designed in view of the GB transmission system in its entirety.

In this research, the main focus has been on the control of automatic devices such as the SVC, HVDC link and TCSC, which will be commissioned to deliver the solutions to the GBSO ‘2020 Gone Green scenario’ [6][152]. The full GB transmission system model will be used in the study to investigate the feasibility and capability of this non-parametric approach for the feedback control system design, which will form the core of the overall SCS strategy.

The overall SCS development would also need to be fitted into the existing GBSO control system, computer systems, and the communication framework. The existing IEMS system is situated at the Electricity National Control Centre (ENCC) and system operation is via a centralised control system. Therefore, the SCS setup is also lined up with a centralised control strategy. The alternative of a decentralised control system is beyond the scope of the current research.

5.4 Theory of the multi-variable Sampled Regulator control design method

This section will introduce the fundamental techniques of a stabilising Sample Regulator (SR) control system design method. The non-parametric approach applied to the power system coordination problem is a sampled Multi-variable control law, which is based on the principle of a passivity energy system to ensure the closed loop system stability [148][150]. The SR controller algorithm, which is explained below, is particularly formulated for computer implementation.

5.4.1 Introduction

With slight extensions from the original integral sampled regulators, the general form of the feedback control law that we shall explore further can be written as follows:

$$u(nT) = C_P \Delta e(nT) + C_I e(nT) + C_D \Delta^2 e(nT) + \sum_{r=1}^n b(rT) u((n-r)T) \quad (5.1)$$

Where $e(nT) = (y^0(nT) - y(n)T)$,

$$\Delta e(nT) = (e(nT) - e((n-1)T))$$

$$\Delta^2 e(nT) = (e(nT) - 2e((n-1)T) + e((n-2)T)).$$

It is clear that this class of Sampled Regulators is an extension of the traditional PID control law (in the discrete form) where it is essential to incorporate additional control terms of u_n in order to achieve both stability and dynamic performance in this formulation. In essence, stability of this class of Sampled Regulators is achieved through the construction of the invertible sequences of the closed loop system transfer function.

This Chapter mainly focuses on the theories of this class of Sampled Regulators. We shall review the stability design method, which was established originally for a class of generalised integral regulators [148][149][150]. Following that the applications of this class of Sampled Regulators to the power systems will be presented in the second part of this Chapter.

5.4.2 Assumption, notations and definitions

Consider a stable time invariant MIMO plant (P) and assume it can be linearised around the neighbourhood of its operating point [150][138].

The time response of this system is denoted as $H(t) = (H_{ij}(t)) \in R^{m \times m}$, where $H_{ij}(t)$ is the step response of the i -th row and j -th column entry of $H(t)$, with $u_j(t)$ and $y_i(t)$ as its input and output, respectively. $u_j(t)$ and $y_i(t)$ are j -th and i -th components of $u(t)$, $y(t) \in R^m$.

Since (P) is assumed to be stable and can be linearised at its operating point for the linearised system, its step response is bounded exponentially. In terms of a pair of parameters $K, \beta > 0$, and with any matrix norm defined on $R^{m \times m}$ that is induced from the measure of linear vectors defined in R^m , this bound can be expressed as $\|H(t) - H(\infty)\| \leq K \exp(-\beta t)$, $t \geq 0$.

The relationship between the output and the input of the linearised plant can be expressed in terms of the system impulse response, h , as $y(t) = h(t) * u(t) = \int_0^{\infty} h(s)u(t-s)ds$, where ‘*’ denotes the convolution operator.

In the discrete form with the sampling rate of T , as shown, in the Åström work [148], this input-output relationship of a linear system can be written in terms of its unit step response:

$$y(nT) = \sum_{r=1}^n \Delta H(rT) u((n-r)T) \quad (5.2)$$

where $n=0, 1, 2, \dots$, $\Delta H(rT) = H(rT) - H((r-1)T)$ with $H(rT) = 0$ for $r \leq 0$. The input vector $u(t)$ is defined as:

$$u(t) = \begin{cases} 0, & t < 0 \\ u(nT), & t \in [nT, (n+1)T) \end{cases} \quad (5.3)$$

Since the sampling rate (T) is a fixed parameter, it is therefore dropped for simplicity. In the sampling signal sequences, numerating subscripts are used instead of the time argument in the subsequent development in this Chapter. For example; (5.1) and (5.2)

can be rewritten more concisely as: $u_n = C_P \Delta e_n + C_I e_n + C_D \Delta^2 e_n + \sum_{r=1}^n b_r u_{n-r}$ and

$$y_n = \sum_{r=1}^n \Delta H_r u_{n-r}.$$

In these equations u and y are vectors, and parameter matrices C 's and b 's have compatible dimensions.

The linearity of the model implied in the unit step responses of $\{H_n\}$ can be understood as the result of the linearisation around an operating point of a nonlinear system. Curly bracket $\{.\}$ denotes either a truncated or an infinite sequence of time series with its elements at a particular time instance of proper dimensions. In the case of a power transmission system, a full system model may contain any dynamic and nonlinear characteristics of generators and control devices (including both controllers and

actuators). At a feasible operating point, the conditions required for linearisation must be clearly satisfied.

Stability in this Chapter is defined in the sense of Lyapunov. For non-linear systems, the stability conditions required in the design ensures the ‘bounded-input and bounded-output’ stability of the closed loop system. When a power system is subject to a short circuit fault with the subsequent fault clearance, the disturbance is of finite energy, hence is a bounded input in that sense.

5.4.3 Stability of the Sampled Integral Regulators

Chronologically, three design approaches that we are most interested in have been developed by Åström in 1980, Lu and Kumar in 1984, and Mossaheb in 1987 respectively. The closed loop stability has been proved for a class of linear integral regulators in this sequence of developments.

Since the development by Lu and Kumar established a general form, where the originating work of Åström can be included as a special case, this approach ensures overall system stability by requiring all roots of the Z-transform of the closed loop character equations to be bounded within the unit disk on the Z-plane.

The design method by Mossaheb is based on a less conservative approach where system passivity is established, which is referred to as passivity method in this Chapter [150]. In a particular parameter selection, further optimisation can be achieved; this is explained further in section 5.4.4.

5.4.4 Passivity method

For the class of Sampled Integral Regulators in the form of (5.4), Mossaheb [150] has developed a design method that ensures system stability by making the closed loop system ‘passive’ [150].

$$u_n = C(y_n^0 - y_n) + \sum_{r=0}^n b_r u_{n-r} \quad (5.4)$$

Lemma 1: Passivity Design - Stability Theorem

It has been established that with the selection of the parameter sequence $\{b_n\}$ such that $b_0=0$, $b_n=C\Delta H_n - \varphi_n$, ($n \geq 1$), then from (5.2) and (5.4) the closed loop transfer functions $y^0 \rightarrow u$ can be obtained as $\psi^*u=Cy^0$, where $\psi = \varphi = \{\varphi_n\}$, $n \geq 1$. Furthermore, if $\{\varphi_n\}$ is selected to be a convex sequence and $\sum \varphi_n$ converges, then ψ is a strictly passive operator. Consequently, the closed loop system that maps $y^0 \rightarrow y$ is stable. It is important to note that the sequence $\{\varphi_n\}$ is termed to be convex if each φ_n is real symmetric positive semi-definite (r.s.p.s.d.) and satisfies $\varphi_n - 2\varphi_{n+1} + \varphi_{n+2} \geq 0$. This has been established in [150].

From this theorem, the design objective for this class of Sampled Integral Regulators is therefore to select a parameter sequence $\{b_n\}$ to make the sequence $C\Delta H_n - b_n$, ($n \geq 1$) be equal to the pre-defined sequence $\{\varphi_n\}$, which is both convex and convergent. One simple example of such a convex sequence $\{\varphi_n\}$ is the sequence of a real symmetric positive semi-definite matrix $\{A, A^2, \dots, A^N, \dots\}$ with $A < I$. By selecting $\varphi_n = A^n$, the closed loop system that is described by φ is then passive.

Property 1: Passivity Design – Zero-Steady-State Criterion

For the selection of the controller parameters $\{b_n\}$ as in Lemma 1 and for a convex sequence $\{\varphi_n\}$, the Sampled Regulator in (5.4) will guarantee the zero-steady-state of the closed loop system given by (5.2) when it is subject to a constant step change, if parameter C satisfies $C = (I + \sum_{n=1}^{\infty} \varphi_n) H_{\infty}^{-1}$.

Remark: With the choice of $\{\varphi_n\} = \{A^n\}$, this condition then is reduced to

$$C = (I - A)^{-1} (H_{\infty})^{-1}.$$

Property 2: Passivity Design – Integrator

For the selection of parameters $\{b_n\}$ as in Lemma 1, $C = (I + \sum_{n=1}^{\infty} \varphi_n) H_{\infty}^{-1}$ is equivalent

to $\sum_{n=0}^{\infty} b_n = I$. In fact $\sum_{n=0}^{\infty} b_n = I$ is the integral operator in the discrete form.

Proof: Sum up the sequence $\{b_n\}$ with its definition in Lemma 1 then applies the expression of C of Property 1, the equality of the sum yields Property 2.

The optimisation of the Passivity design is based on a further Property of Lemma 1, which also helps to the understanding of this control law.

Property 3: Passivity Design – A Two-step Control Law

For a linear system of (5.2) and the Sampled Regulator of (5.4) that is designed using the passivity algorithm with the selection of $\varphi_n=A^n$, the control signal to track a constant step response is a two-step control action:

$$u_n = \begin{cases} (I - A)^{-1} H_\infty^{-1} y^0, & n = 0 \\ H_\infty^{-1} y^0, & n \geq 1 \end{cases} \quad (5.5)$$

Proof: Write out term by term from the definition of the control sequence $\{u_n\}$ in (5.4), and note the assumption on causality of the plant P , one obtains the above result.

There is still a degree of freedom in this design, and the value of A is yet to be determined. Based on the parameters selected as outlined in Lemma 1 and property 1 and property 3, Mossaheb has established the following algorithm [150].

Algorithm 1: Passivity Design - Optimisation

Assume that for a linear system in (5.2) under the control of the Sampled regulator in (5.3) that is designed using Lemma 1 and property 1 and property 3, then when it is subject to a constant step input y^0 , the system mean square tracking error $\sum_{n=1}^{\infty} \|y_n^0 - y_n\|^2$ can be minimised in terms of its trace operator by choosing $A=I-B^{-1}$, with $B>I$ being the solution of the matrix Lyapunov equation:

$$B\Gamma K + K\Gamma B = -(K\Omega + \Omega^T K) \quad (5.6)$$

Where

$$\begin{aligned}
 \Gamma &= \sum_{n=1}^N (\Delta H_n^T \Delta H_n) \\
 K &= H^T_{\infty} H_{\infty} \\
 \Omega &= \sum_{n=1}^N \Delta H_n^T (H_{n-1} - H_{\infty})
 \end{aligned} \tag{5.7}$$

The derivation of this algorithm is given in [150].

It is also important to note that the optimal solution may not always satisfy $A < I$ in this calculation. The existence of an optimal solution however does not affect stability. For stability, sequence $\{\varphi_n\}$ only needs to satisfy conditions of Lemma 1. When an optimal solution exists, this choice of A ensures both stability and the optimal error tracking, hence to achieve the better performance that is featured by decoupling and improved damping.

5.4.5 Algorithm and theorem of passivity design method

The steps for the Passivity design method can be summarised as follows and shown in Figure 5.2:

1. Choose a sampling control period T and obtain the unit step responses of $\{H_n\}$
2. Truncate time series sequence at the N^{th} term;
3. Obtain an optimal real symmetric positive semi-definite parameter matrix A , according to following equation :

$$A = \left[\sum_{n=1}^{\infty} \Delta H_n (H_{\infty} - H_n) \right] * \left[\sum_{n=1}^{\infty} \Delta H_n (H_{\infty} - H_{n-1}) \right]^{-1}$$

4. Calculate $C = (I - A)^{-1} (H_{\infty})^{-1}$ to ensure the zero-error and de-coupled steady state.
5. Calculate $\{b_n\}$ with $b_0 = 0$, $b_n = C \Delta H_n - A^n$, $n \geq 1$.
6. Then implement the control law of (5.4).

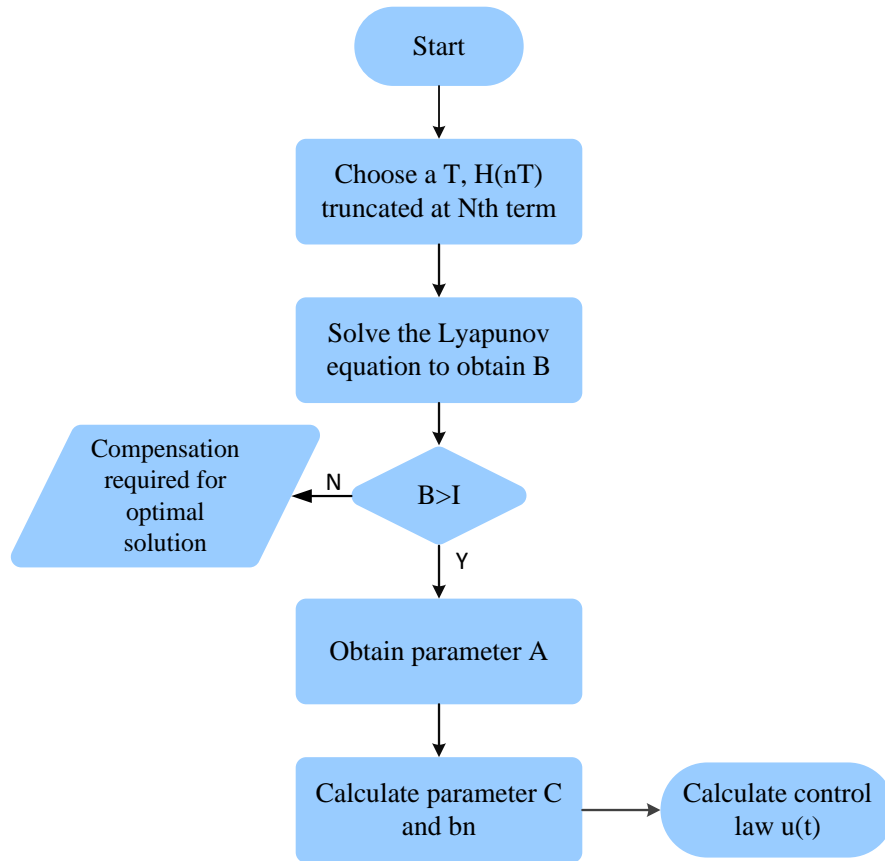


Figure 5.2: Algorithm of Sample Regular design method

5.4.6 Discussion on main features of the SR control.

As for any non-parametric approaches in general, in the design of this class of Sampled Regulators the dimension of the control system is only determined by the number of the controlled variables rather than that of the state variables in the system. In a HV transmission system, there can be as many as several thousand state variables, while there are only a few stabilising control devices, such as HVDC link, TCSC and phase shifters. Therefore, the number of controlled variables of these devices is not in excess of dozens.

In contrast to the heuristic PID design methods, the stability of the closed-loop control system with the proposed regulator is guaranteed meanwhile, the minimal interaction and optimal responses during transient periods are achieved by the optimisation in terms of the system tracking errors.

Stability of the design is independent of the sampling time. However, control can be realistically implemented by a proper choice of the sampling time T in order to refrain the control signal to be within the physical limits of actuating devices. However, the larger the sampling time, the more sluggish the control is.

Also, this algorithm could be further developed into an adaptive self-tuning on-line control algorithm. The self-tuning implementation of this regulator is to address changes in operating conditions and system configurations. It is noted that although the requirement of an open loop system time response implies the open-loop stability of the system, this does not limit this class of regulator to be useful to the power system control, since the intact power systems should be stable at a physically feasible operating point even without the flow control.

5.5 Comparison of the linear characteristics of the actuators under control

The controller behind the actuator sees the plant model through these actuators. If the plant model is compensated by these actuators to become linear, the linear system design techniques can be applied. If the linearity holds for a wide operating range, the linear control design can be expected to be robust through the entire operating range.

For the research into whether the control system development is the best fit for these actuators, in this section, the linearity of the systems under the control of the TCSC, the HVDC link and SVC are investigated and compared which reveals essential information that forms the basis of our control system design. To investigate this, the SMIB test system 1, test system 3 and test system 5 introduced in Chapter 3 are used respectively.

5.5.1 Characteristics of the TCSC as an actuator

Under the TCSC control, in test system 1, if we inject a step input of XI in a regular incremental level into the system, we can obtain the step responses in power flow of the system under the TCSC control. It is observed in the study for the TCSC case, as presented in Figure 5.3, when the step change of XI decreased from 18 Ohm to 13 Ohm in the regular steps of 2 Ohm, the power flows on the controlled circuit show increasing nonlinearities. (The base case start from $XI=20$ Ohm)

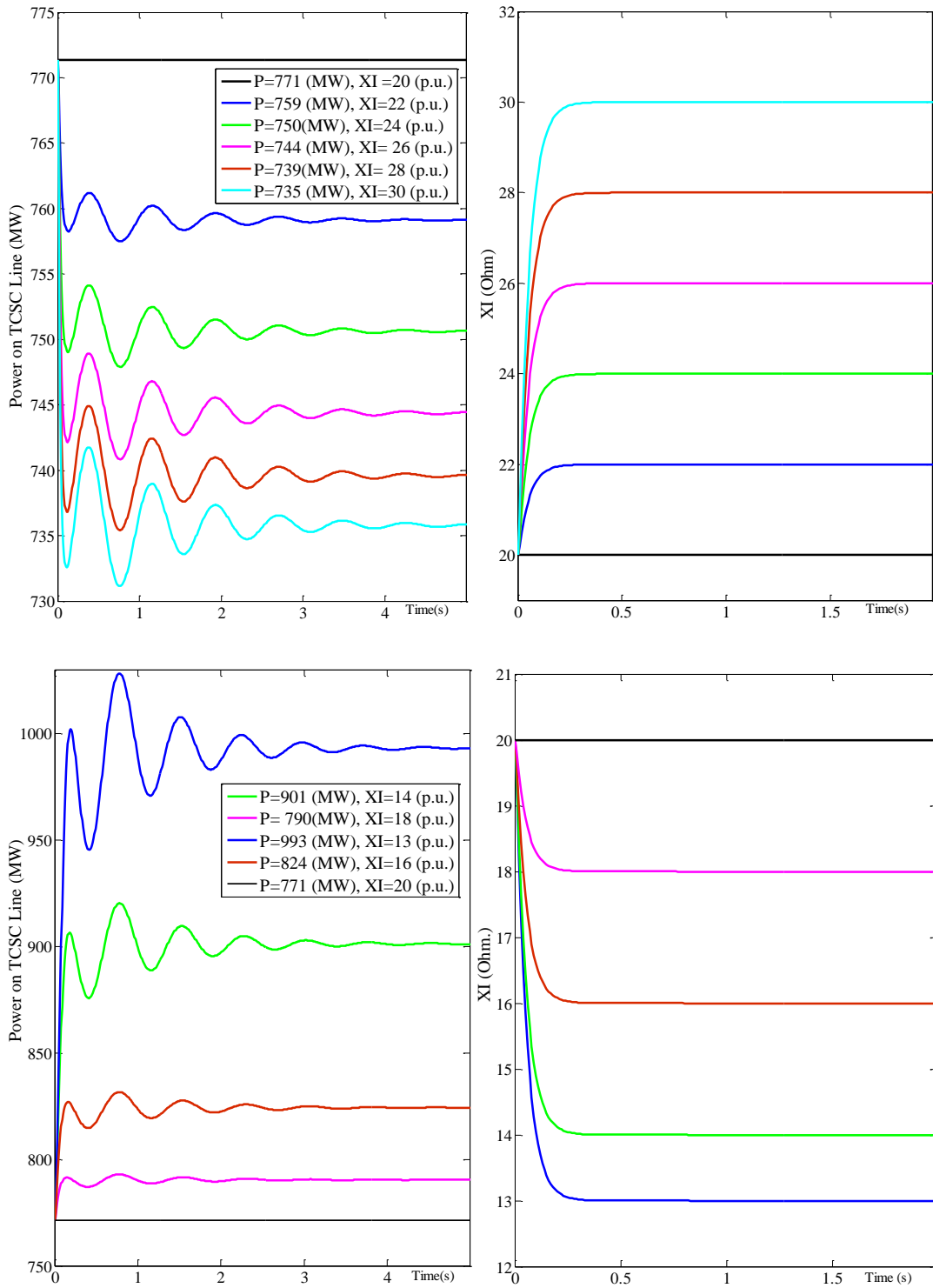


Figure 5.3: TCSC step response

5.5.2 Characteristics of the HVDC link as an actuator

In the case of the HVDC link, using the test system 3, we inject the step changes to the power set-point of HVDC link and obtained the step responses of power flow on the HVDC link as shown in Figure 5.4. Starting from the current operating point of 500MW, increasing up to 1000MW. The results show a consistent linear behaviour. When the power on the HVDC link is decreasing, the nonlinear characteristic starts to appear when the flow is decreased below 300MW. Please note that, this is an observation based on the simulation results, not a generic conclusion.

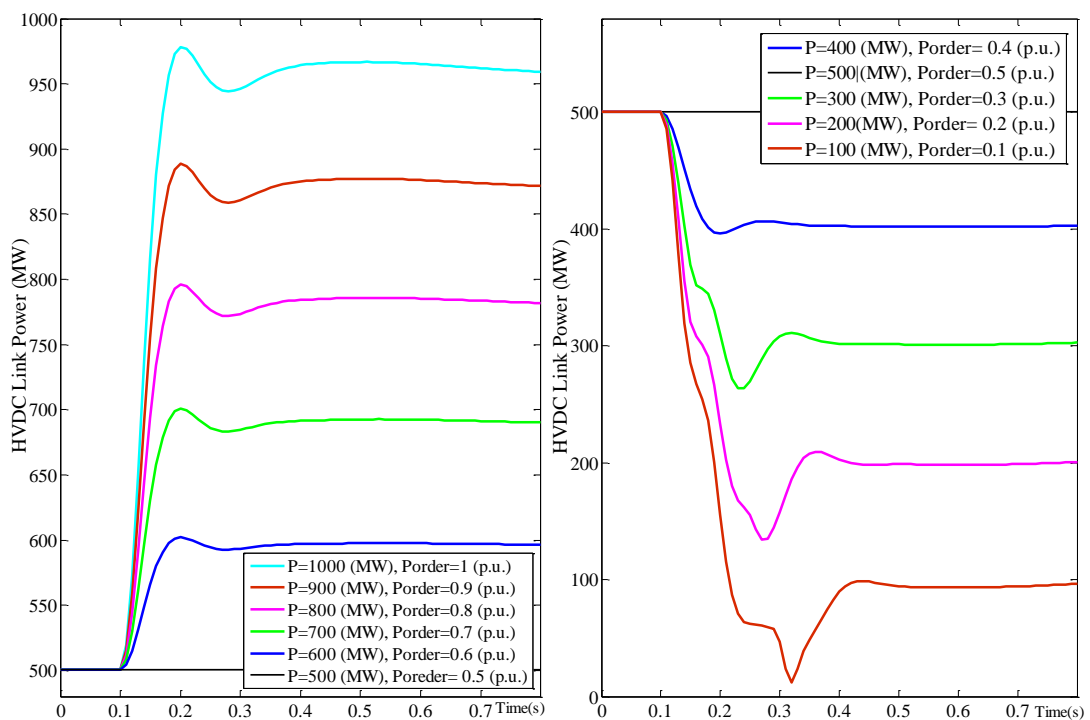


Figure 5.4: HVDC link step response

5.5.3 Characteristics of the SVC as an actuator

The relation between V and B is approximately linear. As shown in (5.8) as long as it is within the droop characteristic range.

$$Q = BV^2 \tag{5.8}$$

Figure 5.5 shows that the change of reactive power, voltage and B of the SVC are reasonably linear within the normal voltage regulating range of the device.

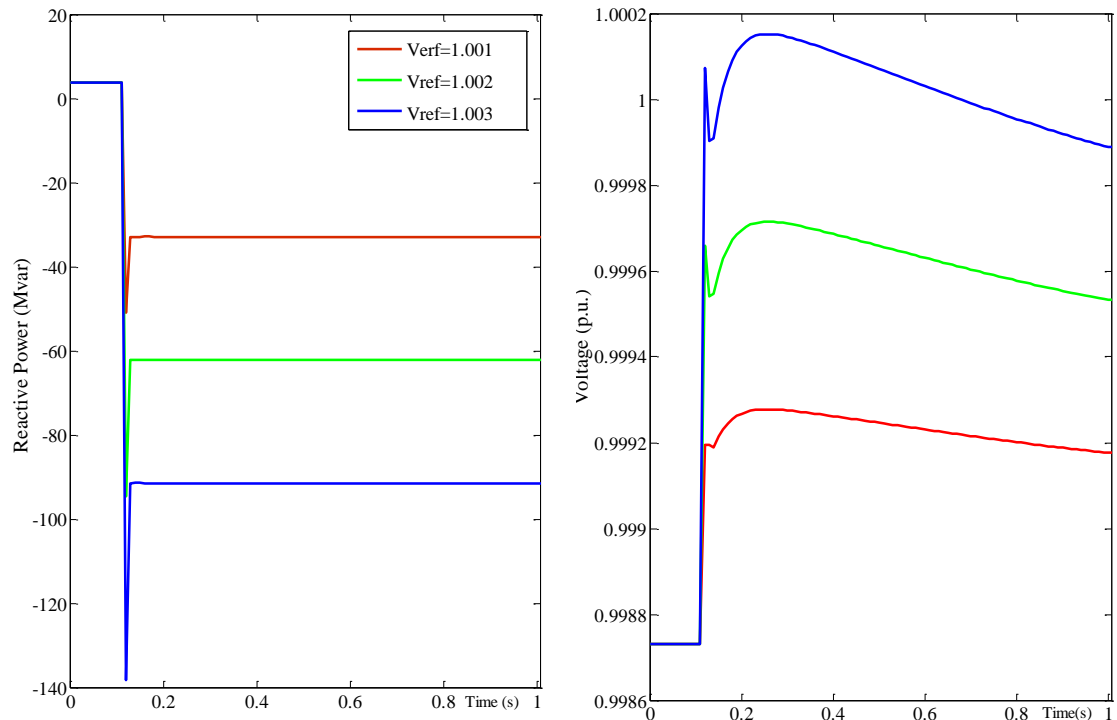


Figure 5.5: SVC step response

5.6 Implications to the stability control system design

The HVDC link as an actuator for the flow regulation can provide a wider linear range of operating points than that of the TCSC. This implies that the control design using the HVDC as an actuator can be more robust for the wider operating ranges without needing to retune the parameters. In fact the linear behaviour presents over the entire increasing operating range of this type of HVDC link. Some preliminary work has demonstrated the advantages due to the HVDC link linearising property in our proposed Stability Control System post-fault strategy. Also, a characteristic of the SVC, within the designed range of voltage regulation, shows a good linear relationship between susceptance (B) and voltage at the controlled bus.

5.7 Considerations affecting the stability control system

For a fault that has occurred directly on the equipment in the primary part of the transmission system e.g. on the HVDC link, it is clear the feedback control system would no longer be capable of functioning as designed. These cases would be considered in the overall SCS and secured by the special protection actions.

5.8 Application of SISO SR control in the stability enhancement

Two study cases are presented in this section (study case 1 and study case 2). The first study case demonstrates the performance of the SISO SR control for the TCSC and the second study case shows the performance of SISO SR control for the HVDC link.

5.8.1 Development of a SISO SR control for the TCSC power flow control (Study case 1)

As previously explained in Chapter 4.7.2, interfacing between Matlab and PowerFactory allows the full exploitation of both packages' capabilities. As a result the various control functions available in the Matlab program can be implemented with the fast and powerful modelling and simulation capability of the PowerFactory simulation tool. In fact, the model or codes in Matlab/Simulink represent the model and algorithms of the external controllers while the PowerFactory model represents the power system. In this research, the interface capability of Matlab and PowerFactory is implemented for the design of the MIMO SR controller. The overall structure of the interface for the SR controller design is presented in Figure 5.6. Since there is no continuous dynamic model in the SR control law, Simulink is not required in the simulation. The discrete SR control algorithm is implemented in an m-file. The definition of all the required variables, inputs and outputs are critical in interfacing Matlab with PowerFactory and a single common definition block in PowerFactory defines all signals as shown in Figure 5.6. The Matlab control slot shown in Figure 5.6 represents the external SR controller in PowerFactory's composite model. This slot defines all inputs from the power system in PowerFactory to the controller in Matlab, which in this case is active power (P) on the TCSC line, and outputs from the Matlab controller back to PowerFactory, which in this case is XI as depicted in Figure 5.6. In addition, a counter (t) is required to coordinate the simulation steps between PowerFactory and Matlab.

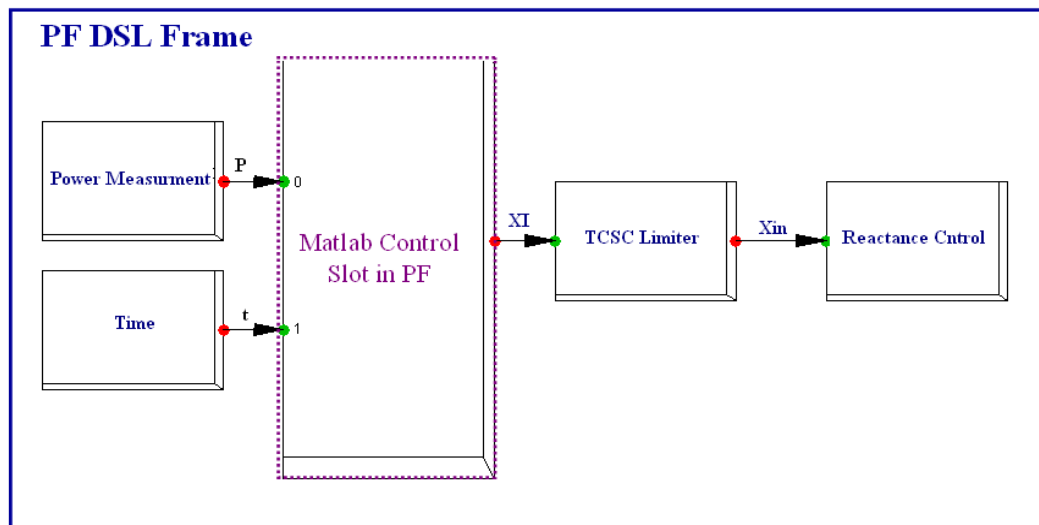


Figure 5.6: Structure of the Interface for SR Control design in PowerFactory

5.8.1.1 Open-loop step response for design of SR controller

For the design of the SR controller, only the knowledge of the open-loop unit step response is required. In this example, the open-loop unit step response is obtained at the steady state operating point with a sampling rate (T) selected to be $T=0.01$ s and then the open-loop response is truncated at $N=2000$.

It is noted that although the stability of the design is independent of T , the magnitude of the control signal is related to T . Therefore, the physical limitation of the actuator can be met by the correct selection of T . An open-loop unit response informs how much the output of the open loop system will change when the input changes by 1 of whatever the appropriate physical unit. In this example, where the TCSC is acting as an actuator in the closed loop control system, the control variable is the reactance of the TCR branch and the system output is the active power on the TCSC line. In fact the active power on the AC line is regulated by varying the reactance of the series reactor. In practical application, the Least Square Method can be implemented along with introducing a Pseudo Random Binary Sequence (PRBS) signal in order to update the system open-loop step response continuously without interrupting the normal closed loop operation [153]. In this study the open-loop step response of the system (Matrix H), depicted in

Figure 5.7, is simply obtained by sampling the active power on the TCSC line when the reactance of the TCSC (XI) increases by 1 Ohm.

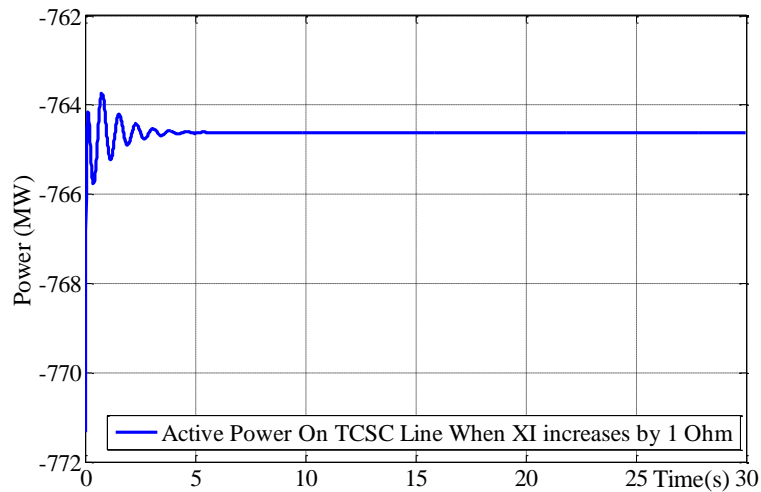


Figure 5.7: Unit step Response of the TCSC line for SR Controller Design

5.8.1.2 Test system

A SMIB test system1 shown in Figure 4.4 is used for this study case. In this model, as explained in detail in Chapter 3, one of the AC lines is equipped with a TCSC, where the initial FSC is 30% of the total line reactance. The TCSC can provide up to 75% compensation to the total reactance of a single line route by changing the reactance of the TCR. In this study case, the performance of the SISO SR controller for the TCSC line is compared with the PI controller. In fact, the designed SR controller provides the control signal (XI, reactance of TCR branch) in the case when the SR controller is used for regulating the power on the TCSC line. Therefore, the active power flow of the TCSC line is the controlled variable, which is fed back to the SR controller for modulating the TCSC's reactance.

5.8.1.3 Simulation results and analysis on study case 1

A comparison study is performed between the PI controller as an internal controller and the SR controller as an externally designed controller using the Matlab interface. The available PI controller block in PowerFactory was used for the model of the PI controller, whereas for the SR controller, which is a user defined controller, it is implemented using Matlab. It is important to note that both PI and SR controller are optimised and their performances are compared when both are working to their

optimised parameters. The selected optimal tuning parameters for PI controller are shown in Appendix C.

In both cases the TCSC physical limits are included. A small change of the TCSC set-point (P_{ref}) at $t=100\text{ms}$ as shown in Figure 5.8.b was applied to avoid exceeding the limit of the TCSC reactance. Following the change of the set-point (P_{ref}), the error between measurement and set-point becomes non-zero. The SR as a controller tries to minimise the error between the measured power on the TCSC line and the set-point by regulating the reactance of the TCR branch. Hence, the controller calculates the optimal control signal (XI) at each simulation step (every 10ms) in Matlab for the best dynamic tracking of the set-point. Consequently, a change of the TCSC's reactance, in this instance, results in increasing the power on the TCSC line by roughly 10 MW. The results in Figure 5.8 show the difference in performance of both controllers in generating the control signal. It can be seen in Figure 5.8.a that the SR generates one control signal immediately after the change of the set-point whereas the PI controller shows more control effort in the subsequent oscillations. Therefore, the XI is more oscillatory using the PI compared to the SR controller. Although the PI controller can provide tighter control, in terms of reference tracking, on the line under the TCSC control, it can be seen from Figure 5.9 and Figure 5.8.d that the SR controller provides better performance with regards to the overall system stability. It is evident in Figure 5.8.c that following the change in set-point of the TCSC line, the degree of oscillation induced in the other lines in the system, which are not under control of any controller, such as line 3, is significantly less when the SR controller is implemented. Also, less voltage variation at the TCSC busbar is observed using the SR controller as presented in Figure 5.8.d.

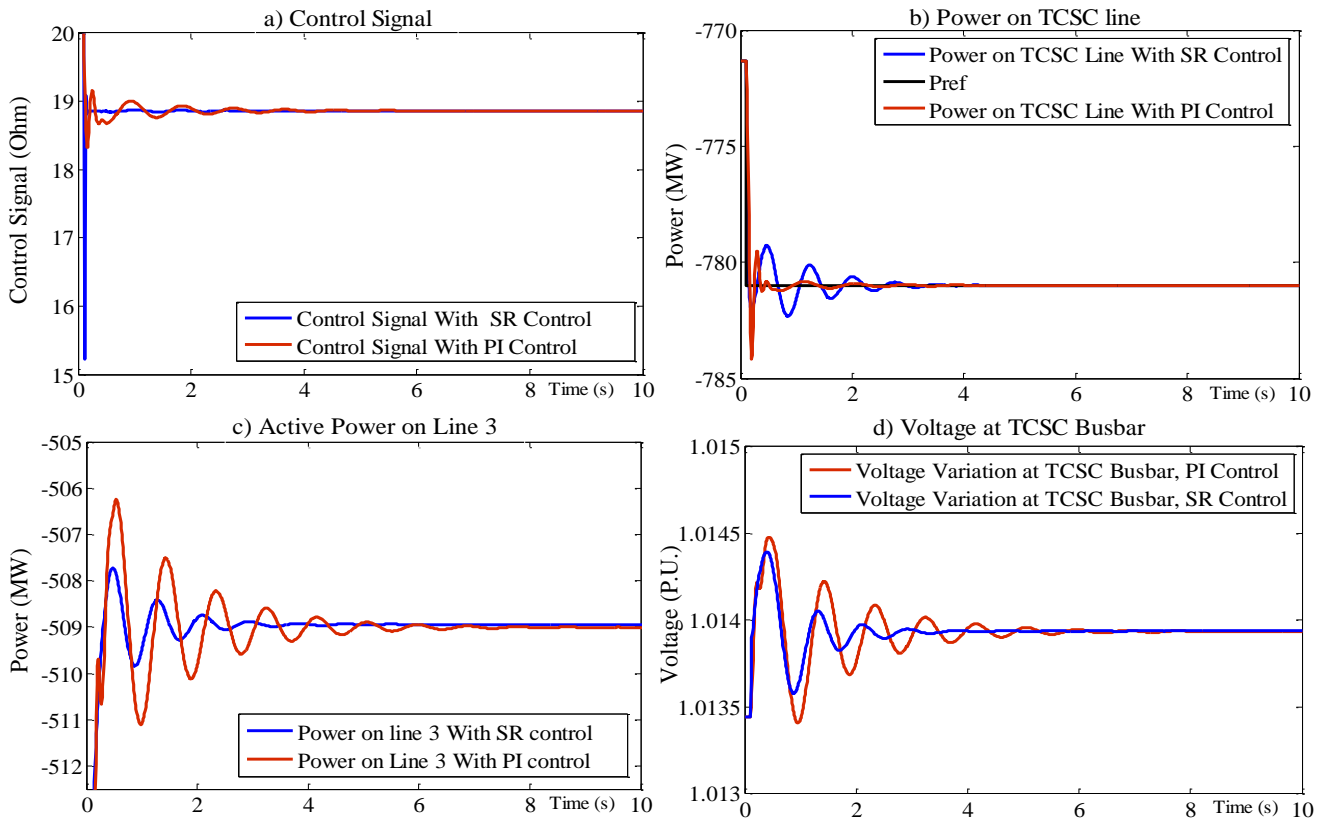


Figure 5.8: Comparison of SR and PI controller Performance

In addition, as presented in Figure 5.9, one can see that the rotor angle oscillation, which is a good indicator of system stability, has greater dampening when the SR controller is implemented instead of the conventional PI controller. All the simulation results demonstrate and propose that, stability wise, the SR controller, when considering the stability of whole system, offers better stability performance in comparison to the PI controller.

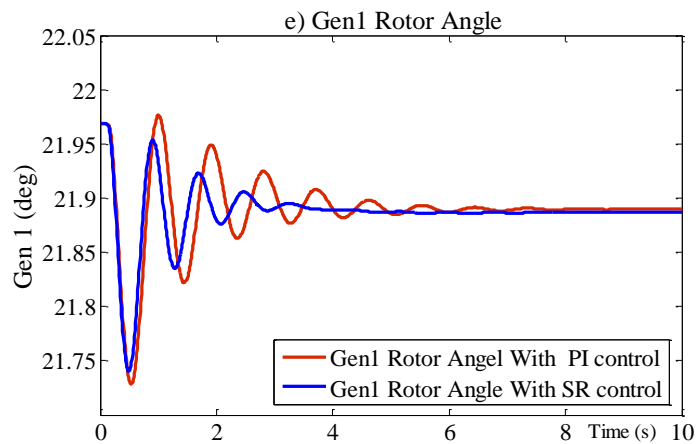


Figure 5.9: Comparison of SR and PI Controller Performance

5.8.2 Development of SISO SR controller for the HVDC link power flow control (Study case 2)

Two sets of tests are carried out to investigate the performance of the SISO SR control for the HVDC link in this section as follows:

- At pre-fault: under normal operating conditions a step change is applied to the HVDC Link.
- At post-fault: when a 100ms, 3-ph fault occurred on one of the two AC transmission lines, and followed by the fault clearance of the faulted line.

The first test is to investigate the impact of the controller by varying the SR control parameters, and the robustness of the SR controller for using the HVDC link as an actuator for flow control; while the second is to test the SR controller design for its fault regulation capabilities, under the proposed transient stability control strategy.

The integration step size of the simulation is 10ms, and the open loop time responses are truncated at 30s of the simulation.

5.8.2.1 Test system

In study case 2, also the SMIB test system 3 with initial transfer level of 1.3 GW including 500MW power flow on the HVDC link, as shown in Figure 3.8 in Chapter 3, is set up to investigate and examine the performance of the SISO SR controller for the HVDC links power flow control. The initial state of the system at pre-fault in presented in Figure 5.10.

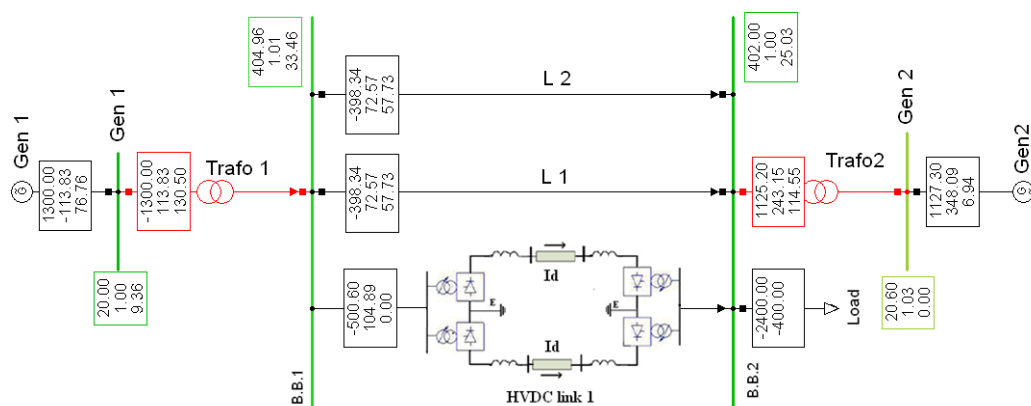


Figure 5.10: Concept proving PowerFactory SMIB test model 3 for study case 2

5.8.2.2 Overall structure of the secondary SISO SR controller for the HVDC link

The overall structure and framework of the SISO SR controller for a CSC-HVDC link is depicted schematically in Figure 5.11. The PowerFactory to Matlab interface facility has been used to extend the capability of PowerFactory for the design of the SISO SR controller. The Matlab SR control slot shown in Figure 5.10 represents the externally designed SISO SR controller, which provides the calculated control signal (U_1) to the HVDC link to track the new set-points and the PowerFactory model represents the power system. The control of the bipole set-point can be set under a single command point.

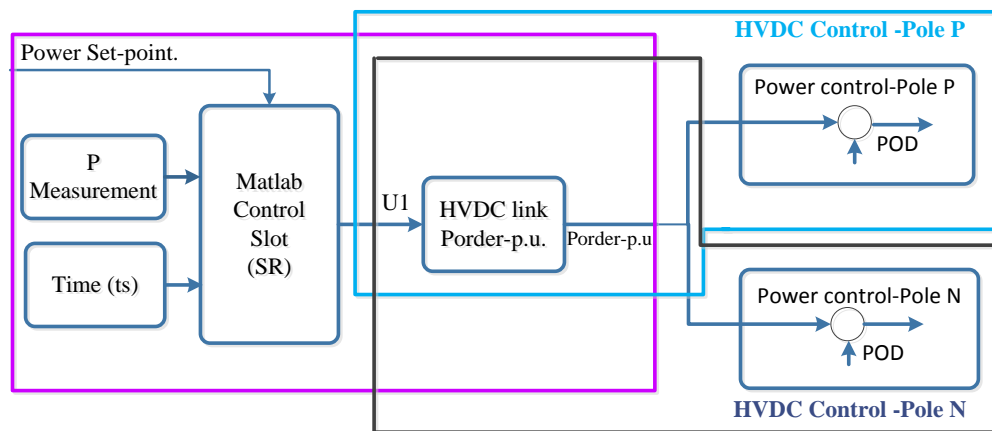


Figure 5.11: Structure of interface for the SISO SR control design for the HVDC link in PF 5.8.2.3 Simulation results and analysis on study case 2

Figure 5.12 presents the dynamic response of the system at pre-fault following a step change applied to the HVDC links set-point from 500MW to 900 MW. It is important to note that in this example the HVDC model is rated at 1000MW.

Also, in this study the impact of the SISO SR controller with various sampling time rates (T) on the system response is investigated. It is important to note that the integration step size for all the simulations in all study cases is 10ms and the open loop time responses are truncated at 30s of the simulation.

The power flow on the HVDC link is shown in Figure 5.12.a where the black line is the set-point of the HVDC links control and the red curve is the time response of the primary internal control system of the HVDC link without cascade control. The other curves show the response of the HVDC link under the SR control with various sampling control rates including 10 ms, 20 ms, 50 ms and 80ms.

It has been noticed that with the internal PI control, there is a small steady state error in set-point tracking when the terminal voltages at the HVDC link end-buses deviate from unity. However, with the SR cascade control this steady state error is eliminated, as shown in Figure 5.12.a. This is because; PI controls I_{order} rather than P_{order} whereas SR design controls P_{order} . Also SR controller guarantees zero steady state by selection of parameters “C” as given in property 1 section 5.4.4.

In fact, Figure 5.12.a shows the optimality of the SR control designed to minimise the sum of the squares of the tracking errors between the set-point and the controlled variable of the HVDC link, which is the power flow on the HVDC link. Although, the squares of the errors are smaller under the SR control with 10ms sampling control rate compared with the dynamic response of the HVDC internal control, the first overshoot is higher. As a compromise, the SR control with a slower sampling control rate of 80ms gives much less overshoot.

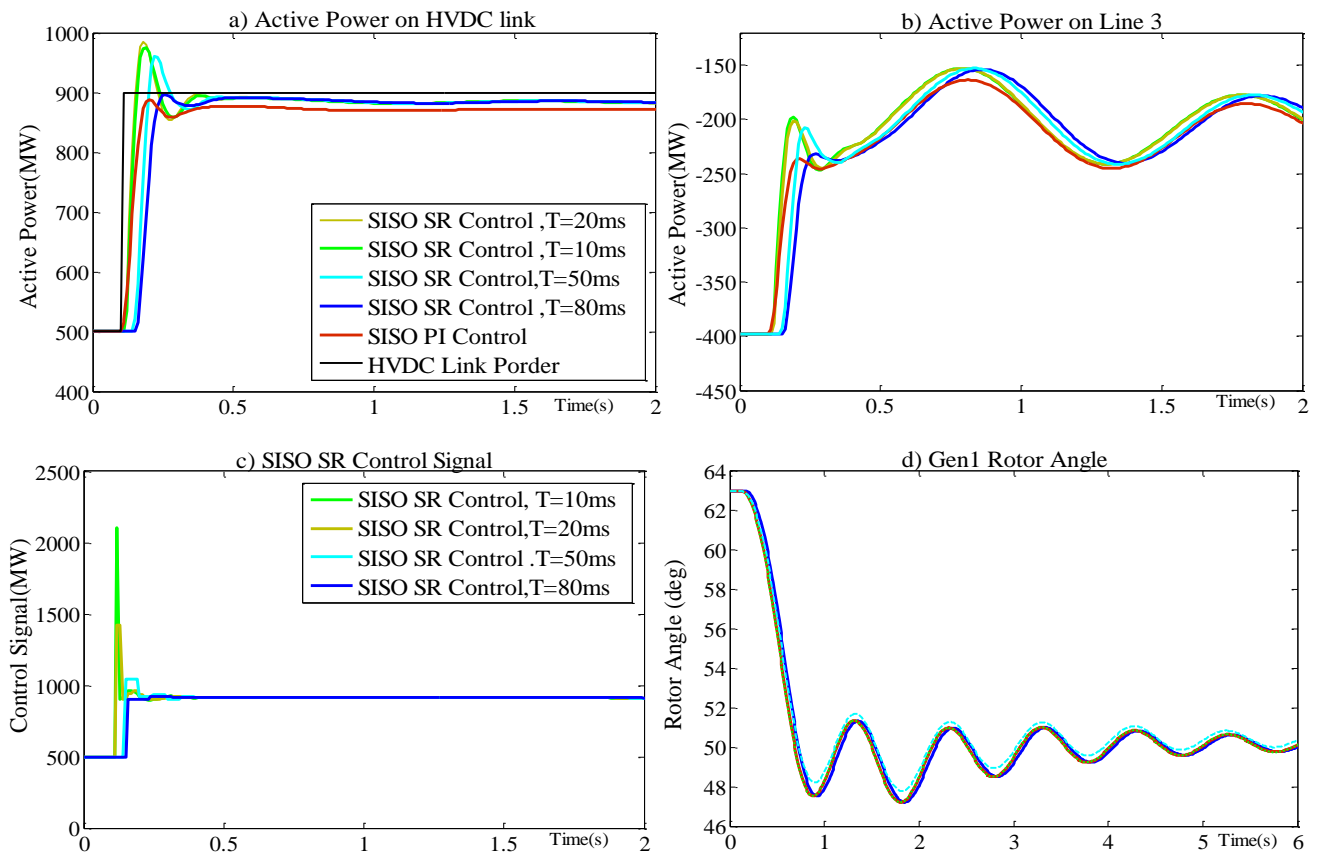


Figure 5.12: Dynamic time responses of the system following a step change to the HVDC link under control of a SISO SR design with different sampling rate.

Additionally, Figure 5.12.c shows the control signals of the SR controller with the same sampling control rates as before. From these results, it is evident that the SR control can be adjusted to produce different levels of control, suitable for the control system performance requirement, while meeting the physical limit of the actuating device.

Moreover, Figure 5.12.b and Figure 5.12.d illustrate the power flows on line 3 and generator1's rotor angle swings respectively, which show that the SISO SR and PI performance is very similar, especially when 80ms sampling is applied.

It is worth pointing out that the stability of the system under the SR control is guaranteed, as long as the system is sufficiently linear with respect to the operating point where the open-loop step responses of the system was measured. In the case of the HVDC link acting as an actuator, the linearity between the input power set-point and its controlled variable, which is the HVDC links power flow, carries over the entire HVDC designed transmission level range, as described in Section 5.4.2

Figure 5.13 presents the dynamic response of the system at post-fault, with the HVDC link controlled by an internal PI controller or the cascade SISO SR control using the SR sampling control rate of 80ms when a three-phase fault occurred on one of the AC lines, followed by the fault clearance at 100ms. This study is to examine the robustness of the SR controller for the power flow control on the HVDC link during the fault occurrence. From the power flow on the HVDC link, shown in Figure 5.13.a, it is clear that not only does the SR controller remain robust in tracking the set-point at post-fault, but also the performance of the SISO SR cascade controller is marginally better than the internal PI controller, which implies that the SR controller can be implemented for the HVDC links set-point adoption at post-fault for stability enhancement. In addition, from both, the power flow on the remaining AC transmission line (Figure 5.13.b) and the generator1 rotor angle swing (Figure 5.13.d), it can be seen that under the SR cascade control the post-fault system is slightly better damped and more stable. Also, it is found that when the control sampling rate of the SR controller increases beyond 80ms the optimal solution of the SR passive design no longer exists, nevertheless the power series that is chosen for the passivity can still be fixed to $B > I$, to reserve the stability that is required in this design approach.

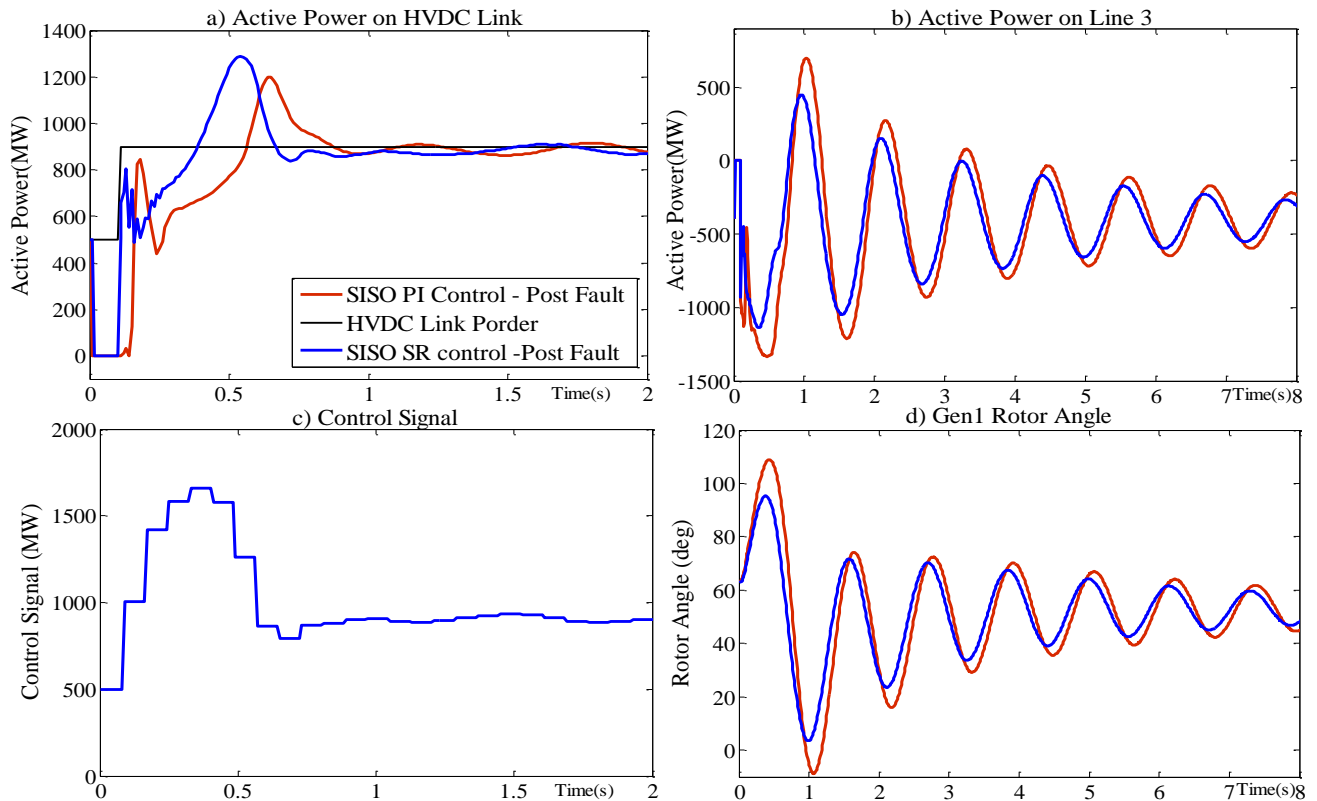


Figure 5.13: Dynamic time responses of the system at post-fault with HVDC link under controls of internal PI controller or the cascade SISO SR control with sampling rate of 80ms

5.9 Application of MIMO SR control for coordinated control of power flow and voltage control devices

Three power system applications of the MIMO SR controller design are demonstrated in three study cases. The first study case demonstrates the coordination of two TCSC lines using MIMO SR control as a primary control. The second study case demonstrates the coordinated control of multiple HVDC links using MIMO SR control as secondary control. Finally, the last study case shows the coordination of the HVDC link and SVC control.

5.9.1 Development of MIMO SR control for coordinated control of two TCSC lines (Study case 3)

5.9.1.1 Test System

The test system 2, depicted in Figure 5.14, with two parallel TCSC lines, is set up to demonstrate the performance and capability of a MIMO SR controller in the coordinated control of two TCSC lines in order to enhance system stability.

The test system consists of two AC lines in parallel with two TCSC lines. The TCSC lines have an initial FSC of 30%. The TCR branch of the TCSC lines can produce up to

75% compensation to the total reactance of a single line route. Further details of the test system characteristic are described in Section 3.6.2. The initial state of the pre-fault system can be read from power flow in Figure 5.14.

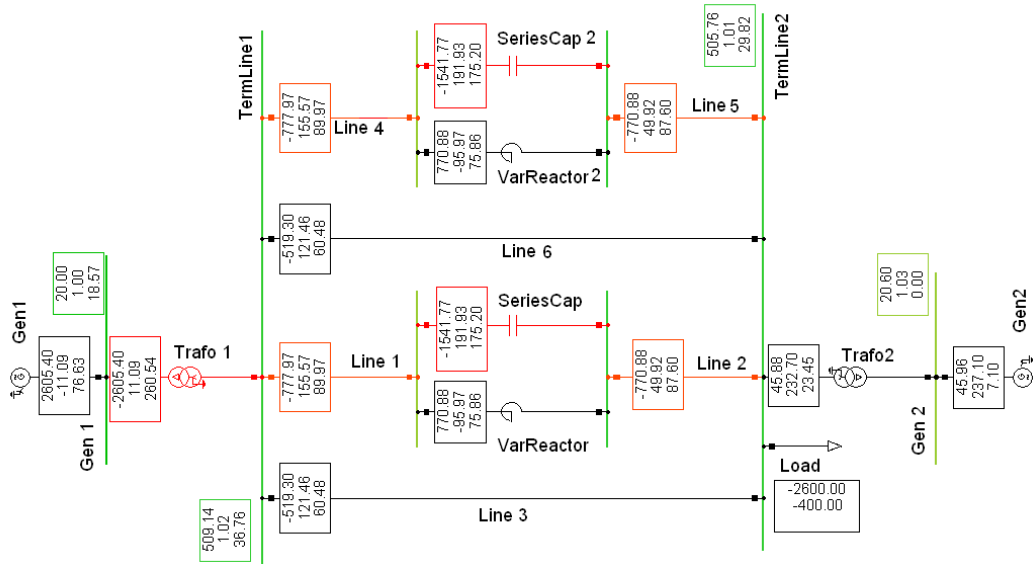


Figure 5.14: Concept proving PowerFactory SMIB test model for study case 3

5.9.1.2 Simulation results and analysis on study case 3

Figure 5.16 illustrates the dynamic response of the system when a small change to the set-point (P_{ref}) of the TCSC line1 is applied. The power on the TCSC line 1 increased from 770MW to 800MW at $t=100$ ms. As presented in Figure 5.16, it is evident that the power on the TCSC line1 is increased by 30MW at $t=100$ ms. Following the change of set-point (P_{ref}) of TCSC line 1, the error between the measurement and the set-point become non-zero and the MIMO SR, as a controller tries to minimise the error between measured power on the TCSC line1 and its set-point by regulating the reactance of the TCR branch. Hence, the controller calculates the optimal control signal (XI) at each simulation step for the best dynamic tracking of the set-point. Also, in the following simulation results, comparison of the MIMO SR performance and the SISO PI controllers is presented. To do so, another SMIB model is set up and two individual PI controllers were implemented for the TCSC's control, as shown in Figure 5.15, instead of a MIMO SR controller. Figure 5.16.b shows the change of reactance of TCSC line 1 (XI) following the change of its set-point.

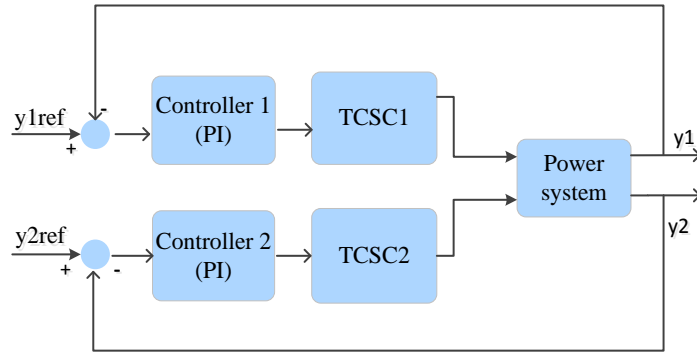


Figure 5.15: Individual SISO PI controller for each TCSC line

The SR provides the new values of XI at each simulation step by calculating the optimal control signal in the Matlab platform. Consequently, change of the TCSC's reactance results in regulating the power flow on the TCSC line 1. It can be seen that XI varies from initial reactance of 20 Ohm to 19 Ohm to alter the power on the TCSC line from 770 MW to 800MW. It is evident in Figure 5.16.b that the MIMO SR controller changes the control variable (XI) much quicker with less oscillation than the SISO PI controller. However, as presented in Figure 5.16.a, the SISO PI controller manages to track the set-point and consequently the power on the line under its control quicker and smoother than the MIMO SR controller.

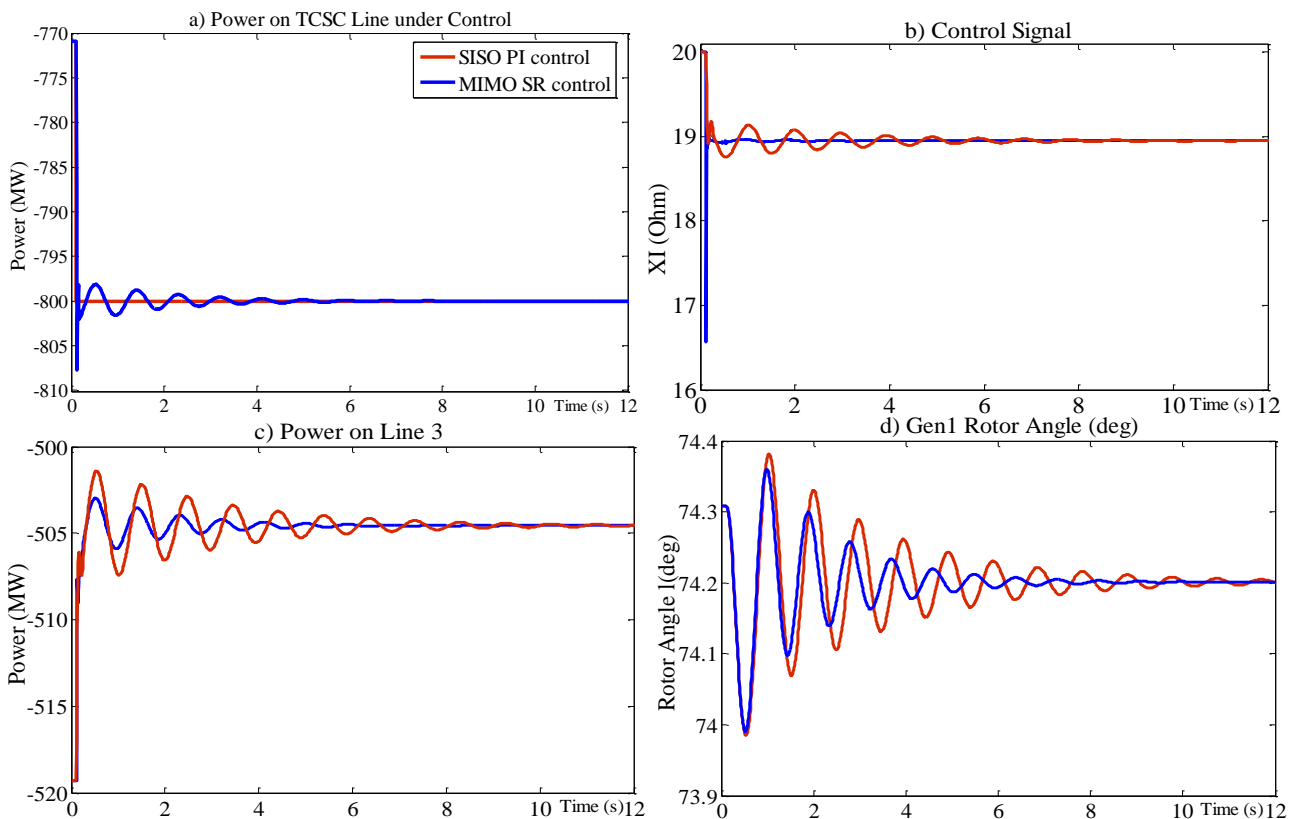


Figure 5.16: Performance comparison of SISO PI control vs. MIMO SR control for TCSC power flow control

This is mainly due to the fact that the main objective of the PI controller is to control power in the line under its control and does not consider the effect on the rest of the system. Although, the SISO PI controller demonstrated slightly better set-point tracking on the line under its control, it can be seen from Figure 5.15.c and Figure 5.15.d that the MIMO SR controller provides better performance with regards to the overall system stability. For example, it can be seen from Figure 5.15.c that following the change of one of the TCSC lines set-point, the degree of the oscillation induced in the other lines in the system which are not under control of any controller, such as line 3, is significantly less than when the SISO PI controller is implemented. In addition, as presented in Figure 5.15.d, we can see that the generator rotor angle oscillations, which are a good indicator of system stability, are considerably damped when the MIMO SR controller is implemented instead of the conventional SISO PI controller. All simulation results demonstrate the performance of the MIMO SR controller, which unlike the SISO PI controller is concerned with the stability of the whole system not only the line under its control. This is the reason why we observed better set-point tracking and fewer oscillations on the line under control in the case of the PI controller. However, the MIMO SR controller provides much better oscillation damping on the generator rotor angle. Therefore, stability wise, we can conclude that the MIMO SR controller, which considers the stability of the whole system, demonstrates better stability performance overall.

5.9.1.3 Limitation of the SR controller for the TCSC line

Although, the above results are presented for a small change of set-point, various operational conditions have been studied to investigate the robustness of the SR controller for the TCSC power flow control. The results of these simulations showed that the SR controller cannot provide robust control when the set-point changes more than 100MW. Through the studies and investigating the source of this limitation of the SR in the control of the TCSC line, it was determined that this was due to the nonlinear characteristics of the TCSC, which was discussed in section 5.4.1 and shown in Figure5.3.

5.9.2 Development of the MIMO SR control for coordinated control of two HVDC links (Study case 4)

For this study case the performance of the MIMO SR controller for the control of multiple HVDC links is investigated by conducting the following tests:

- Pre-fault control: when a step change for one of the HVDC links is applied at pre-fault.
- Post-fault control: when a three-phase fault occurred on one of the AC lines followed by fault clearance and post-fault action of both links after 100ms.

The first test allows investigation into the capability of the MIMO SR controller for pre-fault coordinated control of power flow devices such as the HVDC link, as well as exploring the impact of control by varying the SR control parameters such as the sampling rate (T). Whereas, the second test examines the capability of the MIMO SR controller design for a robust control following a short circuit fault. As aforementioned, the integration step size for all the simulations is 10ms and the open loop time responses are truncated at 30s of the simulation.

5.9.2.1 Test System

The SMIB test system 4, shown in Figure 5.17, is set up in PowerFactory to represent the transmission system connections between the North of England and Scotland. In this study, two HVDC links are connected in parallel and 1.3 W of power is transferred from Generator 1 to the load and each HVDC link carries 500MW of power. This test system is explained in detail in Chapter 3.

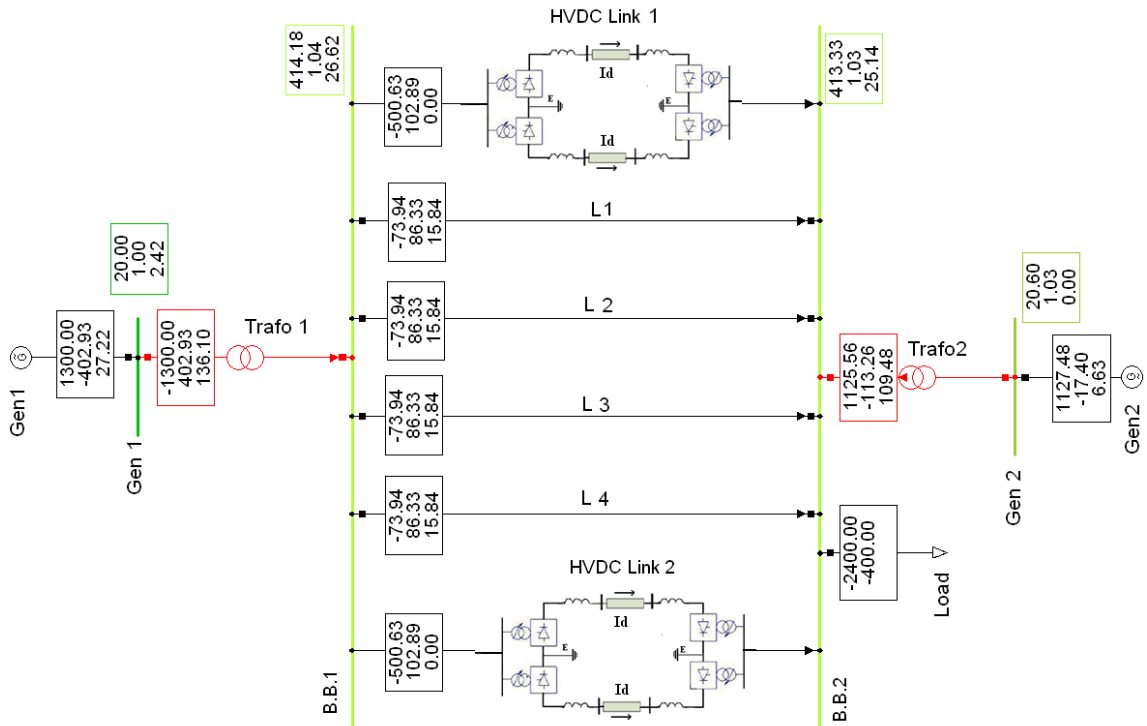


Figure 5.17: Concept proving PowerFactory SMIB test model 4 used for study case 4 5.9.2.2 Overall structure of the secondary MIMO SR control for multiple HVDC links

The overall structure and framework of the MIMO SR controller for the coordinated control of two HVDC links is illustrated schematically in Figure 5.18. Similar to the other presented study cases, the PowerFactory to Matlab interface facility has been used to extend the capability of PowerFactory for the design of the MIMO SR controller. The Matlab SR control slot shown in Figure 5.18 represents the externally designed MIMO SR controller, which provides calculated control signals (U_1 and U_2) to both HVDC links to track the new set-points, and the PowerFactory model represents the power system. It should be noted that the structure of the MIMO SR controller for the study case 3 is also similar to this case.

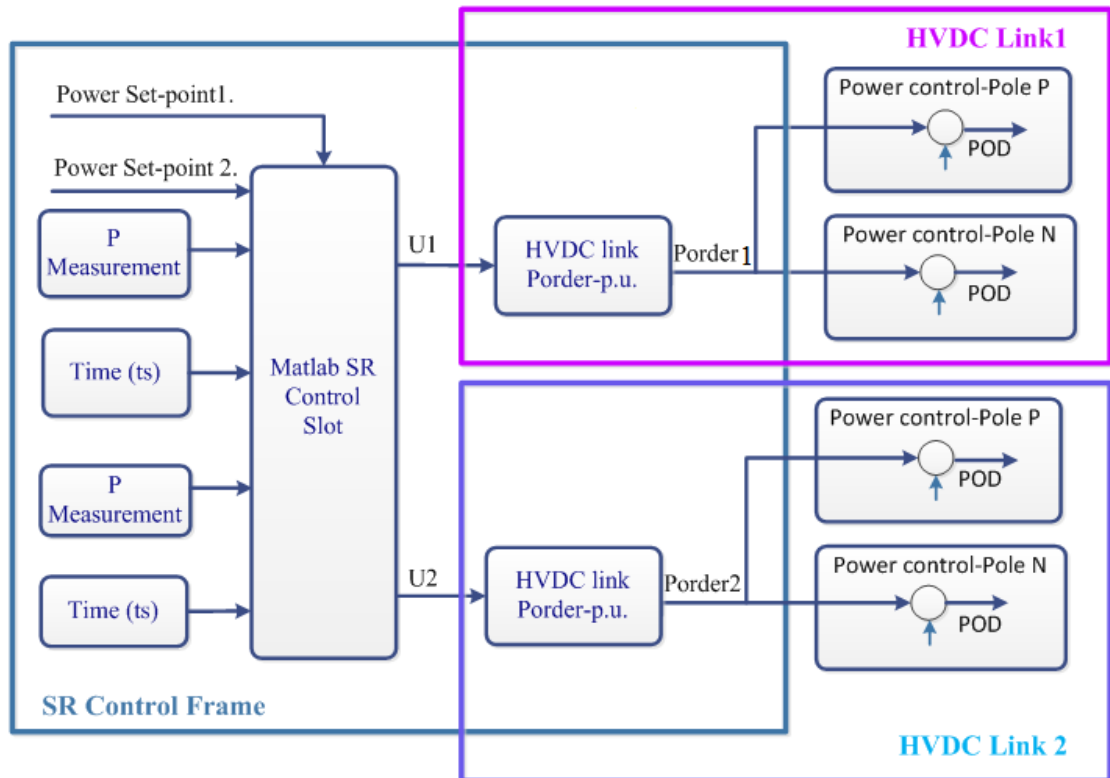


Figure 5.18: Structure of the Interface for the MIMO SR control design for two HVDC links in PowerFactory

5.9.2.3 Simulation results and analysis on study case 4

The results shown in Figure 5.19 represent the time domain responses of the HVDC control system when a step change is imposed on the HVDC link1's set-point, while the second HVDC link remains at its original set-point of 500MW.

Also, Figure 5.19.a and Figure 5.19.c show the power flows on HVDC link 1 and HVDC link 2 respectively where the black line is the set-point of the HVDC links and the red curve is the HVDC links' power flow under the control of the internal PI controller with no cascade control. The green curve also shows the HVDC links' power under SR cascade control with a 10ms sampling control rate, while the blue curve is that under the SR cascade control with a 80ms sampling control rate. In this case again there is a steady state error if the HVDC terminal voltage is not at nominal.

Clearly it is seen that the interactions are significantly reduced with the MIMO SR controller in the case of the 80ms control rate. The control signals of the MIMO SR cascade controls, with 10ms and 80ms sampling rate are presented in Figure 5.19.

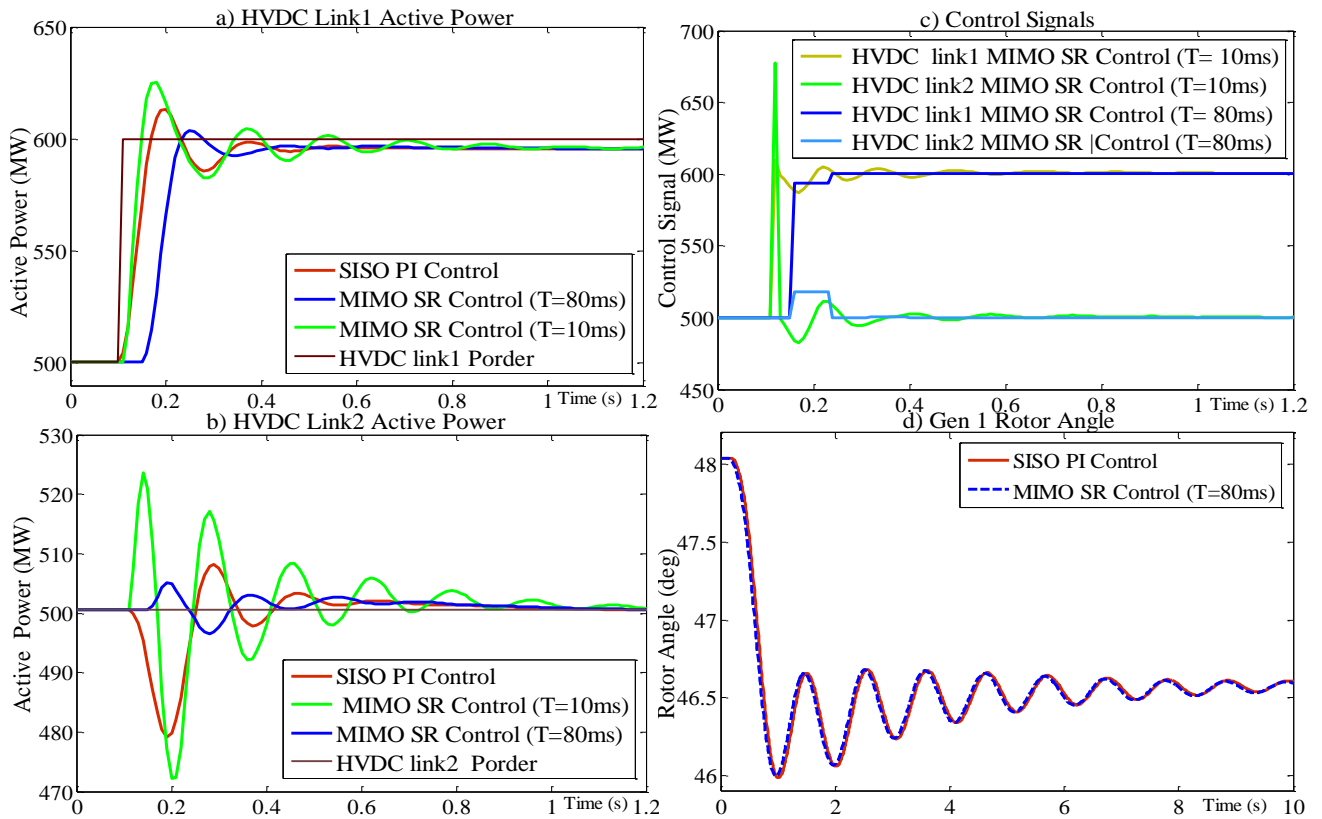


Figure 5.19: Per-fault coordinated control of the two-HVDC links following a step change on one of the HVDC links

The generator1's rotor angles, which reflects the impact of control on the system stability is shown in Figure 5.19.d. In this case there is no significant difference in performance of the MIMO SR controller compared to that of the internal PI controller since the internal PI controller is designed nearly to its optimum for the HVDC control system [138].

The results presented in Figure 5.20 show the dynamic response of the system at post-fault. Also, the performance of the secondary MIMO SR control system is compared with the internal SISO PI control within the HVDC power control system, without the cascade control.

The system is at the operating point where 1750MW is transferred from generator1 side to a load at the infinite Bus side. A 100ms three-phase short circuit fault is applied to one of the AC lines. It was observed that the HVDC link has avoided the 'blocking' mode, and the voltage recovered soon after the fault is cleared. The set-points of both HVDC links are changed from the original 500MW to 800MW at this point to compensate the loss of the faulted AC line [138].

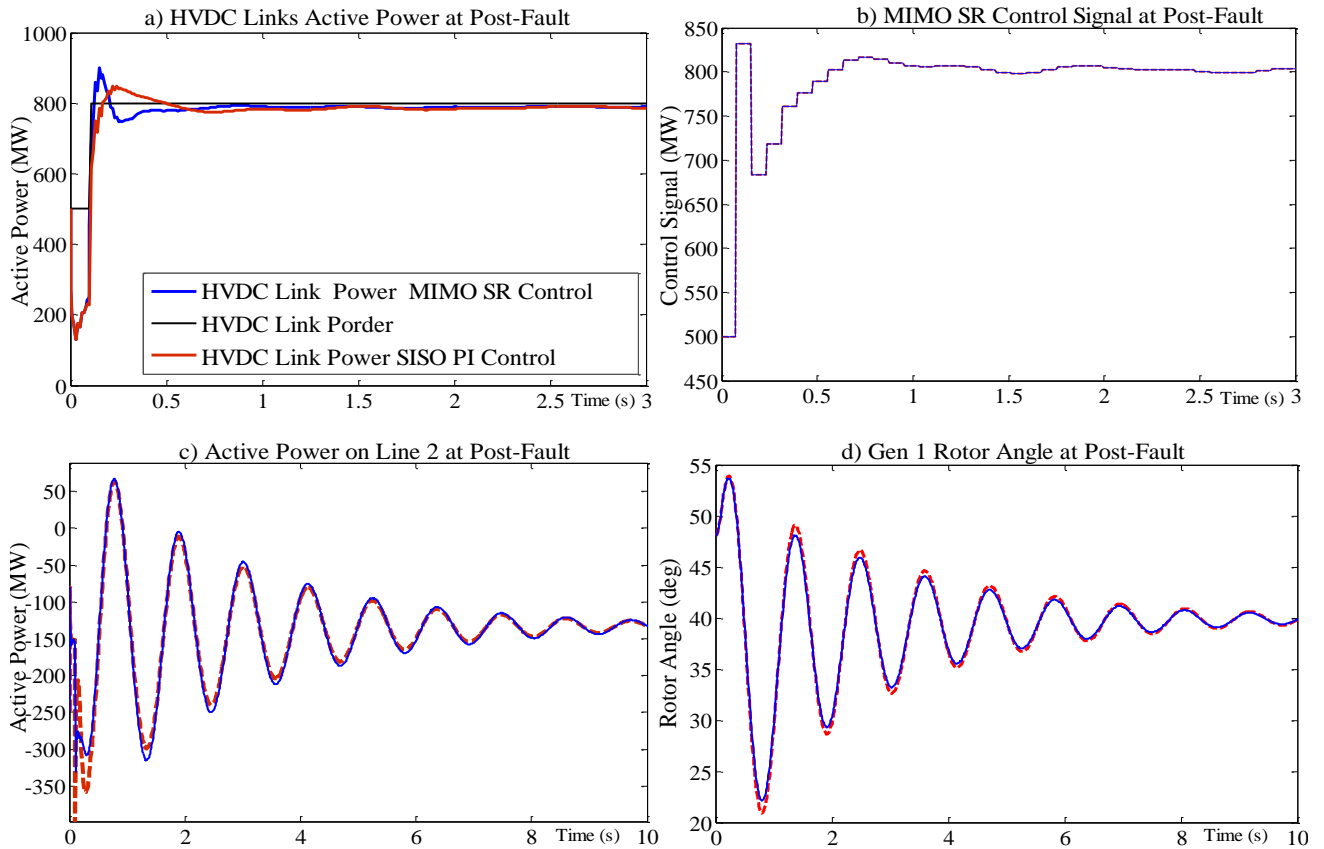


Figure 5.20: Post-fault control of the multiple HVDC links with the immediate increase of both HVDC links' flows to enhance the system stability

The HVDC links power flow presented in Figure 5.20.a shows a steady state error with the internally controlled HVDC link. The control signals for both HVDC links and the power swing on line 2 are presented in Figure 5.20.b and Figure 5.19.c respectively. Also, the rotor angle swing of generator 1 is shown in Figure 5.20.d.

At this operating point, the robust performance of the MIMO SR controller at post-fault can be clearly seen. Although during the fault ride-through period the system has been subjected to various stages of non-linear evolutions, the SR control design based on the linear time responses around the pre-fault operation point (500MW, in this case) has managed to robustly control the post-fault period. In addition, with the loss of one of the AC lines the system configuration has been significantly changed. However, this system change has been tolerated by the robustness of the SR control design method. Therefore, The SR controller remains robust to enhance the system stability by rapid tracking of the set-point change at post-fault.

5.9.3 Coordinated control of the HVDC link and SVC (Study case 5)

The SVC and the embedded HVDC link are fast and automatically controlled devices. Both the SVC and the HVDC link can also incorporate additional POD functions to improve the system oscillation damping. However, the TCSC and the HVDC are primarily used for flow control purposes and the SVC for voltage regulation.

As previously mentioned, the Anglo-Scottish boundary is such a critical transfer boundary in the GB transmission system and as a part of network reinforcement a new embedded HVDC link soon will be commissioned, along with existing SVC's that are equipped with POD control. Primarily, the HVDC embedded link in the GB transmission system is to tie the two parts of the weakly connected AC network together and to control the pre-fault flow and to enhance the boundary transfer capacity under normal operation; while at the immediate post-fault, its fast ramping dynamics and short-term capability (up to 110%) can be utilised to enhance transient stability. While the HVDC link provides fast ramping for taking on extra flow from the faulted AC circuits, the SVC can regulate within the statutory operation limits ($\pm 10\%$ in the GB HV system) to support the voltage for post-fault actions. These post-fault control actions need to be carried out in transient time scales (i.e. in ms).

The control of the HVDC link and SVC together under a MIMO feedback control would address two very different control variables, one is flow and the other is voltage while the interactions could be coupled through the rest of the transmission system. Therefore, the control objectives are for the SVC control to regulate the voltage profile, while for the HVDC link is to track the wide range of operating point changes, at both pre-fault and post-fault, rapidly and accurately, in order to provide stability control.

The aim in study case 5 is to set up a framework and investigate the feasibility of a MIMO control approach that can control both the HVDC link and the SVC meeting their very different objectives within a single framework.

In addition to the voltage regulation function, the SVC is also equipped with a POD for damping control. The damping control senses system oscillation from either frequency or power feedback. In the SMIB system presented in Figure 5.20, the power flows on the AC lines L1, L2, L3, L4, L5 and L6 are monitored by the POD, as is the case in the GB system on the west-side of the AC inter-connectors.

These two control systems, the HVDC link and SVC with POD control, if running separately, could have interactions with both of them trying to achieve their dynamic control objectives via the adjustment of power flows on the same set of boundary circuits.

In this study, a MIMO controller is designed using the SR control design approach to provide a coordinated control for both the HVDC link and the SVC-POD.

Since the HVDC link tends to control power flow and the SVC regulates voltage, in the non-parametric formulation, the SR controller is a 2×2 MIMO system, with the output variables and control variables expressed in vectors as (y) and (u) , respectively. Clearly, the dimension of the control system is determined by the number of system input and output variables, rather than the number of state variables in the system. This can be advantageous when considering a full scale power transmission system, where it is common to have several thousands of state variables, due to the dynamics from both generators and the associated control systems. It is noticed that there is a small steady state error for the HVDC link when it is operated under its internal current control. Kundur suggested that for stability the high speed current control with a superimposed power control is preferable [22]. In this study, the MIMO control system of the HVDC link is placed in cascade with its internal control system, and power control is provided via the HVDC links internal power control set-point. In the case of the HVDC control, both the controlling and controlled variables are power flows whereas, the SVC control system controls voltage by varying the shunt Susceptance. The POD power feedback signal is superimposed on the voltage feedback signal.

The HVDC link power control subsystem has much faster dynamics compared with the SVC voltage control subsystem. For a unit step change in the power control channel the step response settles in under 10s, while the step response in the voltage control channel can take about 50s to settle.

5.9.3.1 Test system

In the this study , the SMIB test model 5 with an initial transfer level of 2GW and 500MW power on the HVDC link, as shown in Figure 5.21, is set up for the control of the HVDC link and SVC together under a single MIMO SR feedback control. In this case, the controller would address two very different controlled variables, one is power flow and the other is voltage, while the interactions are coupled through the rest of the

transmission system. In this study case the performance of the MIMO SR controller for coordinated control of HVDC link and SVC is investigated at pre-fault by applying a change of set-point (P_{order}) by 100 MW. In this study, unlike in the HVDC links power controller, the PI controller within the SVC model is replaced by SRMIMO controller

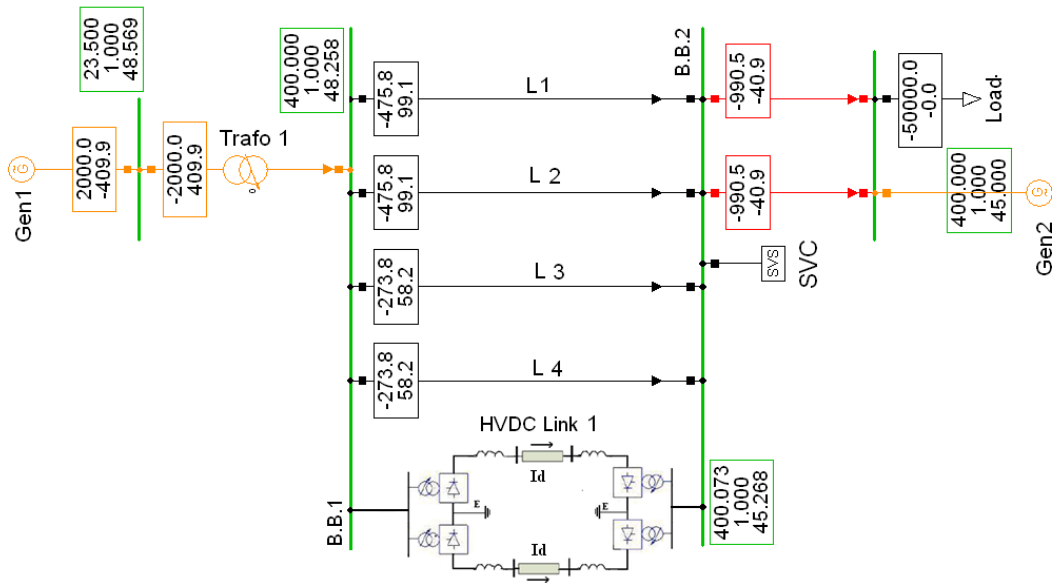


Figure 5.21: Concept proving PowerFactory SMIB test model for study case5

and there is no cascade control in the SVC. The SVC control variable is B and the controlled variable is V (at a selected bus), and this defines the open-loop step response. This relation between V and B is $\sim Q=BV^2$ when it is within the droop range of the SVC, the system should be fairly linear (since $V \sim 1pu$) as demonstrated in Section 5.4.3. In the SMIB model, the POD inputs are power signals from 4 AC lines including L1, L2, L5 and L6 as presented in Figure 5.21.

5.9.3.2 Simulation results and analysis on study case 5

Furthermore, the performance of the MIMO SR controller for the coordinated control of the HVDC link and SVC under a single framework is investigated in study case 5. It is demonstrated in this study case that the interaction is significantly reduced when the MIMO SR is implemented for control of the HVDC link and SVC under a single framework. Under normal operation, a step change in one control channel interacts with the other, coupled through the rest of the system. This is particularly an issue between the HVDC power flow control and the SVC-POD regulation. This is observed in the system where the HVDC link and the SVC are operated under their individually designed SISO control systems (using continuous PI controllers, and HVDC has only its

internal current control system). Figure 5.22 compares the dynamic responses of the system to a step change using a SISO PI or MIMO SR control at pre-fault. To test the interactions between the SVC and HVDC, the control reference points of each of these devices are subject to a step change in turn while the set-point of the other device is kept unchanged. Figure 5.22.a and Figure.5.22.c show the responses of the voltage of SVC and the active power of the HVDC when a 10% step change is imposed on the SVC voltage control set-point, where the HVDC set-point is kept constant at the original operating point. Figure 5.22.b and Figure 5.22.d show the responses of the system when a 100MW step change is added to the HVDC control set-point, where the SVC set-point is constant. With this arrangement, the SVC voltages are shown in the top plots, where Figure 5.22.a shows voltage change by self-excitation and Figure 5.22.b shows voltage change excited by the HVDC disturbance. The HVDC line flows are the bottom plots, with Figure 5.22.c being the response of HVDC link power to disturbance from the SVC's set-point change and Figure 5.22.d is the HVDC link step response following the change of its set-point. It is evident from the Figure 5.22.b (red curve) that the step change in the HVDC flow control causes substantial disturbance in both the SVC voltage and the POD damping control signal, when the system is under the SISO control. Whereas, when the system is under the MIMO sampled regulator control, as shown in Figure 5.22.b, blue curve, the interaction between HVDC power flow control and the SVC-POD control is significantly reduced.

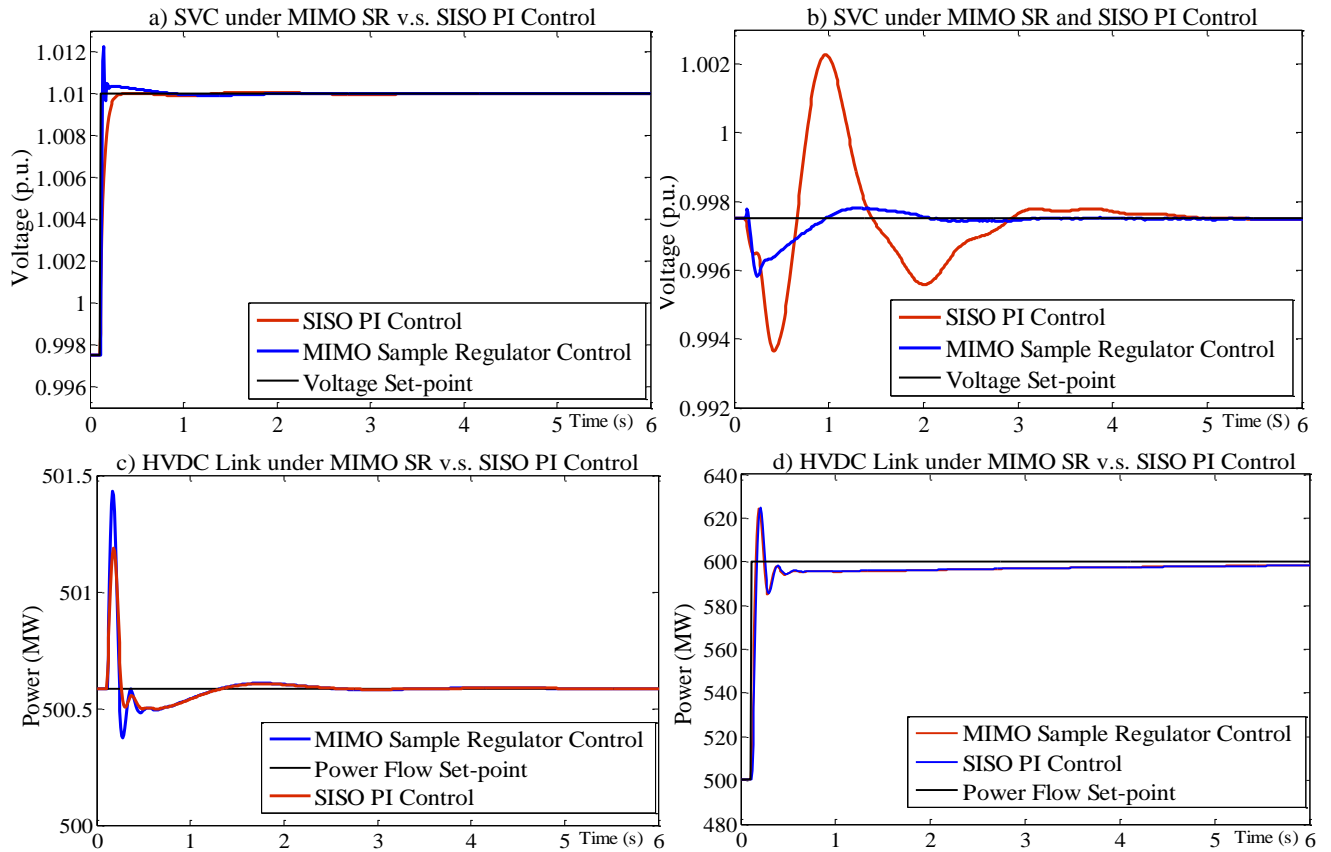


Figure 5.22: Per-fault coordinated control of the HVDC link and SVC using a MIMO SR control

In the case of a fault occurring, if there is no post fault action to adopt the HVDC links set-point, the HVDC link would keep its pre-fault flow, while the loss of a circuit due to the fault clearance would reduce the post-fault transfer capability across the boundary circuits. As a consequence the connection between accelerating and decelerating groups is further weakened. Loss of synchronism between these oscillation groups could ultimately lead to instability.

Under the MIMO SR control the embedded HVDC link can provide a rapid post-fault action, picking up the flow from the lost AC circuit. As a consequence, loading of the machines in the exporting group is quickly restored and system integrity and stability maintained. Figure 5.23 shows the dynamic response of the system at post-fault with and without post-fault stabilising control actions[138].

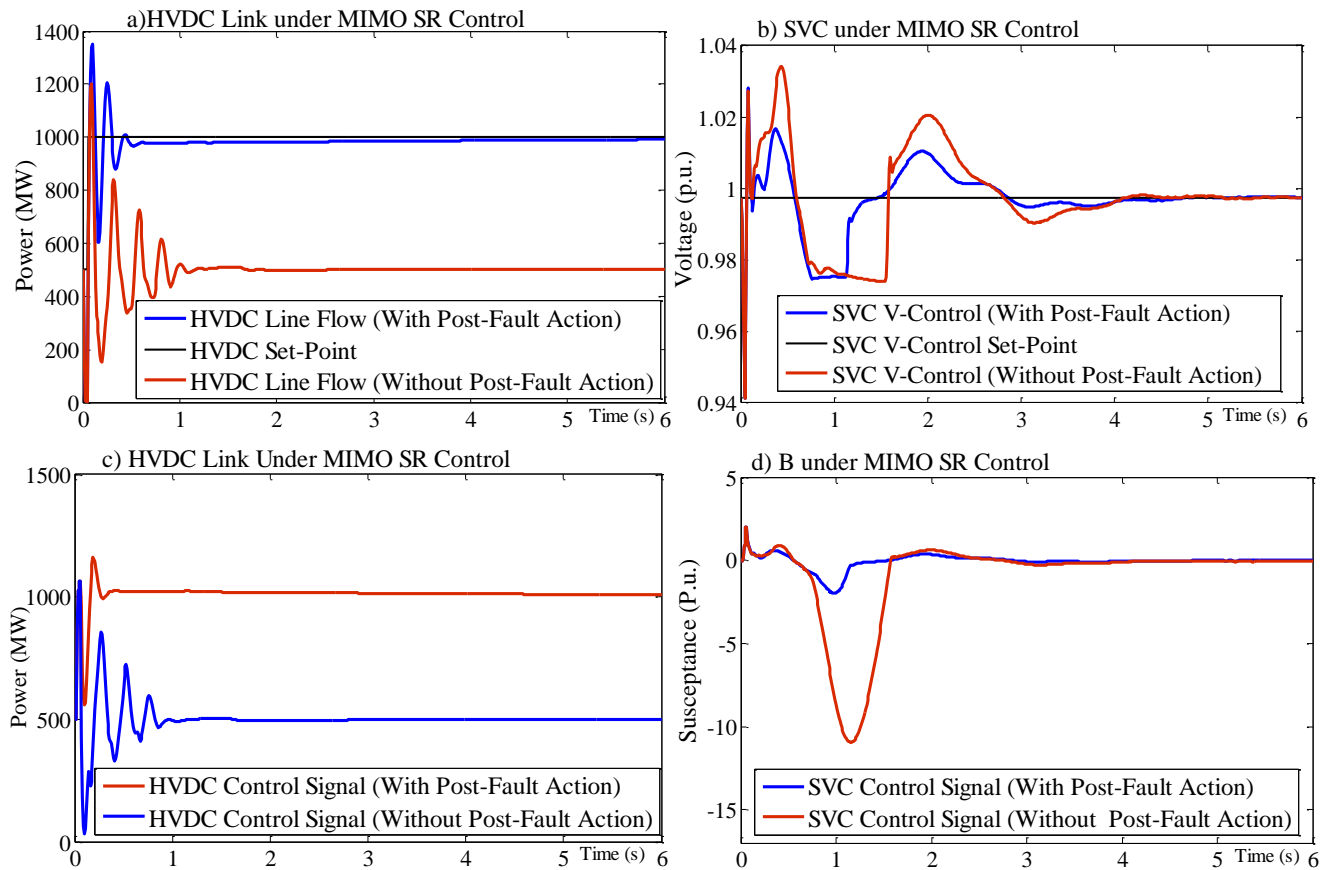


Figure 5.23: Post-fault control of the HVDC link and SVC using MIMO SR control for the immediate increase of the HVDC link's flows to enhance the system stability

In this case, a three-phase fault is placed on line L1 towards the SVC terminal end. At post-fault, line L1 is tripped for fault clearance. In addition, the MIMO SR commanded the HVDC links power flow to increase to 980MW from the pre-fault operating point of 500MW following the fault clearance [138].

Figure 5.23.b shows the power flow in the HVDC link following the loss of an AC line with and without implementing the HVDC link set-point adoption as post-fault action. It is clearly seen that the post-fault action using the HVDC flow control has enhanced post-fault stability, as shown in Figure 5.23 by the blue curves. The MIMO SR control performed a 'tracking' control in the HVDC link control channel with its interaction with the voltage regulation being reduced under the MIMO control design.

Also, Figure 5.23.c presents the control signals from the MIMO SR controller, which demonstrates that the MIMO control signal has not been restricted significantly by the HVDC links physical limit under this design.

In this study, no step change applied to the SVC set-point and MIMO SR control maintains the voltage under the SVC control at post-fault to its pre-fault set point.

Figure 5.23.b demonstrates that less voltage variation is observed when the post-fault action is taken through MIMO SR control.

In addition, the SVC control signal is presented in Figure 5.23.d. The SVC limit on the control variable is $[-0.75, 1.5]$ and with the post-fault stabilising action the SVC control signal is less restricted, hence more effective, than that of no post-fault control. The limiting effects can be seen in the top-right voltage plot.

In post-fault the system has undergone various nonlinear system stages, and these tests have demonstrated robustness of the sampled regulators. The post-fault system is different from the pre-fault system with both the line switching and operating point changed. Desirably the parameters of the controller are updated in post-fault. With the proposed time domain design approach this class of Sampled Regulator control can be further developed into adaptive schemes, using standard recursive online algorithms for the non-parametric system identification [138][152].

5.10 Concluding remarks

In this chapter, firstly the requirement for secondary/supervisory multivariable feedback control system for co-ordinated control of power flow control devices on the future GB transmission system such as the future HVDC link and the TCSC is discussed. Secondly, the Chapter presents a methodology to design a novel Sample Regulator (SR) controller which is capable of providing coordinated control of the HVDC links, TCSC and SVCs at pre-fault as well as providing stability support to the main AC system to enhance the stability limit at the post-fault. Alongside that, the detail of the background theory and main features of the proposed SR design method is presented. Then, the Chapter focuses on the technical development of the SR controller and the overall structure of Matlab to PowerFactory interface for design of SR is presented as initial part of controller design. The proposed SR controller can be implemented as a SISO or MIMO controller. Therefore, further to theoretical development of the SR controller, performance and capability of both SISO and MIMO SR controllers are investigated. Two power system applications, including coordination of power flow control of multiple HVDC links and power flow control of HVDC link with the SVC voltage regulation are presented. The simulation results demonstrated the capability of MIMO

SR for the co-ordinated control of two HVDC links and HVDC link and SVC at pre-fault under one framework.

Also, robustness of this class of sampled regulator has been tested at post-fault which confirmed that the sampled regulators design method is both practical and applicable to power system control even when the systems are subjected to severe disturbances. Therefore, by adopting a MIMO SR control, the HVDC link can also provide rapid post fault action to pick up the flow on the lost AC line and consequently restore system stability.

Chapter 6

Stability control and management system in future GB transmission system

6.1 Introduction

The performance of the non-parametric time domain, MIMO SR control design approach is further tested for the control of various types of control devices, including the HVDC link and SVC with its associated auxiliary POD functions using the full scale GB transmission system model. To do so, a full model of the GB transmission network representing the 2016 generation and demand pattern is set-up.

The control of the HVDC link and SVC together under a MIMO SR feedback control would address two very different control variables. In the case of the HVDC link, the SR controller is a power flow controller, which rapidly and accurately tracks the wide range of operating point changes at both pre-fault and post-fault, to provide support to the AC system and ultimately enhance system stability, whereas in the case of the SVC, the controller regulates voltage. The interactions could be coupled through the rest of the transmission system. In addition, in this Chapter, the optimal operational strategy for the embedded West Coast HVDC link in the GB transmission system with regard to the enhancement of the stability limit across the B6 boundary is investigated using the MIMO SR controller [152].

6.2 Study set-up

In the network access planning process at National grid, offline studies in Power Factory (Off Line Tool Analysis, OLTA) are conducted to ensure that system security is maintained for various planned and unplanned outages. The demand and generation profile could change minute by minute. Consequently security analysis studies need to be updated based on the change of the demand and generation profile. However, it is not practical to repeat all the studies on a minute by minute basis. Therefore, these studies are only conducted for major points of time on the daily demand curve. Representative demand curves for the winter peak, typical winter, typical summer and summer minimum are shown in Figure 6.1. These major points of time, which are called cardinal

points (CP), represent peak, trough and fixed point on the demand curve as illustrated in Figure 6.1. The cardinal points are represented by study cases and a pair scenario in PowerFactory.

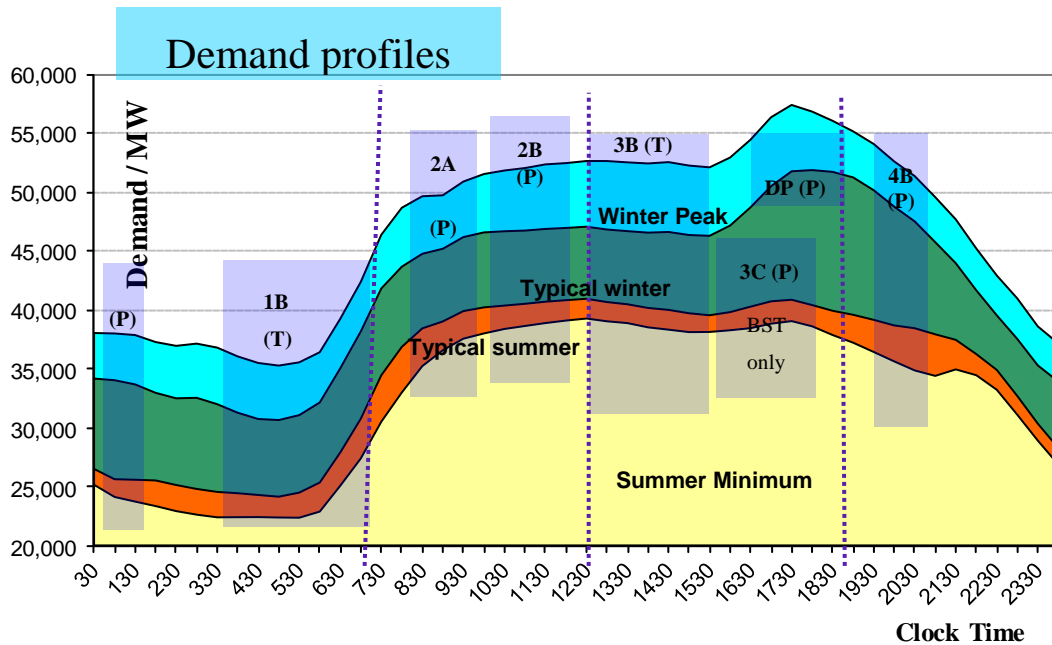


Figure 6.1: Demand curve for typical minimum and maximum winter and summer including Cardinal points such as Peak (P), trough (T) and fixed point (F) [154]

6.2.1 Main steps of setting up a study case which represents 2016 demand and generation profile

This section describes the processes conducted to set up a study, which represents the future model of the GB system with regard to the increase in wind generation level in Scotland and England by 2016. The West Coast HVDC link model is also integrated to this model. The process of study set-up mainly includes importing generation and demand information, balancing the study and ensuring that the study has a good voltage profile. These steps are explained in more detail in the following section.

Firstly a current model is derived containing the Winter Peak (WP) database at 2B cardinal point. As mentioned above, in PowerFactory a cardinal point defines a point in time for which all analysis functions will be executed.

The derived project from the 2013 model contains a generation and demand profile that didn't correspond to the profile scheduled for the cardinal point under consideration of

this study. Therefore, as part of the study set-up process, the generation and demand patterns are updated in such a way that they would represent the generation and demand pattern by 2016, particularly the wind generation increase in Scotland and England.

The OLTA tool provides an interface to the Scheduling Process in a Control Environment (SPICE) to extract generation schedule data. Once generation schedule data has been extracted, we proceed to apply Balancing Mechanism Units (BMUs), so that BMUs dispatch generators in the controlled group according to merit order.

After that, MW and MVar demand data is applied to the OLTA system. This is done through an interface to the Demand Forecasting (DEAF) system although generation has been set up to match the total demand (i.e. load + network losses).

After SPICE imports the BMU application and DEAF imports demand, there is still a large mismatch between generation and load. This is due to the DEAF values being stored in the feeders at this stage but yet to be applied to the load. The demand values are not yet scaled to match the SPICE dispatch. Balancing MW demand in a scenario is conducted by distributing from the Grid Supply Point (GSP) to Bulk Supply Point (BSP), and then scaling demand to meet the total generation. The total system imbalance should not be more than 10 MW [154].

After carrying out the above steps, the AC load flow is run and the tap positions are re-written to the database.

In general a well-balanced study case has the following criteria which were considered in this study setup [154]:

- Active power mismatch (all generators) is less than 10 MW.
- No thermal limit violation for the pre-fault case.
- Can be verified with an “AC Load Flow Report”
- An acceptable national voltage profile based SQSS is obtained
- All equipment such as PV generators, SVCs and Tap changers operate within their limits and no violation of limits are observed.
- Also, the low number of iterations that the load flow calculation needs for convergence is a good indication of the robustness of the solution. A high number of iterations usually indicate that there might be problems in keeping the voltages at all busbars within specified limits or there might be an overload in a part of the system.

Subsequent to setting a balanced study case for the winter peak scenario at the second cardinal point 2B (12:00 h), the study cases described in Section 6.5 are investigated with regards to stability enhancement across the B6 boundary.

6.2.2 Description of the Full GB Transmission system model

The capability of the embedded West Coast HVDC link, which uses Current Source Converter (CSC) technology, in transient stability enhancement, is investigated using the set-up study case for the full model of the future GB transmission system. The dynamic model, which is created in DIgSILENT PowerFactory [144], was set up to represent the 2016 generation profile based on the 2013 Gone Green Future Energy Scenarios [6]. To do so, as previously explained in Section 6.2.1, the generation in Scotland was scaled up to increase the transfer across the B6 boundary for the purpose of the studies. There are many ways in which generation and demand can be scaled up. Therefore, the B6 boundary found in these studies may not represent the actual operating condition in 2016. In this model, the GB transmission system consists of three main areas including the SHETL in the North of Scotland, the SPTL in the South of Scotland and the NGETN for England and Wales. These three regions use three voltage levels of 400kV, 275kV and 132kV. In total, there are 220 synchronous machines in service from which 195 of them are equipped with Automatic Voltage Regulators (AVR). Also, there are 36 substations in NGETN with dynamically-controlled SVCs to maintain the bus voltages within statutory limits. For the operating conditions under study, the total generation is around 62.5 GW. In order to have a dynamic model and obtain realistic results all generators are equipped with excitation system models and governors. Also, all PSS remain connected and in service. In addition, 7801 transmission lines, 5328 busbars, 2,354 transformers, 644 shunts and 1627 loads (all of the loads in the system model are modelled as constant impedance loads) are included in this model.

As previously explained in Chapter 1, the Scottish B6 boundary includes two double 400kV AC lines with each of the four AC lines having a thermal rating of 2.2GW. Based on the Security and Quality of Supply Standards (SQSS) requirements, the system should remain stable following a double circuit fault [15]. Therefore, the two existing double AC lines should be capable of providing 4.4GW of thermal capacity. However, this capability is currently limited by stability constraints. Thus, in line with future reinforcements across the B6 boundary, a 2.2GW, 600kV Bipolar CSC-HVDC

link is planned to be installed between Hunterston (SPTL) and Deeside (NGET) by 2016, as shown in Figure 6.2, to enhance the power transfer capacity of the transmission corridors between Scotland and England. Therefore, a CSC-HVDC model is integrated in this model to represent the West coast HVDC link. The CSC-HVDC link normally controls the DC current at rectifier side and DC voltage at inverter side. The detail of the West coast HVDC link model including the diagrams and parameters of the HVDC link control system are included in Appendix B. It is important to note that the focus of this Chapter is only on the West Coast HVDC link [147][152].

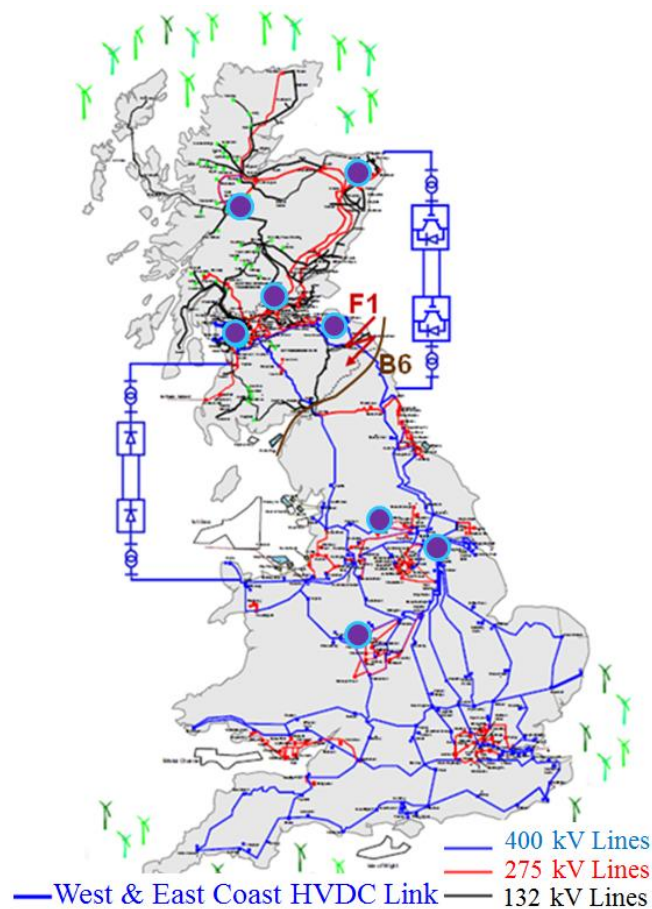


Figure 6.2: GB transmission system with the future West and East Coast embedded HVDC links and location of the monitored generators [6]

6.3 Stability analysis performed for the GB transmission system

As discussed in Chapter 1, the transmission system will require operation closer to its thermal limits to provide cost and operational efficiencies and to offset the requirement for further physical capacity. Therefore, increased monitoring of system stability is necessary to ensure that the network is stable in real-time. National Grid as the Great

Britain System Operator (GBSO) currently monitors and analyses dynamic and transient stability to ensure the SQSS obligations in maintaining security of supply is satisfied [15]. The dynamic stability/oscillation monitoring system provided by Psymetrix (Power System Stability Monitoring) currently monitors dynamic stability, oscillation of synchronous machines by analysing the digital output from Phasor Measurement Units (PMUs) strategically located across the England & Wales transmission network

Off-line transient stability analysis (which is the focus of the studies presented in this Chapter) identifies system stability for all credible faults on the network and ultimately indicates which contingencies will potentially lead to instability [155]. Also, stability analysis identifies the power transfer limit of the Main Interconnected Transmission System (MITS) or the boundaries of interest such as B6 boundary (known also as Anglo-Scottish boundary). The identification of these limits is based on the planning criteria outlined in the SQSS as follows [15].

6.4 Planning criteria

The maximum transmission capacity of the MITS shall be planned such that prior to any fault there shall not be any equipment loadings exceeding the pre-fault rating and voltages outside the pre-fault planning voltage limits.

In addition, the maximum transmission capacity of the MITS is required to be planned such that for any following event of fault outage there shall not be any system instability, unacceptable voltage condition or overloading of the equipment [15]:

- A single transmission circuit or a reactive compensator or provider
- A double circuit overhead line on the super grid
- A double circuit overhead line
- A section of bus-bar or mesh corner

Following the above planning criteria the power transfer stability limit of the B6 boundary is normally identified by increasing the power transfer across the boundary step by step (at 100MW steps). Stability analysis is performed at each step for all the credible faults as outlined in SQSS. The main generators' rotor angle's oscillations across the boundary (shown in Figure 6.2 by blue circles) are monitored as the main index of system stability. 100 MW before the point where system becomes unstable is

considered as the maximum stability limit of the boundary. The SQSS defines the system instability as when there is either [15] [154]:

- Pole Slipping: when a transmission connected generator loses synchronism with the remainder of the system to which it is connected or,
- Poor Damping: when after a 20s simulation period, the electromechanical (e.g. Rotor angle) oscillation has a damping time constant greater than 12 seconds.

With following the above planning criteria the stability limit of the B6 boundary is identified and the study cases in Section 6.5 are conducted to investigate the optimal operating point of the HVDC link with regards to stability enhancement across the B6 boundary using the MIMO SR control.

6.5 Definition of Study cases and scenarios

- **Study case 1:** investigates the optimal operating scheme of the West Coast HVDC link with regard to the system stability enhancement using the Multivariable SR controller. The following two scenarios, as detailed in Figure 6.3, have been considered for this study case.
 - Running the HVDC link at 2.2 GW (case 1.1)
 - Running the HVDC link at 1.9 GW (case 1.2) in order to reserve its fast ramp-up capability for the PFA
- **Study case 2:** investigates the capability of the MIMO SR controller in co-ordinated control of the HVDC link and SVC at pre-fault. In these study cases, the main control objective for the SVC is to regulate the voltage profile. However, the HVDC link's main objective is to track the wide range of operating point changes, rapidly and accurately, at both pre-fault and post-fault in order to enhance system stability.

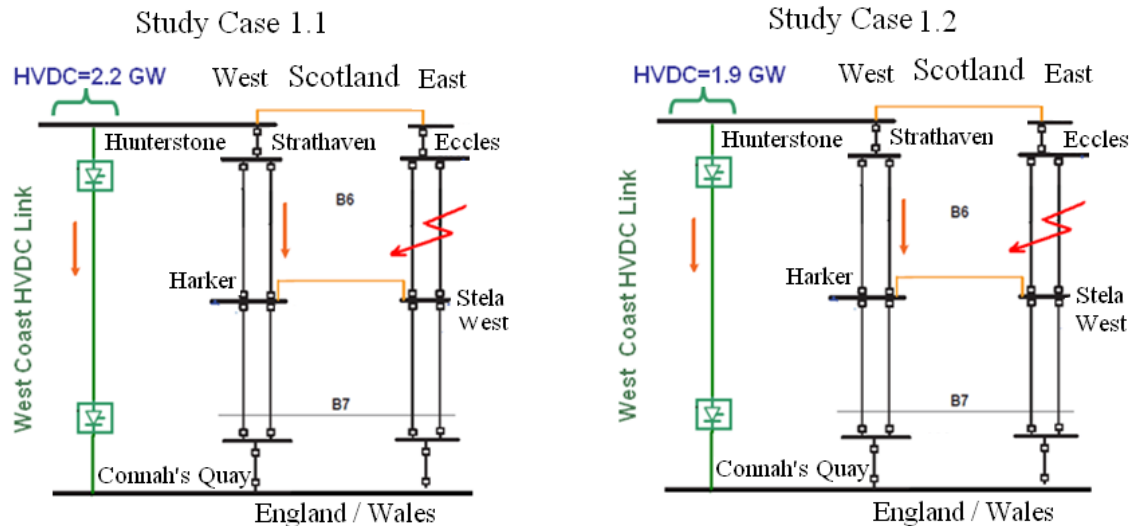


Figure 6.3.: Schematic diagram of B6 boundary in parallel with West coast HVDC link for study case 1

6.6 Capability of the West Coast HVDC link in stability enhancement

The West Coast HVDC link is expected to provide fast ramp-up and a short term overload capability of 2.4 GW (for up to 6 hours) to be implemented for Post Fault Action (PFA). However, according to the West coast HVDC link technical document [156], PFA capability of the West coast HVDC link is not available if it is running at its maximum continuous capacity which is 2.2 GW [156]. Therefore, the main question raised is what would be the optimal operating point of the HVDC link with regard to the enhancement of system stability, whether to run the HVDC link at its maximum capacity or run the HVDC link at recommended lower level (1.9 GW) in order to preserve its fast ramp-up capability for the PFA.

The study case1.1 and study case1.2 are investigating the above question using the full future model of the GB transmission system. (The processes of study set-up were described in Section 6.2.1).

6.7 Simulation results and analysis for the study case 1.1 vs. study case 1.2

Since the fast ramp-up capability of the HVDC link is available when the HVDC link is set maximum up to 1.9 GW (study case 1.1), the stability limit of the B6 boundary is identified (based on the required planning criteria described in section 6.4) with and

without implementing the fast ramp-up capability of the HVDC link for PFA. PFA is implemented through the MIMO SR control, which is controlling the HVDC link and SVC under a single framework in the GB transmission system. To do that, a three-phase fault, shown in Figure 6.2 by F1, on one of the double 400KV AC lines across the B6 boundary is applied and it is cleared after 100ms. It is important to note that in these study cases only the most critical fault is considered for identifying the power transfer stability limit. The fault on the double circuit connecting Eccles and Stela West (shown in Figure 6.2 by F1) has been identified as the most critical fault, which could lead the system to instability depending on the level of power transfer on the B6 boundary, outage pattern and system arrangements. (It is important to note that these cases are defined for the intact system) [152].

In study case 1.1, the total power transfer limit of the B6 boundary including the HVDC links flow without any PFA is identified at operating point A, which implies that without taking any PFA the system will be unstable beyond this point. After that, the power flow across the boundary is increased to identify the maximum stability power transfer limit across the B6 boundary while exploiting the fast ramp-up and overload capability of the HVDC link as a PFA. The summary of total power transfers across the B6 boundary at each of the operating points is presented in Table 6.1.

The same steps are repeated to identify the total stability power transfer limit across the B6 boundary for the case when the HVDC link's set-point is set up to its maximum capacity of 2.2 GW (study case 1.2). However, in this case no PFA is available from the HVDC link due to the link technical limitation. In this case, the maximum transfer limit obtained is point C, which is lower than point D by 150MW. The simulation results revealing the dynamic performance of the system for both study case 1.1 and study case 1.2 at operating points B, C and D are presented in Figure 6.4, Figure 6.5 and Figure 6.6 respectively. In these presented simulation results, as well as the status of the system in term of system stability, the system dynamic response at each operating point including the active power on the HVDC link, voltage at Harker and the rotor angle oscillation of the large generators across the network are monitored and presented for stability performance analysis. Please note that due to the generators' data confidentiality the name of generations have not been provided.

TABLE 6.1: Power transfer limit across the B6 boundary at various operating points

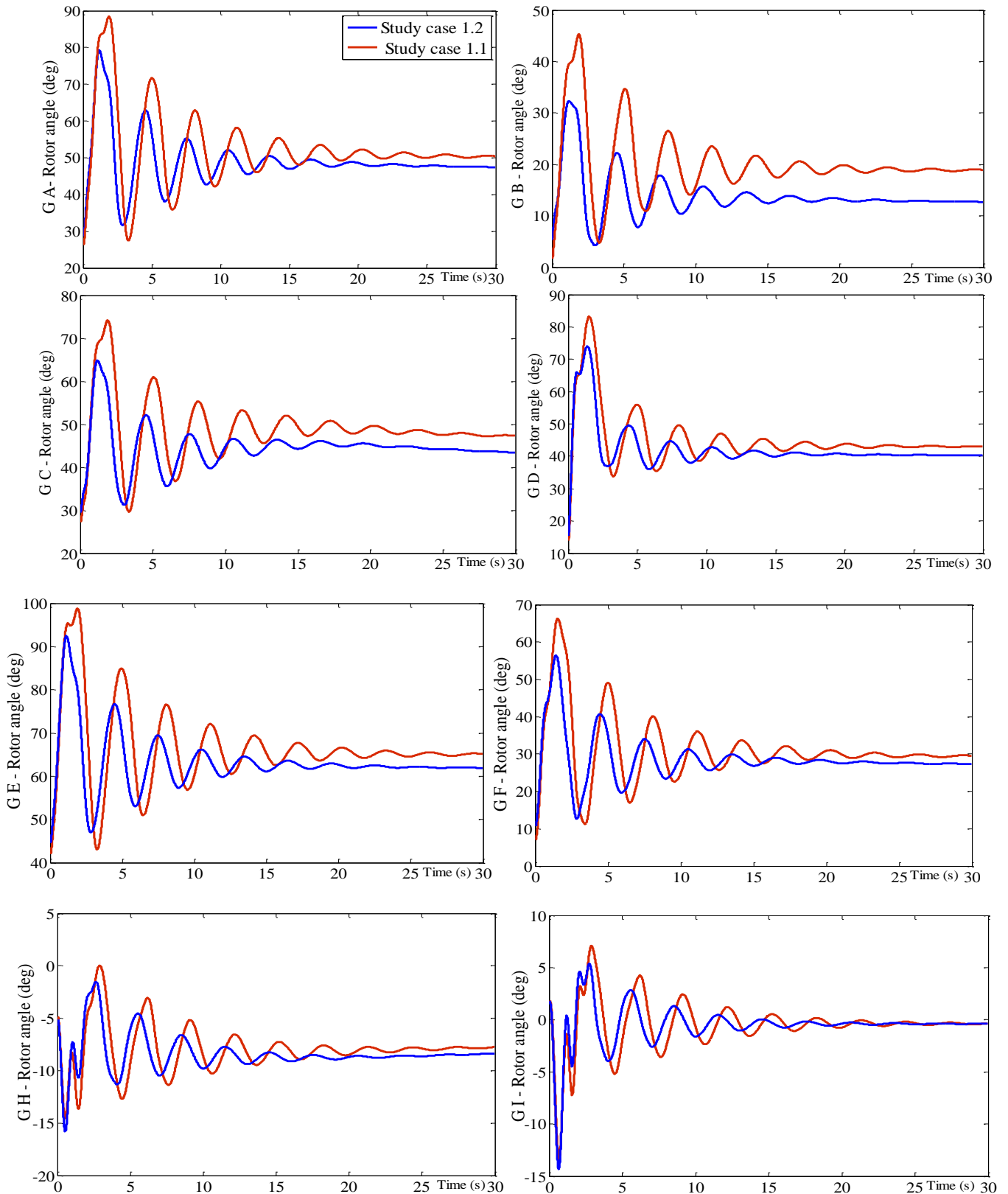
Operating point**	Total PT of B6 boundary* (GW)	HVDC link (1.9 GW) at pre-fault	HVDC link (2.2 GW) at pre-fault
Point A	4540	Stable with No PFA	Stable
Point B	4640	Stable with PFA	Stable
Point C	4735	Stable with PFA	Stable
Point D	4885	Stable with PFA	Not stable
Point E	4944	Not stable	Not stable

** PT: Power Transfer, including the power flow on the DC and AC lines.

* Using generation scaling pattern specific to studies.

It is evident from the simulation results presented in Figure 6.6 that at operating point D the system will be unstable without the use of the PFA provided by the HVDC link. In both study cases as presented in Table 6.1, the system is unstable behind point E even with implementing the PFA from the HVDC link. In addition, it is apparent from the simulation results presented in Figure 6.4 and Figure 6.5 that even though the same total power transfer level is maintained in both study cases (case 1.1 and case 1.2), at operating B and operating point C, the system responses are less oscillatory (blue curves) when the HVDC link is operated at 1.9 GW and the overload capability of the HVDC link is utilised for PFA (case 1.2) compared to the case 1.1 when the HVDC link is operated at its maximum capacity of 2.2GW (red curves).

Also, Figure 6.4, showing the dynamic response of the system at point B, demonstrates that less voltage drop at Harker is observed in the case of running the HVDC link at 1.9GW at pre-fault. Moreover, it is clearly evident from the simulation results that the highest power transfer limit across the B6 boundary is obtained with running the HVDC link at 1.9GW and exploiting overload and fast ramp-up capability of the HVDC link at post-fault using the MIMO SR control [152].



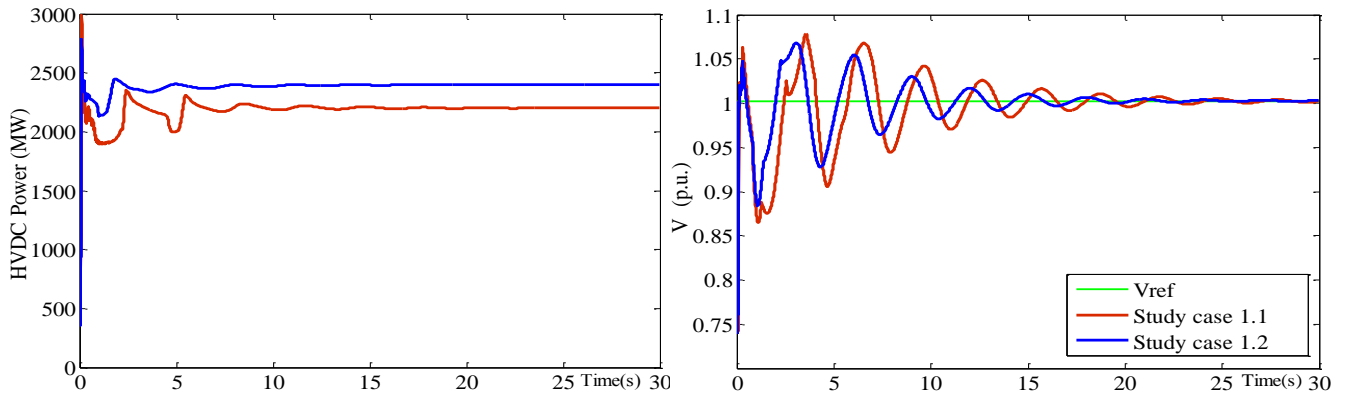
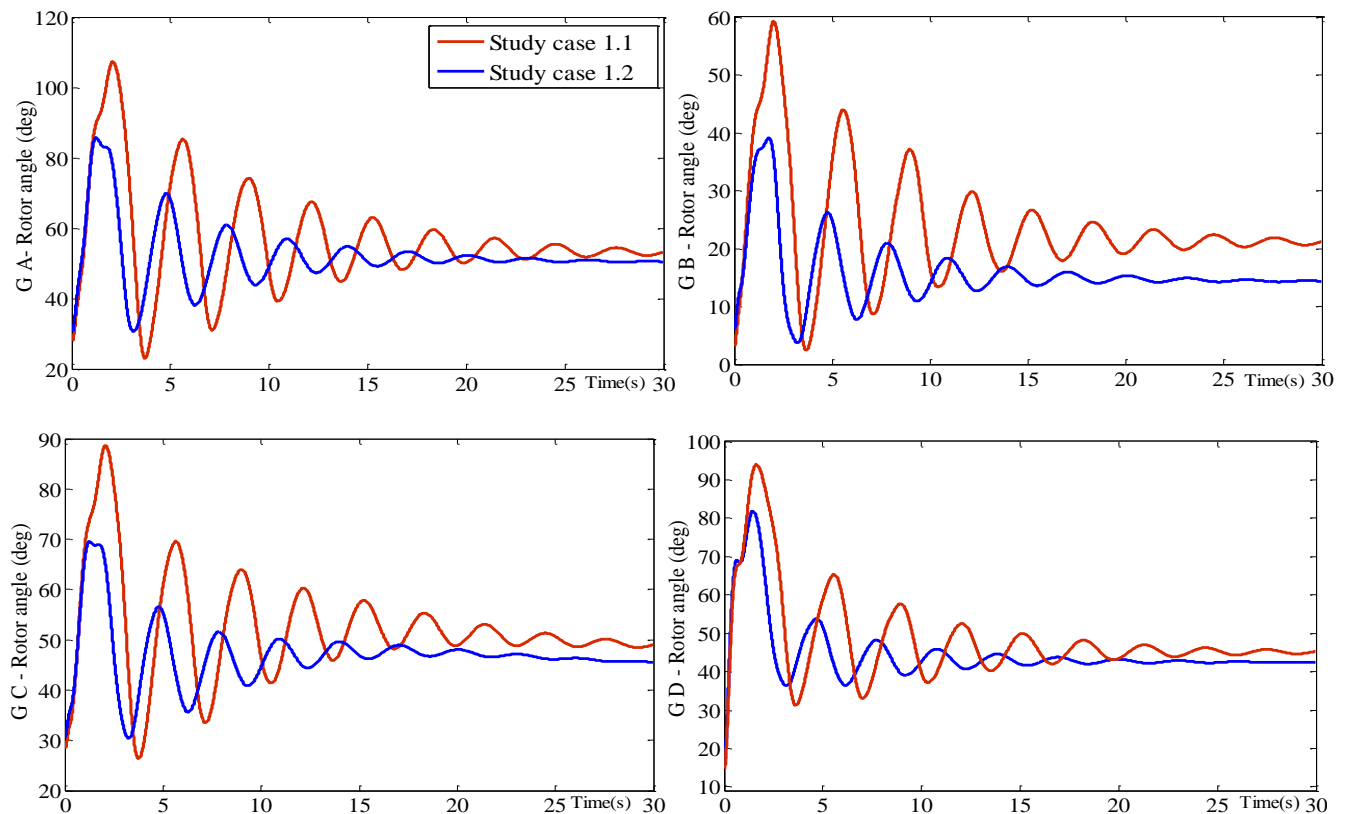


Figure 6.4: Study case 1: operation point B: Dynamic response of the system with/without implementing the HVDC link’s fast ramp-up capability through the MIMO SR control following the occurrence of the AC fault (F1) when the B6 transfer is at point B

Furthermore, operating point C represents the maximum stability transfer limit obtained when the HVDC link is operated at its maximum capacity of 2.2GW. Rotor angle oscillation of the main large generators across the network at this point are compared with the case when the HVDC link is operated at 1.9 GW and PFA is provided by the HVDC link. Simulation results demonstrated that the generators’ rotor angle oscillation is considerably higher in case 1.1. In addition, as shown in Figure 6.5, a higher voltage drop at Harker is detected in case 1.1.



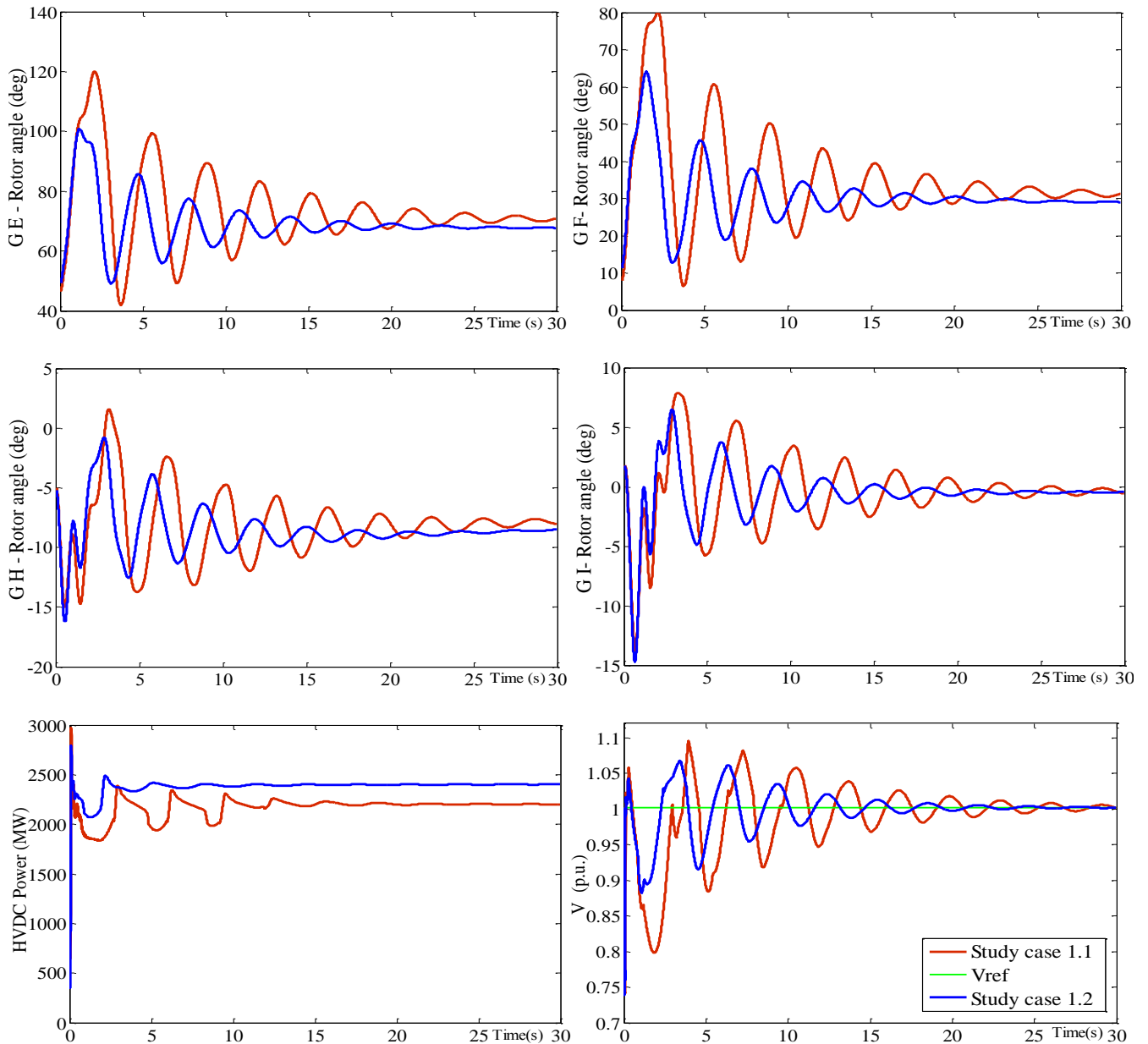
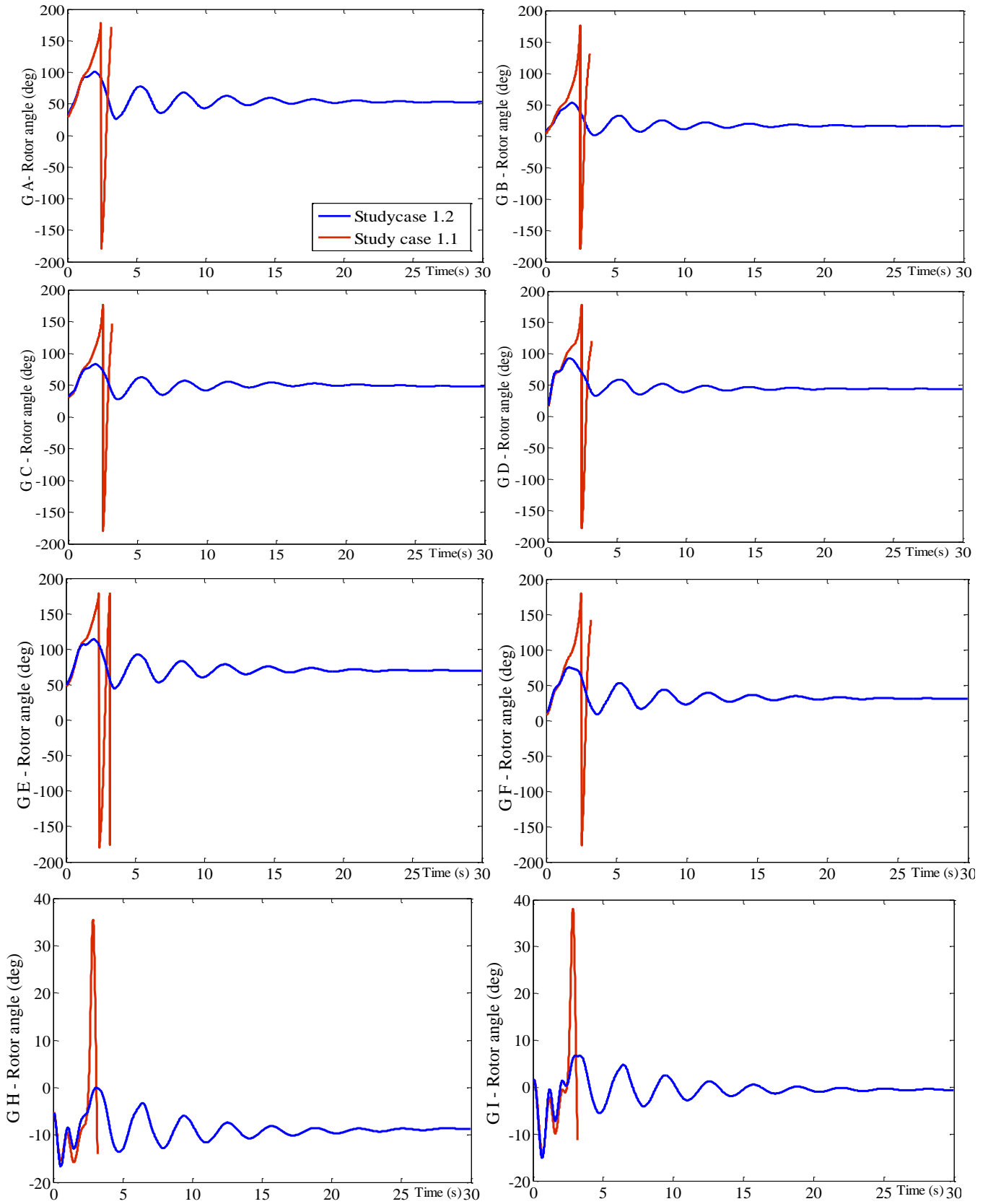


Figure 6.5: Study case 1-operation point C: Dynamic response of the system with/without implementing the HVDC link's fast ramp-up capability through the MIMO SR control following the occurrence of the AC fault (F1) when the B6 transfer is at point C.

At operating point D, where the system becomes unstable for case 1.1, system stability at this point can still be maintained at post-fault if the HVDC link is operated at 1.9 GW at pre-fault in order to implement the PFA action from the HVDC link. Figure 6.6 shows the simulation results at point D for both study cases.



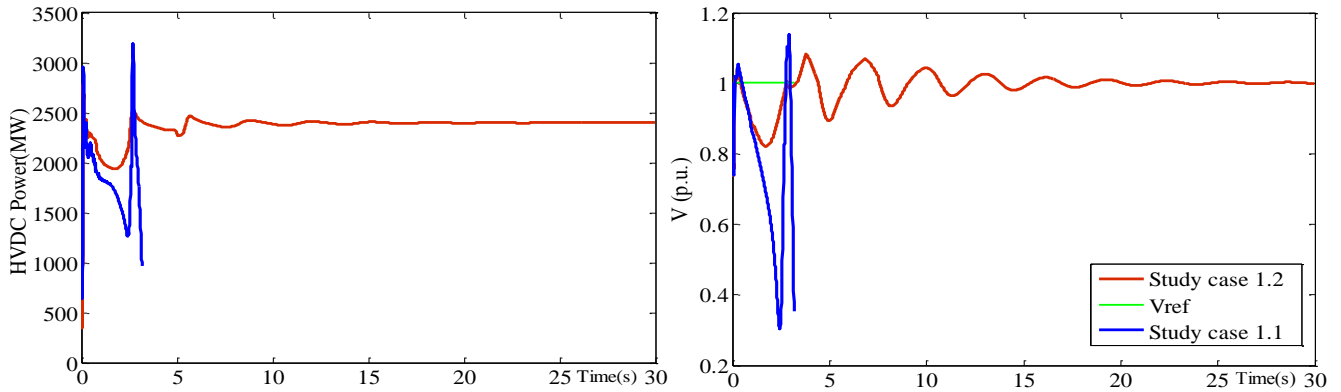


Figure 6.6: Study case 1-operation point D: Dynamic response of the system with/without implementing the HVDC link's fast ramp-up capability through the MIMO SR control following the occurrence of the AC fault (F1) when the B6 transfer is at point D

In conclusion, simulation results for study case1 revealed that higher power transfer limit and better stability performance across the B6 boundary can be attained if the HVDC link is operated at 1.9GW in order to reserve the HVDC link's fast ramp-up and overload capability for PFA. In the next section, the performance of SISO and MIMO controllers at pre-fault is only investigated for the case where the HVDC link is operated at 1.9 GW at pre-fault. This is due to the fact that the second operational strategy for the HVDC link, which was demonstrated in study case 1.2, proved to be more beneficial with regards to achieving higher transfer limit.

6.8 Simulation results and analysis for the study case 2

There is an SVC installed at Harker on the boundary of one of the two 400kV AC interconnectors between Scotland and England-Wales to support the voltage profile across this boundary. In addition to voltage regulation, the SVC is also equipped with a power oscillation damping control module. These two control systems including the HVDC links control and the SVC's power oscillation damping controller, if running separately, could have interactions with both trying to achieve their dynamic control objectives via the adjustment of power flows on the same set of boundary circuits. Therefore, the capability of the MIMO SR control for coordinated control of this SVC and the West coast HVDC link is investigated in this study using the full GB transmission system model. Similar results and dynamic performance to those presented in Chapter 5, Section 5.8.3.3, are also observed in this study case using the full GB transmission system model. The results shown in Figure 6.7 demonstrate that not only does the MIMO SR control cause less disturbance to the voltage control channel but also

provides better voltage control when a small change of set-point is applied to the HVDC link at pre-fault whereas, the interaction on voltage control is higher when the SISO PI control is implemented (green curve).

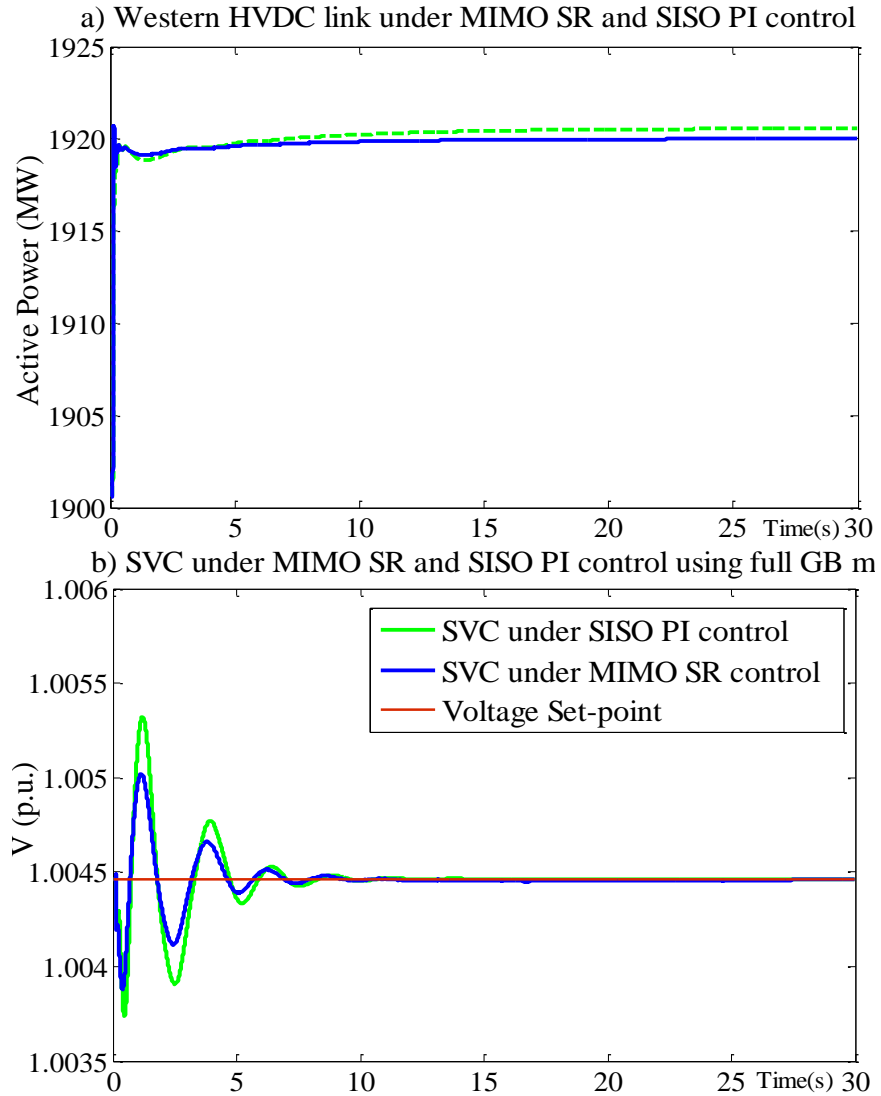


Figure 6.7: Comparison of the SISO PI and MIMO SR control performance for coordinated control of SVC and HVDC link using the full GB transmission system model

6.9 Concluding remarks

This Chapter investigated the optimal operating strategy of the West Coast HVDC link with regard to the system stability enhancement. Also, the capability of the designed multivariable SR controller in providing stability support to the main AC system to enhance the B6 boundary stability limit at post-fault by using the HVDC link's set-point adoption is demonstrated. The simulation results shown that higher power transfer limit and enhanced stability performance across the B6 boundary can be achieved if the HVDC link is operated at 1.9GW in order to spare the HVDC link's fast ramp-up and overload capability for PFA.

Moreover, the capability of the MIMO controller in the coordinated control of the West coast HVDC link and Harker SVC under one framework at pre-fault is presented in this Chapter. Further to the theoretical development of the SR controller, the capability and scalability of the proposed control design method is demonstrated on the full off-line future GB transmission system model for the coordinated control of various types of control devices including the west Coast embedded HVDC link and SVC at pre-fault. Also, the robustness of this class of SR has been tested at post-fault, which confirmed that the SR control design method is both practical and applicable to power system control even when the systems are subjected to severe disturbances. Therefore, by adopting a MIMO SR co-ordinated control, the control of various voltage and power flow devices can be obtained at pre-fault. In addition, if it is required, as mentioned above the HVDC link can also provide rapid post-fault action to pick up the flow on the lost AC line and consequently restore system stability using the MIMO SR controller.

Chapter 7

Wide-area power oscillation damping control for embedded HVDC link

7.1 Introduction

Small signal stability problems have long been identified as one of the major threats to power grid stability and reliability. This is because an undamped low-frequency oscillatory mode can cause large-amplitude oscillations and may result in large-scale blackouts [157]. In this chapter, the application of the HVDC link and TCSC for the design of a supplementary damping controller is presented. Also, two approaches for the design of power oscillation damping control are presented and their performances are investigated through a comparative study using a four-machine test system. In addition, the impact of sharing active power flows between the DC link and the AC lines on the movement of poorly damped inter-area oscillation modes is investigated prior to adding any damping controller to the HVDC control scheme. Finally, the capability of the West Coast HVDC link's damping controller in system stability improvement is demonstrated using the full GB transmission system model.

7.2 History of transient and dynamic instability in GB transmission system

Since the 1980s' the GB system has occasionally experienced low frequency oscillations at around 0.5Hz due to the fact that generator groups in the Scottish network oscillated against generator groups in the England and Wales network. An example of unstable 0.5Hz oscillations between the Scotland-England generators is shown in Figure 7.1. Following some post-event analysis, it was recognised that the oscillation damping reduces as the power flow increases across this boundary. Therefore, a lower limit on the level of power transfer across the Anglo-Scottish boundary was set. Due to the recurrence of large sustained oscillations, PSS were consequently installed on a couple of Scottish generators [158]. However, due to the dynamic characteristics and uncertainty in dynamic network simulation, there is still a significant constraint in the export of power from Scotland to England [159]. Furthermore, in order to monitor the inter-area modes and detection of any oscillations between England and Scotland, a

system was developed, which is capable of performing constant oscillation analysis and determining the frequency, amplitude and damping of the modes of oscillation. The current system has the ability to identify whether the oscillation damping on the system has dropped below predefined stability margins. On identifying any unacceptable damping an alarm is generated to alert the system operators that the system may be approaching instability. In the case of such an alert, the Scottish transfer is to be reduced in 100MW blocks, until the dynamic stability monitor returns to the stable region [160]. However, reducing the power flow across the interconnection incurs cost for consumers. Therefore, in future a more economical approach such as employing an advanced wide area power oscillation damping controller or an overall stability control system is required, in order to enhance the transfer limit across the network [161].

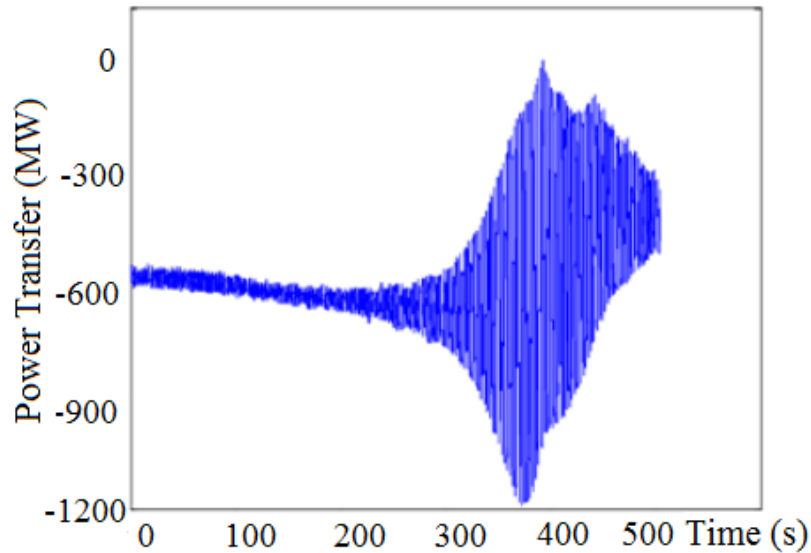


Figure 7.1: Unstable 0.5Hz oscillations between the Scotland and England [159]

7.3 Principle of modal analysis

The nonlinear model of a power system can be linearized around an operating point and presented in the state space format shown in (F.2.2) in Appendix F. The linearised state space model of the system can also be presented in a modal form (7.1) using modal transformation matrix ($M = \phi^{-1}$), which transforms the state variable to modal variables.

$$\begin{aligned} \dot{z} &= \Lambda z + B_M \Delta u \\ \Delta y &= C_M z + D \Delta u, \quad z = M \Delta x \end{aligned} \tag{7.1}$$

In (7.1), the modal state matrix is defined as $\Lambda = MAM^{-1}$, $B_M = MB$ and $C_M = CM^{-1}$ are the mode's controllability and modal observability matrix respectively. The mode controllability matrix is a $(n \times m)$ matrix, which defines how controllable a mode is through a given input. If the element $B_M(i, j)$ is equal to zero, then the j^{th} input will have no effect on the i^{th} mode. Similarly, the mode observability matrix is a $(p \times n)$ matrix which defines how observable a mode is through a given output. If the element $C_M(k, i)$ is equal to zero, then the i^{th} mode cannot be observed in the k^{th} output [22].

Overall, the transfer function of the above system can be defined in terms of input and output matrices, right and left eigenvectors and residue values as presented in (7.2). R_i is the residue of a specific mode, which gives a measure of that mode's sensitivity to the feedback between the output (y) and the input (u). It is in fact the product of the mode's observability and controllability [163][164]. All the parameters are defined in Table 7.1.

$$G(s) = \frac{\Delta y(s)}{\Delta u(s)} = \sum \frac{C\phi(:, i) * \Psi(i, :) B}{(s - \lambda_i)} = \sum \frac{R_i}{(s - \lambda_i)} \quad (7.2)$$

TABLE 7.1: Definition of parameters

ΔX	State vector	A	State matrix	λ_i	Eigenvalue
Δy	Output vector	B,C	Input and output matrix	Φ	Right eigenvector
Δu	Input vector	D	Feedforward matrix	Ψ	Left eigenvector

7.4 Application of the TCSC and the HVDC link in damping the inter-area oscillation

Traditionally HVDC links are mainly installed in a system to provide a transmission route for bulk power transfer over a long distance, or have been implemented for the connection of asynchronous networks. However, the application of embedded HVDC links which are installed in parallel with AC lines has increased. A good example of this is the future West Coast HVDC link in the GB transmission network. It is therefore, critical to investigate the impact of embedded HVDC links on system stability. Also, as previously mentioned, fast power controllability of the HVDC link can be implemented for the design of a supplementary power oscillation damping controller. The supplementary control scheme for the HVDC link, which provides modulation to the

rectifier current controller, is an effective means for the mitigation of inter-area oscillations of interconnected power systems [164][162]. Similarly, the TCSC lines are primarily installed in series with the AC line to increase the power transfer capacity in the network by reducing the impedance of the AC line. However, their fast response and capability in the control of power can be implemented to improve the system oscillation damping using a supplementary power oscillation damping control. Thus, in this Chapter the applications of the TCSC and the HVDC link for the design of a supplementary damping controller are demonstrated using the two approaches for the design of power oscillation damping control, which are presented in the next section.

7.5 Supplementary power oscillation damping control design approaches and specification

Low frequency oscillations are inherent in large integrated power systems. To improve the damping of oscillations in power systems, a supplementary power oscillation damping control can be employed for existing devices such as FACTS devices or the HVDC links. In this Chapter, two approaches for the design of power oscillation damping controller are presented. These are the PSS-based damping controller and the Modal Linear Quadratic Gaussian (MLQG) control design method. Both damping controllers are designed to shift the poorly damped oscillatory modes of the system into the left side of the complex plane in order to make the system stable and improve system oscillation damping. The selected mode of interest must be both controllable by the chosen input and observable in the chosen output for a feedback control to have any effect on the mode. Selection of suitable feedback variables is therefore critical to the design of any damping controller [164][162]. The overall structures of both damping controllers are presented in the next section.

7.5.1 PSS-based damping controller design

The PSS-based damping controller has a similar structure to that of a generator' PSS, incorporating a phase compensation block, washout filter, gain and limiter. The transfer function and structure of the PSS-based damping controller is shown in (7.3) and Figure 7.2 respectively. The main advantage of this damping control design approach is due to the fact that its control structure is uncomplicated, effective and easily tuned. However, it can only be optimally tuned for a single mode. In this study the PSS-based controller is tuned using a residue-based method [164]. The details of this method are also provided in [164].

$$H(s) = K_D \frac{1}{1 + sT_m} \frac{sT_w}{1 + sT_w} \left[\frac{1 + sT_{lead}}{1 + sT_{lag}} \right]^N \quad (7.3)$$

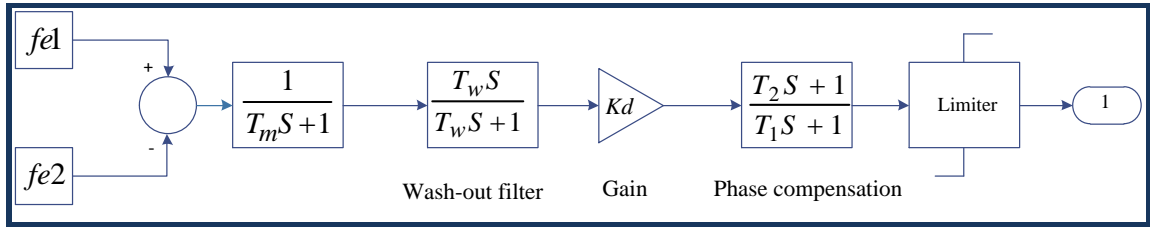


Figure 7.2: Structure of PSS-base damping controller

7.5.2 Principle of the MLQG control design method

The linearised model of a power system is defined in (7.4), where w and v are assumed to be uncorrelated process noise and measurement noise respectively [165].

$$\begin{aligned} \Delta \dot{x} &= A\Delta x + B\Delta u + \Gamma w \\ \Delta y &= C\Delta x + D\Delta u + v \end{aligned} \quad (7.4)$$

The standard LQG control is based on optimal control theory and designed to find the control input $u(t)$ signal that minimises the quadratic cost function in (7.5) which is formulated in terms of the modal variable. In this design the objective is to minimise the energy of the controlled output (states' deviation) and the energy of the input signal (control effort). However, there is continuously a trade-off between error minimisation and control effort. Matrixes “ Q_m ” and “ R ”, in (7.5), are the weighting factors which determine the trade-off between these two goals [90]. In (7.5), M is the modal transformation matrix that maps between the system modal variables (z) and system state variables (x). As explained in section 7.3, matrix (M) which is associated with the matrix of right eigenvectors ($M = \phi^{-1}$), transforms state variable to modal variables as shown in (7.6) [166].

$$J = \lim_{t \rightarrow \infty} E \int_0^t \left[x^T (M^T Q_m M) x + u^T R u \right] dt \quad (7.5)$$

$$Z(t) = M x(t) \quad (7.6)$$

The values of each diagonal element of matrix “ Q_m ” is associated to the modal variables and consequently to the equivalent mode $e^{\lambda_i t}$. Elements of the “ Q_m ” matrix are selected to penalise the corresponding states when deviating from their steady-states values. This implies that giving higher weight to a modal variable results in higher effort by the

controller to stabilise the corresponding mode. This property of the MLQG design method, allows the controller to focus only on stabilising the poorly damped mode of interest by giving weight only to the element of the “Q_m” matrix that corresponds to the mode of interest while the other modes’ weights are set to zero. In this way, the control effort of the designed MLQG is only on damping the modes of interest by shifting them to the left side of the complex plane and keeping locations of other modes unchanged. To ensure that the MLQG controller give the best damping, a search algorithm in Matlab is used to find Q_m. Similarly, the values of the diagonal elements of “R” are set in order to penalise the corresponding system inputs [166]. For the LQR problem, the solution of (7.5) can be written in the form of standard state feedback law presented in (7.7) and the LQR controller gain is computed by solving the associated Algebraic Riccati Equation (ARE), shown in (7.8), based on the cost function presented in (7.5).

$$u(t) = -K \hat{x}(t) \quad \text{where } K = \text{Const. Matrix} \quad (7.7)$$

$$K = R^{-1} B^T X, \quad X = \text{Solution of ARE} \quad (7.8)$$

$$\text{ARE} : A^T X + XA - XBR^{-1}B^T X + Q \quad (7.9)$$

In (7.7), all the system states must be measurable in order to find gain K. However, in reality all the system states are not available. Consequently, an observer is required to estimate the unavailable system states. The $\hat{x}(t)$ is therefore an estimation of the state variable (x), obtained using a Kalman filter shown in Figure 7.3. The Kalman filter is defined in (7.10), where L is a constant estimation error feedback matrix, which minimises $E = [(x - \hat{x})^T (x - \hat{x})]$ and is designed and calculated by solving the cost function defined in (7.11).

$$\hat{x}(t) = A \hat{x} + Bu + L(y - C \hat{x}) + Lv \quad (7.10)$$

$$J_L = \lim_{t \rightarrow \infty} E \int_0^t [(x^T W x + u^T V u)] dt \quad (7.11)$$

The weighting matrices W and V are calculated as in (7.12) and tuned based on the Loop Transfer Recovery (LTR) procedure at either plant input or output [166][165].

$$W = \Gamma W_0 \Gamma^T + q B \theta B^T \quad \text{and} \quad V = V_0 \quad (7.12)$$

Where W_0 and V_0 refer to the nominal model noise and θ is any positive definite matrix. As shown in Figure 7.3, the MLQG is an optimal controller obtained as the combination of an optimal MLQR state feedback gain and feedback from an optimal state estimator (Kalman filter). Therefore, the MLQG closed loop poles are simply the combination of the poles of the MLQR system and the poles of the Kalman filter, Therefore, the separation principle can be used to solve the MLQG control problem, which has the same order as the plant [166]. In addition, it is important to note that a linear state-space model that correctly captures the dynamics of the power system is required to be obtained before the design of the model-based MLQG damping controller, which will be further explained in section 7.9.

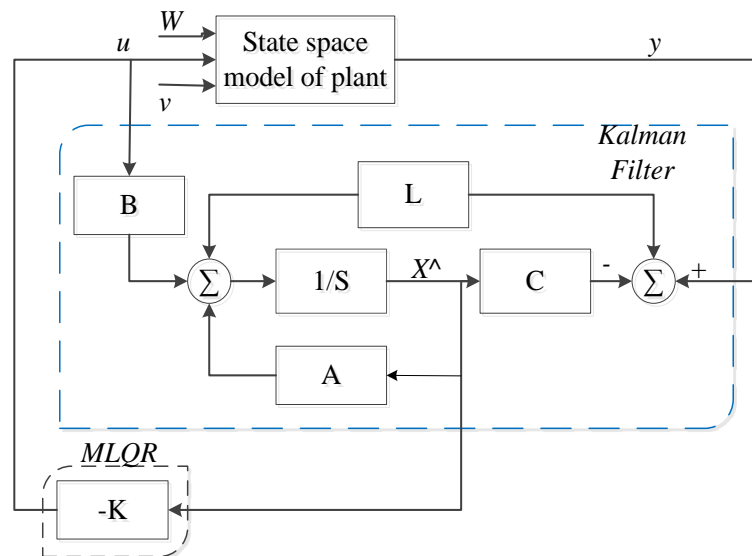


Figure 7.3: Structure of the MLQG damping controller

7.6 Test systems under study

Two power system network models have been used in this Chapter for the purpose of small stability analysis. First, a simple concept proving test system is used for demonstrating the application of the TCSC and the HVDC link in dynamic stability enhancement. Then the full GB transmission system model is used to investigate the capability and effectiveness of the West Coast HVDC embedded link in improving the system power oscillation damping and transient stability.

7.6.1 Two Area , four- machine concept proving test network

This simple test model is based on a four-machine multi-bus system as shown in Figure 7.4. This model is suitable for the purpose of small disturbance stability analysis.

This is because a large volume of power is transferred from bus 3 to bus 5 over a long distance line. Also, generators at both sides are likely to oscillate against each other following a disturbance due to the existence of a poorly damped inter-area mode of oscillation. In addition, the model is modified and a HVDC link is added in parallel with AC lines. The HVDC link, which is modelled as a CSC-HVDC link carries 100MW of active power. Also, a dynamic model of the generator is implemented in this test system. The eigenvalues of the system under study are presented in Table 7.2, which will be further explained in section 7.9.4.

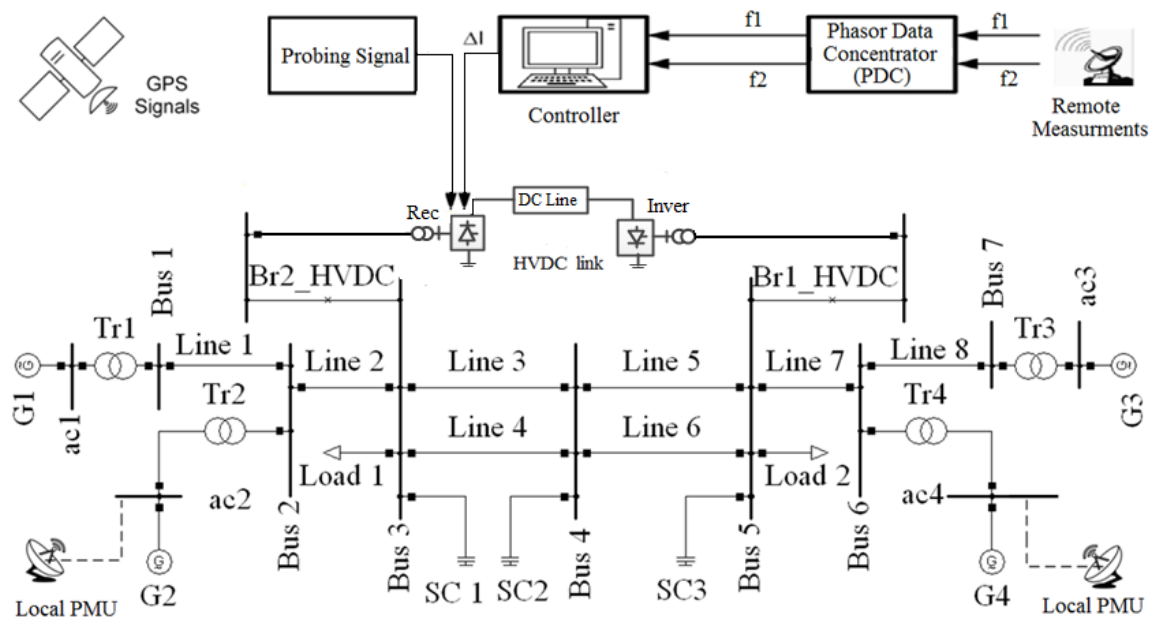


Figure 7.4: Four-machine test system in DIgSILENT with HVDC link

TABLE 7.2: Eigenvalues /Modes of the two-area, four-machines test system with HVDC link

Mode	Real part 1/s	Imaginary part rad/s	Frequency Hz	Damping 1/s	Damping Ratio
Mode 1	-0.49	6.25	0.99	0.48	0.08
Mode 2	-0.48	6.47	1.03	0.48	0.07
Mode 3	0.002	3.21	0.51	-0.002	-0.0008
Mode 4	-1.7	1.67	0.27	1.73	0.72
Mode 5	-0.33	1.02	0.16	0.33	0.312
Mode 6	-0.94	1.03	0.163	0.94	0.68
Mode 7	-0.42	0.65	0.102	0.4207	0.55
Mode 8	-0.42	0.64	0.101	0.421	0.55

7.6.2 Full GB Transmission system model

The effectiveness of the West Coast HVDC embedded link in improving power oscillation damping is investigated using the full dynamic model of the GB transmission system. This model represents the 2016 generation profile based on the Gone Green future energy scenario [6][134]. In addition, in order to have a dynamic model and obtain realistic results all generators are equipped with excitation system models and governors. Also, all PSS remain connected and in service. The detailed description of the model and the processes of creating this model from the current year model are explained in section 6.2 of Chapter 6. Also, as previously mentioned in Chapter 6, the B6 boundary is currently limited by stability constraints. In line with future reinforcements across the B6 boundary, a 2.2GW, 600kV Bipolar CSC-HVDC link to enhance the power transfer capacity of the transmission corridors between Scotland and England is planned to be installed by 2016 on West Coast between Hunterston (SPTL) and Deeside (NGET), as shown in Figure 7.17. A CSC-HVDC model is therefore integrated in this model to represent the West Coast HVDC link. In this study, the high volume of power transfer ($\approx 4.7\text{GW}$) exported from Scotland to England on the B6 boundary is shared between the AC lines and the DC link.

7.7 Design of the supplementary power oscillation damping controller for the TCSC line

Ideally, all generators in the power system are synchronous machines and rotate with the same angular velocity. In reality this is not the case and the generators have slightly different rotor speeds or angles to deliver the required energy demand. Disturbances may increase the severity of such oscillations. Apart from the generator PSS, various FACTS devices such as the TCSC can be equipped with supplementary power oscillation damping controllers to damp the aforementioned inter-machine (area) oscillations [146][167]. In this section the PSS-based design approach is implemented in the design of the supplementary damping control for the TCSC as an actuator. The controller is tuned using the residue based method to shift the undamped eigenvalue/mode of the system into the left side of the complex plane to improve oscillation damping [164]. As previously mentioned, the selection of suitable feedback variables is critical to the design of any damping controller. In this study, the difference between the generators frequency is implemented as an input signal for the damping controller.

7.7.1 Characteristics of modified the test system under the study for design of the TCSC's damping controller

The two-area four-machine test system introduced in section 7.6.1 is modified as shown in Figure 7.5 for investigating the application of the TCSC for the design of power oscillation damping. At the mid-point, the AC line is compensated with a TCSC, which provides 40% compensation of the line reactance. As described in section 2.1, the TCSC is an impedance compensator component that is added in series to an AC transmission line to increase the power transfer capability of the line. It is also able to contribute to the power system stability enhancement by load flow control of the system. For power system stability studies, the Thyristor operation is negligible in the simulations. Consequently, for such studies, a TCSC can be represented using a simplified and ideal model with only a fixed capacitor in parallel with a variable reactor. During the steady state operation of the system the TCSC reactance is controlled to provide the expected power flow. In addition, the TCSC can also play an important role in improving the damping of low frequency power oscillations. This can be realised by adding a supplementary damping controller that provides a damping signal to dynamically change the TCSC's reactance. In the presented study case, a typical PSS-based power oscillation damping supplementary controller (with the same structure presented in section 7.5.1) for the TCSC is designed and tuned based on the modal and residue analysis [164][141]. The performance and ability of the TCSC damping controller in enhancing the system oscillation damping is investigated following the occurrence of a large disturbance such as a 3-phase fault on the system.

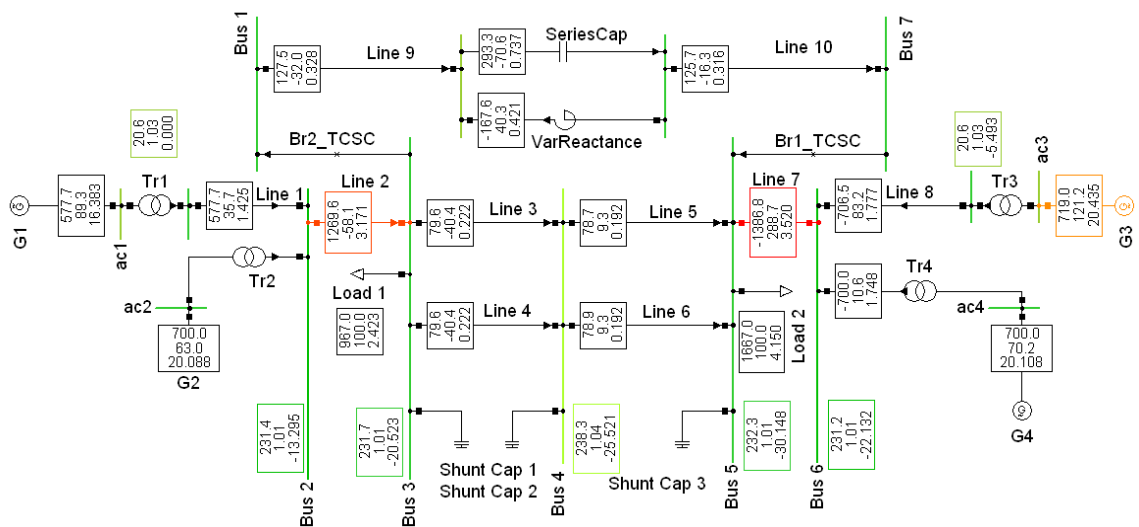


Figure 7.5: Four-machine test system in DIgSILENT including the TCSC line

TABLE 7.3: Eigenvalues /Modes of the two-area, four-machines test system with No damping control for TCSC

Mode	Real part 1/s	Imaginary part rad/s	Frequency Hz	Damping 1/s	Damping Ratio
Mode 1	-0.552	6.27	0.99	0.55	0.087
Mode 2	-0.0875	3.245	0.51	0.078	0.025
Mode 3	-0.460	6.452	1.027	0.46	0.071
Mode 4	-1.60	1.537	0.24	1.60	0.72
Mode 5	-0.333	1.015	0.16	0.33	0.312
Mode 6	-0.827	0.980	0.156	0.82	0.644
Mode 7	-0.403	0.62	0.993	0.403	0.543
Mode 8	-0.407	0.642	0.101	0.407	0.536

Prior to that, a modal analysis is conducted to observe the impact of the TCSC damping controller on the poorly damped mode of the system. The Table 7.3 shows the modes of the system integrated with the TCSC line with no damping controller. As can be seen, although all the modes are stable, mode 2 has damping ratio of 2.5%, which is less than 5%. The parameters of TCSC damping controller is presented in Appendix C.

7.7.2 Simulation results on performance of the PSS-based damping controller for TCSC

The results provided in Figure 7.6 present the effect of the power oscillation damping controller on the system response including the rotor angle of generators (Figure 7.d,e, f), Power on line3 (Figure 7.c) and power on the TCSC line (Figure 7.a). The modulation signal generated from the damping controller is also shown in Figure 7.6.b. The performance of a supplementary damping controller for the TCSC is observed following the occurrence of a severe disturbance such as a three phase short circuit fault on line 2. It is clearly evident that the controller is able to improve the systems power oscillation damping following a sever disturbance and stabilise the system in less than 12s as required by SQSS [15]. Also, as Table 7.4 shows, after adding the damping controller the damping ratio of mode 2 increases significantly to 12.9%.

TABLE 7.4: Modes of the two-area, four-machines test system with damping cont. for TCSC

Mode	Real part	Imaginary part	Frequency	Damping	Damping Ratio
Mode 1	-0.646	3.66	0.99	0.646	0.173
Mode 2	-0.815	6.240	0.58	0.815	0.129
Mode 3	-0.518	6.357	1.01	0.517	0.082
Mode 4	-1.63	1.584	0.25	1.62	0.716
Mode 5	-6.90	6.25	0.99	6.908	0.741
Mode 6	-0.333	1.016	0.167	0.333	0.312
Mode 7	-0.815	0.977	0.155	0.815	0.641
Mode 8	-0.406	0.631	0.100	0.405	0.539

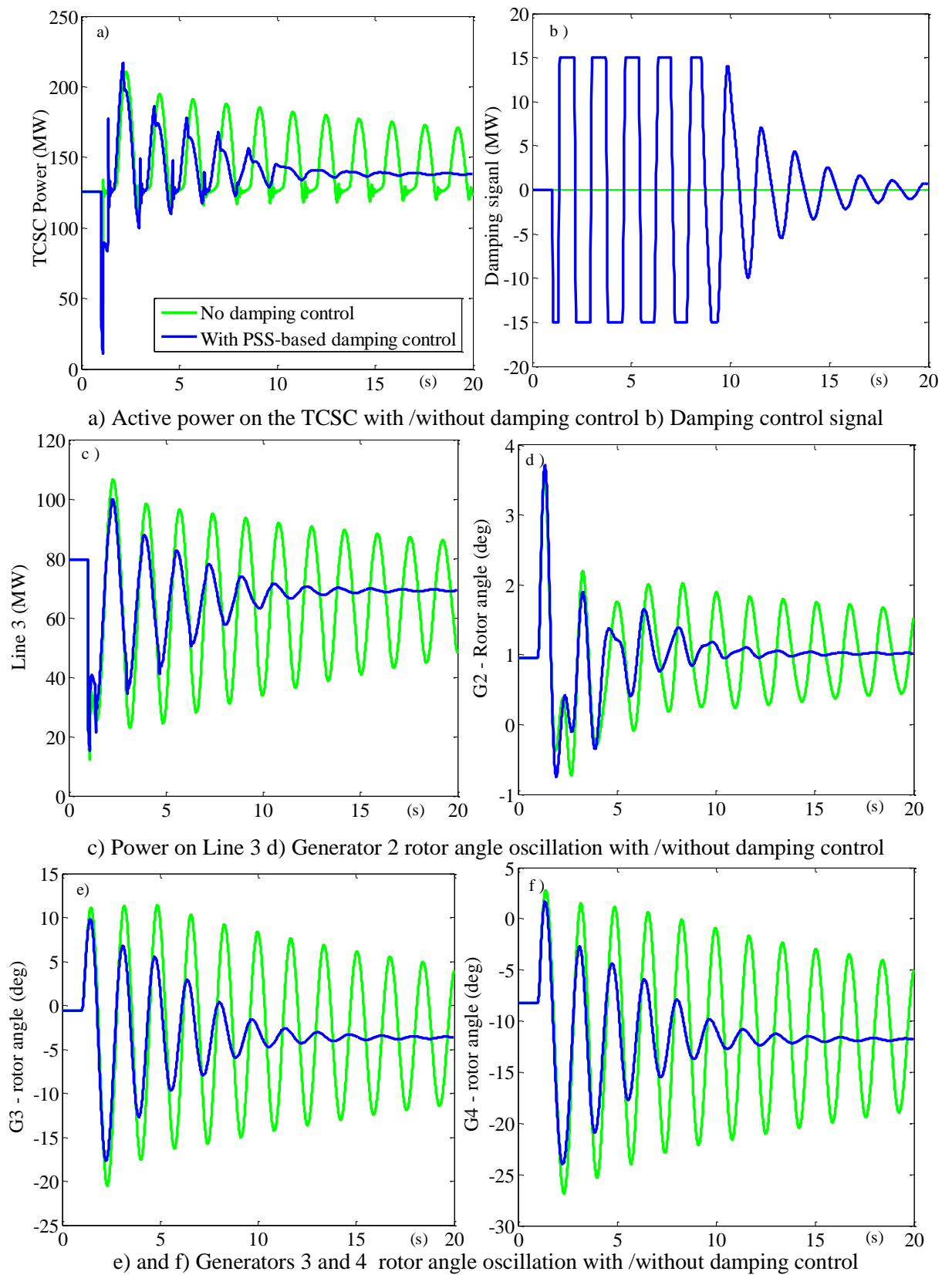


Figure 7.6: The effect of the TCSC damping controller on the system stability

7.8 Impact of the sharing of active power on the AC and DC lines on the system small-signal stability

The impact of sharing active power flows between the DC link and the AC lines on the movement of poorly damped inter-area oscillation modes was investigated prior to adding any damping controller to the HVDC control scheme using the test system 3. It was observed that as the active power on the DC link is gradually increased from 600MW to 1.2GW and more power is pushed from the AC lines to the DC link the synchronising and damping ratio of oscillatory modes are increased as shown in Figure 7.7, which consequently results in improving the dynamic stability of the network. Also, as can be seen in Figure 7.8 that the frequency of the poorly damped oscillatory mode increases by increasing the power flow on the HVDC link.

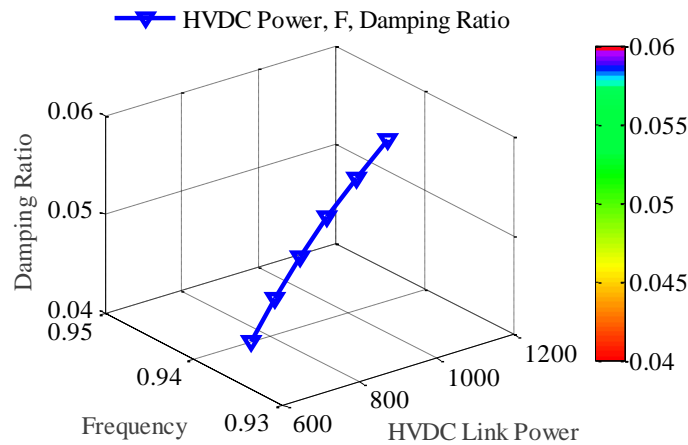


Figure 7.7: Impact of the HVDC link power flow variation on the damping ratio of the oscillation mode

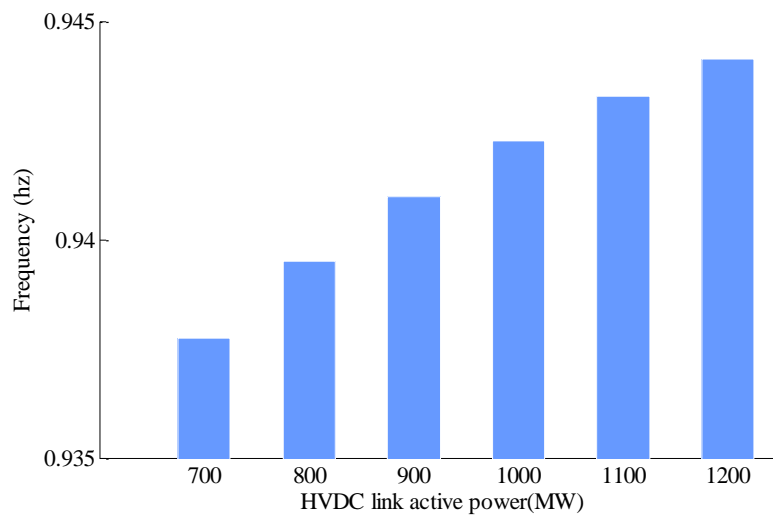


Figure 7.8: Impact of the HVDC link power flow variation on the damping ratio of the oscillation mode

7.9 Design of supplementary power oscillation damping control for the CSC-HVDC link (study case on small test system)

Performance of both PSS-based and MLQG-based supplementary damping controllers for the HVDC link are investigated and presented in the following sections. Also, the requirements for the design of model-based MLQG damping controller is discussed in next section.

7.9.1 Requirements for the MLQG-based damping controller for the HVDC link

The MLQG controller design method is a model-based design approach and requires a linear model of the system, which correctly captures the dynamic properties of the power system under control. NG utilises PowerFactory as a simulation tool for power system modelling and performing off-line security studies. However, PowerFactory doesn't provide the linearised model of the system. This limits the capability of PowerFactory for the design of the controller [141]. The PowerFactory and Matlab interface capability is therefore, implemented in order to utilise the available system identification algorithm in Matlab to obtain the linearised model of the system for the design of the MLQG damping controller. With having the linear model of the system, the linear analysis methods, which are standard functions in the analytical tool, can be implemented for the investigation of low frequency oscillation in power systems. The system identification method, which is a measurement-based approach, estimates the low-order, linear, mathematical models of the dynamic systems from the measured input-output data [168][169]. Various identification algorithms are available for the identification and construction of the system's linear model. For example, the state-space identification algorithm, which provides the system model in linear state-space form, as given in (F.2.2) in Appendix F, is a common and reasonable approach to model a large power system around its operating point. The resultant linear model captures the critical modes of the original nonlinear system, which can be implemented for the damping controller to enhance system dynamic stability. Since the estimated linear model of the system is based on the obtained WAM outputs, resulting from the response to the injected low-level band-limited input signals, the selection of input and outputs signals and the validation of the estimated model are considered as the main steps in obtaining the linear model of the system using the system identification approach [59][170].

7.9.1.1 Selection of signals for system identification

Not only the appropriate selection of input and output signals is essential in the accurate estimation of the system model, but also, the selection of suitable stabilising input signals is critical in the design of any damping controller. Since the design of the damping controller is based on the modulation of the actuators' active power set-point, the controllable input of actuators such as the HVDC link's active power set-point is considered as an input point to inject the input signal. A probing signal such as a Pseudo Random Binary Sequence (PRBS), which causes low disturbances to the power system, is selected for the input signal. The signal amplitude has to be chosen high enough to sufficiently excite the critical modes yet keeping the responses within the linearisable zone of the operating condition [171][100]. The system response to the injected signal is selected as the output signal for system identification. This selected output could be WAM tie-line flows, bus voltage phase angles or bus frequencies at various points, which give a high observability of the inter-area modes compared to local signals. However, the frequency difference is a better option since its value is independent of the system operating point and consequently the estimated model will show more robustness [168].

7.9.1.2 System model validation and reduction

The identified linear model needs to be validated through a step response test against the actual measurements in PowerFactory DIgSILENT. This is done by comparing the response of the estimated model with the response of the actual model of the system in PowerFactory to another set of un-correlated probing PRBS signals different from the original PRBS signal used for system identification. Another key factor in system identification is the selection of a suitable system order. The singular value decomposition is used as a means to select the best model order. The singular value corresponding to order (n) is a measure of how much the (nth) component of the state vector contributes to the input-output behaviour of the model. A good choice of model order 'n' is one where the singular values to the right of the selected order are small compared to those to the left [172]. To evaluate the fitness of the identified model the following fitness value equation presented in (7.13) can be used.

$$\bar{Y}_{\text{fit}} = 100 \left[1 - \frac{\bar{y} - \hat{y}}{\bar{y} - \bar{y}} \right] \quad (7.13)$$

Where y is the measured output, \hat{y} is the simulated output and \bar{y} is the mean of the y over the simulation period [170]. A description on procedure and steps of the system identification routine to identify the linear model of non-linear systems is provided in Appendix D.

7.9.2 Linearised model of the test system using system identification

The four-machine test system shown in Figure 7.4 is used to investigate the performance of both PSS and MLQG-based damping controllers. As detailed in the previous section, the linear model of the system is required for the design of the MLQG. Therefore system identification is applied in MATLAB/Simulink to derive the state-space model from the input-output measurements. As the first step of the identification process, the appropriate input and output signals are selected. A PRBS-based probing signal, shown in Figure 7.9.a, is given to the active power set-point of the HVDC link as the input signal.

The amplitude of the input signal is selected to be high enough to excite the critical modes. The amplitude of the chosen signal should not result in high variation in the active power set-point of the HVDC link. The selected input signal and response of the system to that (such as generator's rotor angle oscillation) is presented in Figure 7.9.b. Also, as explained in section 7.9.1.1, the frequency difference between two areas is chosen as the system output for the system identification. Thus, the measurements from the PMUs installed at Bus 2 and Bus 6, shown in Figure 7.4, are collected to be used as output signals. Following the processing of the input/output data to remove any trend, the system identification function available in Matlab is applied to obtain a state-space linear model of the system.

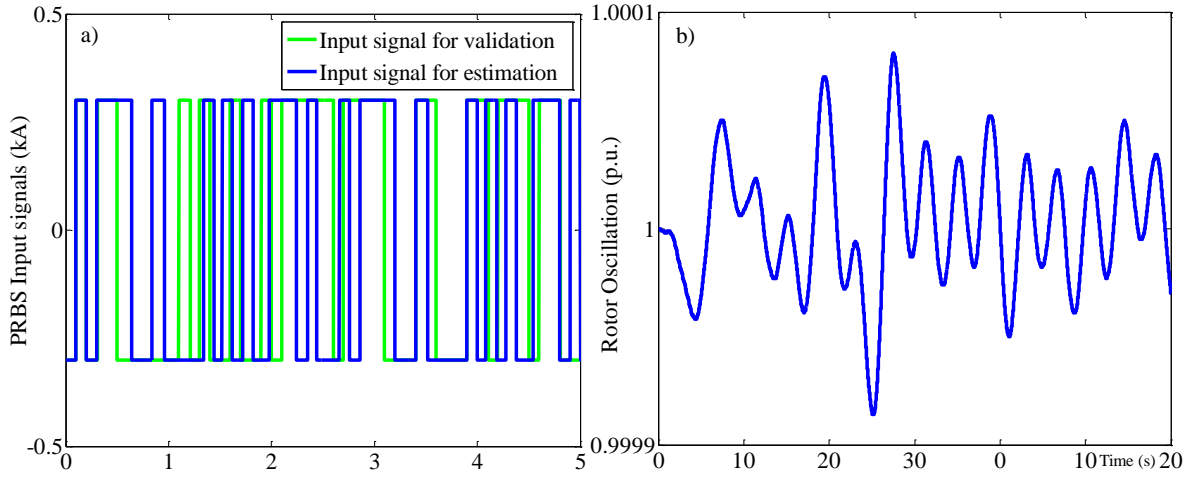


Figure 7.9: a) The injected signal for system identification, b) System response (rotor oscillations) following the injection of the PRBS signal

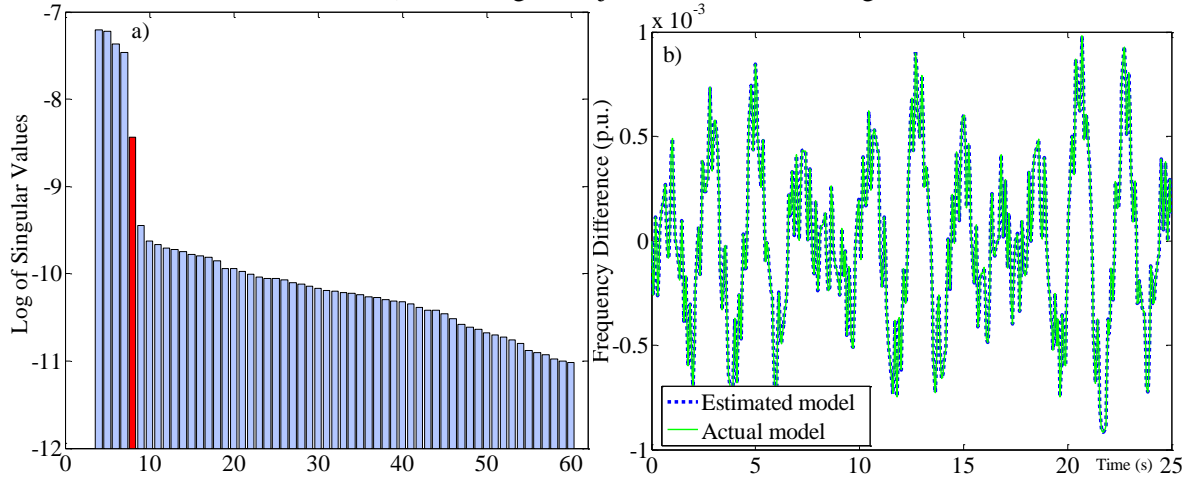


Figure 7.10: a) Model order selection using the singular value, b) Validation of the estimated linear model and actual non-linear system

In addition, an appropriate order of the obtained state-space model is chosen based on the log of singular values. The criterion is to select an order where the singular values to the right of the selected system order “n” are small compared to those to the left. As presented in Figure 7.10.a, the order (8) satisfies this criterion and therefore selected as the order of obtained state-space system model. However, in order to reduce the size of the controller, the identified model was further reduced to order 6. Finally, the obtained model is validated to ensure that the estimated linear model is a good match for the actual non-linear system model using a different set of independent input-output data generated by DIgSILENT. Figure 7.9.a shows the un-correlated PRBS signal (green line) implemented as a new set of input signal injected to the estimated linear model for model validation. As can be seen in Figure 7.10.b the estimated model is accurately identified based on the obtained data with a high fitness value of 99.62% calculated using (7.13).

7.9.3 Main features of the MLQG damping controller design

Firstly, as previously mentioned in section 7.5.2, the MLQG damping controller is capable of shifting the oscillatory mode of interest towards the stable part of the complex plane by assigning a non-zero value to the corresponding element within the “ Q_m ” matrix without the need for calculation of the participation factor matrix. The higher weighting value leads to a larger displacement of the targeted mode. Very high values of “ Q_m ” element have to be avoided as this could create instability within the system [166].

Secondly the individual robustness of the MLQR and the Kalman filter is lost when they are combined together to form the MLQG controller. The Loop Transfer Regulator (LTR) procedure at plant input or output is a commonly used method to achieve robustness recovery. In this procedure, the LQR is designed first in order to add damping to the lightly damped inter-area modes. Then, the Kalman filter is added such that the loop transfer function of $K_{LQG}(s)G(s)$ (where $G(s)$ is plant transfer function and $K_{LQG}(s)$ is LQG controller transfer function) approaches the LQR loop transfer function [90][166]. Figure 7.10 presents the LTR procedure for various values of (q) including 1, 10, and 100 and 1000. The measurement noise covariance is selected quite low (0.001) to reflect the characteristics of high quality PMUs [170][173]. As can be seen in Figure 7.11, for $q=1000$ the LQG controller closely maintains the LQR robustness around the desired frequency range of the inter-area modes. The overall structure of MLQG controller and the parameters of the designed controller are presented in Appendix C.

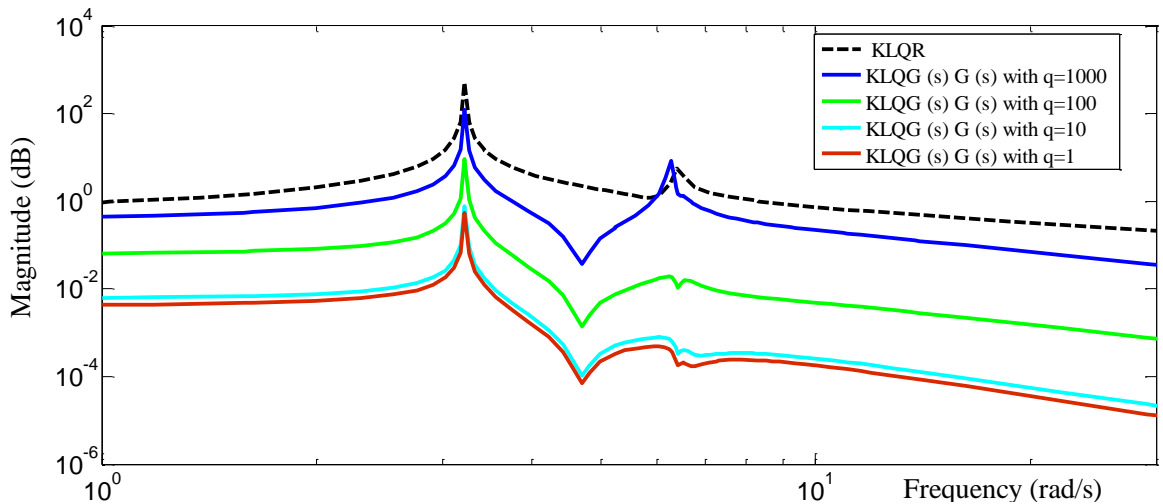


Figure 7.11.: LTR with different value of q

7.9.4 Capability of the MLQG and PSS-based damping controller for the HVDC link

The model analysis was performed for the test system under the study presented in Figure 7.4 and the results revealed three electromechanical modes, including two local modes and one inter-area oscillatory mode with a damping ratio less than 5%, which is shown in Table 7.5. As shown in Figure 7.12, the inter-area mode of the test system is unstable (mode 3, shown with the red arrow) and additional damping is required to be provided to maintain the system stability. Hence, a supplementary damping controller is added to the HVDC link control system to investigate the effect of the damping controller on moving the poorly damped oscillatory mode to the left side of the complex plane. Both approaches introduced in section 7.5 for the design of a damping controller for the HVDC link are implemented.

TABLE 7.5: Eigenvalues /Modes of the two-area, four-machines test system

Mode		Effective machine	Eigenvalues	Damping Frequency	Damping	Damping Ratio
Mode 1	Local	G1 and G2	$-0.49 \pm 6.25j$	0.99	0.48	0.076
Mode 2	Local	G1 and G4	$-0.48 \pm 6.47j$	1.023	0.48	0.073
Mode 3	Inter-area (IA)	IA	$0.002 \pm 3.21j$	0.51	-0.002	-0.0008

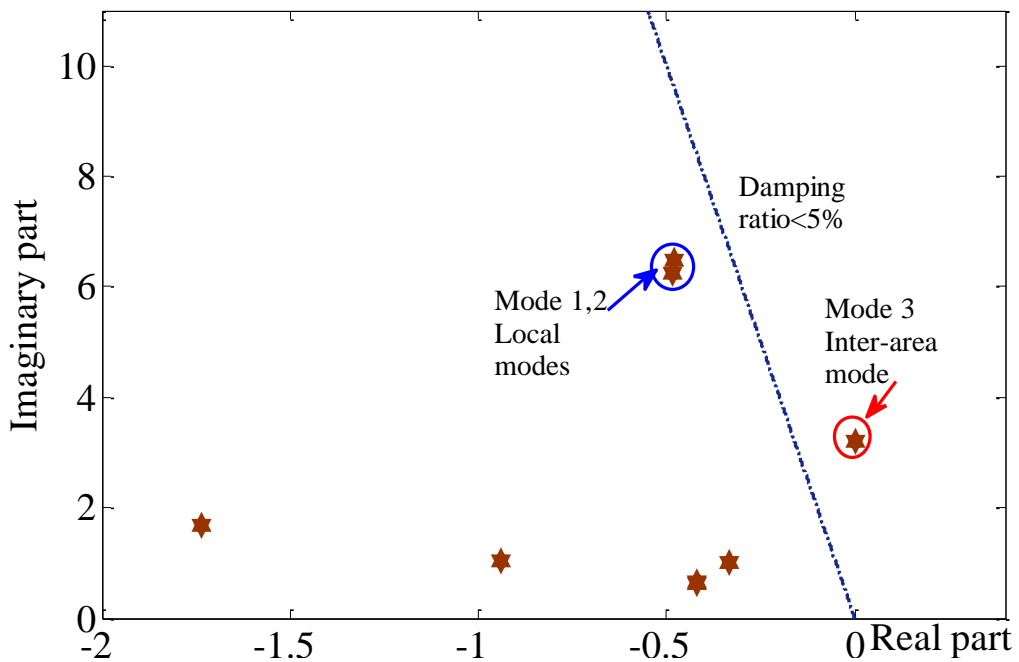


Figure 7.12: Modes of the four-machine test system in complex plane

7.9.4.1 Definition of the study cases to investigate the effectiveness of both designed damping controllers for the HVDC link

In order to investigate the performance, capability and robustness of both the MLQG and the PSS-based damping controllers in the enhancement of system stability, two study cases are defined. For the first study case the performance of both damping controllers and the system responses are investigated following the occurrence of a small change to the system. A small disturbance in the system is created to excite the inter-area mode of the system by increasing the mechanical torque of generator 2 by 0.01(p.u.) and simultaneously decreasing the mechanical torque of generator 4 by 0.01(p.u.). In the second study case, the robustness of the damping controllers is examined by applying a large disturbance to the test system. A large disturbance in the system is created by applying a three-phase fault on line 2. Prior to performing the above mentioned study cases the nominal performance of both damping controllers is investigated by conducting a modal analysis with and without damping controllers in service. The impact of both the PSS-based and the MLQG damping controllers on the modes of the system's frequency, damping ratio and damping constant are presented in Table 7.6. Also, the movement of the system modes are presented in Figure 7.13, which shows that without implementing a damping controller, there is a critical unstable inter-area mode on the right side of the complex plane, which has a time constant of 379s. However, following the implementation of the damping controller, it is evident from the results presented in the plot of poles in Figure 7.13 that both controllers are capable of moving unstable modes to the stable side of the complex plane and achieve a damping ratio of higher than 5%.

TABLE 7.6: Impact of the damping controllers on the modes of the system's frequency , damping ratio and damping constant

System Modes		No damping control	PSS	MLQG
Damped Frequency	Mode 1	0.995	0.996	0.950
	Mode 2	1.023	1.033	0.994
	Mode 3	0.51	0.59	1.029
Damping Ratio	Mode 1	0.076	0.0761	0.092
	Mode 2	0.073	0.083	0.077
	Mode 3	-0.0008	0.408	0.074
Damping time constant	Mode 1	2.073	2.071	1.804
	Mode 2	2.083	1.843	2.072
	Mode 3	379.59	0.599	2.0727

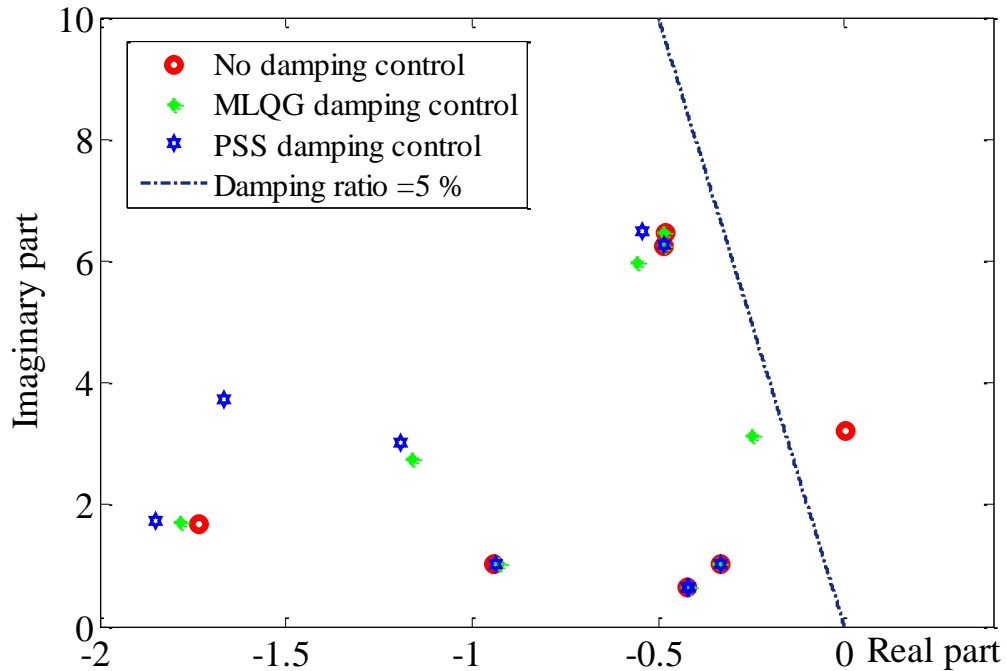


Figure 7.13: Damping of system poles with and without damping controller

In addition, as can be seen from the results in Table 7.6, both controllers increase the system modes' damping ratio and damping frequency. However, the MLQG controller shows more effectiveness on local mode1 and increases the damping ratio of mode 1 from 7% to 9% whereas; the PSS controller is hardly effective on mode1. On the other hand, the PSS damping controller is more effective on damping mode 2 and mode 3. This is because the PSS damping controller is tuned based on a poorly damped mode of interest which is inter-area mode 3. Whereas in the MLQG design method, weighting factors not only affect the poorly inter-area damped mode of interest, but also affect all local modes in the system. Therefore, the performance of the MLQG can be improved if the weighting is only given to oscillatory inter-area modes of interest in order to achieve targeted damping for the critical inter-area system modes [166][146].

7.9.4.2 Simulation results on the performance of the PSS-based and MLQG-based damping controller (study case1)

The system responses including the generator rotor angle oscillation, frequency differences between busbar 2 and 6 and active power in line 3 to a small disturbance with and without implementing a damping control are presented in Figure 7.14. Following the occurrence of a small change in the system without damping controller the system is instable as shown in Figure 7.14.a,d,e,f (grey dotted lines). However, with the designed MLQG and PSS-based damping controllers installed, the system oscillation damping is

improved significantly; particularly the inter-area mode 3 achieves very good damping. However, the simulation results confirm that the PSS-based controller provides slightly better performance with regard to improving inter-area oscillation damping when the system is subjected to a small disturbance.

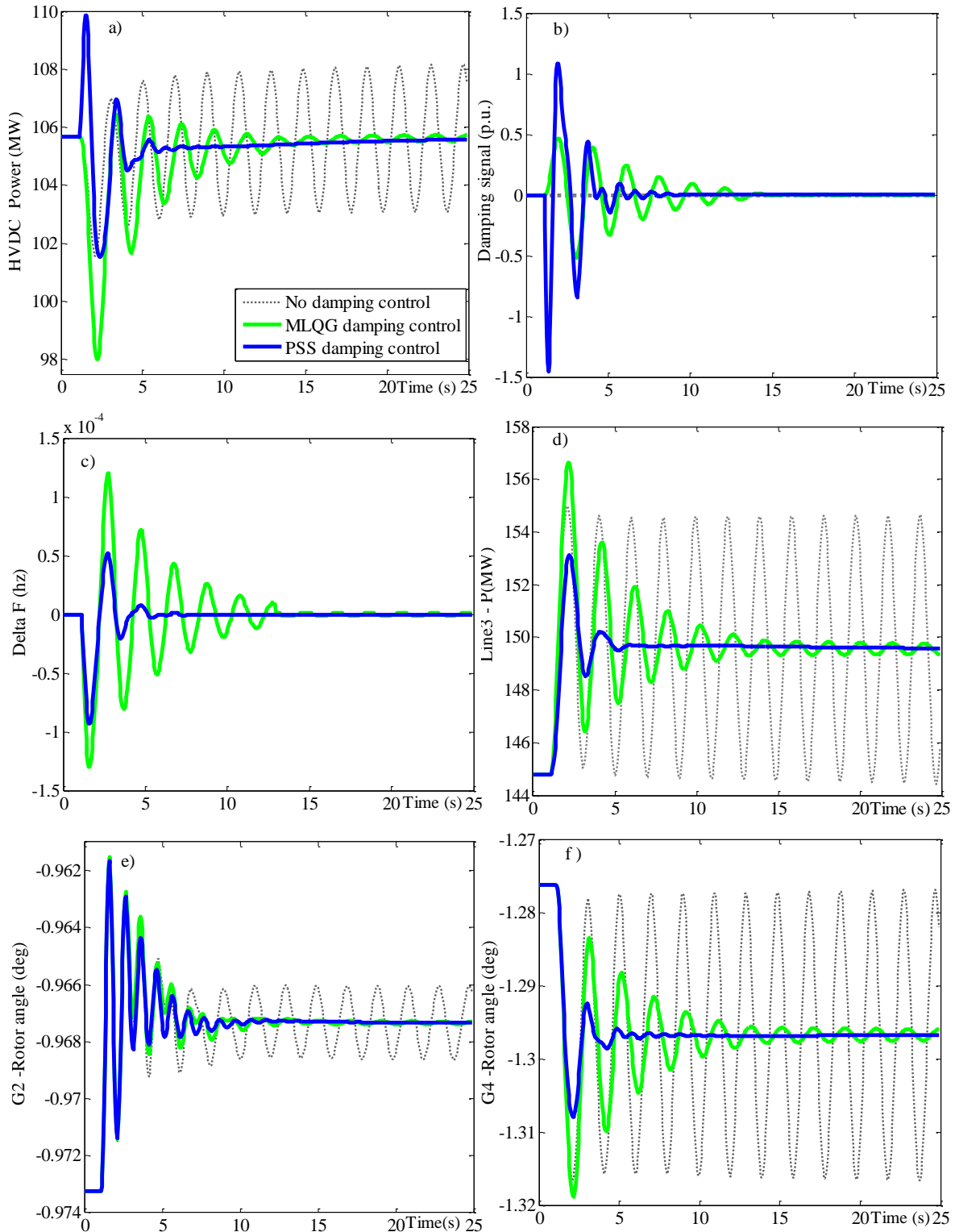


Figure 7.14: Comparative study on performance of PSS and MLQG damping controller, system response with/ without damping controller following a small disturbance

7.9.4.3 Simulation results on the performance of the PSS-based and MLQG-based damping controllers (study case 2)

Similarly, the system responses to a large disturbance with/without implementing a damping control are presented in Figure 7.15.

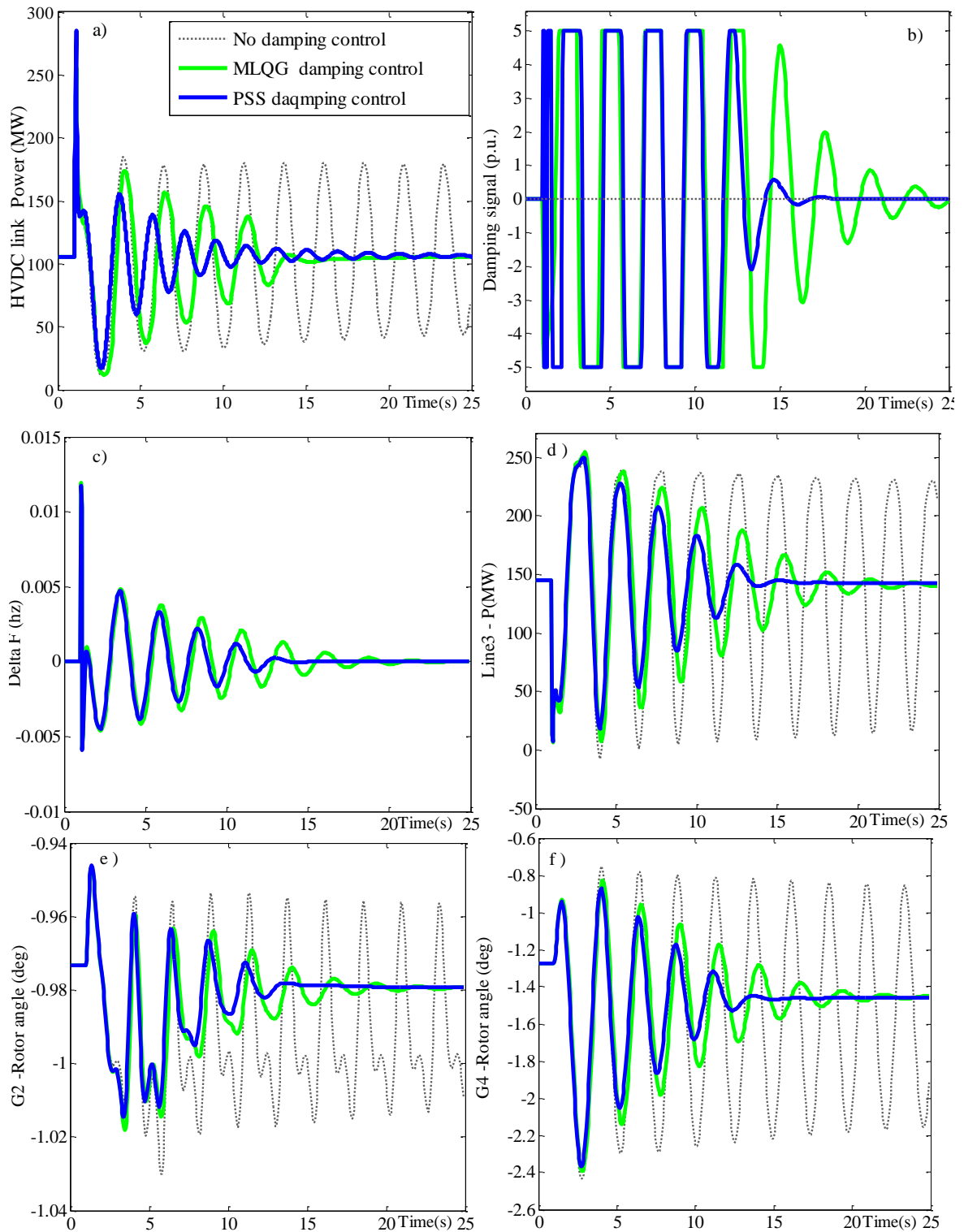


Figure 7.15: Comparative study on performance of PSS and MLQG damping controller, system response with/ without damping controller following a large disturbance

It is evident from the results that both MLQG and PSS-based damping controllers improve the damping ratios of the oscillatory modes significantly. Also, the simulation results demonstrate that both damping controllers are robust and remain effective in providing oscillation damping following the occurrence of a large disturbance such as a 3-phase fault. However, the PSS-based controller displays a slightly better performance with regard to improving the inter-area oscillation damping as it is merely tuned for poorly damped inter-area mode 3. The damping constant for various system variables such as power flow on the AC and DC lines, generators rotor angle and frequency are presented in Figure 7.16. It is clear that with implementation of damping controllers all the variables' oscillation are settled in less than 12s which implies that the performance of both controllers meet the SQSS requirement of 12s damping constant. However, in overall, the PSS-based damping controller with more focus on damping mode 3 achieves better damping constant for all variables. For example the generator 2 rotor angle oscillation is settled and reached the steady state point within 10.5s with the PSS damping controller and within just 10.8s with the MLQG controller. The level of modulation of the DC link presented in Figure 7.15.a, which shows that following the initial swing after the disturbance, only small levels of modulation are required to efficiently stabilise the unstable oscillatory AC network. It is important to note that in both the above-presented study cases no communication delay has been included. This is to reduce complexity for the purposes of the initial assessment into the feasibility of using supplementary MLQG damping controller for the DC links.

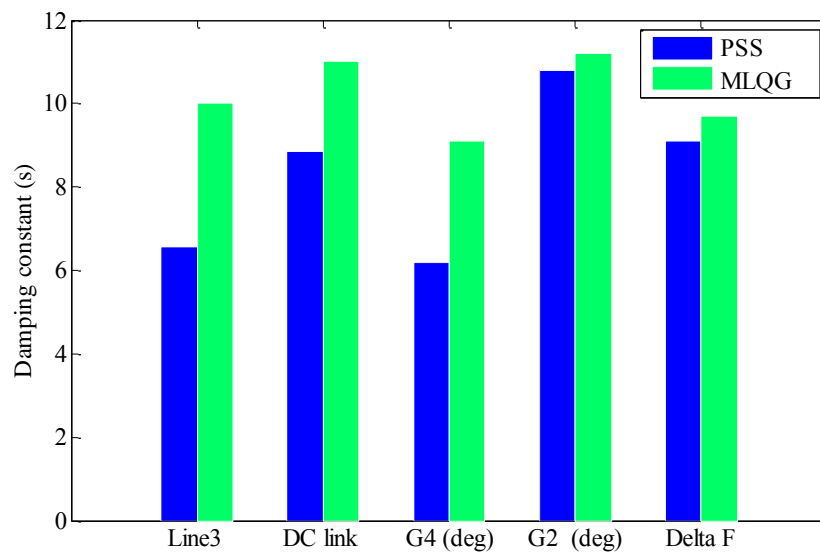


Figure 7.16: Damping constant for various system variables following a large disturbance

7.10 Capability of the West Coast HVDC link's damping controller in the system stability improvement (Study case on the full GB transmission system model)

The impact of sharing active power flows between the DC link and the AC lines on the movement of poorly damped inter-area oscillation modes is investigated in section 7.8 and results show that as the active power on the DC link is gradually increased and more power is pushed from the AC lines to the DC link the synchronising and damping ratio are increased, which accordingly results in improving the dynamic stability of the network. In addition, the application of supplementary power oscillation damping control for the HVDC link to mitigate the oscillation of inter-area modes is demonstrated on the simple test system. It is observed that modulation of the HVDC link's DC current can improve damping of the system oscillation following a disturbance. Further to the above studies on the simple test system, the capability of the future embedded West Coast HVDC link in system oscillation damping is investigated using the full model of the future GB transmission system described in section 7.6.2.

7.10.1 Inter-area oscillation studies using the full GB transmission system model

The assessment on the inter-area power flow on the transmission lines connecting the Harker and Hutton substations revealed the existence of low frequency inter-area oscillatory modes [99]. The location of the selected Harker –Hutton line, which is used for monitoring the inter-area oscillations, is presented in Figure 7.19. In order to excite the inter-area oscillatory mode in the GB power system, a large disturbance such as a 100ms 3-phase short-circuit fault was initiated on a critical transmission line, this is described in detail in the next section. Also, the rotor angle oscillations of some large generators across the network between England and Scotland are monitored in simulation to observe the inter-area oscillations between the England and Scotland networks (this occurs when the group of generators in Scotland are swinging against the generators in England). Moreover, frequencies at points where wide area input signals for the damping controller are obtained are monitored in off-line studies. In this study case, the HVDC link is scheduled at 1.9GW in order to reserve its overload capability to be implemented for DC current modulation. The location of monitored generation in off-line stability studies and the location of where the input signals used for the design of power oscillation damping controller are presented in Figure 7.17.

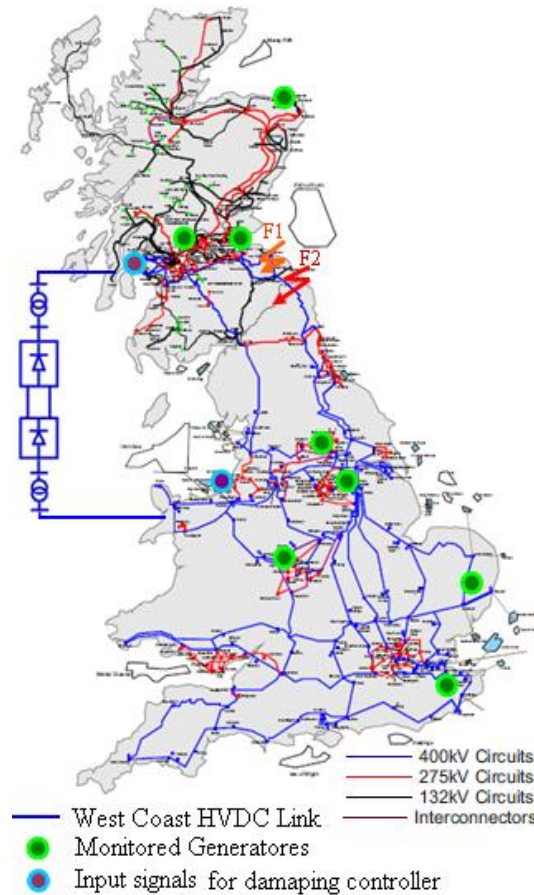


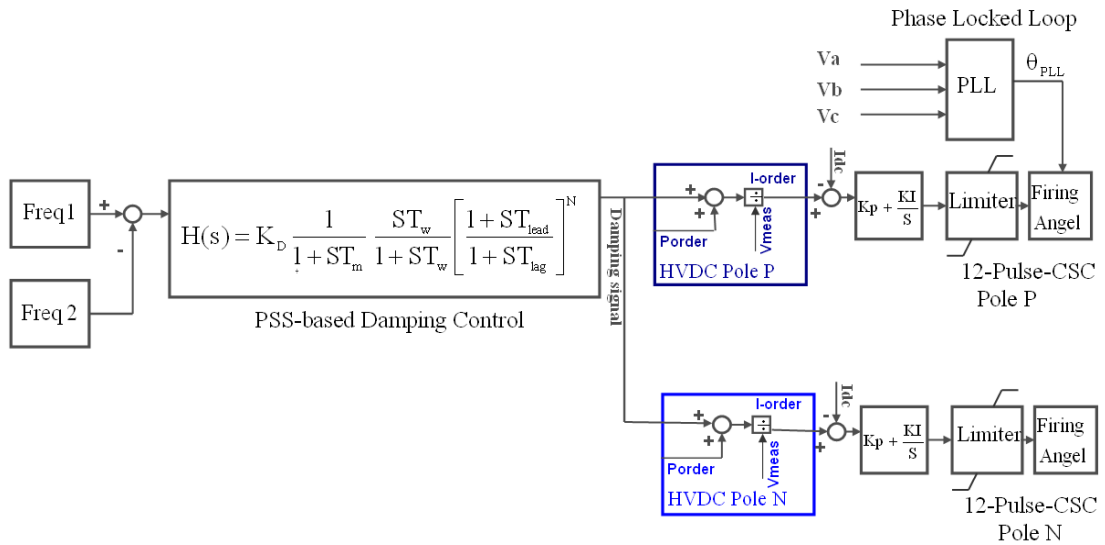
Figure 7.17: GB transmission system including embedded West Coast HVDC link presenting the location of generators monitored for the inter-area oscillation assessment and location of required damping controller's input signal on the GB transmission system

All the wide-area data/signals used for design of the West coast HVDC link damping controller such as active power on the line connecting Harker to Hutton, damping controller's input signal and frequency of monitored generators across the B6 boundary are shown in Figure 7.17 are required for real-time inter-area damping assessment. This data can be obtained from the Wide-Area Monitoring and Control Centre (WAMCS), which receives the installed PMUs data across the networks [99]. Currently, there are twelve PMUs in the synchronized data acquisition system. Two PMUs are installed in the 400kV substations Harker (HARK) and Hutton (HUTT) which could provide the active power on the transmission lines connecting the substation at Harker (HARK) and Hutton (HUTT). Also, more PMUs are required to provide frequency or speed of monitored generators across the B6 boundary [161]. However, for the purpose of this study to investigate the capability of the HVDC link's damping controller in mitigating the inter-area oscillation, the off-line stability analysis is conducted using the PowerFactory simulation tool. Therefore, for small signal

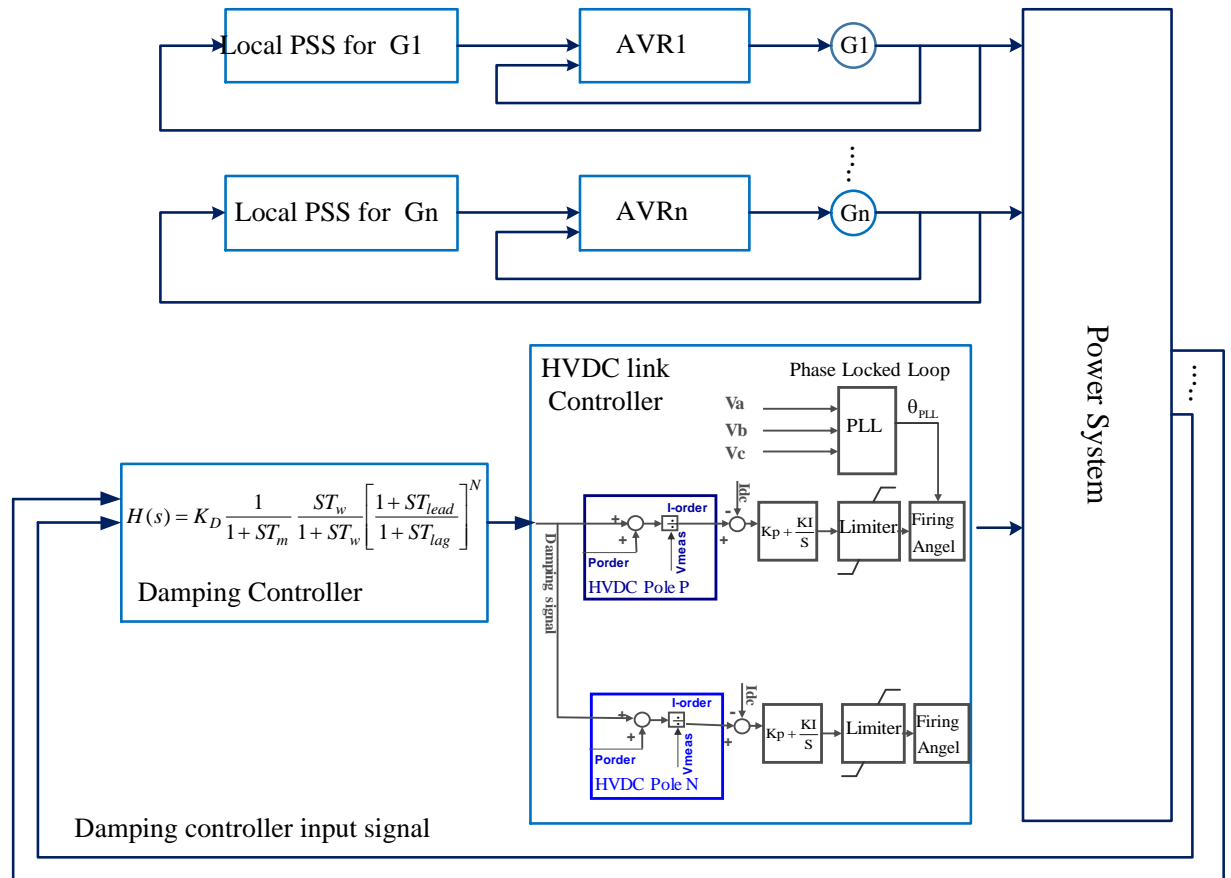
stability studies, generators' rotor angle and damping controller's input signals are monitored in simulation.

7.10.2 Structure of the PSS-based damping controller for the bipole West Coast CSC-HVDC link

The PSS-based damping controller design approach is selected for the design of a supplementary damping controller for the Western HVDC link due to its simplicity in design and the fact that it performs better in the case of single mode oscillations. Thus, a PSS-based damping controller is added to the current controller at the rectifier side of both poles of the Western HVDC link. As previously mentioned, the selection of the controller's input signal is critical in the design of an effective damping controller to ensure the maximum observability at dominant oscillation mode for the selected input signal. Also; research shows that wide area signals have proven to be more effective in the design of power oscillation damping control [146][174]. Therefore, following a sensitivity assessment, the frequency oscillations at Hunterston and Deeside substations, which allow clear observation of the inter-area mode, are given as input signals of the damping controller. In future, these signals can potentially be obtained from the PMUs installed at converter stations. It is important to note that at this stage no signal latency is considered in this study. The output signal of the damping controller is given to both poles of the HVDC link to modulate the DC current on the HVDC link. The overall structure of the HVDC link's supplementary control is shown in Figure 7.18. It can be seen that the damping control signal generated by the damping controllers is added to the current references of the rectifier controllers (P_{order}) to dynamically modulate the DC power. Also, as Figure 7.18 indicates, all generators' PSS in the network model are kept in service in order to have a practical scenario[147]. In this study, the parameters of the HVDC supplementary damping controllers, which are provided in Appendix E, were determined by modal and residue analysis [164].



a) Structure of supplementary PSS-based damping controller for the Bipole CSC-HVDC link



b) PSS-based damping controller for the CSC-HVDC link with respect to local generators' PSS


Figure 7.18: Supplementary damping controller for the Bipole CSC-HVDC link

7.10.3 Definition of the study cases to investigate the effectiveness of the HVDC link's damping control (using full GB transmission system mode I)

As previously mentioned, a 100ms 3-phase short-circuit fault is initiated on a critical transmission line to excite the inter-area oscillatory mode in the GB power transmission corridor between SPTN and NGETN. Faults on two double circuits, shown in Figure 7.19, have been identified as the most critical faults, which could lead the system to instability depending on the level of power transfer on the B6 boundary, outage pattern and system arrangements. The first critical route is the double circuit connecting Torness and Eccles (fault on this line denoted as F1) and the second route is the double circuit connecting Eccles, Blyth and Stella West (fault on this line denoted as F2). As the double circuit connecting Stella West and Eccles is carrying more power at pre-fault compared to the double circuit connecting Torness and Eccles, F2 is considered as a more critical fault compared to F1. The locations of these faults on the network are presented in Figure 7.19. It is important to note that the impact of faults close to the West coast HVDC link have not been considered in this study.

Two study cases representing two different system operating points with different power transfers on the B6 boundary at each point are set up. In study case1, which represents operating point 1, the power transfer on the B6 boundary is 4.5GW including 1.9GW power on the DC link, whereas in study case2, which represents operating point2, 4.7GW of power is transferred on the B6 boundary including 1.9GW power on the DC link. For both cases, the system dynamic responses and effectiveness of the West Coast HVDC link's damping controller in improving the system oscillation damping have been examined following the occurrence of fault F1 and F2 on the identified critical lines. It is important to note that these cases are defined for the intact system.



Figure 7.19: Location of line monitored for inter-area assessment  and location of faults simulated on the GB transmission system in study case1 and study case 2

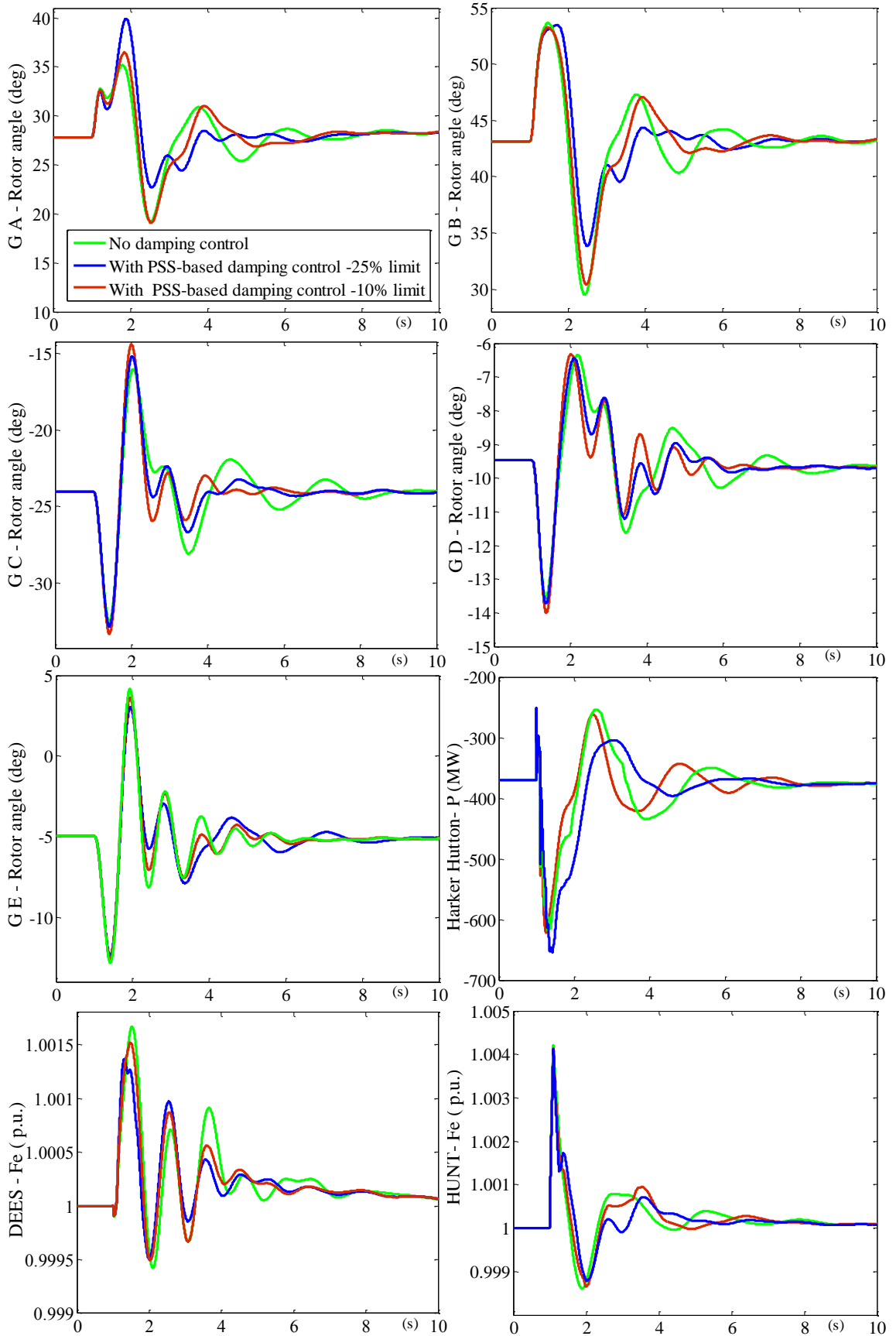
In summary, the following study cases are explored to investigate the effectiveness of the West Coast HVDC link’s damping controller with regard to system stability enhancement at various operating points:

- **Study case 1:** investigates the effectiveness of the West Coast HVDC link’s damping controller at operating point 1 with lower power transfer across the B6 Boundary when the following faults occurs:
 - Study case 1.1: 3-phase Short Circuit (SC) fault (F1) occurs on circuit connecting Torness and Eccles
 - Study case 1.2: 3-phase SC fault (F2) occurs on the double circuit connecting Eccles, Blyth and Stella West, which is considered as the most onerous fault.

- **Study case 2:** investigates the effectiveness of the West Coast HVDC link's damping controller at operating point 2 when following faults occurs :
 - Study case 2.1: 3-phase SC fault (F1) occurs on the circuit connecting Torness and Eccles
 - Study case 2.2: 3-phase SC fault (F2) occurs on the double circuit connecting Eccles, Blyth and Stella West, which is considered as the most onerous fault.

7.10.4 Simulation results and analysis on study case 1

Figure 7.20 and Figure 7.21 show the dynamic response of the system with and without the HVDC link's damping controller following two severe faults occurrence where the B6 transfer is at operating point 1 at pre-fault. The dynamic responses presented in the simulation results include active power on the AC line, frequencies (where damping controller input signal are obtained) and a couple of generators' rotor angles across the B6 boundary for both study cases. Furthermore, Figure 7.20 presents the dynamic response of the system with and without the HVDC link's damping controller following occurrence of F1. This is where the B6 transfer is at operating point 1 at pre-fault (study case 1.1). In addition, the impact of limitation on modulation capacity of the HVDC link is investigated in study case 1.1. The simulation results presented in Figure 7.20 compare the effectiveness of the damping controller when using various allowances on the HVDC link capacity for the modulating damping control signal. The red curves show 10% limit on the HVDC link capacity and blue curves show 25% limit on HVDC link capacity for modulating the power oscillation damping control signal. This is in line with the available HVDC link overload capability which is 20% to 25% of the HVDC link maximum capacity. In a practical installation, the limit of available modulation capacity will be determined by the system operator based on the physical and technical limitation of the HVDC link. Nevertheless, from simulation results, it is clear that a higher allowance for modulation capacity (blue curves) improves the oscillation damping more effectively. Also, it is observed that when the power transfer across the B6 boundary is low, the HVDC damping control is only marginally effective on improving system oscillation damping.



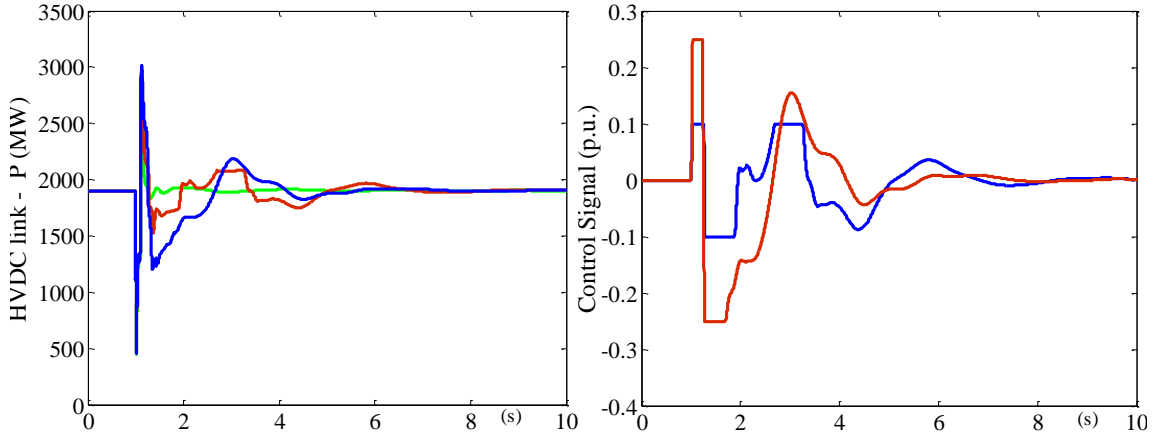
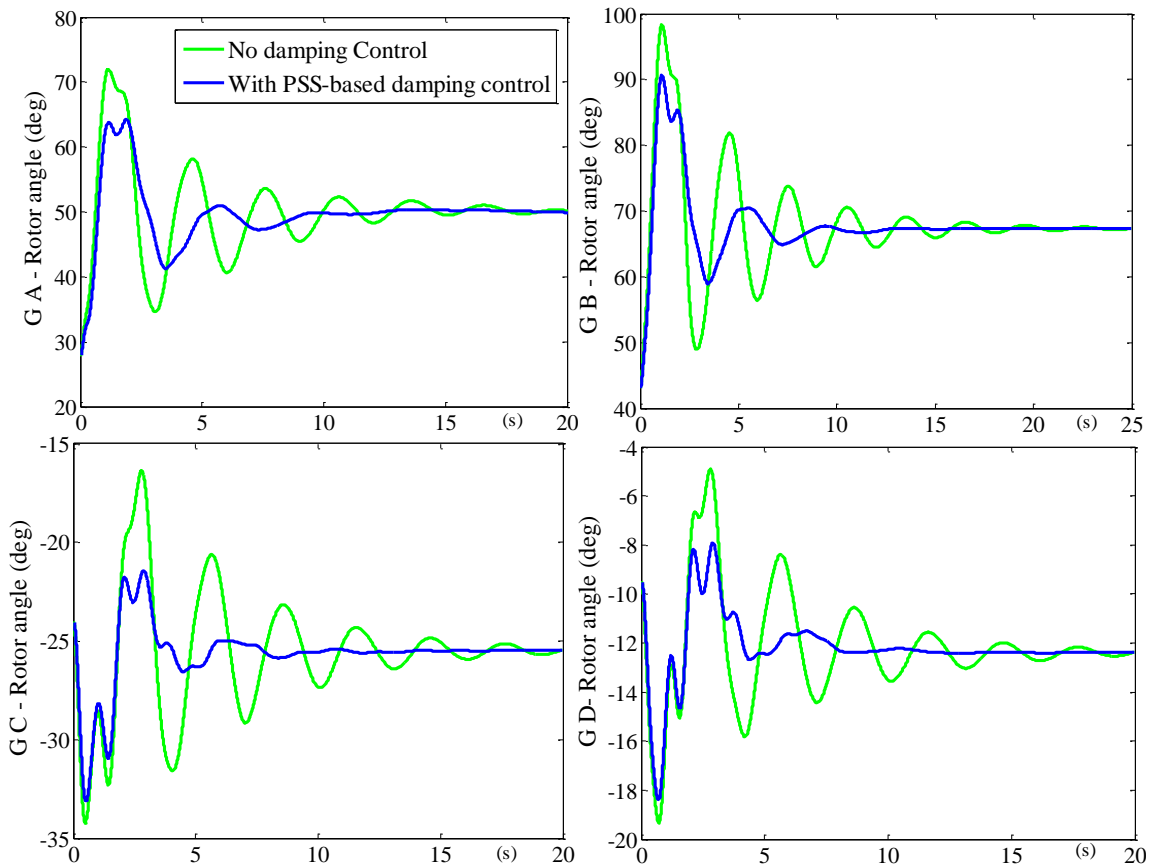


Figure 7.20: Study case 1.1: Response of the full GB transmission system with/without damping controller following occurrence of F1 when B6 transfer is at point 1

Similarly, the dynamic response of the system with and without the HVDC link's damping controller following occurrence of F2 is shown in Figure 7.21. This is where the B6 transfer is at operating point 1 at pre-fault (study case 1.2). In this study, the damping control signal is limited to 25% of the modulation capacity.

It is observed that power oscillation damping control is more effective following the occurrence of F2 compared to F1 when the B6 transfer is at lower transfer limit of point 1.



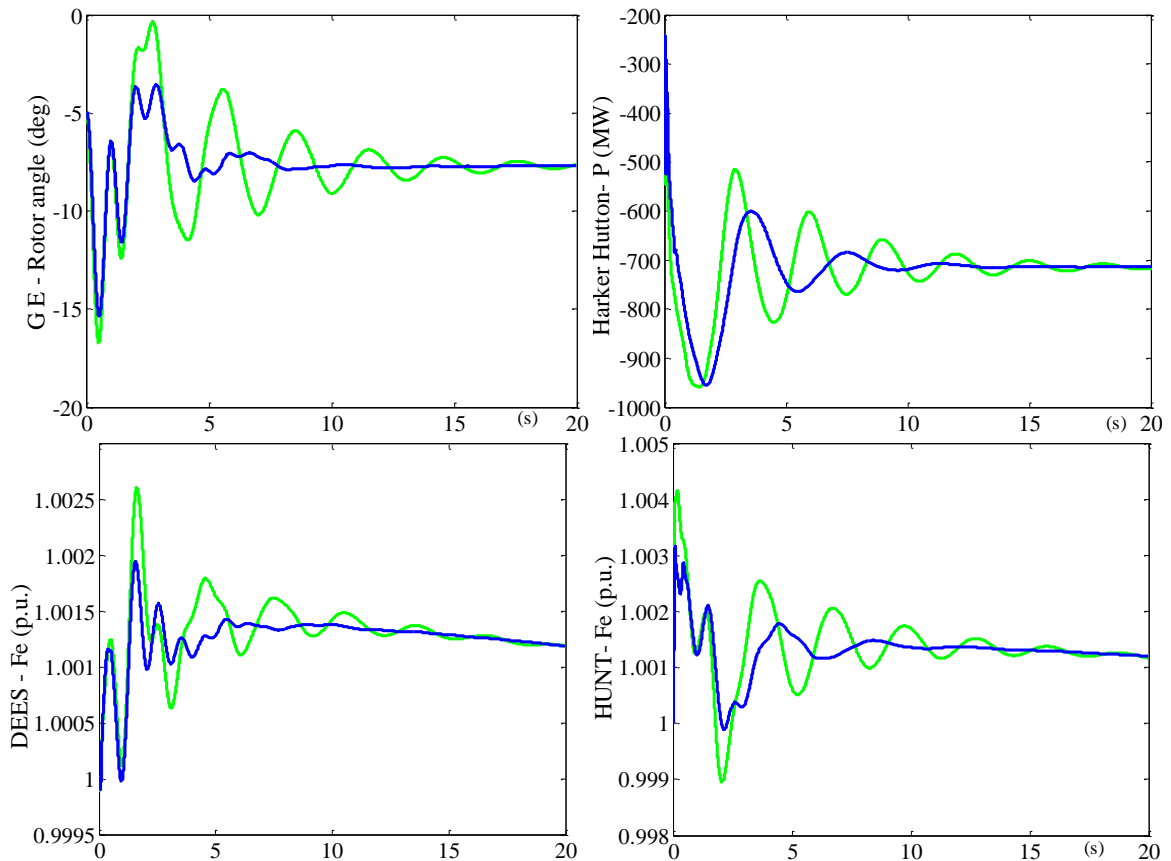


Figure 7.21: Study case 1.2: Response of the full GB transmission system with/without damping controller following occurrence of F2 when B6 transfer is at point 1

7.10.5 Simulation results and analysis on study case 2

Figure 7.22 and Figure 7.23 show the dynamic response of the system with and without the HVDC link's damping controller following a severe fault occurrence where the B6 transfer is at operating point 2 at pre-fault. Similar to study case 1, this includes the active power on the AC line, frequencies for input signal and couple of generators' rotor angle across the B6 boundary for second study case.

The dynamic response of the system with and without the HVDC link's damping controller following occurrence of F1 is presented in Figure 7.22 (study case2.1). Also, the dynamic response of the system with and without the HVDC link's damping controller following occurrence of F2 is presented in Figure 7.23 (study case2.2).

It can be seen that, at operating point 2, the damping controller is even effective for F1 whereas at point 1 the damping controller is only effective for F2 and has almost no impact in case of the F1 occurrence at point 1.

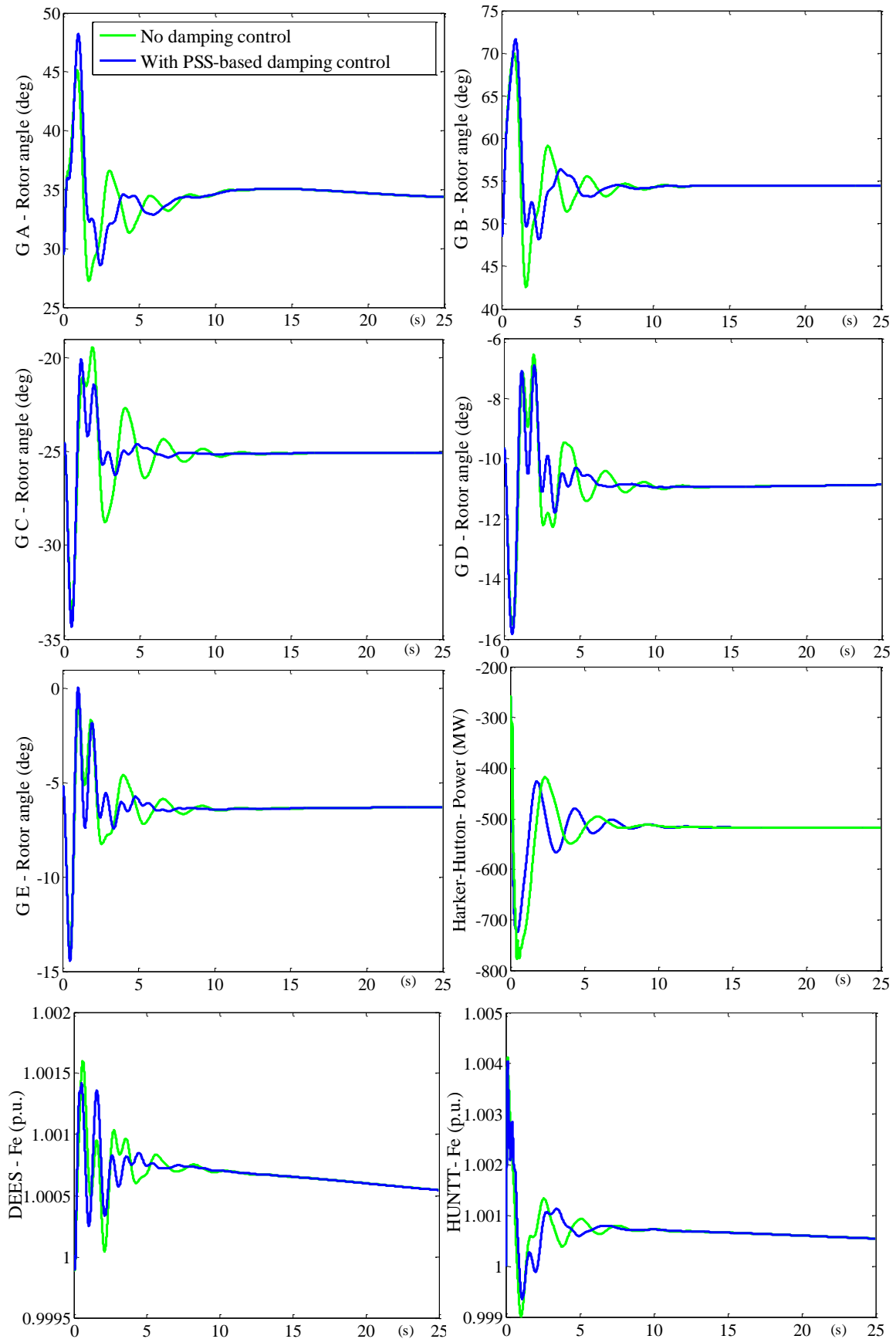


Figure 7.22: Study case 2.1: Response of the full GB transmission system with/without damping controller following occurrence of F1 when B6 transfer is at point 2

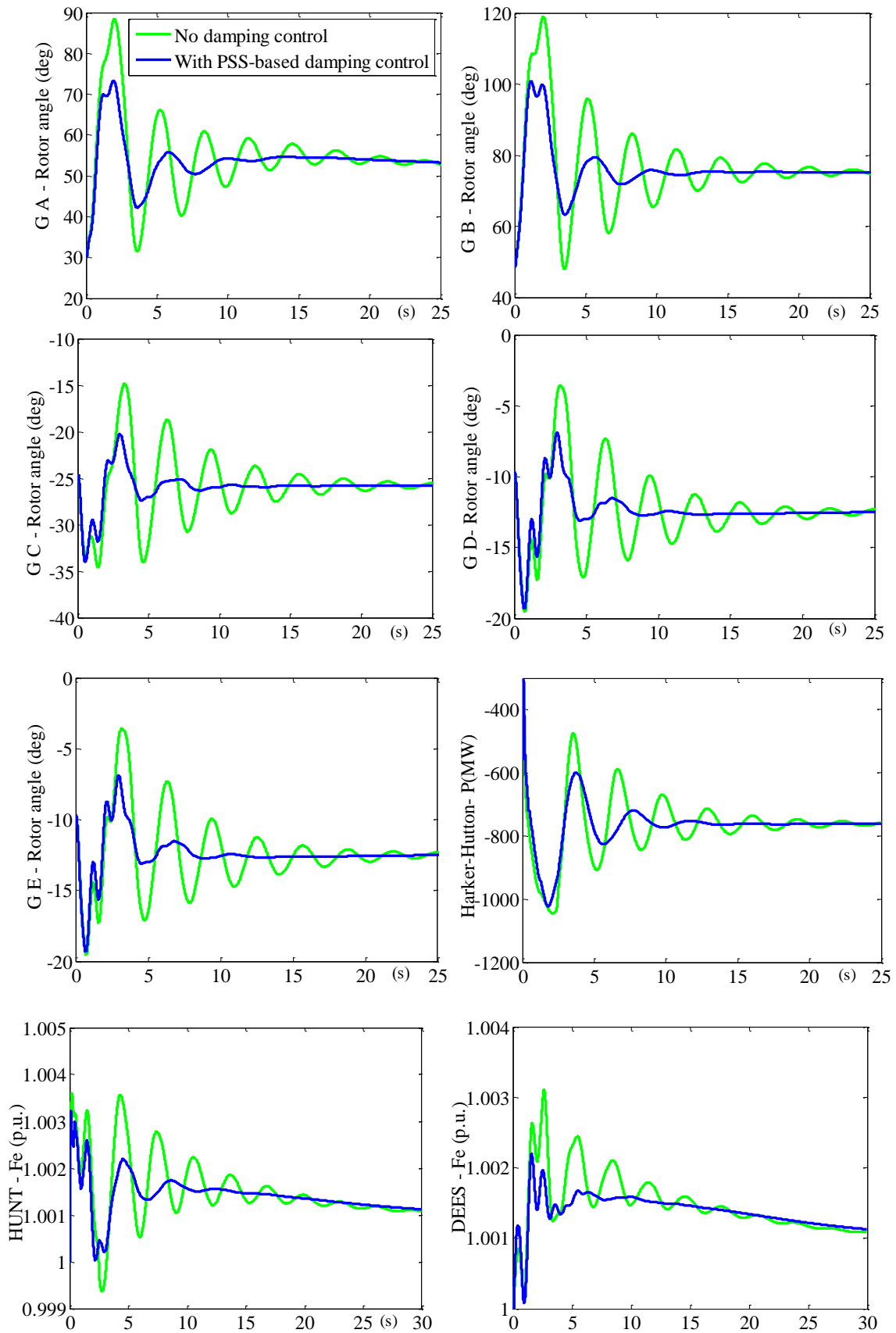


Figure 7.23: Study case 2.2: Response of the full GB transmission system with/without damping controller following occurrence of F2 when B6 transfer is at point 2

7.10.6 Discussion on effectiveness of the West Coast HVDC link damping controller at various operating points

Performance of the West Coast HVDC link damping controller at operating point 1 and point 2 with various transfer limits on the B6 boundary following the occurrence of F1 and F2 are presented in Figure 7.24 and Figure 7.25 respectively based on the generators' delta damping constant, which is the difference between the generators damping constants with and without the implementation of the damping controller at each operating point.

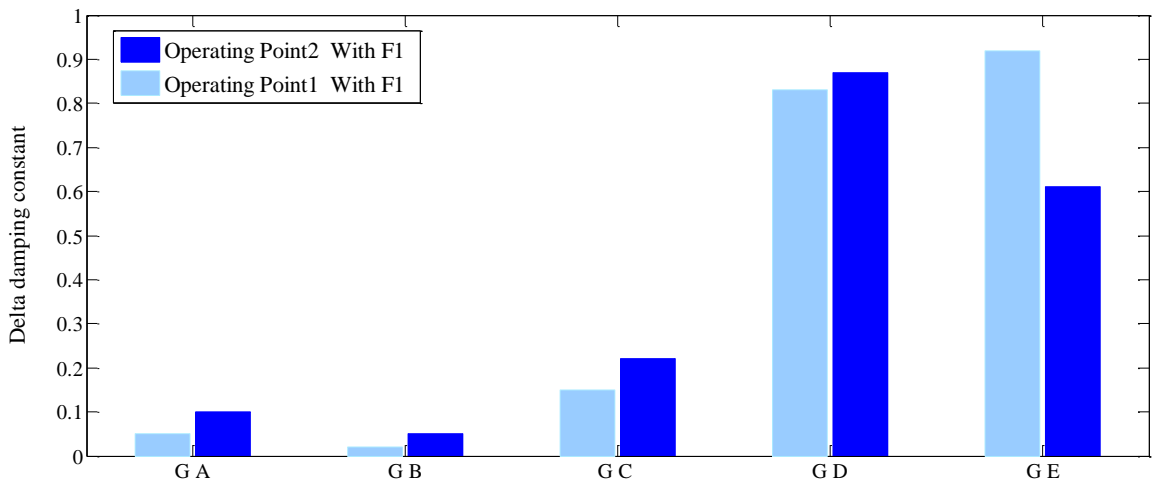


Figure 7.24: Comparison of damping controller effectiveness at operating point 1 & 2 when F1 occurs

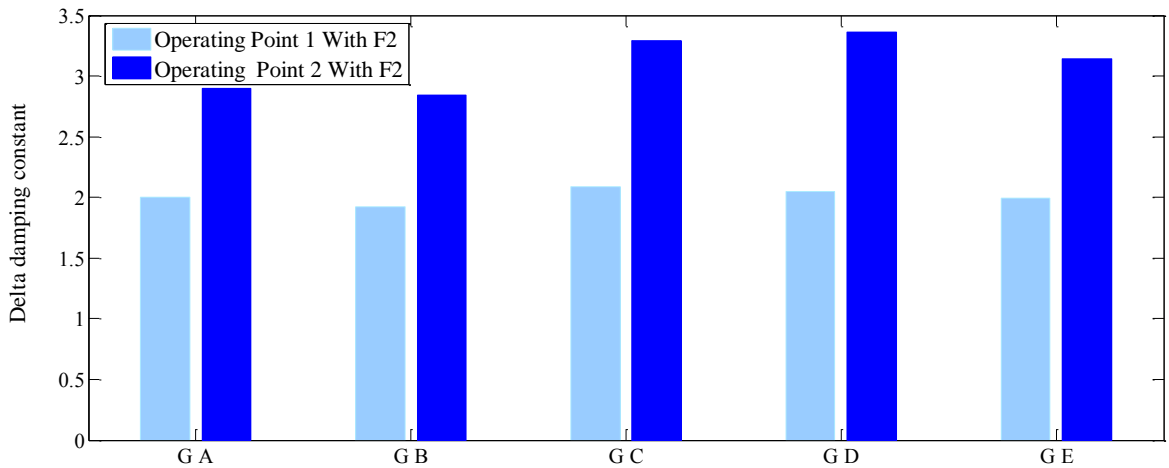


Figure 7.25: Comparison of damping controller effectiveness at operating point 1 & 2 when F2 occurs

In both Figure 7.24 and Figure 7.25, it can be seen that the difference between the generators damping constants with and without a damping controllers are higher at operating point 2 (dark blue bars) compared to point 1 (light blue bars) with either F1 or F2 faults. This implies that the power oscillation damping controller is more effective when lines are operated at a higher power transfer level (dark blue bar) compared to

lower power transfer level at point 1. However, as can be seen in Figure 7.25 when a fault is more onerous such as F2 the damping controller is more effective and the difference between the generators damping constants with and without damping controllers are higher compared to the case when F1 occurs. In summary, it is observed that at the higher transfer level of point 2, the damping controller is even effective for the less onerous fault of F1 whereas at lower transfer level of point 1, the damping controller is only effective on the more onerous fault of F2 and has almost no impact in the case of the F1 occurrence at point 1.

7.11 Comparative study on effectiveness of a range of supportive control actions for stability enhancement

7.11.1 Introduction to smart demand control and generator inter-trip

For comparison purposes, another two methods explored in this Chapter include a smart demand controller and a generator inter-trip. This study also shows how a generator inter-trips and demand management schemes can improve power system stability. Smart demand management involves new communication technologies to make sure actions can be fast enough to prevent instability situations. The study presented in this Chapter uses Power Transfer Distribution Factor (PTDF) to set up an algorithm that will switch on and off demand in an effective way [175].

Inter-trip of a generator is an automatic action that will trip the selected generator to release the system overload and stability issues [176]. This inter-trip service is normally operated through protection and is used to increase transmission capacity. [177][176].

7.11.1.1 Generator inter-trip

Generation inter-trip is a conventional technology that is used by TSOs to alleviate overload and improve system stability. It is a protection controlled automatic action that will disconnect a selected generator and solve system thermal overload, voltage and stability issues and improve system security. As specified in the connection agreement, TSOs can ask generators to select their contracted machines to be armed to inter-trip to attain a more secure situation at post-fault/disturbance. Should the fault happen, the selected generator circuit breaker will open in a specified time [177]. This service is also known as generation curtailment.

7.11.1.2 Smart demand control

With the improvement of communication technology, demand in the future will be more flexible. It will be either from domestic or industry, for example electric vehicles [178][179] and smart fridges. As explained further in the study presented in [175], demand can be managed and dispatched pre-fault and post-fault. The best way to choose the most effective demand to dispatch is the PTDF methodology. The smart demand controller with the PTDF algorithm can be used to dispatch demand according to different geographical areas depending on different faults.

As demonstrated in paper [175], demand changes on different locations have a different impact on system security. The effectiveness of demand for a certain fault can be calculated and used as a ranking algorithm for different demand control selection. The demand sensitivity can be calculated as follows;

$$\alpha = \frac{\partial P_{line}}{\partial P_{load}} \quad (7.14)$$

$$\beta = \frac{\partial Q_{line}}{\partial Q_{load}} \quad (7.15)$$

α and β are defined as the sensitivity factors to manage demand in a certain area. ∂P_{line} is the MW change in affected circuits, ∂P_{load} is the MW demand change in the certain area. Similarly ∂Q_{line} is the Mvar change in affected circuits. ∂Q_{load} is the Mvar demand change on the certain area.

Before starting any demand management, smart demand control management will rank the demand selection sequence according to sensitivity factors. For this study only active power is used to calculate sensitivity factors. For this logic, the ranking sequence should follow the absolute value of the sensitivity. However if the sensitivity factor is positive, it means reduce/switch off demand is improving the stability situation. If the sensitivity factor is negative, it means increase/switch on demand is improving the stability situation [175]. Hence the smart demand controller will switch on or off demand according to the location of the fault to get a more effective result.

7.11.2 Simulation results and analysis on the effectiveness of introduced supportive control actions (comparative study)

As discussed in the previous section, at any power transfer level on the B6 boundary, following a double circuit fault, the remaining AC tie-lines across the B6 boundary must remain stable. Based on the SQSS, this implies that no generation should pole slip and an oscillation must be damped and settled within 12s, otherwise power transfer must be reduced to the point where system security is maintained [15]. To achieve that, a range of post-fault actions such as conventional generation inter-trip and smart demand management can be taken to assist with maintaining system stability. Also, the HVDC link can provide additional supportive control actions to enhance both transient stability and power oscillation damping using various control schemes, such as the supplementary damping controller or the set-point adoption of the HVDC links at the post-fault. The application of the HVDC link's set-point adoption in stability enhancement is presented using the SR control design method for the design of secondary control. The main reason to implement a SR controller for the HVDC link's set-point adoption at post-fault is due to the fact that the SR controller can be extended to a MIMO controller, which has the capability of co-ordinated control of various power flow control devices in the power system. However, in this study, only the performance and robustness of a SISO SR controller in stability improvement at post-fault is demonstrated.

Finally, in this study, a comparative study is performed to investigate how and to what extent each action is capable of improving system stability and consequently enhancing the power transfer limit on the Scottish boundary by releasing the existing network capacity. The dynamic response of the system at operating point2 following the occurrence of F2 is presented in Figure 7.26, which includes power flow on one of the AC lines close to the boundary, frequency at Hunterstone where the damping controller input signal is obtained and a couple of generators' rotor angle across the B6 boundary.

It can be seen from Figure 7.26 (red graphs) that without any control, the magnitudes of the power swings are relatively large following the clearance of the above-mentioned fault. Whereas, system oscillation damping can be considerably improved at post-fault by implementing a range of supportive post-fault actions such as generation inter-trip, smart demand control, HVDC link's set-point adoption and HVDC link's damping controller.

As presented in the Figure 7.26, the green curves show the dynamic response of the system including the generators' rate of change of rotor angle following a generation inter-trip of 600MW. The first swing curve has been improved considerably and system damping is also improved slightly.

The pink curves show the dynamic response of the system including the generators' rotor angle rate of change for 600MW demand side management. By using the algorithm of smart demand control, for this fault, negative demand has a better effectiveness. Hence for this fault, the smart controller has switched on the negative demand according to the ranking sequence. The assumption of the speed to switch on demand through the smart demand controller is 1s, where it can be found that the rotor angle of the pink curve is similar to the red curve (no action curve) at the beginning of the fault and 1s later, it starts to improve the first swing situation and the system damping has also been improved with the smart demand control. It is evident that generator inter-trip and smart demand control have achieved the task of improving system stability, and it also helps with the system oscillation damping. However, there is a cost associated with these actions.

Alternatively, the loss of the AC line can be compensated using the HVDC link's set-point adoption. The generators' rotor angle responses (blue graph) clearly show that the HVDC links set-point adoption can improve both first swing and oscillation damping following a fault occurrence. Also, it can be seen in Figure 7.26 (blue curves), that the response of the system following the HVDC link's set-point adoption is very similar to the generator inter-trip with providing slightly better damping.

Furthermore, in comparison, it can be seen in Figure 7.26 (black graph) that the HVDC link damping controller presents the best performance by providing better damping at post-fault. The damping constant has reduced significantly. To achieve this, a dynamic variation of up to 25% of HVDC capacity is used, which is well within the short term rating of the HVDC link.

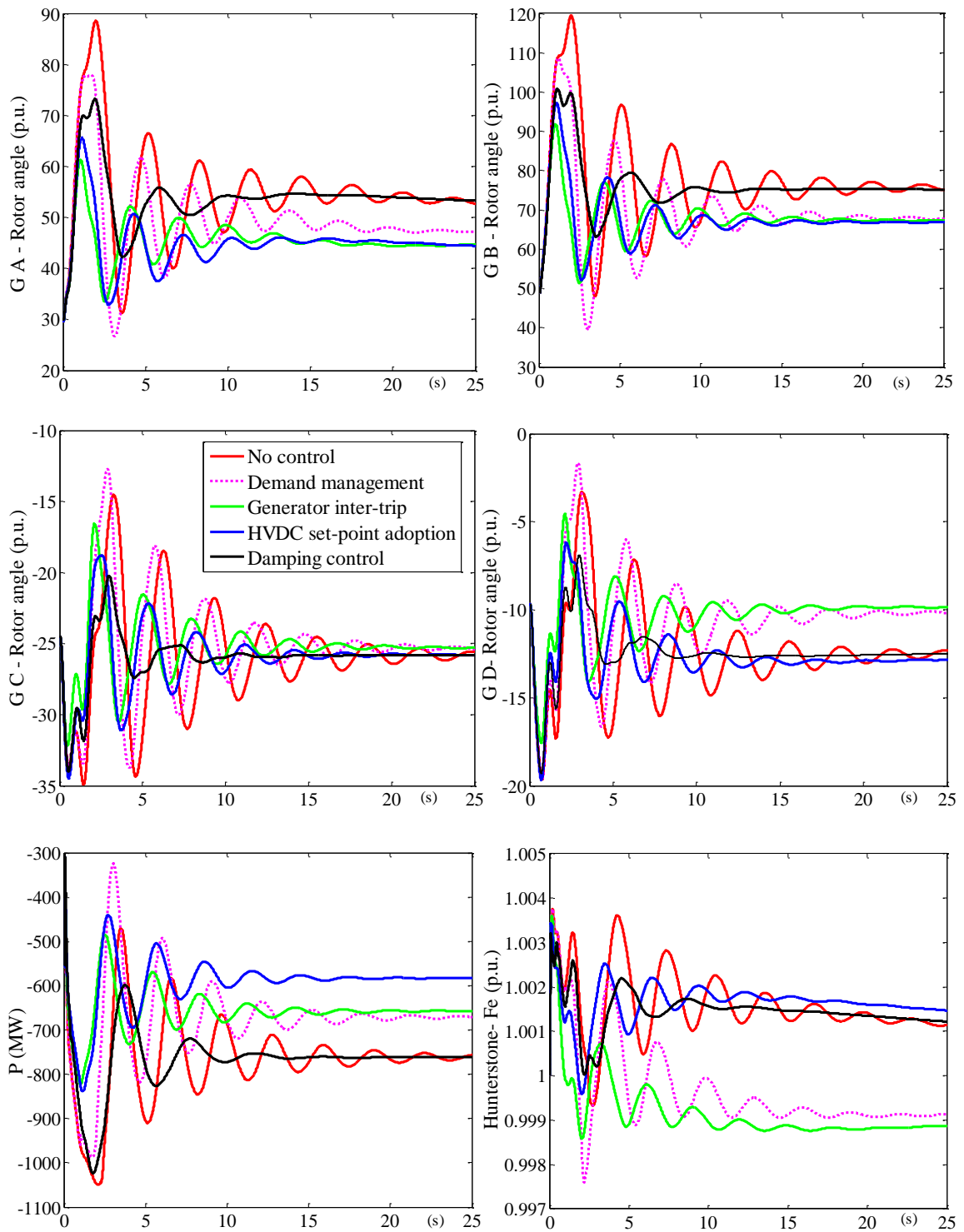


Figure 7.26: Response of the full GB transmission system following a fault occurrence using various supportive actions

7.12 Concluding remarks

Low frequency oscillations have been a cause for concern for many large power system networks as well as the GB transmission system. Thus, firstly an overview and history of the dynamic instability issue in the GB transmission system is provided. Then the Chapter proceeds with presenting the fundamentals of model analysis, which is required for identification of the oscillatory mode of the system and the design of the supplementary oscillation damping controller for the upcoming HVDC link and TCSC devices. Two approaches with different design requirements have been presented including the PSS-based and the MLQG damping controllers. Also, the structures of both controllers are described in this chapter.

The linear state-space model of the system is required for the design of the MLQG damping controller. Therefore the system identification method is introduced and implemented to obtain the linear model of a system that maintains the key oscillatory low frequency mode of the system. To implement this algorithm the interface between Matlab and PowerFactory introduced in Chapter 4 is implanted.

Two comparative study cases on the performance of both damping controllers are presented using a simple test system. The results show that both controllers are significantly effective on improving the system oscillation damping. The PSS-Based damping controller has proven slightly more effective on inter-area mode of oscillation as it is tuned only for the inter-area mode of oscillation. However, the MLQG performance also met the SQSS damping requirement and achieved damping ratio of more than 5% for the inter-area mode of interest. It is important to note that the MLQG damping controller has advantage over the PSS-based controller due to the fact that it can be expanded to a multivariable controller. Therefore in the case of the damping controller for VSC-HVDC link, it can make an effective use of the multiple points of controlled power injection available in VSC-HVDC link to provide a significant method of stabilising system oscillations.

Following the demonstration of the effectiveness of the HVDC link's supplementary control in system oscillation damping using a small test system, further comparative investigation has been conducted into the capability of the West Coast HVDC link in the system inter-area oscillation damping using the full GB transmission system model. Two study cases, which explore the performance of PSS-damping controller for the West

Coast HVDC link at different operating points with various power transfers across the B6 boundary have presented. The results revealed that the HVDC link damping controller is more effective when there are higher power transfer across the B6 boundary. Also, the location of the fault has an impact on the level of effectiveness that can be obtained from the HVDC link supplementary damping controller.

Finally a comprehensive comparative study with regard to the effectiveness of a selection of supportive control actions to ensure system stability during the immediate post-fault period is performed in this Chapter. These control actions comprise the set-point adoption of the embedded HVDC link that involve the fast ramp-up capability of the HVDC link, supplementary power oscillation damping control for the HVDC links, smart demand side control and conventional generation inter-trip schemes. Results demonstrated that the HVDC link damping controller presents the best performance and provide better damping at post-fault compared to the other control schemes.

Chapter 8

Conclusions and Further work

8.1 Summary and conclusions

This Chapter summarises and brings together the main contributions and advances that have been made in this research and presented in this thesis.

The motivation and drive for the research presented in the thesis were outlined in detail in the first Chapter, as stemming from the fact that a substantial amount of change needs to be implemented to the GB transmission system in order to accommodate the forthcoming renewable generation and meet the climate change legislation enforced from both by UK Government and EU [1][2][3].

According to the Future Energy Scenarios, since the majority of the new wind generation will be in Scotland and offshore in the UK as a whole, there will be an immense increase in the power export from Scotland resulting in the exceeding of the maximum capability of the existing network and consequently being non-compliant with the requirements of the NETS SQSS. There will therefore, be a significant increase in the power transfer capability requirement across the Anglo-Scottish boundary (B6 boundary). This is currently stability-limited to approximately 2.2GW and at present managed by limiting the power transfer across this boundary [131]. For that reason, more state-of-the-art transmission technologies such as embedded HVDC links and TCSC are planned to be deployed within the existing AC transmission system to provide additional capacity and raise the boundary limit up to its thermal limit.

Ultimately, such power flow controller devices could potentially affect the system stability. Also, as the network in this area is now congested with many types of new and automatic control devices, there is a potential risk of interaction between these various control devices. Therefore, without the development of a supervisory stability control system much of the potential advantages of these costly individual reinforcements to enhance the AC systems stability could bring much less benefit than expected. Consequently, this will result in constraining the output of the renewable energy

sources. For that reason, a stability control scheme is needed at transmission system level to ensure optimum dynamic performance in providing stability support to the main AC power system using the HVDC link and the co-ordination of power flows in such an integrated large power system [152].

In addition, although the embedded HVDC link will add to the current transmission capacity, identification of their optimal operational points requires further investigation. It is also essential to consider smarter ways of operating the transmission network and gaining additional benefit, in view of the system operator, from the future DC links' capability with regard to system stability enhancement in order to meet the growing challenge of accommodating large amounts of variable wind power generation [147].

Chapter 2 presents a comprehensive review conducted on past research surrounding the issue of power system stability and the latest proposed solution for stability enhancement using the HVDC link and TCSC. This is done through the deployment of various controller design methods and implementation of various control schemes and strategies.

This completed evaluation represents the first contribution of the thesis which reveals that hardly any of these methods proposed in past researches has looked into the scalability, difficulty and mostly the requirements for implementation of these proposed controllers in a large practical network.

This thesis in Chapter 3 covers and reviews the modelling of the large-scale CSC-HVDC link, which could be used for stability studies and analysing complex system dynamic behaviour. DIgSILENT PowerFactory is used as the main simulation tool for developing power system models including test study systems and HVDC link's control systems.

Besides the intensive and economical capability of PowerFactory in power system modelling and analysis, the other driving factor in choosing it as a simulation tool was that National Grid and both Scottish Power Transmission Network Owners (TOs) in the U.K use DIgSILENT PowerFactory as their off-line tool to perform system studies for system design, planning and the development of a roadmap of the GB system for 2015 and beyond [14]. However, this software cannot directly provide all control system components required for specific computation or design of a complex control law. Therefore, it is sometimes essential to combine two programs so that each could provide

particular features either for more detailed modelling or for higher computational capability [142].

As the second original contribution of this research, interfacing between PowerFactory and Matlab tools is proposed and deployed to extend the computational facilities and capability of PowerFactory for the implementation of advanced control design methods [141]. The overall structure and process of interfacing between Matlab/Simulink to PowerFactory is illustrated in Chapter 4.

In addition, in the same Chapter a framework of strategies for the hierarchical stability control system which meets the NG's requirements at the transmission level is proposed. This implies that the proposed framework fits into the NG's operational business procedures and takes into consideration other control systems on the NG system such as Energy Balancing System (EBS) , Operational Tripping Scheme (OTS) and on-line Stability Assessor (OSA) [136].

Following the setting of the overall strategy for stability control and outlining the role of each component of the proposed stability control system, Chapter 5 of this thesis focuses on the technical developments of a feedback control system. Prior to that, the necessity to have a secondary/supervisory multivariable feedback control system for the co-ordinated control of power flow control devices on the future GB transmission system such as the future HVDC link and TCSC is discussed. This is a results of the internal SISO controllers as implemented by manufacturers being typically tuned only for a single control variable which is sufficient for cases where the individual controls are near 'optimal' on their own and variables under control in the system are relatively uncoupled. However, the controller will not be able to coordinate several individual actuators and control all outputs coherently in the feedback control system. With the presence of these interactions the overall system stability and control performance can be severely compromised. Interactions in a real system may depend on the system operating conditions. Within power systems, planned or unplanned outages may change the interactions between control variables and sometimes this can be fairly rapid and severe. In these cases control systems designed based on the SISO control will be challenged.

As a third original contribution of this research, a multivariable feedback control is designed using a non-parametric control design method. This design method, which is

called Sample Regulator (SR) control, is developed for unknown systems and is based on their open loop step responses. In contrast to any model based methods, in this approach the models are non-structural time responses. Therefore, these algorithms can be applied to the design of the controller for large and complex power systems without any model simplification required.

The trade-off to the dimensionality in this non-parametric approach, however, is the length of the time series that would be needed to capture a dynamic process. For a parametric approach when stability is obtained with simplification it is critical to justify its validity to the original system, while in the non-parametric time response approach an estimate of the truncation errors can be established with relative ease. Between these two approximations, quantifying impacts of structural simplification often can be a more open problem than formulating the truncation error from a well-constructed sequence [180].

It is important to note that, despite a wide range of model-based control design techniques developed and implanted in the latest research, scarcely any of them has examined the scalability of the proposed method on the large practical power networks.

The proposed SR controller is capable of providing coordinated control of the HVDC links, TCSC and SVCs at pre-fault as well as providing stability support to the main AC system to enhance stability limit at the post-fault. Alongside that, the detail of the background theory and main features of the proposed SR design method is presented in Chapter 5. The Chapter then focuses on the requirements for the development of the SR controller. Hence, the overall structure of the Matlab to PowerFactory interface for the design of the SR is presented as an initial part of controller design. The proposed SR controller can be implemented as a SISO or MIMO controller. Therefore, further to the theoretical development of the SR controller, the performance and capability of both SISO and MIMO SR controllers are investigated. Two power system applications, including the coordination of the power flow control of the multiple HVDC links (Study case 4) and the power flow control of the HVDC link with the SVC' voltage regulation (Study case 5) are presented. The simulation results demonstrated the capability of the MIMO SR for the co-ordinated control of the HVDC link and SVC at pre-fault condition under a single framework. Simulation results in the case of the coordination control of the power flow of the multiple HVDC links (Study case 4) demonstrated that

following the change of the set-point of one HVDC link, the interaction and impact on the other link is significantly reduced using the MIMO SR control. Whereas with individual SISO PI controllers for each HVDC link, the interaction is higher and cannot be controlled (Figure 4.b).

Similarly in the second case (study case 5), it is evident from the results, that under normal operation condition, a step change in the HVDC link's power flow control (Figure 5.a) causes a significant disturbance in the SVC voltage control when the system is under the SISO PI control. Whereas the interaction on voltage control is reduced using a MIMO SR controls [138].

In addition, the implication of actuators' characteristic, including HVDC link, SVC and TCSC, on the stability control system is investigated in this research. It was revealed that, the control design using the HVDC link as an actuator can be more robust for the wider operating ranges without needing to re-tune the parameters. In fact the linear behaviour presented over the entire increasing operating range of this type of the HVDC link demonstrates its advantages compared to other actuators such as the TCSC with regard to proposed stability control system. Also, the robustness of this class of Sampled Regulator has been tested at post-fault which confirms that the sampled regulators design method is both practical and applicable to power system control even when the systems are subjected to severe disturbances. Therefore, by adopting a MIMO SR control, the HVDC link can also provide rapid post fault action to pick up the flow on the lost AC line and consequently restore system stability.

Furthermore, as the fourth original contribution of the thesis, the performance of the non-parametric time domain, MIMO SR control design approach is further tested for the control of various types of control devices including the HVDC link and SVC with its associated auxiliary POD function using a full scale model of the GB transmission system representing the 2016 future generation scenarios profile. In order to perform this study, the current model of the GB transmission system is extended to represent the model of future GB transmission system with 2016 demand and generation profile sand including the West Coast HVDC link. Furthermore, the optimal operational strategy for the embedded West Coast HVDC link in the GB transmission system with regard to the enhancement of the transient stability limit across the B6 boundary is investigated using the MIMO SR controller [152].

As discussed further, in more detail in Chapter 7, the HVDC Link can be implemented to enhance power oscillation damping as well as assisting with transient stability enhancement using a variety of control schemes, such as the supplementary damping controller or the post fault set-point adoption of the HVDC links correspondingly. As the fifth contribution of the thesis, the capability of the HVDC link in improving both transient and dynamic stability is investigated in Chapter 7. Firstly, the capability of the HVDC link in improving inter-area power oscillation damping is investigated and two control design approaches including PSS-based and MLQG for the design of a supplementary damping controller have been introduced and implemented. These control design methods have very different design requirements. For example, the MLQG damping control design method is a model based approach and required the linear modal of the system. Therefore, system identification is used to derive the linear model of the system. The process of the system identification algorithm is also provided in this Chapter.

The main advantage of the MLQG compared to the other control design method such as LQG method is that its tuning process in order to obtain an exact target damping ratio is relatively straightforward through the novel implementation of a modal representation of the control design problem. Whereas in the LQG control design method, the controller tuning process can become excessively complex within large power systems where several generators participate in the critical modes which need additional damping. This is because, in this case, the LQG design method requires the participation factor analysis in order to identify the electromechanical states involved in critical system oscillatory modes and assigning the weightings to these states. However, if these states are involved in other modes that do not require further damping, the damping of these modes could be affected adversely. This results in a complex and time-consuming tuning process in which it is often not possible to obtain exact target damping factors.

A comparative study on the performance of both introduced damping controllers is presented using a simple test system. The results confirm that both controllers are considerably effective on improving the system oscillation damping. The PSS-Based damping controller has proven slightly more effective on inter-area mode of oscillation as it is tuned only for the inter-area mode of oscillation. However, the PSS-based damping controller is considered as single mode damping controller whereas the MLQG

damping controller can be extended to a multivariable controller. This property of the MLQG damping controller make it a better control design option for design of supplementary damping controller for the VSC-HVDC links with the multiple points of controlled power injection.

As the sixth and final contribution of this research further comparative investigation has conducted into the capability of the West Coast HVDC link in the system inter-area oscillation damping using the full GB transmission system model. The results evidently demonstrated that West Coast HVDC link, not only can be implemented for the bulk power transfer, but also can be implemented for stabilising action within power systems. Also, The initial studies presented have shown that with the installations of supplementary damping control for the HVDC link, various factors such the operating conditions, level of transfer across the B6 boundary, level of s allowances on the HVDC link capacity for modulating damping control signal and location of the fault can all effect on the performance of the HVDC link supplementary damping control and consequently on the damping of oscillatory modes. Thus, these details may require cautious analysis and real-time monitoring, particularly when critical modes are near the stability margin.

In addition, a range of advanced and economically efficient assistive control actions including the set-point adoption of the embedded HVDC links using the SR control design method (which involve the fast ramp-up capability of the HVDC link), supplementary power oscillation damping control for the HVDC links, smart demand side control and conventional generation inter-trip schemes has been introduced and their effectiveness in releasing the latent network capacity have been investigated using the full model of GB transmission system. It was demonstrated based on studies performed on the full dynamic model of the GB transmission system that the proposed transient supportive actions/schemes could improve the overall system stability and potentially improve the limit on the B6 boundary. However, there is a significant cost associated with the conventional post-fault actions such as generation inter-trip and smart demand management whereas the other two aforementioned supportive actions are free. In addition ,the results of comparative study demonstrated that the HVDC link damping controller presents the best performance and provide better damping at post fault compared to the other control schemes [147].

8.2 Further research opportunities

The work presented within this thesis has satisfied all of the research aims which were initially defined. Nevertheless there are a number of areas where this work could be extended in order to further develop the ideas and methods which have been developed. The following are a few probable future research directions:

Further investigation into the robustness of the proposed SR control for wider range of operational points:

The performance and robustness of the designed SR can be further investigated for various system operating point and system outage patterns.

Extension of SR control to an adaptive control:

The SR control can be extended to an adaptive control to develop solutions that can automatically adapt the active power set-point of the HVDC links and consequently release the burden on the B6 boundary during heavily loaded operating conditions. The feasibility and requirement of the adaptive SR controller need to be further investigated.

Investigating the performance of the proposed controller for co-ordinated control of East and West Coast HVDC link:

Additional to the Western HVDC link, the Eastern Coast HVDC links are planned to be connected to the transmission system in order to increase the B7 boundary power transfer capability. Further investigation is required with regard to coordinated control of future DC links and determining their set-points in a coordinated manner. The coordination of the power flow controlling devices can potentially optimise the transmission capacity as well providing enhanced system security management [181].

Investigation on the performance of the MLQG damping controller for the West Coast HVDC link:

The Feasibility of model-based MLQG damping controller for the West Coast HVDC link need further investigation. Also, the WAMS-based multivariable control structure of the MLQG damping control can be also implemented for co-ordinated control of West and East HVDC links damping controllers to provide improved stability performance across B6 and B7 boundaries.

Robustness assessment of the designed damping controller for the HVDC link : Power system networks are continuously subjected to the uncertainty introduced by load and wind energy variations which can change the power system operating condition to the point that the tuning of the damping controller are no longer effective. This is more evident for the model-based damping controller such as MLQG controller where design method relies on linearized model of the system. Consequently this could results in deterioration of performance of the designed Wide-area controller. In the worse scenario, the controller can even introduce an adverse effect on system stability. This necessitates a thorough investigation of the controller's performance over a wide range of operating points. To show the satisfactory performance and practical applicability over a wide range of operating points, a robustness assessment is required to be performed at different operating points obtained by implementation of the probabilistic distribution of system operating points using probabilistic method such as the Monte Carlo method [174].

Impact of time delays to a wide-area damping controller:

As it was demonstrated in Chapter 7, the HVDC links' supplementary damping controllers can provide damping to the system oscillation. Although, Wide-Area Measurement system signals provide better damping of the inter-area oscillation [182], the damping performance can be affected or may even cause instability of the closed-loop system due to existence of communication time delay for transfer of input signals. Therefore, a further investigation into controller design approaches that provide a balance between the delay margin and the damping performance is required [183].

Examine the performance of wider range of control design methods:

As discussed in Chapter 2, wide range of alternative controller design methods used in past researches for design of control systems mostly for power oscillation damping controller. These included model-based, MPC, non-linear optimisation methods such as evolutionary genetic algorithms, Prony-based adaptive control, Lyapunov energy functions and fuzzy control. It would be appropriate to conduct a comprehensive comparative study using the same test system and operational condition to investigate the capability and performance of each in a like to like cases. This would assist the system operators to decide on type and method of controller design [146]

Appendix A

Correct modelling of the synchronous generators and their excitation systems is essential in studying the dynamic behaviour of power systems. Various test systems have been considered throughout this thesis as described in Chapter 3. The parameters of the key components of the test systems such as generators and their excitation and governor, transformer, line, load and SVC are provided in the Appendices.

A.1: Dynamic parameters of the SMIB test system 1

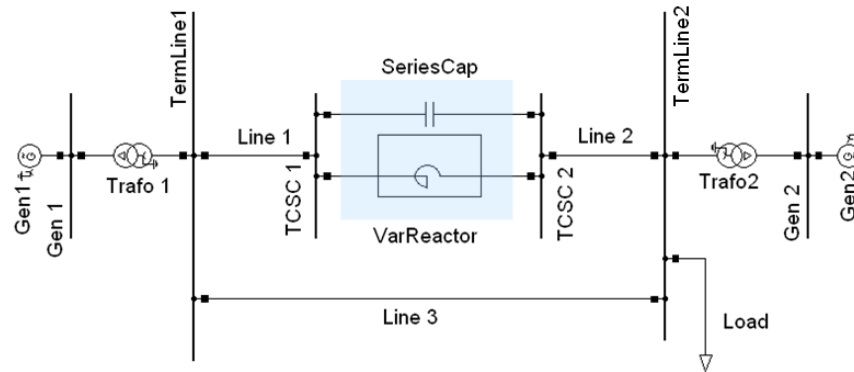


Figure A.1. 1: SMIB test system 1

Both generators dynamic data in test system 1 is presented in Table A1.1. Also, both generators' rotors are salient pole rotor type.

Table A.1 1: Synchronous machine dynamic parameters

Generator	symbol	Unit	G1	G2
Inertia time constant	H	s	10	10
Mechanical damping		p.u.	0	0
Stator resistance	$rstr$	p.u.	0.001	0.001
Stator leakage reactance	x_l	p.u.	0.1	0.1
Synchronous reactance	x_d	p.u.	2	2
Synchronous reactance	x_q	p.u.	2	2
Transient reactance	x_d'	p.u.	0.3	0.3
Transient reactance	x_q'	p.u.	-	-
Sub-transient reactance	x_d''	p.u.	0.2	0.2
Sub-transient reactance	x_q''	p.u.	0.2	0.2
Transient time constant	T_{d0}'	s	1	1
Transient time constant	T_{q0}'	s	-	-
Sub-transient time constant	T_{d0}''	s	0.05	0.05
Sub-transient time constant	T_{q0}''	s	0.05	0.05

Load flow data and bus type for the in test system 6 is presented in Table A.1.2

Table A.1 2: Bus type and load flow data

Gen No	Bus node	Bus	Gen Rating	V_{L-L}	P_L (MW)	Q_L (MVar)	V
G1	Gen1	PV	1700	20	1300	97	1.05
G2	Gen2	SL	1700	20	1300	428	1.05
-	TermLine1	PV	-	500	-	-	1.05
-	TermLine2	PV	-	500	-	-	1.05
-	TCSC1	PV	-	500	-	-	1.05
-	TCSC2	PV	-	500	-	-	1.05

Both generators use the following exciter data as shown in Table A.1.3

Table A.1 3: Generators' exciter data

Voltage regulator gain	K	400	p.u.
Voltage regulator time constant	T_e	0.02	s
Transient gain reduction time constant	T_a	1	s
Transient gain reduction time constant	T_b	10	s
Maximum voltage regulator output	V_{max}	6	p.u.
Minimum voltage output	V_{min}	0	p.u.

All the generators use the following Governor data as shown in Table A.1.4

Table A.1 4: Generators' governor parameters

Speed droop	R	0.05	p.u.
Controller time constant	T_1	0.05	s
Actuator time constant	T_2	0	s
Compressor time constant	T_3	0.5	s
Ambient temp.	AT	1	s
Turbine factor	K_t	1	s
V_{max} controller Maximum output	V_{max}	0	p.u.
V_{min} controller Minimum output	V_{min}	1.5	p.u.

All the generators' transformer use the following data as shown in Table A.1.5

Table A.1 5: Generators' transformer parameters

Generator	G1	G2
Rated power (MVA)	1000	1000
Rated voltage (HV)	500	500
Rated voltage (LV)	20	20
Short circuit voltage (positive Sequence %)	8	8
Short circuit voltage (zero Sequence %)	3	3
Winding connection (HV)	YN	YN
Winding connection (LV)	YN	YN

The load data are presented in Table A.1.6.

Table A.1 6: Load data

Load	P (MW)	Q (MVar)
Load 1	2600	400

The TCSC parameters are given in Table A.1.7.

Table A.1 7: The TCSC's Reactor and Capacitor parameters.

Series Capacitor	20	ohm
Reactor parallel with series Capacitor	35	ohm

The lines parameters are presented in Table A.1.8.

Table A.1 8: Lines parameters

	V_{L-L} (kV)	L (km)	Rated	R(Ohm/km)	Reac.(Ohm/km)	Susc.(μ s/km)
Line1	500	100	1	0.03	0.3	5
Line2	500	100	1	0.03	0.3	5
Line3	500	200	1	0.03	0.3	5

A.2: Dynamic parameters of the SMIB test system 2

All the parameters including generators, generators' governor/exciter, generator transformer and lines are the same as SMIB test system 1.

A.3: Dynamic parameters of the SMIB test system 3

All the parameters for generators and generators' governor/exciter are the same as SMIB test system 1. Only a HVDC link is added in place of the TCSC. The rest of parameters which are different from the test system1 are presented as follows.

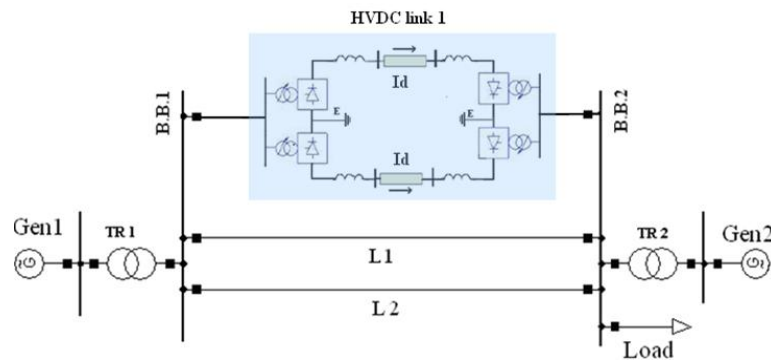


Figure A.3. 1: Test system 3 with HVDC link

The load data are presented in Table A.3.1.

Table A.3 1: Load data

Load	P (MW)	Q (MVar)
Load 1	2400	400

The lines parameters are presented in Table A.3.2

Table A.3 2: lines parameters

Lines	V_{L-L} (kV)	L (km)	Rated	R(Ohm/km)	Reac.(Ohm/km)	Susc. ($\mu\text{s/km}$)
L1	400	200	1	0.03	0.3	5
L2	400	200	1	0.03	0.3	5

Table A.3 3: Bus type and load flow data

Gen No	Bus node	Bus	Gen Rating	V_{L-L}	P_L (MW)	Q_L (MVar)	V_{\max}
G1	Gen1	PV	1700	20	1300	114	1.05
G2	Gen2	SL	1700	20	1200	350	1.05
-	BB1	PV	-	400	-	-	1.05
-	BB2	PV	-	400	-	-	1.05

All the generators' transformer use the following data as shown in Table A.3.4

Table A.3 4: Generators' transformer parameters

Generator	G1	G2
Rated power (MVA)	1000	1000
Rated voltage (HV)	400	400
Rated voltage (LV)	20	20
Short circuit voltage (positive Sequence %)	8	8
Short circuit voltage (zero Sequence %)	3	3
Winding connection (HV)	YN	YN
Winding connection (LV)	YN	YN

A.4: Dynamic parameters of the SMIB test system 4

All the parameters including generators, generators' governor/exciter, generator transformer and lines are the same as SMIB test system 3.

A.5: Dynamic parameters of the SMIB test system 5

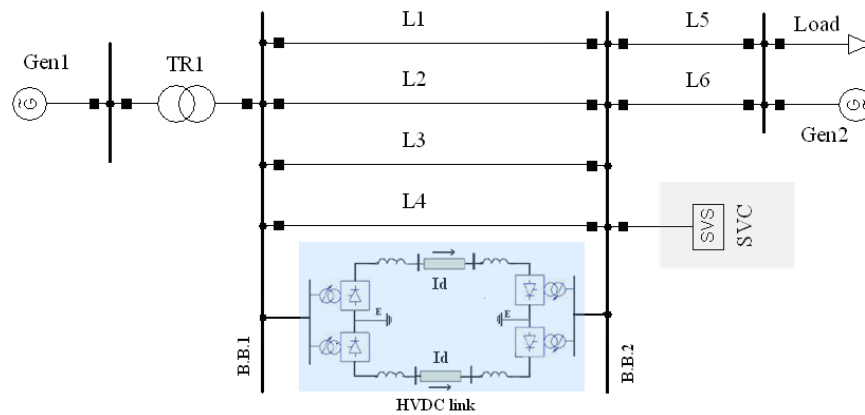


Figure A.5. 1: Test system 5 with SVC and HVDC link

All the parameters for generators and generators' governor/exciter are the same as SMIB test system 1. The rest of parameters are presented in as follows:

Table A.5 1: Synchronous machine dynamic parameters

Generator	symbol	Unit	G1	G2
Inertia time constant	H	s	10	10
Mechanical damping		p.u.	0	0
Stator resistance	r_{str}	p.u.	0.0023	0.0023
Stator leakage reactance	x_l	p.u.	0.182	0.182
Synchronous reactance	x_d	p.u.	2.68	2.68
Synchronous reactance	x_q	p.u.	2.456	2.456
Transient reactance	$x_{d'}$	p.u.	0.29	0.29
Transient reactance	$x_{q'}$	p.u.	2.45	2.45
Sub-transient reactance	$x_{d''}$	p.u.	0.228	0.228
Sub-transient reactance	$x_{q''}$	p.u.	0.228	0.228
Transient time constant	T_{d0}'	s	0.55	0.55
Transient time constant	T_{q0}'	s	0.55	0.55
Sub-transient time constant	T_{d0}''	s	0.0115	0.0115
Sub-transient time constant	T_{q0}''	s	0.0115	0.0115

Load flow data and bus type for the in test system 6 is presented in Table A.5.2

Table A.5 2: Bus type and load flow data

Gen No	Bus node	Bus	Gen Rating	V_{L-L}	P_L (MW)	Q_L (MVar)	V
G1	Gen1	PV	2500	23	2000	410	1.05
G2	Gen2	SL	2500	23	48019	72	1.05
-	BB1	PV	-	400	-	-	1.05
-	BB2	PV	-	400	-	-	1.05

All the generators' transformer use the following data as shown in Table A.5.3

Table A.5 3: Generators' transformer parameters

Generator	G1	G2
Rated power (MVA)	1000	1000
Rated voltage (HV)	400	400
Rated voltage (LV)	23	23
Short circuit voltage (positive Sequence %)	0.677	0.677
Short circuit voltage (zero Sequence %)	0.009	0.009
Winding connection (HV)	YN	YN
Winding connection (LV)	YN	YN

The load data are presented in Table A.5.4.

Table A.5 4: Load data

Load	P (MW)	Q (MVar)
Load 1	50000	0

The lines parameters are presented in Table A.5.5.

Table A.5 5: lines parameters

Line	V_{L-L} (kV)	L (km)	Rated	R(Ohm/km)	Reac.(Ohm/km)	Susc.(μ s/km)
L1	400	1	2.309	1.815	17.39	5753.8
L2	400	1	2.309	1.815	17.39	5753.8
L3	400	1	2.309	1.815	17.39	5753.8
L4	400	1	2.309	1.815	17.39	5753.8
L5	400	1	2.309	1.815	17.39	5753.8
L6	400	1	2.309	1.815	17.39	5753.8

The parameters of the SVC and its voltage control are presented in Table A.5.6 and Table A.5.7.

Table A.5 6: SVC parameters

Target voltage	K	275	p.u.
Reactance	$TCR(Q)$	75	Mvar
Capacitor	$TCS(Q)$	-75*2	Mvar
Droop	T_b	5%	%
Max steady state voltage	V_{max}	1.05	p.u.
Min steady state voltage	V_{min}	0	p.u.

Table A.5 7: SVC voltage control parameters

Voltage regulator gain 1	$K1$	0.03	p.u.
Voltage regulator gain 2	$K2$	3.87	p.u.
Lead time constant	T_1	0.0057	s
Lag time constant	T_2	0.0042	s
Lead time constant	T_3	0.0059	s
Lag time constant	T_4	0.0043	s

A.6: Dynamic parameters of the test system 6

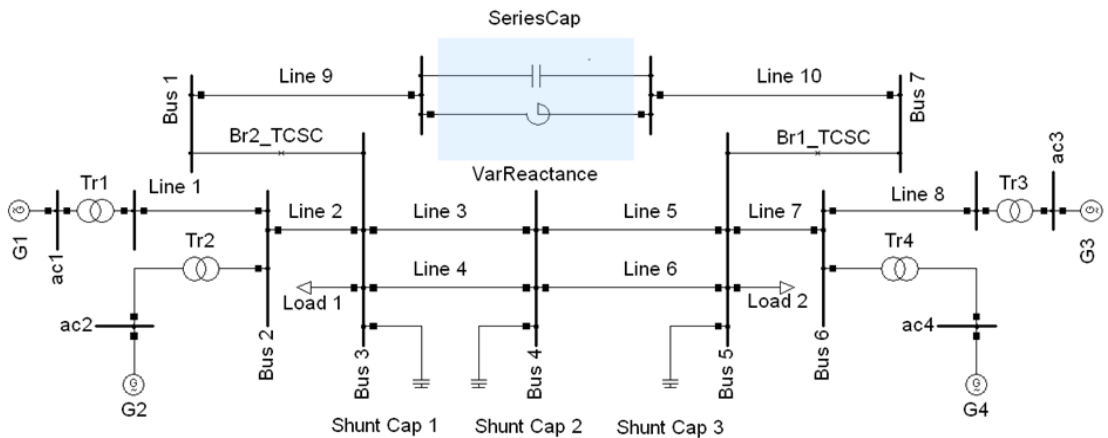


Figure A.6. 1: Single line diagram of the four-machine test system 6 with TCSC

All the generators dynamic data in test system 6 is presented in Table A.6.1 [22].

Table A. 6. 1: Synchronous machine dynamic parameters

Generator	symbol	Unit	G1	G2	G3	G4
Inertia time constant	H	s	6.5	6.5	6.5	6.5
Mechanical damping		p.u.	0	0	0	0
Stator resistance	r_{str}	p.u.	0.0025	0.0025	0.0025	0.0025
Stator leakage reactance	x_l	p.u.	0.2	0.2	0.2	0.2
Synchronous reactance	x_d	p.u.	1.8	1.8	1.8	1.8
Synchronous reactance	x_q	p.u.	1.7	1.7	1.7	1.7
Transient reactance	$x_{d'}$	p.u.	0.3	0.3	0.3	0.3
Transient reactance	$x_{q'}$	p.u.	0.55	0.55	0.55	0.55
Sub-transient reactance	$x_{d''}$	p.u.	0.25	0.25	0.25	0.25
Sub-transient reactance	$x_{q''}$	p.u.	0.25	0.25	0.25	0.25
Transient time constant	T_{d0}'	s	8	8	8	8
Transient time constant	T_{q0}'	s	0.4	0.4	0.4	0.4
Sub-transient time constant	T_{d0}''	s	0.03	0.03	0.03	0.03
Sub-transient time constant	T_{q0}''	s	0.05	0.05	0.05	0.05

Load flow data and bus type for the in test system 6 is presented in Table A.6.2

Table A. 6. 2: Bus type and load flow data

Gen	Bus type	R (MVA)	V_{L-L}	P_L (MW)	Q_L (MVar)	V (p.u.)
G1	SL	900	20	750	185	1.03
G2	PV	900	20	700	235	1.01
G3	PV	900	20	719	176	1.03
G4	PV	900	20	700	202	1.01

All the generators use the following AVR data as shown in Table A.6.3

Table A. 6. 3: Generators' AVR data

Transducer filter time constant	T_r	0.01	s
Voltage regulator gain	K	200	p.u.
Voltage regulator time constant	T_e	0.05	s
Transient gain reduction time constant	T_a	1	s
Transient gain reduction time constant	T_b	10	s
Maximum voltage regulator output	V_{max}	3	p.u.
Minimum voltage output	V_{min}	-3	p.u.

All the generators use the following Governor data as shown in Table A.6.4

Table A. 6. 4: Generators' governor parameters

Governor gain	K	50	p.u.
Servo time constant	T_s	0.1	s
Transient gain time constant	T_3	0	s
HP turbine time constant	T_c	0.5	s
Time constant to set HP ratio	T_4	1.25	s
Reheat time constant	T_5	5	s
Maximum power	P_{max}	1	p.u.
Minimum power	P_{min}	0	p.u.

All the generators' transformer use the following data as shown in Table A.6.5

Table A. 6. 5: Generators' transformer parameters

Generator	G1	G2	G3	G4
Rated power (MVA)	900	900	900	900
Rated voltage (HV)	230	230	230	230
Rated voltage (LV)	20	20	20	20
Short circuit voltage (positive Sequence %)	15	15	15	15
Short circuit voltage (zero Sequence %)	3	3	3	3
Winding connection (HV)	YN	YN	YN	YN
Winding connection (LV)	YN	YN	YN	YN

The load data are presented in Table A.6.6.

Table A. 6. 6: Load data

Load	P (MW)	Q (MVar)
Load 1	967	100
Load 2	1667	100

The Shunt Capacitors (SC) data are presented in Table A.6.7.

Table A. 6. 7: Shunt capacitors data

No. of	V(kV)	At bus	Q (MVar)	Q/ per tap	No tap	Q max
SC1	230	3	189.88	100	6	600
SC2	230	5	0	100	5	500
SC3	230	5	341.61	50	10	500
SC4	230	Rec.	118.67	125	1	125
SC5	230	Rec.	122.00	125	1	125

The lines parameters are presented in Table A.6.8.

Table A. 6. 8: Shunt capacitors data

Line	line1	line2	line3	line4	line5	line6	line7	line8	line9	line10
V_{L-L} (kV)	230	230	230	230	230	230	230	230	230	230
L (km)	25	10	110	110	110	110	10	25	10	10
R(Ohm/km)	0.05	0.05	0.05	0.05	0.05	0.05	0.05	0.05	0.52	0.52
Reac.(Ohm/km)	0.52	0.52	0.52	0.52	0.52	0.52	0.52	0.52	0.52	0.52
Susc.(μ s/km)	3.30	3.30	3.30	3.30	3.30	3.30	3.30	3.30	3.30	3.30

The TCSC parameters are given in Table A.6.9.

Table A. 6. 9: TCSC Reactor and Capacitor parameters.

Series Capacitor	20	ohm
Reactor parallel with series Capacitor	35	ohm

Appendix B

The details on the modelling and primary control of CSC-HVDC link using the DiGSILENT PowerFactory are provided in Chapter 3. Power Factory use a composite frame as a hierarchical framework for modelling purposes. Appendix B presents illustrative snapshots of the CSC-HVDC models implemented in PowerFactory [124] with the main design aspects of the future West Coast HVDC link presented in Table B.1 [156].

Parameter	Value
HVDC link Converter continuous rating	2.2GW
Nominal Direct Current (without redundant cooling)	1875A
Nominal Direct Voltage	600kV
Nominal AC Voltage	360kV to 440kV (440kV for 15min)
Power reversal	Limited by Q constraints
DC submarine cable	385km
Short Circuit Level (At Connah's Quay, Intact system)	29652MVA
Short Circuit Level (At Hunterston, Intact system)	18150MVA

B1: The converters' control model associated with HVDC link

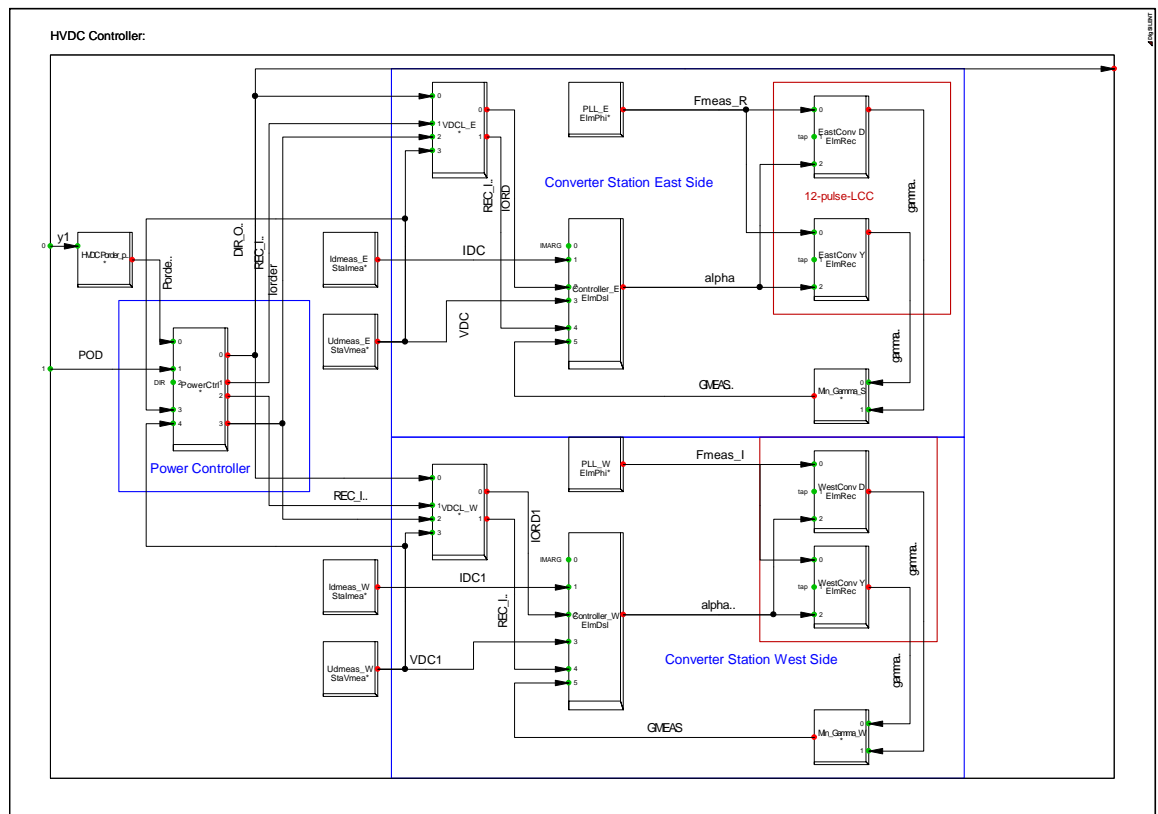


Figure B. 1: Overall framework of the CSC-HVDC link converters control

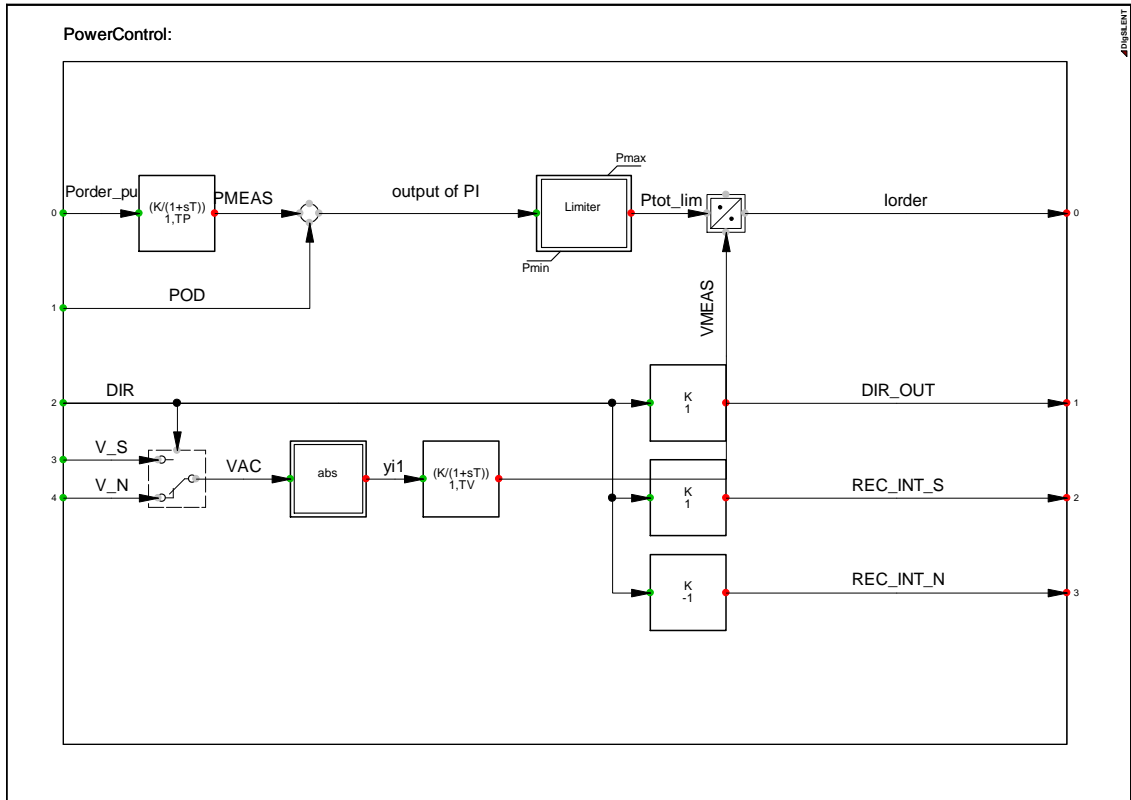


Figure B. 2: CSC-HVDC link and DC power control

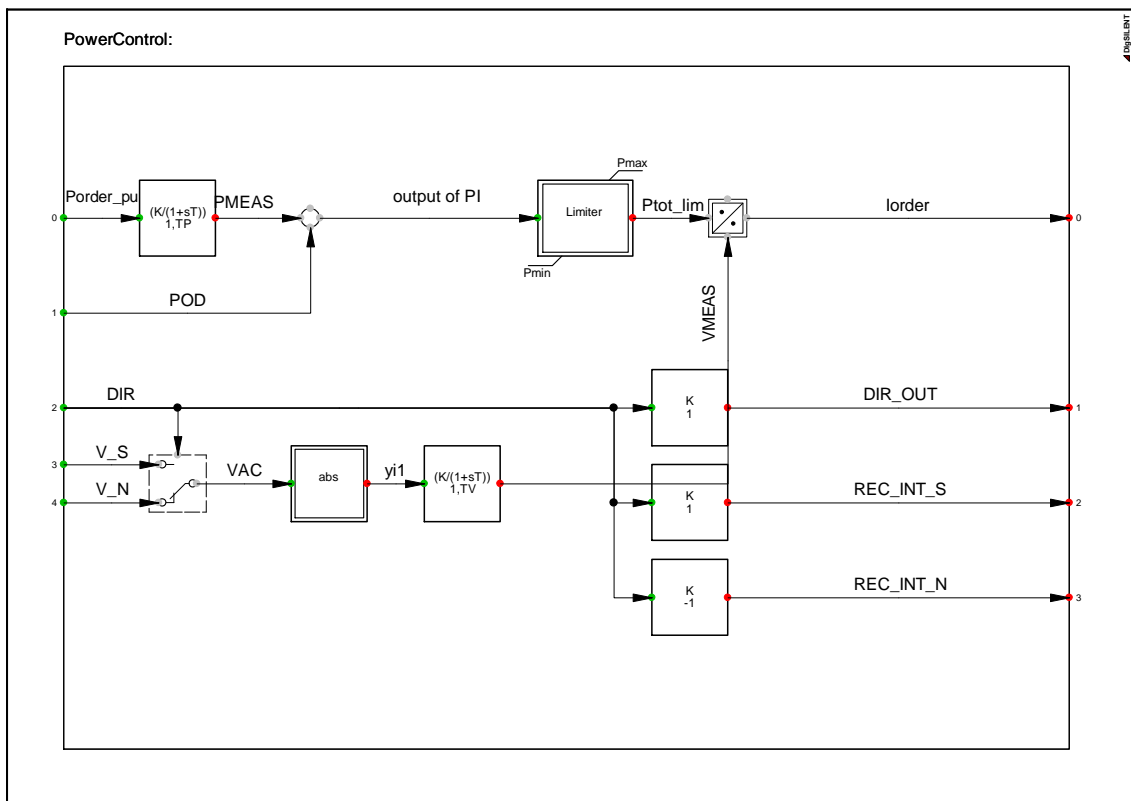


Figure B. 3: CSC-HVDC link Voltage Dependant Current Order Limiter (VDCOL) model

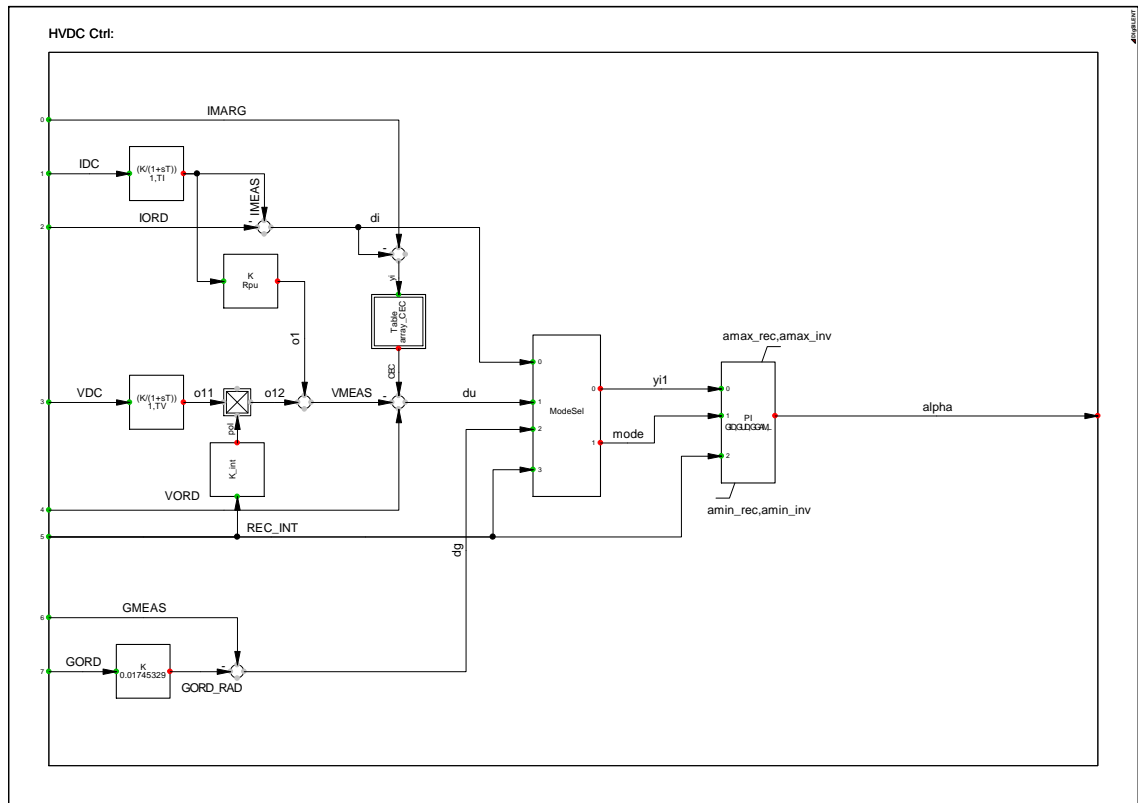


Figure B. 4: The HVDC link CC, CV and CEA control framework

Appendix C

C 1: Model and parameters of the PSS-based power oscillation damping control for the TCSC

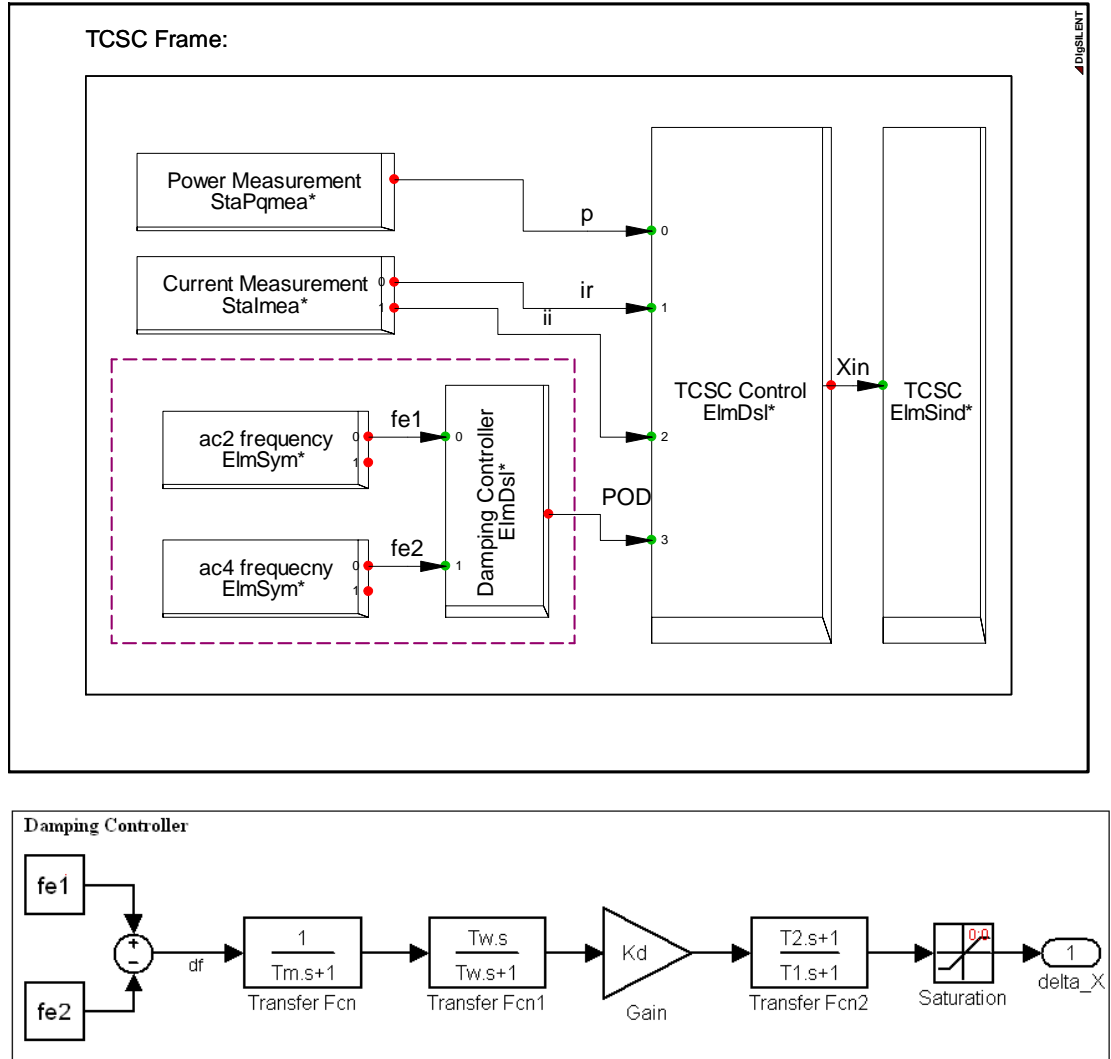


Figure C. 1: PSS-based damping control model for the TCSC

Table C.2: PSS-based damping control design parameters for the TCSC

Washout time constant	T_w	10	s
Filter time constant	T_m	0.1	
Controller gain	K	22000	s
Lead phase compensation	T_1	0.11	s
Lag Phase compensation	T_2	0.566	s
Lead phase compensation	T_3	1	s
Lag Phase compensation	T_4	1	s
Maximum power	P_{max}	15	p.u.

C 2: Model and parameters of the PSS-based power oscillation damping control for the HVDC link

Table C. 3: PSS-based damping control design parameters

Washout time constant	T_w	10	s
Filter time constant	T_m	0.1	
Controller gain	K	1600	s
Lead phase compensation	T_1	0.1	s
Lag Phase compensation	T_2	1	s
Lead phase compensation	T_3	0.1	s
Lag Phase compensation	T_4	1	s
Maximum power	P_{max}	5	p.u.

Damping controller:

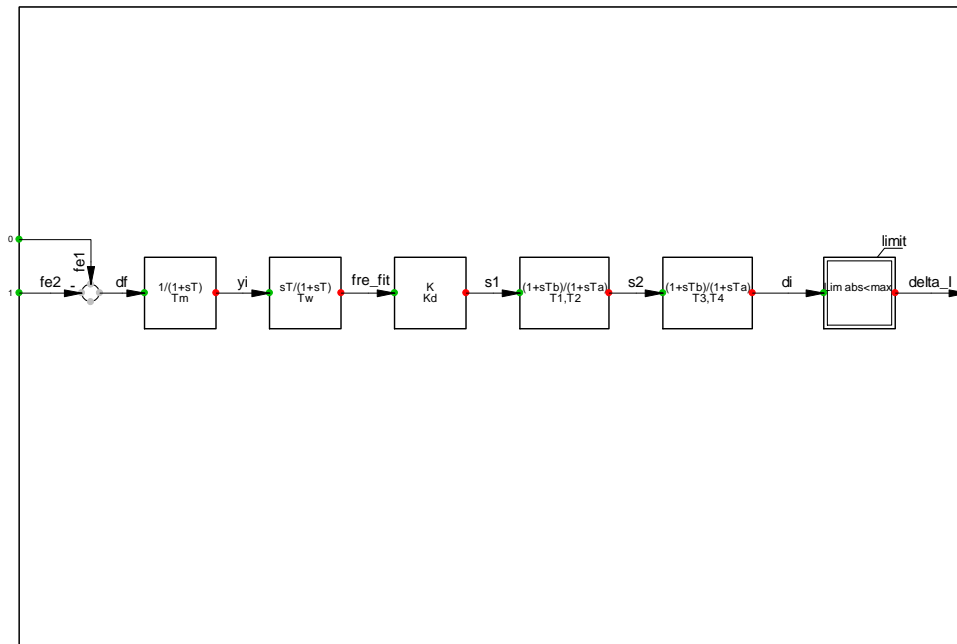


Figure C. 2: PSS-based damping control model for the HVDC link in PowerFactory

C 3: Model and parameters of the MLQG-based power oscillation damping control for the HVDC link

Table C 4: MLQG-based damping control design parameters

Washout time constant	T_w	10	s
Controller size	<i>order</i>	6	-
WAC output limiter	K	± 5	p.u.
weight matrix of output deviations (Q)	Q	1e5	p.u.
Weight matrix of control inputs (R)	R	1	p.u.

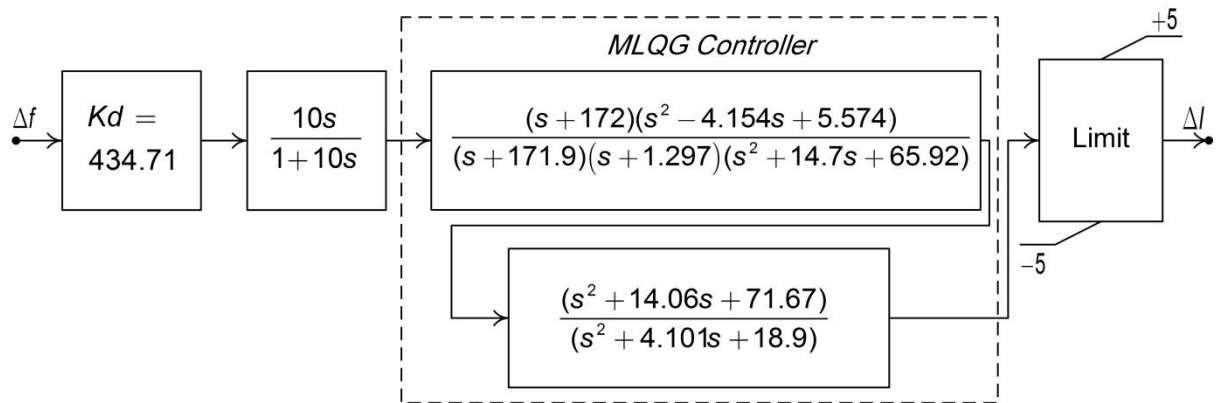


Figure C. 3: MLQG-based damping control model for the HVDC link in PowerFactory

C 4: Parameters of the PI control for the TCSC

Table C 5: PI controller parameters

Time constant	T_f	0.05	s
Gain (Ki)	K_i	0.5	p.u.
Integral time	T_i	0.01	s
Minimum reactance	X_{min}	12.8	p.u.
Maximum reactance	X_{max}	30	p.u.

Appendix D

D.1: Procedure and steps of the system identification routine to identify the linear model of non-linear systems are presented in Figure D.1.

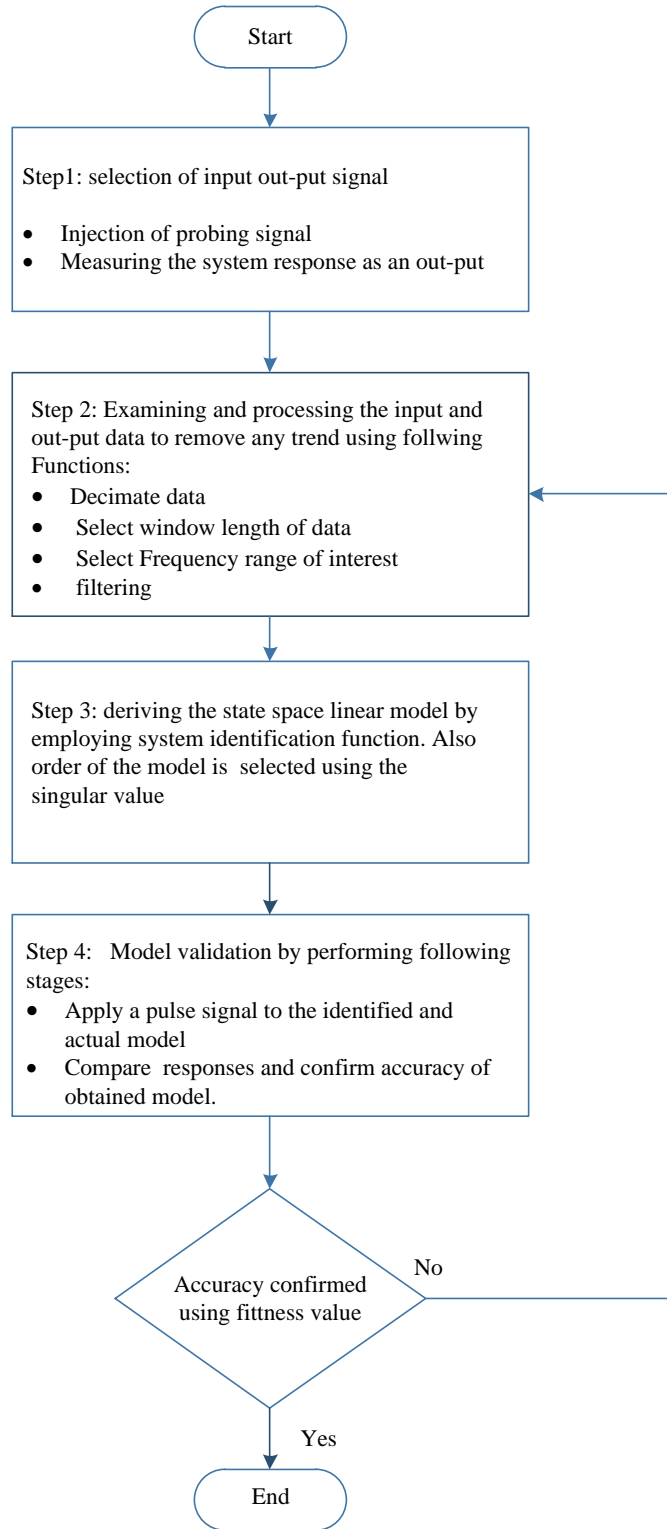


Figure D. 1: System identification procedure [59]

Appendix E

E.1: The overall structure of the West coast HVDC link supplementary damping controller in Power Factory

POD Frame:

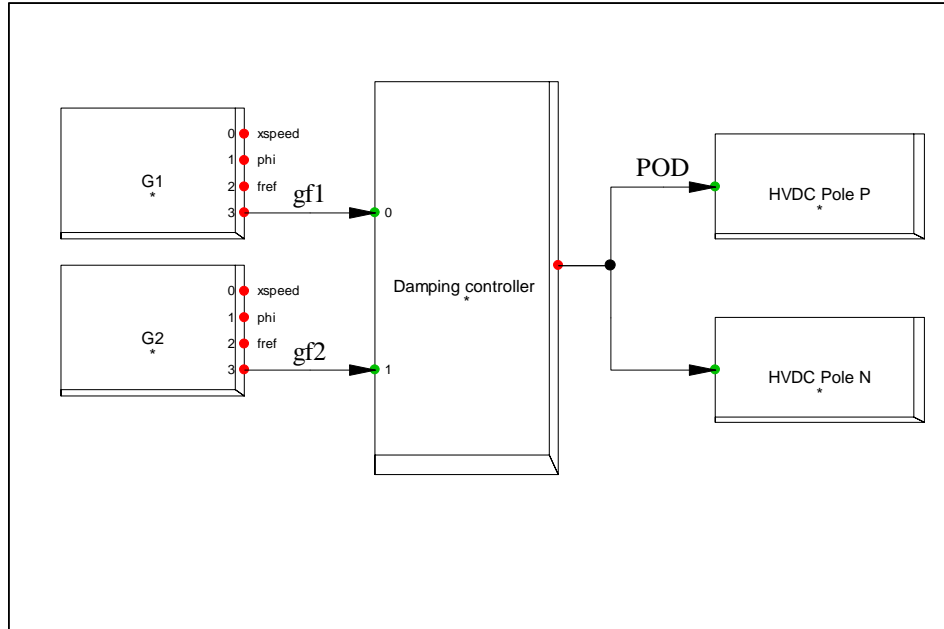


Figure E 1: Overall structure of the PSS-based damping control model for West Coast HVDC link in PowerFactory

E 2: Model and parameters of the PSS-based power oscillation damping control for the West coast HVDC link

Table E 2. 1: PSS-based damping control design parameters for the West coast HVDC link

Washout time constant	T_{w1}	10	s
Washout time constant	T_{w2}	10	s
Filter time constant	T_m	0.1	
Controller gain	K	100	s
Lead phase compensation	T_1	1	s
Lag Phase compensation	T_2	1	s
Lead phase compensation	T_3	0.1	s
Lag Phase compensation	T_4	1	s
Maximum power	P_{max}	0.2	p.u.

Damping controller:

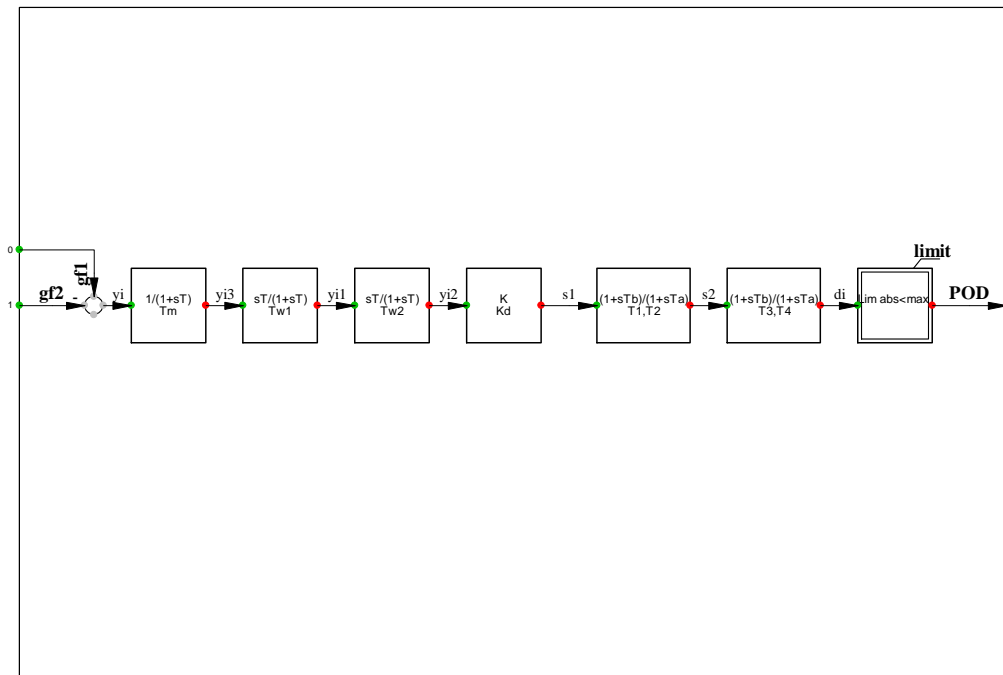


Figure E 2: PSS-based damping control model for West Coast HVDC link in PowerFactory

Appendix F

F.1 Overview of Inter-area oscillation/small signal stability

Small signal stability studies have been mainly based on eigenvalue analysis to identify the modes of the system. The two main approaches for finding power system modes are component-based methods and measurement-based methods. In the component-based method, the nonlinear differential equations of the system are linearised around an operating point [57]. The power system modes are then obtained through eigenvalue analysis of the characteristic matrix derived from the linearised model of the power system. A brief overview of eigenvalue analysis using component-based method is given in the next section.

F.2 Power System linearisation for stability analysis

A power system can be described as a set of nonlinear differential algebraic equations as shown in (F.2.1), where x is the state vector, y is the algebraic output vector, and u is the input vector.

$$\begin{cases} \dot{X} = f(x, y, u) \\ 0 = g(x, y, u) \end{cases} \quad (\text{F.2.1})$$

The system can be linearised around its operating point for small-stability analysis purposes. This is because the small-disturbance stability is defined as the ability of a power system to maintain synchronous operation when subjected to a small disturbance and as long as the disturbance is small the power system equations can be linearised and presented in a state space form as shown in (F.2.2).

$$\begin{aligned} \Delta \dot{x} &= A \Delta x + B \Delta u \\ \Delta y &= C \Delta x + D \Delta u \end{aligned} \quad (\text{F.2.2})$$

Based on Lyapunov's first method, the small-disturbance stability of a system is determined by the roots of the characteristic equation of the system. In the case of a state space model of the system, the characteristic equation of the system based on matrix A is given in (F.2.3) [22].

$$A \phi = \lambda \phi \quad (\text{F.2.3})$$

Where λ are scalar values called the eigenvalues of system and the eigenvalues of a linearised power system models are the oscillation modes of the power system. There

are (n) solutions for (F.2.3), which form a set of (n) eigenvalues. Equation (F.2.3) can be solved to find the eigenvalues of a system using the following determinant:

$$|A - \lambda I| = 0 \quad (F.2.4)$$

It should be noted that the eigenvalues (modes) of the system can be influenced by adjusting or changing the operating point of the power system. Also, matrix in (F.2.3) is a corresponding eigenvectors where which satisfies (F.2.3) for the i^{th} eigenvalue is called right eigenvector of matrix A. Similarly, the modified characteristic equation in (F.2.3) can be defined in term of left eigenvalues as shown in (F.2.5).

$$\psi A = \psi \lambda \quad (F.2.5)$$

The eigenvalue characteristic of the system can be briefly expressed by modal matrices presented in (F.2.6)-(F.2.8) where ϕ is the matrix of right eigenvectors, Ψ is the matrix of left eigenvectors, and Λ is a diagonal matrix of system eigenvalues.

$$\phi = [\phi_1 \ \phi_2 \dots \ \phi_n] \quad (F.2.6)$$

$$\Psi = [\psi_1^T \ \psi_2^T \dots \ \psi_n^T] \quad (F.2.7)$$

$$\Lambda = [\lambda_1 \ \lambda_2 \dots \ \lambda_n] \quad (F.2.8)$$

The mode of the system's performance in time-based format is defined by where, It can be seen that eigenvalues (λ) with only real part are not oscillatory. Also, a complex eigenvalue with a negative real part will result in a decaying time response whereas positive real eigenvalues will lead to a growing time response which leads to instability. Therefore, eigenvalues/modes of the system are expressed by their damping and frequency of their oscillation where the real part of the eigenvalue of the system gives the damping, and the imaginary part gives the frequency of oscillation. The damping ratio of the modes, which is shown in (F.2.9), is defined as a rate of decay of the amplitudes of oscillation associated with the mode. In general, the oscillatory modes having damping ratio less than 5% are considered to be critical [162][22].

$$\zeta = \frac{-\sigma}{\sqrt{\sigma^2 + \omega^2}} \quad (F.2.9)$$

References

- [1] Department of Trade and Industry, “Meeting the Energy Challenge: A White Paper on Energy,” *Nucl. Eng. Des.*, vol. 236, no. May, p. 343, 2007.
- [2] “The Climate Change Act 2008. HM Government United Kingdom, 2008.” pp. 111–124, 2012.
- [3] European Commission, “Communication from the Commission to the European Parliament, the Council, the European Economic and Social Committee and the Committee of the Regions - A Roadmap for moving to a competitive low carbon economy in 2050,” *Change*, vol. 34, pp. 1–34, 2011.
- [4] Ensg. “Our Electricity Transmission Network: A Vision for 2020,” *Office*, no. February, p. 148, 2012.
- [5] Ensg. “Our Electricity Transmission Network : A Vision for 2020,” *Network*, no. July, pp. 1–151, 2009.
- [6] “UK Future Energy Scenarios UK gas and electricity transmission July 2013,” 2013.
- [7] Entso-E “Ten-Year Network Development Plan 2012 ” 2012.
- [8] UK Ofgem “Project Discovery - Energy Market Scenarios. 2009” 2009.
- [9] “Summer Outlook” no. October, 2014.
- [10] National Grid, “Winter Outlook 2013/14,” no. October, pp. 1–70, 2013.
- [11] Food Department for Environment and Rural Affairs (Defra), “Food Department for Environment and Rural Affairs (Defra), Large Combustion Plant Directive (LCPD) - Update No. 7 , UK National Plan. www.defra.gov.uk, October 2012.”
- [12] Ofgem, “RIIO: A new way to regulate energy networks ” p. 58, 2010.
- [13] T. C. Estate, “The future is bright - the future is wind ! Round 3 Offshore Wind Farm Launch Programme for The Crown Estate The future is bright - the future is wind !”
- [14] Decc, “UK Renewable Energy Roadmap” *Carbon N. Y.*, vol. 5, no. November, pp. 293–298, 2011.
- [15] “System Security and Quality of Supply Standards(SQSS) ” [Online] available on: [<http://www2.nationalgrid.com/UK/Industry-information/Electricity-codes/System-Security-and-Quality-of-Supply-Standards>]
- [16] Commission of the European Communities “Modular Development Plan of the Pan-European Transmission System 2050,” *e-Highway2050*, 2013.
- [17] “Coordination of Electricity System Operators (Coreso), Company Overview , [Online] available on: www.coreso.eu, 2014.

References

- [18] “Engineering Doctorate Handbook. Brunel University London.” .
- [19] “Historical Review of Power System Stability Problems.” [Online]. Available: <http://electrical-engineering-portal.com/historical-review-of-power-system-stability-problems>.
- [20] Sushama Rajaram “Robust WAM-based Controller Coordination of FACTS Devices for Power System Transient Stability Enhancement,” University of Western Australia, 2011.
- [21] North American Electric Reliability Council, *Reliability concepts in bulk power electric systems*. Princeton, N.J., 1985.
- [22] Prabha-Kundur, *Power System Stability and Control*, 1st ed. New York; McGraw- Hill.
- [23] “L Gyugyi IN. Hingorani “FACTS Concept and General System Considerations,” Wiley-IEEE Press, 2000, pp. 1–35.
- [24] S. Rahimzadeh, M. Tavakoli Bina and H. Viki “Simultaneous application of multi-type FACTS devices to the restructured environment: achieving both optimal number and location,” *IET Gener. Transm. Distrib.*, vol. 4, no. December 2008, p. 349, 2010.
- [25] E. Ghahremani and I. Kamwa, “Analysing the effects of different types of FACTS devices on the steady-state performance of the Hydro-Québec network,” *IET Gener. Transm. Distrib.*, vol. 8, no. August 2013, pp. 233–249, 2014.
- [26] Stéphane Gerbex “Optimal location of multi-type facts devices in a power system by means of genetic algorithms,” pp. 70–73, 2001.
- [27] S. R. Najafi, M. Abedi, and S. H. Hosseinian “A Novel Approach to Optimal Allocation of SVC using Genetic Algorithms and Continuation Power Flow,” *2006 IEEE Int. Power Energy Conf.*, no. 4, pp. 202–206, 2006.
- [28] G. I. Rashed, H. I. Shaheen and S. J. Cheng “Optimal location and parameter settings of multiple TCSCs for increasing power system loadability based on GA and PSO techniques,” *Proc. - Third Int. Conf. Nat. Comput. ICNC 2007*, vol. 4, no. Icnc, pp. 335–344, 2007.
- [29] Kazemi, D. Arabkhabori, MYari and J. Aghaei “Optimal location of UPFC in power systems for increasing loadability by genetic algorithm,” *41st Int. Univ. Power Eng. Conf. UPEC 2006, Conf. Proceedings*, vol. 2, pp. 774–779, 2006.
- [30] M. Behshad, a. Lashkarara and H. Rahmani “Optimal location of UPFC device considering system loadability, total fuel cost, power losses and cost of installation,” *PEITS 2009 - 2009 2nd Conf. Power Electron. Intell. Transp. Syst.*, vol. 2, pp. 231–237, 2009.
- [31] S . Gerbex, R. Cherkaoui and A. J. Germond “Optimal Location of FACTS Devices to Enhance,” 2003.
- [32] M. Santiago-Luna and J. R. Cedeño-Maldonado “Optimal Placement of Facts Controllers in Power Systems via Evolution Strategies,” *Survival (Lond.)*, pp. 1–6, 2006.

References

- [33] R. P. Kalyani, M. L. Crow, and D. R. Tauritz “Optimal Placement and Control of Unified Power Flow Control devices using Evolutionary Computing and Sequential Quadratic Programming,” *2006 IEEE PES Power Syst. Conf. Expo.*, pp. 959–964, 2006.
- [34] S. Jamhoria, L. Srivastava, and S. M. Ieee “Applications of Thyristor Controlled Series Compensator in Power System : An Overview,” no. January, pp. 8–10, 2014.
- [35] L. Kirschner, D. Retzmann, and G. Thumm “Benefits of FACTS for power system enhancement,” *Proc. IEEE Power Eng. Soc. Transm. Distrib. Conf.*, vol. 2005, pp. 1–7, 2005.
- [36] J. Y. J. Yong, W. X. W. Xiaochen, D. Z. Du Zhongming, J. X. J. Xiaoming, W. Y. W. Yuhong, D. H. Zhang, and J. Rittiger “Digital simulation of AC/DC hybrid transmission system,” *Proceedings. Int. Conf. Power Syst. Technol.*, vol. 3, 2002.
- [37] N. P. Padhy and M. Moamen “Power flow control and solutions with multiple and multi-type FACTS devices,” *Electr. Power Syst. Res.*, vol. 74, pp. 341–351, 2005.
- [38] M. Basu “Optimal power flow with FACTS devices using differential evolution,” *Int. J. Electr. Power Energy Syst.*, vol. 30, pp. 150–156, 2008.
- [39] S. Meikandasivam, R. K. Nema, and S. K. Jain “Fine power flow control by split TCSC,” *Int. J. Electr. Power Energy Syst.*, vol. 45, pp. 519–529, 2013.
- [40] Venu Yarlagadda, .B.V.Sankar Ram and M.Rao “Voltage Stability Improvement using Controlled Series Capacitor based on Lmn and VCPI Stability Indices,” *Int. J. Electr. Power Energy Syst.*, vol. 3, pp. 1–5.
- [41] R. Shizawa, K. Nishida, T. Ohtaka and S. Iwamoto, “Allocation of TCSC from transient stability viewpoint,” *2004 Int. Conf. Power Syst. Technol. 2004. PowerCon 2004.*, vol. 1, no. November, pp. 21–24, 2004.
- [42] C. Venkatesh, T. Deepak, K. Rajesh, K. Krishna, and K. Kamath, “Flatness based TCSC controller for transient stability enhancement of power system,” *2010 Mod. Electr. Power Syst.*, pp. 1–6, 2010.
- [43] S. K. Rautray, S. Choudhury, S. Mishra and P. K. Rout, “A Particle Swarm Optimization based Approach for Power System Transient Stability Enhancement with TCSC,” in *Procedia Technology; 2nd International Conference on Communication, Computing & Security ICCCS-2012*, 2012, vol. 6, pp. 31–38.
- [44] M. Ishimaru and R. Yokoyama “Allocation and design of robust TCSC controllers based on power system stability index,” *Power Eng. ...*, vol. 00, no. c, pp. 573–578, 2002.
- [45] A. Samimi “A New Method for Optimal Placement of <i>TCSC</i> Based on Sensitivity Analysis for Congestion Management,” *Smart Grid Renew. Energy*, vol. 03, no. February, pp. 10–16, 2012.
- [46] G. Huang and T. Zhu “TCSC as a transient voltage stabilizing controller,” *2001 IEEE Power Eng. Soc. Winter Meet. Conf. Proc. (Cat. No.01CH37194)*, vol. 2, no. C, pp. 628–633, 2001.

References

- [47] D. Chatterjee and A. Ghosh “TCSC control design for transient stability improvement of a multi-machine power system using trajectory sensitivity,” *Electr. Power Syst. Res.*, vol. 77, pp. 470–483, 2007.
- [48] I. A. K. and T. H.T.Hassan, Usman Farooq Malik and Khalid, “Stability Improvement of Power System Using Upfc Stability Improvement of Power System,” *Electr. Eng.*, 2007.
- [49] D. Mondal, a Chakrabarti, and a Sengupta, “Small Signal Stability Improvement and Congestion Management Using PSO Based TCSC Controller,” vol. 02, pp. 12–17, 2011.
- [50] R. Benabid, M. Boudour and M. a Abido “Optimal placement of FACTS devices for multi-objective voltage stability problem,” *Proc. IEEE/PES Power Syst. Conf. Expo. PSCE '09*, pp. 1–11, 2009.
- [51] M. Gitizadeh and M. Kalantar “A New Approach for Congestion Management via Optimal Location of FACTS Devices in Deregulated Power Systems,” no. April, pp. 1592–1597, 2008.
- [52] Y. Wu and L. Li, “Transfer capability study of tie-line installed TCSC considering transient stability constraints,” *PEAM 2011 - Proc. 2011 IEEE Power Eng. Autom. Conf.*, vol. 2, pp. 260–263, 2011.
- [53] D. N. Kosterev, C. W. Taylor, and W. a. Mittelstadt, “Model validation for the August 10, 1996 WSCC system outage,” *IEEE Trans. Power Syst.*, vol. 14, no. 3, pp. 967–979, 1999.
- [54] R. a. Jabr, B. Pal and N. Martins “A sequential conic programming approach for the coordinated and robust design of power system stabilizers,” *IEEE Trans. Power Syst.*, vol. 25, pp. 1627–1637, 2010.
- [55] a. L. B. Do Bomfim, G. N. Taranto, and D. M. Falcao “Simultaneous tuning of power system damping controllers using genetic algorithms,” *IEEE Trans. Power Syst.*, vol. 15, no. I, pp. 163–169, 2000.
- [56] X. Lei, E. N. Lerch, and D. Povh “Optimization and coordination of damping controls for improving system dynamic performance,” *IEEE Trans. Power Syst.*, vol. 16, no. C, pp. 473–480, 2001.
- [57] R. Preece “A Probabilistic Approach to Improving the Stability of Meshed Power Networks with Embedded HVDC Lines” PhD thesis, University of Manchester, 2013.
- [58] Balarko Chaudhuri , B. Pal, A. C. Zolotas, I. M. Jaimoukha, and T. Green “Mixed-sensitivity approach to H_{∞} control of power system oscillations employing multiple facts devices,” *IEEE Trans. Power Syst.*, vol. 18, pp. 1149–1156, 2003.
- [59] Y. Pipelzadeh, “Coordination of Damping Control in Transmission Networks with HVDC links” PhD thesis, Electrical and Electronic Engineering Imperial College, London, 2012.
- [60] D. Van Hertem and J. Driesen “Transient Stability Enhancement By Tcsc.”
- [61] F. Liu, R. Yokoyama, Y. C. Zhou, and M. Wu “TCSC wide-area damping controller to enhance the damping of inter-area oscillation for power systems with considering the

References

- time delay of wide-area signals” *2010 Int. Conf. Power Syst. Technol. Technol. Innov. Mak. Power Grid Smarter, POWERCON2010*, pp. 1–6, 2010.
- [62] M. O. Hassan, Z. A. Zakaria, and S. J. Cheng, “Impact of TCSC on enhancing power system stability,” *Asia-Pacific Power Energy Eng. Conf. APPEEC*, pp. 14–15, 2009.
- [63] C. E. Ugalde-loo, J. B. Ekanayake, and N. Jenkins, “Subsynchronous resonance in a series-compensated Great Britain transmission network,” no. January 2012, pp. 209–217, 2013.
- [64] D. Rai, S. O. Faried, G. Ramakrishna, and A. A. Edris “An SSSC-based hybrid series compensation scheme capable of damping subsynchronous resonance,” *IEEE Trans. Power Deliv.*, vol. 27, no. November 2009, pp. 531–540, 2012.
- [65] D. Rai, S. O. Faried, G. Ramakrishna, and A. A. Edris, “Damping inter-area oscillations using phase imbalanced series compensation schemes,” *IEEE Trans. Power Syst.*, vol. 26, no. 3, pp. 1753–1761, 2011.
- [66] D. Rai, G. Ramakrishna, S. O. Faried “Enhancement of Power System Dynamics Using a Phase Imbalanced Series Compensation Scheme,” vol. 25, no. 2, pp. 966–974, 2010.
- [67] S. R. Joshi, E. P. Cheriyan, and a. M. Kulkarni, “Output feedback SSR damping controller design based on modular discrete-time dynamic model of TCSC,” *IET Gener. Transm. Distrib.*, vol. 3, no. December 2008, p. 561, 2009.
- [68] C. E. Ugalde-Loo, J. B. Ekanayake, and N. Jenkins, “Subsynchronous resonance on series compensated transmission lines with quadrature boosters,” *2011 IEEE PES Trondheim PowerTech Power Technol. a Sustain. Soc. POWERTECH 2011*, pp. 1–7, 2011.
- [69] H. F. Latorre, M. Ghandhari, and L. Söder, “Use of local and remote information in POD control of a VSC-HVdc,” *2009 IEEE Bucharest PowerTech Innov. Ideas Towar. Electr. Grid Futur.*, pp. 1–6, 2009.
- [70] G. F. Reed, H. a. Al Hassan, M. J. Korytowski, P. T. Lewis, and B. M. Grainger, “Comparison of HVAC and HVDC solutions for offshore wind farms with a procedure for system economic evaluation,” *2013 IEEE Energytech, Energytech 2013*, 2013.
- [71] G. G. K. Jicheng Yu, “Applications of Embedded HVDC in Power System Transmission,” *IEEE Trans. Power Syst.*, pp. 2–7, 2012.
- [72] ABB, “ABB Reference Projects” [online] Available at: <http://www.abb.com/hvdc>, 2009., 2009. [Online]. Available: <http://www.abb.com/industries/us/9AAF400191.aspx>. [Accessed: 01-Jan-2009].
- [73] N. Flourentzou, V. G. Agelidis, and G. D. Demetriades “VSC-Based HVDC Power Transmission Systems: An Overview,” *IEEE Trans. Power Electron.*, vol. 24, no. 3, pp. 592–602, 2009.
- [74] C. Nguyen-Mau, K. Rudion, and Z. a. Styczynski “HVDC application for enhancing power system stability,” *2011 EPU-CRIS Int. Conf. Sci. Technol.*, no. C, pp. 1–6, 2011.

References

- [75] R. Preece, a. M. Almutairi, O. Marjanovic, and J. V. Milanović “Damping of electromechanical oscillations by VSC-HVDC active power modulation with supplementary wams based modal LQG controller,” *IEEE Power Energy Soc. Gen. Meet.*, pp. 1–7, 2011.
- [76] H. Wang, C. He, and L. Fu, “Stability mechanism analysis of HVDC control system for power system restoration using HVDC,” *DRPT 2011 - 2011 4th Int. Conf. Electr. Util. Deregul. Restruct. Power Technol.*, no. 50877044, pp. 433–437, 2011.
- [77] O. Daniel Adeuyi, N. Jenkins, and J. Wu “Topologies of the North Sea Supergrid,” *Proc. Univ. Power Eng. Conf.*, 2013.
- [78] D. R. L. Sellick and M. Akerberg “Comparison of HVDC Light (VSC) and HVDC Classic (LCC) Site Aspects , for a 500MW 400kV HVDC Transmission Scheme,” *IET ACDC 2012 Conf.*, no. Lcc, pp. 1–6, 2012.
- [79] D. T. Oyedokun, K. a. Folly, a. V. Ubisse, and L. C. Azimoh, “Interaction between HVAC - HVDC system: Impact of line length on transient stability,” *Univ. Power Eng. Conf. (UPEC), 2010 45th Int.*, no. 1, pp. 1–6, 2010.
- [80] T. Zhu, C. Wang, and J. Zhang “Influence of the AC system faults on HVDC system and recommendations for improvement,” *2009 IEEE Power Energy Soc. Gen. Meet. PES '09*, pp. 1–6, 2009.
- [81] C. J. Chou, Y. K. Wu, G. Y. Han, and C. Y. Lee “Comparative evaluation of the HVDC and HVAC links integrated in a large offshore wind farman actual case study in Taiwan,” *IEEE Trans. Ind. Appl.*, vol. 48, no. 5, pp. 1639–1648, 2012.
- [82] Sigurd Skogestad and Ian Postlethwaite, *Multivariable Feedback Control: Analysis and Design*, 2nd Editio. Wiley, 2005, p. 590p.
- [83] W. a Mittelstadt, “R. L. Cresap W. A. Mittelstadt Bonneville Power Administration Portland, Oregon,” 1975.
- [84] G. Liu, Z. Xu, Y. Huang, and W. Pan, “Analysis of inter-area oscillations in the South China Interconnected Power System” *Electr. Power Syst. Res.*, vol. 70, pp. 38–45, 2004.
- [85] N. Encinas, N. Encinas, C. Alvarez, D. Alfonso, D. Alfonso, a. Perez-Navarro, C. Lvarez, F. Garcia-Franco, and a Perez-, “Energy market segmentation for distributed energy resources implementation purposes” *Gener. Transm. Distrib. IET*, vol. 1, no. 1, p. 324, 2007.
- [86] M. Xiao-Ming, Z. Yao, G. Lin, and W. Xiao-Chen, “Coordinated control of interarea oscillation in the China Southern power grid” *IEEE Trans. Power Syst.*, vol. 21, no. 2, pp. 845–852, 2006.
- [87] M. Ghandhari, I. a Hiskens, “Control Lyapunov Functions for Controllable Series” *IEEE Trans. Power Syst.*, vol. 16, no. 4, pp. 689–694, 2001.
- [88] Balarko Chaudhuri , R. Majumder and B. Pal “Wide area measurement based stabilizing control of power system considering signal transmission delay” p. 1447 Vol. 2–, 2005.

References

- [89] Balarko Chaudhuri and B. Pal, "Robust Damping of Multiple Swing Modes Employing Global Stabilizing Signals With a TCSC" *IEEE Trans. Power Syst.*, vol. 19, no. 1, pp. 499–506, 2004.
- [90] A. C. Zolotas, B. Chaudhuri, S. Member, and I. M. Jaimoukha, "Brief Papers," *Ieee Trans. Control Syst. Technol.*, vol. 15, no. 1, pp. 151–160, 2007.
- [91] M. Zarghami, M. L. Crow and S. Jagannathan, "Nonlinear control of FACTS controllers for damping interarea oscillations in power systems," *IEEE Trans. Power Deliv.*, vol. 25, no. 4, pp. 3113–3121, 2010.
- [92] M. M. Alamuti, C. S. Saunders and G. A. Taylor, "A Novel VSC HVDC Active Power Control Strategy to Improve AC System Stability" 2014.
- [93] M. M. Alamuti, R. Rabbani, S. K. Kerahroudi, and G. A. Taylor, "System Stability Improvement through HVDC Supplementary Model Predictive Control."
- [94] S. Cole and R. Belmans "A proposal for standard VSC HVDC dynamic models in power system stability studies" *Electr. Power Syst. Res.*, vol. 81, pp. 967–973, 2011.
- [95] Y. Li, C. Rehtanz, S. Rüberg, L. Luo, and Y. Cao "Wide-area robust coordination approach of HVDC and FACTS controllers for damping multiple interarea oscillations," *IEEE Trans. Power Deliv.*, vol. 27, no. 3, pp. 1096–1105, 2012.
- [96] D. D. Simfukwe, B. C. Pal, R. a. Jabr, and N. Martins "Robust and low-order design of flexible AC transmission systems and power system stabilisers for oscillation damping," *IET Gener. Transm. Distrib.*, vol. 6, no. September 2011, p. 445, 2012.
- [97] L. J. Cai and I. Erlich "Simultaneous coordinated tuning of PSS and FACTS damping controllers in large power systems" *IEEE Trans. Power Syst.*, vol. 20, no. 1, pp. 294–300, 2005.
- [98] P. Pourbeik and M. J. Gibbard "Simultaneous coordination of power system stabilizers and FACTS device stabilizers in a multimachine power system for enhancing dynamic performance" *IEEE Trans. Power Syst.*, vol. 13, no. 2, pp. 473–479, 1998.
- [99] Deyu Cai, "Wide Area Monitoring, Protection and Control in the Future Great Britain Power System" PhD Thesis, University of Manchester, 2012.
- [100] Y. Pipelzadeh, Balarko Chaudhuri , T. Green "Control Coordination Within a VSC HVDC Link for Power Oscillation Damping : A Robust Decentralized Approach Using Homotopy" vol. 21, no. 4, pp. 1270–1279, 2013.
- [101] Y. Li, C. Rehtanz, D. Yang, S. Rüberg, and U. Häger "Robust high-voltage direct current stabilising control using wide-area measurement and taking transmission time delay into consideration," *IET Gener. Transm. Distrib.*, vol. 5, no. April 2010, p. 289, 2011.
- [102] P. K. Dash, S. Mishra and G. Panda "Damping multimodal power system oscillation using a hybrid fuzzy controller for series connected FACTS devices," *IEEE Trans. Power Syst.*, vol. 15, no. 4, pp. 1360–1366, 2000.

References

- [103] H. Weng and Z. Xu “WAMS based robust HVDC control considering model imprecision for AC/DC power systems using sliding mode control,” *Electr. Power Syst. Res.*, vol. 95, pp. 38–46, 2013.
- [104] W. Juanjuan, F. Chuang, and Z. Yao “Design of WAMS-based multiple HVDC damping control system,” *IEEE Trans. Smart Grid*, vol. 2, no. 2, pp. 363–374, 2011.
- [105] Y. Pipelzadeh, Balarko Chaudhuri and T. Green “Coordinated damping control through multiple HVDC systems: A decentralized approach,” *IEEE Power Energy Soc. Gen. Meet.*, pp. 1–8, 2011.
- [106] E. Belenguier, R. Vidal, and H. Beltrán “Wind Power Plants Connected through a VSC-HVDC Link,” pp. 5252–5257, 2013.
- [107] H. F. Latorre, M. Ghandhari, and L. Söder, “Active and reactive power control of a VSC-HVdc,” *Electr. Power Syst. Res.*, vol. 78, pp. 1756–1763, 2008.
- [108] N. Encinas, N. Encinas, C. Alvarez, D. Alfonso, D. Alfonso, a. Perez-Navarro, C. Lvarez, F. Garcia-Franco, and a Perez-, “Energy market segmentation for distributed energy resources implementation purposes,” *Gener. Transm. Distrib. IET*, vol. 1, p. 324, 2007.
- [109] H. Jingbo, L. Chao, W. Xiaochen, W. Jingtao, and T. S. Bi, “Design and experiment of heuristic adaptive HVDC supplementary damping controller based on online Prony analysis,” *2007 IEEE Power Eng. Soc. Gen. Meet. PES*, pp. 1–7, 2007.
- [110] H. F. Wang, “Selection of robust installing locations and feedback signals of FACTS-based stabilizers in multi-machine power systems,” *IEEE Trans. Power Syst.*, vol. 14, no. 2, pp. 569–574, 1999.
- [111] M. Imhof and Z. Eth, “Power System Stability Control using Voltage Source Converter Based HVDC in Power Systems with a High Penetration of Renewables,” 2010.
- [112] S. Pirooz Azad, R. Iravani, and J. E. Tate “Damping inter-area oscillations based on a model predictive control (MPC) HVDC supplementary controller,” *IEEE Trans. Power Syst.*, vol. 28, no. 3, pp. 3174–3183, 2013.
- [113] J. Zhu, C. D. Booth, G. P. Adam, A. J. Roscoe, and C. G. Bright “Inertia emulation control strategy for VSC-HVDC transmission systems,” *IEEE Trans. Power Syst.*, vol. 28, no. 2, pp. 1277–1287, 2013.
- [114] Y. Liu and Z. Chen “A flexible power control method of VSC-HVDC link for the enhancement of effective short-circuit ratio in a hybrid multi-infeed HVDC system,” *IEEE Trans. Power Syst.*, vol. 28, no. 2, pp. 1568–1581, 2013.
- [115] J. Hazra, Y. Phulpin, and D. Ernst “HVDC control strategies to improve transient stability in interconnected power systems,” *2009 IEEE Bucharest PowerTech*, pp. 1–6, 2009.
- [116] I. Martinez Sanz, Balarko Chaudhuri and G. Strbac, “Corrective control through HVDC links: A case study on GB equivalent system,” *IEEE Power Energy Soc. Gen. Meet.*, 2013.

References

- [117] P. M. Anderson, "Industry experience with special protection schemes," *IEEE Trans. Power Syst.*, vol. 11, no. 3, pp. 1166–1179, 1996.
- [118] "HVDC Classic, Siemens" [Online]. Available: <http://www.energy.siemens.com/mx/en/power-transmission/hvdc>.
- [119] G. I. DR. T. ADHIKARI "THE CHANDRAPUR - PADGHE HVDC BIPOLE TRANSMISSION," *Cigré Symp.*, no. September, Kuala Lumpur, Malaysia, 1999.
- [120] G. Corbetta, "EWEA: The European offshore wind industry - key trends and statistics 2013," no. July, pp. 1–7, 2014.
- [121] EWEA, "EWEA ,Wind power in 2013 European statistics." .
- [122] T. M. Haileselassie and K. Uhlen, "Power system security in a meshed north sea HVDC grid," *Proc. IEEE*, vol. 101, no. 4, pp. 978–990, 2013.
- [123] L'Abbate, G. Migliavacca, U. Häger, C. Rehtanz, S. Rüberg, H. Ferreira, G. Fulli, and a. Purvins "The role of facts and HVDC in the future PAN-European transmission system development," *9th IET Int. Conf. AC DC Power Transm. (ACDC 2010)*, pp. O16–O16, 2010.
- [124] "DiGSILENT PowerFactory, Version14.0.522.[Online], Available: <http://www.digsilent.com>." [Online], Available: <http://www.digsilent.com>.
- [125] Dragan Jovcic and Khaled Ahmed, "*High-Voltage Direct Current Transmission: Converters, Systems and DC Grids.*" Wiley 2015, 201AD.
- [126] S.R. Joshi, E.P. Cheriyan, A.M. Kulkarni, P. C. and A K. S.R. Joshi "Output feedback SSR damping controller design based on modular discrete-time dynamic model of TCSC" *Generation, Transmission & Distribution, IET, Vol: 3, no. 6, 2009, pp: 561 – 573*.
- [127] Z. X. and J. Z. X.Zheng "A Supplementary Damping Controller of TCSC for Mitigating SSR" *Power & Energy Society General Meeting, 2009, PES '09, IEEE, pp. 1.,* in *Power & Energy Society General Meeting, 2009, PES '09, IEEE, pp. 1.*
- [128] Dragan. Jovcic, NG. Pillai "Analytical modeling of TCSC dynamics" *Power Delivery IEEE Transaction. , vol.20, no.2, pp.1097,1104, April 2005*.
- [129] S. Meikandasivam, R. K. Nema, and S. K. Jain, "Behavioral Study of TCSC Device – A MATLAB / Simulink Implementation," pp. 694–699, 2008.
- [130] H. Ambriz-Pérez, E. Acha, and C. R. Fuerte-Esquivel, "Advanced SVC models for Newton-Raphson load flow and Newton optimal power flow studies," *IEEE Trans. Power Syst.*, vol. 15, no. 1, pp. 129–136, 2000.
- [131] "National Grid, UK Gas and Electricity Transmission "UK Future Energy Scenarios", July 2013. [Online] Availabe on :<http://www.nationalgrid.com/NR/rdonlyres/2450AADD-FBA3-49C1-8D63-7160A081C1F2/61591/UKFES2013FINAL3.pdf>."

References

- [132] “DECC Energy Trends March 2014” [Online] Available on: https://www.gov.uk/government/uploads/system/uploads/attachment_data/file/295362/ET_March_2014.PDF.”
- [133] “ENSG, ‘Our Electricity Transmission Network: A Vision for 2020’ [Online]. Available: https://www.gov.uk/government/uploads/system/uploads/attachment_data/file/48275/4264-ensg-summary.pdf,2012.”
- [134] National Grid “2013 Electricity Ten Year Statement,” 2013.
- [135] Kerahroudi, Shadi.K, Zobaa. A.F, Taylor G.A, M.E.Bradley, Yang,L "Investigating the impact of stability constraints on the future GB transmission system," *Universities Power Engineering Conference (UPEC), 2012 47th International*, vol., no., pp.1, 6, 4-7 Sept. 2012
- [136] Kerahroudi, Shadi, Taylor G.A, M.E.Bradley, Zobaa A.F "A framework for coordinated stability control in the future GB transmission system using HVDC and power flow controller devices," *AC and DC Power Transmission (ACDC 2012), 10th IET International Conference* , vol., pp.1,6, 4-5 Dec. 2012
- [137] Kerahroudi, Shadi, Taylor G.A, F.Li, M.E.Bradley "Initial development of a novel stability control system for the future GB transmission system operation," *Power Engineering Conference (UPEC), 2013 48th International Universities'* , vol., no., pp.1,6, 2-5 Sept. 2013
- [138] S. K. Kerahroudi, G. A. Taylor, F. Li, and M. E. Bradley “Application of a Novel Stability Control System for Coordination of Power Flow Control Devices in the Future GB Transmission System ” in *EEE PES General Meeting, USA, Washington DC* , July 2014, pp. 1–5.
- [139] “On line stability control system overview,” Internal Business procedure at National Grid.
- [140] “National grid intertrip services [Online].Available:<http://www2.nationalgrid.com/uk/services/balancing-services/system-security/intertrips>.” .
- [141] Shadi Khaleghi- Kerahroudi , Mohsen. M. Alamuti , F. Li , G. A.Taylor “ Application and Requirement of DIgSILENT PowerFactory to Matlab/ Simulink Interface “Springer publication, ISBN 978-3-319-12957-0,” .
- [142] J. A. Filizadeh, S. Heidari, M.; Mehrizi-Sani, A.Jatskevich, J.Martinez, ““Techniques for Interfacing Electromagnetic Transient Simulation Programs With General Mathematical Tools IEEE Taskforce on Interfacing Techniques for Simulation Tools " *Power Deliv. IEEE Trans. , vol.23, no.4, pp.2610,2622, Oct. 2008, 2008.*
- [143] A.M. Gole, A. Daneshpooy “Towards Open Systems: A PSCAD/EMTDC to MATLAB Interface,” *Submitt. to IPST '97.*
- [144] “DIgSILENT PowerFactory, Version14.0.522. [Online]. Available: <http://www.digsilent.com>.” .

References

- [145] “MATLAB Toolbox Release 2009a, the MathWorks, Inc., Natick, Massachusetts, United States. [Online]. Available: <http://www.mathworks.co.uk>.”
- [146] R. Preece, J. V. Milanović, A. M. Almutairi, and O. Marjanovic “Damping of inter-area oscillations in mixed AC/DC networks using WAMS based supplementary controller,” *IEEE Trans. Power Syst.*, vol. 28, no. 2, pp. 1160–1169, 2013.
- [147] Kerahroudi, Shadi.K, F.Li, Z. Ma, M.M.Alamuti, Rabbani.R, Taylor G.A, M.E. Bradley “Critical Evaluation of the Power System Stability Enhancement in the Future GB Transmission Using the HVDC link ,” *AC and DC Power Transmission (ACDC 2015), 11th IET International Conference* , vol., no., pp.1,6, 4-5 Feb. 2015
- [148] K. J. Åström, “A robust sampled regulator for stable systems with monotone step responses,” *Automatica*, vol. 16, pp. 313–315, 1980.
- [149] W.S. Lu and K. S. P. Kumar, “A staircase model for unknown multivariable systems and design of regulators,” *Automatica*, vol. 20, pp. 109–112, 1984.
- [150] Mossaheb, S., Cameron, R. G. and Li, F., “Passivity and the design of sampled regulators: extended results,” *Int. J. Control*, vol. 51, pp. 503–519, 1990.
- [151] N. Patel, R. V. and Munro, “Multivariable System Theory and Design,” *Pergamon Press*.
- [152] Shadi K. Kerahroudi, F. Li, M. Mohammadi Alamuti, R. Rabbani, Martin E. Bradley and G. A. Taylor, “Novel Operational Stability Control Schemes for Embedded HVDC Links in the Future GB Transmission System,” *IEEE Transactions on Power Delivery*, Submitted Sept. 2015.
- [153] H.F. Wang and F.Li, “Multivariable sampled regulators for the co-ordinated control of STATCOM AC and DC voltage” in *IEE Proc.-Gener., Transm. and Distrib*, 2000, pp. Vol147–2 pp93, 2000.
- [154] National Grid “Orange box training module on OLTA application,” 2014.
- [155] National Grid “Power System Stability Management ((INVP 2465 - Stability Control System).”
- [156] National Grid “West Coast CSC-HVDC link Technical Note Guide(TNG),” 2012.
- [157] N. Zhou, Z. Huang, F. K. Tuffner, and S. Jin “Oscillation Detection Algorithm Development Summary Report and Test Plan,” no. October, 2009.
- [158] K. M. Trantor “Installation of power system stabilisers and the evaluation of settings,” *IEE Proc. C Gener. Transm. Distrib.*, vol. 135, p. 244, 1988.
- [159] D. H. Wilson, “Wide area monitoring systems in the Uk: Operational experience and systems Development, ‘Monitoring and system operation control based on synchronized phasor measurements’, Monitoring of Power System Dynamics Performance,” *Proc. Cigre Sess. S1-9*.
- [160] Market Operation National Grid, “Market Operations Business Procedures, BP1612 – Power System Oscillation Identification. National Grid, UK internal.”

References

- [161] Phillip Ashton, "Exploiting Phasor Measurement Units for Enhanced Transmission Network Operation and Control," Brunel Institute of Power Systems (BIPS) at Brunel University London, 2014.
- [162] Kerahroudi, Shadi.K, Rabbani.R, F.Li, Taylor G.A, Alamuti. M. Mohammadi, M.E.Bradley "Power system stability enhancement of the future GB transmission system using HVDC link," *Power Engineering Conference (UPEC), 2014 49th International Universities* , vol., no., pp.1,6, 2-5 Sept. 2014
- [163] H. N. H. Ni, G. T. Heydt, and R. G. Farmer, "Autonomous damping controller design for power system oscillations," *2000 Power Eng. Soc. Summer Meet. Cat No00CH37134*, vol. 2, no. 1, pp. 1133–1138, 2000.
- [164] a. Adamczyk, R. Teodorescu, F. Iov, and P. C. Kjar, "Evaluation of residue based power oscillation damping control of inter-area oscillations for static power sources," *IEEE Power Energy Soc. Gen. Meet.*, pp. 1–8, 2012.
- [165] S. Atique Malik, *Multivariable Feedback Control: Analysis and Design*. Wiley, Chichester, U.K, 1996, p. xi+559 pp.
- [166] A. Almutairi "Enhancement of Power System Stability Using Wide Area Measurement System Based Damping Controller" The University of Manchester, 2010.
- [167] A. A. Hashmani "Damping of Electromechanical Oscillations in Power Systems using Wide Area Control" University of Duisburg-Essen, 2010.
- [168] R. Eriksson and L. Söder, "Wide-Area Measurement System-Based Subspace Identification for Obtaining Linear Models to Centrally Coordinate Controllable Devices," *IEEE Trans. Power Deliv.*, vol. 26, no. 2, pp. 988–997, 2011.
- [169] P. Zhang, D. Y. Yang, K. W. Chan, and G. W. Cai "Adaptive wide-area damping control scheme with stochastic subspace identification and signal time delay compensation" *IET Gener. Transm. Distrib.*, vol. 6, no. May, p. 844, 2012.
- [170] M.Mohammadi Alamuti, Kerahroudi Shadi.K, Rabbani.R, Taylor G.A "Probabilistic Evaluation of Power System Stability Enhancement Using Supplementary MLQG and MPC Schemes for Embedded HVDC ink " *IEEE Transactions on Power Delivery* , Submitted Sept. 2015.
- [171] Y. Pipelzadeh, Balarko Chaudhuri , T. C. Green "Wide-area Power Oscillation Damping Control through HVDC : A Case Study on Australian Equivalent System," pp. 1–7, 2010.
- [172] M. A. Pai and A. Stankovic, *Robust Control in Power Systems*. 2005.
- [173] A. C. Zolotas, Balarko Chaudhuri, and I. M. Jaimoukha, "Brief Papers," vol. 15, no. 1, pp. 151–160, 2007.
- [174] R. Preece, J. V. Milanović, A. M. Almutairi and O. Marjanovic "Probabilistic evaluation of damping controller in networks with multiple VSC-HVDC lines," *IEEE Trans. Power System.*, vol. 28, no. 1, pp. 367–376, 2013.

References

- [175] Shadi Khaleghi, Kerahroudi, Ma Zhibo, Redfern Miles, M.E. Bradley and G.A. Taylor “Transmission System Stability Enhancement using Demand Management Technology” *Power Engineering Conference (UPEC), 2014 49th International Universities*, vol., no., pp.1,5, 2-5 Sept. 2014
- [176] NG, “Nationalgrid Demand Management services,” http://www2.nationalgrid.com/uk/services/balancing-services/reserve-services/demand-management/National_grid_intertrip_services. .
- [177] NG, “Available:<http://www2.nationalgrid.com/uk/services/balancing-services/system-security/intertrips>.” .
- [178] K. Qian, C. Zhou, M. Allan, and Y. Yuan, “Modeling of load demand due to EV battery charging in distribution systems,” *IEEE Trans. Power System.*, vol. 26, no. 2, pp. 802–810, 2011.
- [179] Y. Ma, T. Houghton, A. Cruden and D. Infield, “Modeling the benefits of vehicle-to-grid technology to a power system,” *IEEE Trans. Power Syst.*, vol. 27, no. 2, pp. 1012–1020, 2012.
- [180] Shadi.K.Kerahroudi, F.Li, M.E.Bradley and G.A. Taylor, “Evaluating the Application of a Class of Sampled Regulators for Power System Control” *IEEE Transactions on Control Systems Technology - Paper ID TCST-2015-0052, Accepted*.
- [181] S. De Boeck and D. Van Hertem, “Coordination of multiple HVDC links in power systems during alert and emergency situations,” *2013 IEEE Grenoble Conf. PowerTech, POWERTECH 2013*, 2013.
- [182] L. Power and S. A. Decentralized, “Wide-Area Measurement Based Stabilizing Control vol. 16, no. 1, pp. 136–153, 2001.
- [183] W. Yao, L. Jiang, J. Wen, Q. H. Wu, and S. Cheng, “Wide-Area Damping Controller of FACTS Devices for Inter-Area Oscillations Considering Communication Time Delays,” vol. 29, no. 1, pp. 318–329, 2014.